THE EPIGENETIC REGULATION OF GENE EXPRESSION BY ECDYSONE HORMONE SIGNALING

Christopher Mitsuo Uyehara

A dissertation submitted to the faculty at the University of North Carolina at Chapel Hill in partial fulfillment of the requirements for the degree of Doctor of Philosophy in the Curriculum in Genetics and Molecular Biology in the School of Medicine.

Chapel Hill
2021

Approved by:

Daniel J. McKay

Joseph J. Kieber

Robert J. Duronio

Jill M. Dowen

Stephen T. Crews

© 2021
Christopher Mitsuo Uyehara
ALL RIGHTS RESERVED

ABSTRACT

Christopher Mitsuo Uyehara: The epigenetic regulation of gene expression by ecdysone hormone signaling
(Under the direction of Daniel J. McKay)

The development of a multicellular organism from a single progenitor is a complex process that involves the establishment of gene expression profiles specific to each stage and tissue. In *Drosophila*, pulses of the steroid hormone ecdysone play a central role in coordinating development events throughout the life cycle, including the larval molts and the onset of the larval-to-adult transition. The initial response to ecdysone is mediated by its receptor, EcR, which activates a series of downstream transcription factors that amplify and temporally progress the cascade. The genetic response has tissue- and temporal-specificity; each successive pulse initiates different developmental events in tissues throughout the animal. However, our understanding of how this specificity is achieved remains incomplete. In this work, we examined how EcR and one of its downstream transcription factors, E93, coordinate changes in gene expression. We found that changes in chromatin accessibility are a central means by which specificity to the response is achieved but that EcR and E93 have different roles. E93 is required to temporally progress the accessibility profile and binds many sites dependent on E93 for their accessibility, indicating that it may have pioneer-like activity. In contrast, EcR appears to be a passive factor in which tissue-specific differences in open chromatin direct its binding to different sites between the two tissues. Since EcR functions at the top of a transcriptional hierarchy, we further investigated its direct role in

promoting changes in gene expression. We found that EcR plays a broad role in coordinating the response to ecdysone and that changes in its binding profile are an important means by which specificity is achieved. To determine the function of EcR binding, we investigated its role in regulating enhancer activity. As expected, we found that it regulates the temporal activity of enhancers. Unexpectedly, however, we also found that it regulates the spatial pattern of enhancers. This indicates that EcR may regulate gene expression differences that occur within tissues, as well as between them. Collectively, this work has provided new insights into how tissue- and temporal-specific gene expression responses can be generated by a single, extrinsic signal.

“Here’s to trouble-free tomorrows.

May all your sorrows all be small.

Here’s to the losers.

Bless them all.”

–Frank Sinatra

ACKNOWLEDGEMENTS

My father died on Thursday, January 10, 2019 from prostate cancer. He was 64. Eight days earlier, I left in the early hours of the morning to take a bus from Fairfax, VA back to Chapel Hill, NC. My father was asleep, and I didn't wake him. I whispered, "goodbye", walked out into the cold, dark winter morning, the stars just beginning to fade from the sky, and got into an Uber to Union Station, wondering if I had just seen my father alive for the last time. I had made plans to return the following Friday, on January 11th. He died on the 10th. If I could do it again, knowing that my father only had eight days left to live, I would have stayed, or at least said something more than a simple, "goodbye".

But it didn't work out that way.

In the days, and weeks, that followed, a question kept coming up, asked of me by family members and acquaintances and my own inner-reflections, seemingly well-meaning, but ever so-slightly painful to consider: How had my father most shaped me? I pondered this. People I knew in science sometimes spoke of their parents helping them with class projects, or sending them to space camp, or, perhaps, as was sometimes the case, their parents were, themselves, scientists or doctors. My father didn't really do any of that for me. He was a career Foreign Service Officer – a US diplomat – with a mind that was quietly expansive. Give him a topic on foreign policy, or history, or economics, and he would either happily expound his thoughts on it, or, if this were your area of expertise, launch a barrage of

questions – genuinely curious about the answers. When he was a child, he read the World Book Encyclopedia for fun. He loved watching Jeopardy.

However, as I grew older, and increasingly enamored of science, I slowly became aware that although my father was fascinated by history, public policy, international relations, and economics, the natural sciences never much appealed to him. The more I learned, the more distant our conversations became, as I rapidly surpassed not only his expertise, but also his interest. I could never quite understand why that was – whether that reflected some flaw in my ability to communicate just what it was I found so fascinating, or whether it, instead, reflected some aspect of his character. I never had the courage to tell him that, tell him how as I went off to college to study biology, and got a B.S., then an M.S., then began working towards my Ph.D., that I was saddened, and, if I am being honest, hurt by his disinterest in my job, which I was so passionate about. I regret that I never had that conversation with him.

Outside of science, I can point to a lot of things that I get from my father. When my father was young, he read a lot of science fiction – Heinlein, Asimov, Clarke, Laumer. I read those too. My father always wore a calculator watch. For years, I, too, wore a calculator watch, and still wear a watch every day. My father taught me how to cook fried rice, the right way to hold a chef's knife, and how to curl my fingers while chopping vegetables so that I didn't slice the tips of my fingers off. Like many fathers, he loved puns, and corny jokes, and would chuckle at the most egregious ones. His favorite was the one about a panda walking into a bar, eating, shooting, and leaving. Though now famous from an eponymous book, my father had been telling it for years before. I tell that joke, too.

However, when I contemplated the question of what influenced me *most* from my father, my mind kept coming back to something: when I asked questions growing up, my father never answered them as though I were a child. He never talked down to me. He never smiled condescendingly and told me that I would understand when I grew older, or to stop asking silly questions. He just patiently answered to the best of his knowledge, no matter the topic. He would talk politics with the 10-year-old me with the same tone of voice he'd use with anyone else. I kept coming back to that aspect of our relationship as perhaps the greatest gift he gave to me, but a part of me felt embarrassed that it was my answer. It didn't seem adequate. Like, it was too subtle, or not striking enough, or just too simple a thing. And, really, it is simple. But where is it written that a simple thing can't shape you profoundly? Isn't it those things that often matter most?

My father's willingness to answer whatever question caught my fancy taught me, first and foremost, to never be embarrassed to ask a question. I never felt ashamed to ask my father questions, and he never acted like I was dumb for asking them. It taught me that being confronted with something I don't know didn't make me stupid and gave me the confidence to believe that anyone who thought otherwise was wrong. It wasn't stupid to ask questions. It was stupid to not seek out answers. I can't say that I've always followed that lesson – that I've never held back a question out of embarrassment of my own ignorance or been intimidated by a large crowd filled with people that I knew were smarter than me. However, I believe that those who have known me at UNC can attest that I have asked a mind-numbingly massive number of questions over the years – many of which were quite simple and reflected a profound level of ignorance. I don't regret a single one.

Although I wonder if he intended it, my father also taught me to never respect other peoples' ideas. Respect people; treat them intelligently; listen carefully. But ideas don't have feelings. Ideas are ideas are ideas. My father never treated his own views as necessarily correct or his own beliefs as sacrosanct and above reproach. He *thought* he was right; sometimes he was even stubbornly wedded to his own views, but, whenever I disagreed, whether I was ten years old, or twenty, he always treated it as a discussion worth having. He always listened to what I had to say. Even when he thought I was wrong, I never got the impression he thought poorly of me, and I never thought poorly of him, in turn. He taught me that it was okay to disagree with someone smarter than you, or someone you respected, and that it's possible to think that people, including my father, can be smart and be wrong; there's no contradiction. I like to think that I'm not afraid to disagree with others, and that I've always been willing to probe and poke and push back against arguments, even when coming from people who knew more than me. And I like to think I've never taken it *too* personally when someone does the same to me.

I didn't speak at my father's funeral. I didn't know what to say. It wasn't that there was too little, but that there was too much. How could I hope to portray even one iota of who my father was, what he meant to me, and what our relationship was? It was too much. Too much pain. Too much regret. Too much loss. Too much to say, and not enough time in all the universe with which to say it. I've spent the last two years thinking about my relationship with my father, writing pages of journal entries, spending fitful nights consumed in loss, and regretting all the questions I never asked him, all the things I'd wish I'd said, and all the conversations we never had, and, now, never will. What I've written here doesn't come close to capturing any of it. It's barely a footnote.

One of my sorrows is that my father died before my defense. In the years before he passed away, we had drifted apart, even as I never stopped wanting his approval and respect. I like to imagine that, at my thesis defense, he would have more clearly seen the person I had become. I wish he could have gone to my talk and heard the passion and excitement in my voice and seen how I had matured as a speaker. I wish he could have come to see where I work and met the people I work with. I wish I could have celebrated my accomplishment with him and discussed my hopes and dreams for the future. I can be…quirky. Dan, my research adviser, once described me as whimsical. Excitable. In love with what I do in a way only a scientist can be. You have to be in love, because that love, that passion, gets you through all the days when something goes wrong, you have to repeat an experiment *again*, or you have to do something that's just a slog, even though you know it probably won't even work, and you come home, and you're a mix of frustrated, anxious, and absolutely, soul-crushingly tired, only you know you won't sleep well, and, shoot, you still have to cook dinner… The only thing that got me through those days was that spark of passion. So, I like to imagine that, at my defense, my father would have seen and appreciated those parts of me.

But it didn't work out that way.

My father never had a chance to see my defense. I wish he had. My only solace is this: He may never have fully appreciated it, but he played an integral role in shaping this thesis. More than that – every person I interacted with here has seen glimpses of my father's influence on me. Every time I asked a question, every time I dared to contradict some statement, every time I raised some interesting point, a part of what my father taught me came through. For good or ill, my father's lessons, intentional or not, remain with me to this day.

I have many uncertainties about my relationship with my father, and, really, the world at large. It is in my nature to wonder, to question, and to doubt. There are so few things that I believe, that I *know*, with certainty. However, I have no question that my father made me a better scientist and shaped the man I am today.

Goodbye, Dad. Thank you for all that you gave me. I miss you dearly.

TABLE OF CONTENTS

LIST OF TABLES

LIST OF FIGURES

LIST OF ABBREVIATIONS

20E / 20HE	20-hydroxyecdysone
Ac	Achaete
AEL	After egg laying
AME	Analysis of motif enrichment
AF1/2	Activation function 1/2
A/P	Anterior/Posterior
APF	After puparium formation
ATP	Adenosine triphosphate
BDSC	Bloomington drosophila stock center
bp	base-pair
br	Broad-Complex
C	Celsius
ChIP	Chromatin immunoprecipitation
CNS	Central nervous
CUT&RUN	Cleavage Under Targets and Release Using Nuclease
DamID	DNA adenine methyltransferase identification
DAPI	4′,6-diamidino-2-phenylindole
dsGFP	Destabilized green fluorescent protein
D/V	Dorsal/Ventral
DBD	DNA binding domain
DE	Differentially expressed
DGRP	Drosophila genetic reference pool

Dl	Delta
DNA	Deoxyribonucleic acid
DNase	Deoxyribonuclease
DREME	Discriminative Regular Expression Motif Elicitation
DSHB	Developmental studies hybridoma bank
E93 / Eip93F	Ecdysone-induced protein 93F
EcI	Ecdysone importer
EcR	Ecdysone Receptor
EcR^{DN}	EcR Dominant-Negative
EcRi	EcR-RNAi
ECRE	Ecdysone response element
FAIRE	Formaldehyde-Assisted Isolation of Regulatory Elements
FDR	False discovery rate
FIMO	Find individual motif occurrences
flp	Flippase
FRT	Flippase recognition target
GFP	Green fluorescent protein
GFSTF	EGFP-FlAsH-Strep-TEV-3xFlag
GO	Gene Ontology
HRP	Horse-radish peroxidase
hs	Heat-shock
kb	Kilo base-pair
kDa	Kilo dalton

LBD	Ligand binding domain
MEME	Multiple Em for Motif Elicitation
MiMIC	Minos Mediated Integration Cassette
ml	milliliter
mmol	millimole
MNase	Micrococcal Nuclease
mt	Mutant
N	Notch
NICD	Notch intracellular domain
NIH	National institutes of health
nls	Nuclear localization signal
NR	Nuclear receptor
n.s.	Not significant
OR	Oregon Roseburg
PARP	Poly(ADP)-ribose polymerase
pAdj	Adjusted p-value
PCR	Polymerase chain reaction
PG	Prothoracic gland
PTTH	Prothoracicotropic hormone
PWM	Position weight matrix
RFP	Red fluorescent protein
RNA	Ribonucleic Acid
RNAi	RNA interference

RNase	Ribonuclease
RT	Room temperature
SEM	Scanning electron microscopy
SG	Salivary gland
SOP	Sensory organ precursor
SPRI	Solid Phase Reversible Immobilization
Su(H)	Suppressor of hairless
tdTomato	Tandem tomato
teg	Tegula
TF	Transcription factor
tTF	Temporal transcription factor
UAS	Upstream activating sequence
UNC	University of North Carolina
VDRC	Vienna Drosophila Research Center
WT	Wildtype

CHAPTER 1: INTRODUCTION

A brief overview of gene regulation

The epigenetic landscape

A central feature of metazoans is that life begins as a single cell. Over the course of development, daughter cells adopt specialized properties and become progressively limited in their ability to take on alternative cell fates. In his oft-cited, 1957 work, "The Strategy of Genes", Conrad Waddington creatively imagined development as a three-dimensional surface with canals, or "creodes", that cells travelled down (1). By dint of these downward sloping canals, cells were both resistant to moving backwards along their own lineages, into earlier stages of development, as well as transitioning to adjacent canals and adopting other cell fates. He referred to this as the "Epigenetic Landscape" and posited that the guide ropes that dictated the shape of each canal, the elements that tugged the canals into troughs and hills, were the biochemical products of genes present in each cell. As a paradigmatic example, Waddington further noted that, in *Drosophila*, wing development was affected by multiple genes, which frequently produced phenotypes in multiple tissues. Based off this, and other examples, he proposed that each gene controlled more than one canal, and each canal was controlled by more than one gene. The combination of all genes active in each cell gave rise to their unique properties.

In the 64 years since Waddington published his work, we now understand that each stage in *Drosophila* wing development, and animal development more broadly, is indeed

characterized by the expression of specific complements of genes, most of which are expressed across multiple times and tissues. The biochemical products and downstream effects of some of these genes, including histone readers and writers, components of cell signaling pathways, and transcription factors, provide information that is inherited across cell divisions to ensure that the correct genes are expressed at the right time and in the right place. Collectively, this information forms the basis of Waddington's epigenetic landscape – a term we still use today.

Transcription factors and enhancers

Specific cis-acting, DNA regulatory elements control the transcription of nearby genes. Although originally broadly classified into enhancers and silencers, depending on whether they enhanced or silenced the expression of the genes they regulate, it's now known that this distinction is largely artificial – the same cis-regulatory element can promote or inhibit transcription in different contexts (2, 3). For that reason, throughout this dissertation, I will use the terms, "cis-regulatory element" (or "cis-regulatory module") and "enhancer" interchangeably. In most cases, individual enhancers act on a single gene. However, the converse is not true. Each gene is usually acted on by multiple enhancers, each of which may exhibit independent spatially- and temporally-restricted patterns of activity (4–7). In some cases, the activity of multiple enhancers results in higher aggregate transcription, while, in others, enhancers appear to act redundantly – as in the case of so-called, "shadow enhancers" – to promote developmental robustness (4–8).

Enhancers effect changes in gene expression by serving as platforms for transcription factors that recognize specific DNA sequence motifs found within each enhancer (9–11).

When bound to an enhancer, transcription factors form protein complexes that either promote or inhibit transcription (12). These complexes perform this function through multiple, non-mutually exclusive mechanisms, including by directly altering RNA polymerase recruitment and release, as well as by promoting specific histone modifications. Similar to enhancers, although sometimes described as activators or repressors, many transcription factors have context-dependent activity; they promote transcription in certain circumstances, and repress it in others (13). This often occurs in the context of extrinsic cell-signaling pathways, in which the effectors of signaling pathways repress transcription when the pathway is off, but, upon signal induction, switch modalities and become transcriptional activators (13). For instance, the downstream effector of Notch signaling, Su(H) acts as a repressor until association with the Notch-intracellular domain (NICD) converts it into an activator (13, 14). Members of the Wnt, hedgehog, and nuclear receptor families, amongst many others, also behave this way (13).

The presence of transcription factor motifs in individual enhancers can dictate not only which transcription factors can bind, but also the strength of the enhancer, and whether it acts as an enhancer or silencer (2, 9, 11). Enhancers are often bound by multiple transcription factors, and, in some cases, transcription factors change their behavior depending on which other transcription factors co-occupy the enhancer. Consequently, the specific combination of motifs in an enhancer is an important means by which enhancer activity is determined. Similarly, the optimality of motifs can also modulate the spatial patterns of activity. Low-affinity binding sites, for instance, can tune the strength of enhancer activity, as well as altering how they respond to graded signals, such as morphogens (15–17). Lastly, although some enhancers exhibit tissue-specific regulation by a fixed set of transcription factors, an emerging

body of literature indicates that some enhancers are pleiotropic – they are active in multiple different contexts and perform different roles during development (18, 19). Compared to normal enhancers, pleiotropic enhancers are information dense; their activity in different tissues has been shown to be controlled by multiple, partially- or non-overlapping sets of transcription factors (18, 19).

Chromatin accessibility and pioneer transcription factors

Most transcription factors cannot stably bind nucleosome-associated DNA. Consequently, the pattern of nucleosome-associated and nucleosome-free DNA – the open chromatin pattern – determines which enhancers are utilized throughout the genome. The open chromatin state can dictate not only whether a gene is on or off, but also whether the enhancers that act on it are competent to respond to extrinsic signaling pathways (20, 21). Consequently, the open chromatin pattern is a central means by which cell- and tissue-specific gene expression profiles are established. Changes in the open chromatin profile are ubiquitous throughout development – they have been observed during embryo development, neural-differentiation, as well as in many cancers, which some researchers have characterized as a disease of development (11, 22–26).

A special class of transcription factors, called “pioneer” transcription factors, have the ability to bind nucleosome-associated DNA (27). Pioneers comprise a diverse group of transcription factors that are functionally defined by their ability recognize their motifs even when nucleosome-bound (21, 28). Upon binding, pioneers can evict nucleosomes to render the site accessible. They perform this function through a variety of different ways. One of the best-characterized pioneers, FoxA1, has a winged-helix DNA binding domain that resembles

H1 and is thought to have the ability to directly evict nucleosomes (27). Other pioneers, however, seem to require the assistance of ATP-dependent chromatin remodeling complexes (20, 26, 27). One of the striking features of pioneers is that although they have the ability to open chromatin, their pioneering activity is context-specific - they do not pioneer at all their binding sites or, in some cases, in all cells. Some of this specificity occurs through differences in the concentration of the transcription factors expressed in each cell. In *Drosophila*, for example, the *Bicoid* pioneer transcription factor, is expressed along a gradient, and only pioneers at high concentrations (29, 30). Additionally, pioneer-specificity can occur with assistance of non-pioneer transcription factors. During hormone signaling, for instance, low-affinity binding of non-pioneer nuclear receptors can recruit and stabilize pioneer binding to new binding sites (31, 32).

Ecdysone hormone signaling

Ecdysone timing and release

Decades of work have established the central role that the steroid hormone ecdysone plays in controlling developmental transitions in *Drosophila*. Ecdysone is produced in the prothoracic gland (PG) of *Drosophila* and secreted into the hemolymph (33, 34). Pulses of ecdysone occur throughout *Drosophila* development where they initiate egg-hatching, each of the larval molts, and the initiation of metamorphosis (33, 35, 36). Additionally, during the 3rd larval instar, which directly precedes metamorphosis, there are several, lower amplitude pulses that initiate a variety of events that prepare the animal for metamorphosis (37, 38). Each of these pulses is dependent on internal organismal checkpoints that ensure that the animal is the correct size, and has developed sufficiently to transition to the next stage (34).

The timing of the synthesis and release of ecdysone from the PG has traditionally been seen as being primarily controlled by neurons that directly innervate the PG and secrete prothoracicotropic hormone (PTTH) (33, 34). PTTH release is controlled through a variety of inputs, including photoperiod, which synchronizes development with the day/night cycle, as well insulin and TOR signaling that provide important information about animal weight and size. However, although PTTH undoubtably plays an important role, ablation of PTTH producing neurons delays, but does not arrest, larval development (39). More recent work has demonstrated that many of the same pathways that act on the PTTH-producing neurons also act on the PG itself, including insulin and TOR signaling (38, 40). Consequently, the timing and release of ecdysone is now thought to be a consequence of a variety of interconnected inputs that act on both PTTH-producing neurons and the PG directly.

In the PG, ecdysone is produced in an inactive form which is secreted into the hemolymph prior to being converted into an active form, 20-Hydroxyecysone, by the P450 cytochrome Shade (*shd*) (41). Shade itself is expressed in variety of peripheral tissues, including the epidermis, midgut, Malpighian tubules, and fat body. This conversion is essential for *Drosophila* development, as mutants of *shd* are embryonic lethal and exhibit a similar phenotype to upstream genes involved in the biosynthesis of ecdysone (the so-called, "Halloween" genes) (41, 42). The timing and expression of *shd* appears to play an important modulatory role in controlling developmental timing. *Shd*, itself, is dynamically expressed throughout development, and its expression in peripheral tissues at later stages is important for the correct timing of pupariation (43).

Unlike other steroid hormones, the active form of ecdysone is incapable of freely diffusing across the cell membrane. Instead, uptake of ecdysone by target tissues occurs via

the organic anion transporting polypeptide Oatp74d, also called EcI (44), a membrane channel that allows ecdysone to enter cells via facilitated diffusion. Expression of *EcI* in the epidermal cells that demarcate the blood brain barrier in *Drosophila* is also essential to render the CNS competent to respond to ecdysone (45). Although modENCODE data indicate that *EcI* is expressed in tissues throughout the animal, its relative expression level does vary. However, it is currently unknown what role that variations in the expression level of *EcI* might play in modulating the response to ecdysone.

History of the Ashburner Model

The genetic response to ecdysone was originally characterized through cytological studies of the salivary glands in *Drosophila* and the midge *Chironomus tentens* (46–48). Salivary glands are highly polyploid, with thousands of copies of the genome existing in register with one another. When stained with a DNA marker, salivary gland chromosomes have a pattern of dense, compacted bands and lighter, decondensed interbands along the length of each chromosome that correlate with the transcriptional state of their associated genes (49–51). The pattern of bands and interbands is reproducible which allows, though careful analysis, genomic loci to be identified cytologically. In addition to bands and interbands, work done by Ulrich Clever, in *C. tentens,* and Michael Ashburner, in *D. melanogaster,* found that salivary gland chromosomes also contained visible, decondensed regions called “puffs” (46, 47, 52). The appearance and disappearance of these puffs occurs in a stereotypical pattern across development that corresponds to the activation of specific genes.

Ashburner and colleagues extended the initial observations of puffs in *Drosophila* using *ex vivo* cultured salivary glands. By adding ecdysone and performing careful time-lapse experiments, they were able to more precisely map the temporal progression of puffs. They found that the initial response to ecdysone involves both the regression of pre-existing, intermolt puffs, as well as the induction of a series of "early" puffs that appeared in distinct phases over the course of several hours ultimately numbering several hundred (48, 53, 54). Following several hours of ecdysone addition, the early puffs began regressing, while a second series of "late" puffs appeared. Treatment with the protein synthesis inhibitor cycloheximide demonstrated that while the appearance of early puffs occurred independently of protein synthesis, their regression, as well as the appearance of late puffs, were inhibited by cycloheximide (53–55). This suggested that the appearance of early puffs occurred through a pre-existing protein that directly responded to ecdysone, while late puff formation was dependent on the protein products of early puffs. The observation that early puff regression also required protein synthesis further indicated that early puffs were responsible for their own inhibition (53). This became what is now known was the Ashburner model – a genetic cascade in which the ecdysone, acting through a then-unidentified receptor, directly induced a series of primary response genes found in early puffs. Some of the protein products of early puffs then acted to both activate late puffs, as well as inhibit their own transcription, presumably by antagonizing the receptor activity (52).

Although the Ashburner model has held up relatively well in the decades since it was first proposed, it was almost immediately complicated by several observations. First, the regression of a subset of the intermolt puffs argued that this response was part of the canonical ecdysone cascade (55). This led Ashburner and his colleague Geoffrey Richards to

suggest their induction might occur in response to an earlier ecdysone pulse. However, how this induction and regression interacted with the products of the early puffs was unclear (55). Additionally, subsequent studies on salivary glands after the onset of metamorphosis (pupariation), demonstrated that several puffs were induced multiple times – during both late-larval stages, and after pupariation – while others were only induced at the later time point (56, 57). These data indicated that there was stage-specificity to the ecdysone response during both the larval and pupal stages of development that the Ashburner Model was not sufficient to explain.

The ecdysone hormone receptor

The development of the Ashburner model is broadly remarkable for two reasons. First, it was a largely accurate account of a genetic cascade that was characterized using cytology; Ashburner and colleagues' experiments were performed without the ability molecularly identify and directly characterize the expression of the genes in the ecdysone cascade. Second, the existence of a receptor to ecdysone was, at that point, hypothetical. Ashburner and colleagues reasonably presumed that such a receptor existed, and they were able to make inferences about its behavior, but it wasn't until 1991 and 1992, when the ecdysone receptor (*EcR*) and its binding partner, ultraspiracle (*usp*) were identified, respectively (58–60).

The canonical ecdysone receptor is comprised of a heterodimer of EcR and Usp, the *Drosophila* homologs of the mammalian Farnesoid X receptor and RXR, respectively (58–61). EcR and Usp both bear similarity to other nuclear receptors. They both contain a core, conserved DNA binding domain (DBD), a ligand-binding domain (LBD), and a C-terminal

activation domain. Although EcR binds ecdysone, Usp is an orphan-nuclear receptor whose ligand, if any exists, is unknown. Binding of ecdysone with EcR promotes the formation of a functional complex by stabilizing its heterodimerization with Usp, as well as its association with DNA (62–64).

The EcR/Usp heterodimer recognizes a palindromic Ecdysone Response Element (ECRE) of the format 5'-RGKTCAWTGAMCY-3', that is similar to other nuclear receptor (NR) motifs indicating a high degree of sequence conservation (62, 65–72). Crystal structures of EcR/Usp bound to DNA indicate that EcR and Usp preferentially bind along two adjacent major grooves, with interaction of the DNA binding domains occurring through residues across the minor groove, and further interaction occurring in the ligand-binding domains (73, 74). In addition to the palindromic motif, EcR and Usp are also capable of binding as monomers or homodimers to direct-repeats of each half-site which can substitute for inverted-repeats in some cases, though with less affinity than the palindrome (75, 76). However, although there is evidence to suggest that EcR and Usp may have independent functions *in vivo*, the extent to which this occurs, as well as its biological significance remain incompletely understood (77–79).

Figure 1.1: EcR/Usp association with DNA

Crystal structure from Devarakonda et al., 2003 showing EcR's DBD (cyan) and Usp's DBD (magenta) bound to adjacent half-sites of an ECRE (grey). Structure was visualized using pymol.

In contrast to other steroid hormone receptors (type I nuclear receptors), but similar to non-steroid hormone receptors (type II nuclear receptors), EcR modulates transcription during periods of both high and low ecdysone titer. In the absence of ligand-binding, EcR has been shown to function as a transcriptional repressor, but transitions into an activator upon its association with ecdysone. This switch is thought to occur through changes in EcR's association with binding partners. A central player in this process is thought to be the protein SMRTER which interacts with EcR through its ligand-binding domain and forms a complex with the Sin3a repressor complex. This complex has been shown to mediate repression through recruitment of histone deacetylases (HDACs) and may play an important role in mediating basal repression in the absence of ecdysone (46). Similarly, members of the NURF and NURD ATP-dependent chromatin remodeling complexes also undergo ligand-dependent changes in their association with EcR (81, 82).

In addition to ligand-dependent changes in EcR's binding partners, further modulation of EcR's activity occurs through the expression of different protein isoforms. EcR has three protein isoforms, EcR-A, -B1, and -B2, that share C-terminal DBDs and LDBs, but differ in their N-terminal domains (83–85). All three isoforms can activate gene expression through a shared, AF1, activation domain found in the LBD, but their different N-

terminal, AF2, domains cause the strength of activation to vary. EcR-B1 and -B2 isoforms are more effective activators than EcR-A whose AF2 domain appears mostly non-functional (83, 84). This effect appears to be at least somewhat independent of cell-type specific coactivator complexes, as expression of the different EcR isoforms in mammalian cell culture reveals a similar effect.

Extending the Ashburner Model

Ashburner's work in salivary glands focused on a relatively limited number of puffing sites. However, in the decades since then, it's become apparent that the response to ecdysone is both widespread and diverse. A comprehensive experiment performed as part of the modENCODE project assayed gene expression in 41 different cell lines prior to and after the addition of ecdysone (86). They found that the majority of genes that responded to ecdysone did so in fewer than half the cell lines they observed, indicating a substantial degree of heterogeneity across cell types (86). In agreement with those data, experiments performed on *in vivo* tissues, as well as cultured organs treated with ecdysone, including the wing, fat body, and salivary gland, have identified thousands of genes with tissue-specific expression that are dependent on ecdysone for their normal expression (87–92).

Different metamorphic responses to ecdysone are, in part, achieved through the expression of different EcR isoforms. During the original characterization of EcR isoforms, a striking association was observed between the relative expression of EcR isoforms across larval tissues, and their subsequent behavior during pupal development (85). Strictly larval tissues that do not persist into adulthood tend to express high-levels of EcR-B1, while imaginal tissues that form the precursors to the adult appendages tend to express EcR-A (85).

Consistent with this, isoform-specific mutations have different effects in different tissues (93–97). However, although, compelling, several lines of evidence have demonstrated that the situation is more complex. EcR-A mutants, for instance, prevent proper death of the salivary gland, even though it's the minor EcR isoform expressed in that tissue (95). Additionally, targeted over-expression of dominant-negative isoforms followed by rescue with individual EcR isoforms indicates that isoforms have partially-overlapping functionality – some developmental phenotypes are rescued regardless of which isoform is used to rescue, while others require the expression of specific isoforms (94). Consequently, while tissue-specific and temporally-dynamic expression of different EcR isoforms is undoubtedly important for development, it is far from sufficient to explain the diversity of responses that ecdysone elicits.

Ashburner's model originally posited that EcR acts at the top of a signaling cascade whose downstream targets both activated the next wave of puffing, as well as repressed the current wave. Consistent with this, many of the genes that map to early, primary response, puffing sites were subsequently molecularly characterized and, as expected, a subset of them correspond to transcription factors, including the BTB-transcription factor, *Broad*, the pipsqueak-domain transcription factor *E93F*, and the nuclear-receptors *ftz-f1* and *Hr39* (98–101). These primary response transcription factors are one means by which the ecdysone signal is amplified to generated a widespread transcriptional response (98–101).

Differences in the response to ecdysone across time is mediated, in part, through the expression of stage-specific, primary response transcription factors that respond selectively to specific ecdysone pulses (56, 57, 102). The gene, *E93*, for instance, was originally identified as puff that was unresponsive to larval ecdysone pulses and only appeared during

pre-pupal development (56). Expression of E93 during pre-pupal stages in the salivary gland is one means by which the salivary gland responds differently to the larval and pre-pupal ecdysone pulses (100, 101). Many of the primary response transcription factors exhibit similar stage-specificity, which occurs not only at the level of individual genes, but also through changes in isoform expression (88, 99, 102, 103).

The expression of stage-specific primary response transcription factors occurs, in part, through genetic interactions between each other. For instance, *ftz-f1* is a transcription factor that is insensitive to larval ecdysone pulses but is subsequently activated during pre-pupal development. The stage-specificity of *ftz-f1* expression is controlled by the repressor, *Blimp-1*, which prevents it from becoming activated (43, 104). Following pupariation, *Blimp-1* levels drop and permit *ftz-f1* to become activated during the subsequent ecdysone pulse (43, 104). *Ftz-f1* subsequently controls not only its own expression, but also the expression of other primary response genes, including *Broad* and *E74* (98, 105). Both *broad* and *E74*, in turn, regulate overlapping targets with other primary response transcription factors (106, 107).

EcR has also been shown to play a role in mediating different responses across tissues. The genes that mapped to intermolt puffs, which regress upon ecdysone addition, responded to ecdysone even in the presence of protein synthesis inhibitors, indicating that they might be direct targets of EcR (53, 108). These were subsequently molecularly identified as the new glue (*ng*) and glue (*sgs*) genes, which have salivary gland-specific functions (109–111). Consistent with this, ECREs have been identified in the *sgs* genes, as well as other genes with tissue-specific gene expression (69, 112–114). However, EcR's function at the top of the ecdysone transcriptional hierarchy has made it difficult to determine

whether genes are direct targets of EcR, or one of its myriad downstream transcription factors. Consequently, one of the primary focuses of this work has been to elucidate the molecular and epigenetic mechanisms by which tissue- and temporal-specific responses to ecdysone are achieved.

CHAPTER 2: HORMONE-DEPENDENT CONTROL OF DEVELOPMENTAL TIMING THROUGH REGULATION OF CHROMATIN ACCESSIBILITY[1]

Introduction

A defining feature of metazoan development is the organization of cells into tissues. The physiological function of a given tissue is determined by the identity of its constituent cells, as well as by their arrangement within the tissue. As a result, building tissues during development requires precise spatial control of gene expression over extended periods of time. Whereas many of the genes required for the development of different cell and tissue types have been identified, the mechanisms through which spatial information is coordinated with temporal information remain incompletely understood.

Spatially, a select and conserved group of transcription factors, sometimes termed "master" transcription factors, often specify the distinct identities of different cell and tissue types (115, 116). Genetic studies from a range of organisms show that loss of function of a given master transcription factor can result in the loss of a given cell type or tissue. Conversely, ectopic expression of a given master transcription factor can result in transformation of identities. Hence, master transcription factors are major determinants of cell fate. Consistent with their importance in development, the dysregulation of master transcription factors is associated with a range of diseases. Thus, understanding of the

[1] This chapter originally appears as an article in Genes and Development. The original citation is as follows: C. M. Uyehara, *et al.*, Hormone-dependent control of developmental timing through regulation of chromatin accessibility. *Genes Dev.* (2017) https:/doi.org/10.1101/gad.298182.117 (May 30, 2017).

mechanisms through which these factors function is an important goal in biomedical research.

One proposed mechanism to explain the distinctive power of master transcription factors is that they control where other transcription factors bind in the genome by regulating chromatin accessibility (116–118). *In vivo*, DNA is wrapped around histone proteins to make nucleosomes, the basic unit of chromatin. Due to their tight association with DNA, nucleosomes act as barriers to transcription factor binding. For a given transcription factor to bind DNA, a nucleosome must be moved or evicted, creating a site of "open" or "accessible" chromatin. Several lines of evidence support an important role for chromatin accessibility in transcription factor targeting in the genome. Chief amongst these are the observations that only a small fraction of transcription factor DNA binding motifs is occupied at a given point in time, and that many sites of transcription factor binding do not contain a recognizable DNA binding motif (119, 120). Thus, regulation of chromatin accessibility plays a potentially pivotal role in controlling cell identity by determining where transcription factors can bind in the genome, and hence the sets of genes that are expressed.

If nucleosomes prevent transcription factors from accessing DNA, how then do transcription factors come to occupy their binding sites? Biochemical studies have identified a class of transcription factor termed "pioneer" factors that have the unique ability to bind nucleosomal DNA, and to subsequently enable binding by other transcription factors (27). The prototype pioneer factor is FoxA1, a master regulator of liver development (121). FoxA1 has also been shown to play an important role in controlling targeting of the estrogen and androgen receptors in breast and prostate cancer cells, respectively (25). More recently, the master transcription factors of embryonic stem cell identity, Oct4, Sox2, and Klf4, were

shown to have pioneering activity during induction of pluripotency in iPS cells (21). While pioneers have the potential to be pivotal regulators of gene expression programs, much remains to be learned about their function. For example, it is not clear why they exhibit pioneering activity only in a subset of the cells in which they are expressed. Pioneers may also not be the only factors that control chromatin accessibility. Other transcription factors can work together to compete nucleosomes off DNA, consistent with earlier *in vitro* work on transcription factor binding to nucleosomal templates (122).

In addition to spatial control, gene expression patterns are also temporally regulated in development. For example, in a variety of animals, neural stem cells produce daughter cells with distinct identities at different times of development to create the vast diversity of neurons and glia found in the nervous system (123). In *Drosophila* embryos, an intrinsic cascade of transcription factor expression specifies the distinct temporal identities of neural stem cell progeny (124). A similar mechanism, using a different transcription factor cascade, diversifies neural identities in the *Drosophila* larval brain (125). In contrast to stem cell lineages, coordinating the timing of gene expression across fields of cells, such as a tissue, often involves the use of secreted signals. For example, thyroid hormone controls the initiation and progression of metamorphosis in frogs, whereas the sex hormones control the development of secondary sex traits during adolescence in mammals (126, 127).

In *Drosophila* and other insects, developmental timing is controlled by the steroid hormone ecdysone (52, 128). Secreted by the prothoracic gland at stereotypical stages of development, ecdysone travels through the hemolymph to reach target tissues, where it binds to its receptor, the Ecdysone Receptor (EcR) (129). Like other nuclear hormone receptors, EcR is a transcription factor that differentially regulates gene expression in the presence and

absence of ligand. Studies initially performed in the larval salivary gland revealed that upon binding ecdysone, EcR activates transcription of a set of early genes, many of which are transcription factors (52). The early gene products then work with EcR to activate a set of late genes, which encode the proteins that mediate the physiological response to hormone signaling (e.g., the glue proteins made by the salivary gland that adhere the pupa to a substrate during metamorphosis). Transcriptional profiling from a diverse collection of cell lines showed that the response to ecdysone is both widespread and highly cell type specific (86). Mapping of hormone-responsive enhancers in cultured cells recently revealed that tissue-specific responses to ecdysone are influenced by motif content in DNA regulatory elements (130). Despite these efforts, the precise mechanisms through which ecdysone signaling controls temporal specific gene expression in *Drosophila* remain elusive.

To ask how spatial and temporal information are integrated by regulatory DNA during specification of tissue identities, we recently performed open chromatin profiling at two stages of *Drosophila* appendage development (131). In flies, the distinct identity of each appendage is determined by the expression of different master transcription factors with different DNA binding domains. For example, leg identity is determined by the homeodomain transcription factor *Distal-less* and the zinc finger transcription factor *Sp1* (132). By contrast, dorsal appendage identities, including the wing and haltere, are specified by *vestigial* and its TEA-domain containing DNA binding partner, *scalloped* (133). Despite the differences in master transcription factor identities between these tissues, and contrary to our expectations, we found that the open chromatin profiles in wings, legs, and halteres are nearly the same, with the exception of the master regulator loci themselves, which exhibit differential accessibility between the appendages (131). The similarity in appendage open

chromatin profiles indicates that the master transcription factors are not the sole determinants of chromatin accessibility, if they do so at all. This leaves the question: which factors are responsible for controlling chromatin accessibility in the appendages?

One clue to the potential identity of these factors came from comparisons of open chromatin profiles between appendages at different stages of development. We found that the different adult appendages shared very similar open chromatin profiles, similar to our findings from an earlier stage of appendage development, the third instar imaginal discs. However, open chromatin profiles of the adult appendages were markedly different from those of the imaginal discs. This indicates that a coordinate change in chromatin accessibility occurs during appendage development, and it also suggests that passage through developmental time has a greater impact on chromatin accessibility than does cell lineage. Because the appendages are not in physical contact with each other inside the developing fly, we reasoned that a systemic signal, such as ecdysone, contributes to control of chromatin accessibility.

Here, we examine the mechanisms controlling temporal gene regulation in *Drosophila*. Using a time course of wing development that encompasses the transition between larval and pupal stages, we used RNA-seq to show that gene expression is temporally dynamic as wings differentiate and undergo the complex morphogenetic events that create the adult appendage. We then carried out open chromatin profiling and transgenic reporter analysis to show that these changes in gene expression are accompanied by genome-wide changes in the accessibility of temporal specific transcriptional enhancers. Finally, we used ChIP-seq and loss of function analyses to show that the ecdysone-induced transcription factor E93 is required to drive the normal sequence of chromatin accessibility changes.

Importantly, E93 is required not only for increasing accessibility of late-acting enhancers, but also for decreasing accessibility of early-acting enhancers. Together, these findings demonstrate that E93 specifies temporal identity by directly regulating accessibility of temporal specific transcriptional enhancers. More broadly, this work helps to explain how hormone signaling can influence tissue specific gene expression programs to drive development forward in time.

Materials and methods

Drosophila culture and genetics

Flies were grown at 25C under standard culture conditions. The genotype of the wildtype strain was *w*^{1118}*/yw, hs-FLP*. Late wandering third instar larvae were used for the L3 stage. White prepupae were used as the 0-hour time point for pupal staging. The following genotypes were also used: *UAS-E93 RNAi* (VDRC#104390), *E93 protein trap* (DGDP, BDSC#43675), *UAS-nls::GFP* (chromosome II, BDSC#4775), *UAS-nls::GFP* (chromosome 3, BDSC#4776), *E93*^{4} (gift of Craig Woodard), *Df(3R)93F*^{x2} (gift of Eric Baehrecke), *UAS-destabilized::GFP* (gift of Brian McCabe).

Sample preparation for High Throughput Sequencing

A minimum of 40 wings were dissected from staged female flies in 1x PBS and transferred to ice for subsequent processing. RNA was prepared as previously described and the KAPA stranded mRNA-seq kit was used for library construction (134). FAIRE-seq was performed as previously described, and the Rubicon Thruplex DNA-seq kit was used for library construction. ChIP-seq was performed on 24hr +/- 1hr manually-dissected wings (n=717 Rep1, n=1,280 Rep2) from both male and female E93 protein trap flies (131). Wings were dissected in 1x PBS and kept on ice. Batches of wings from 20 pupae were fixed in 4% paraformaldehyde, 50mM HEPES, 100mM NaCl, 1mM EDTA, 0.5mM EGTA for 20-minutes at room temperature, followed by quenching with 125mM glycine in 1x PBS, 0.01% Triton. Fixed wings were Dounce homogenized in 10mM HEPES, 10mM EDTA, 0.5mM EGTA, 0.25% Triton, 1mM PMSF. Nuclei were pelleted at 4,500xg for 20-minutes, and re-suspended in 10mM HEPES, 200mM NaCl, 1mM EDTA, 0.5mM EGTA, 0.01% Triton,

1mM PMSF. After nutating at 4C for 10-minutes, nuclei were pelleted again and re-suspended in 140mM NaCl, 10mM HEPES, 1mM EDTA, 0.5mM EGTA, 1mM PMSF, 0.1% SDS, followed by sonication on ice with a Branson Sonifier until average chromatin fragment size was 200bp. The soluble chromatin fraction was used for ChIP. Briefly, extracts were pre-cleared with protein-A dynabeads for 2 hours at 4C, and cleared extracts were incubated with 5µg of rabbit anti-GFP antibody (Abcam cat# ab290) overnight at 4C. Bead pulldown was performed for 3-hours the following day. Antibody-bead complexes were washed successively, and then eluted with 1% SDS, 250mM NaCl, 10mM Tris, 1mM EDTA. Samples were treated with RNase A and proteinase K, heated overnight at 65C to reverse crosslinks, and purified DNA was recovered by phenol-chloroform/ethanol precipitation. Rubicon Thruplex DNA-seq kit was used for library construction. All samples were sequenced on an Illumina HiSeq 2500 at the UNC High Throughput Sequencing Facility. Additional details are available upon request.

Sequencing data analysis

Sequencing reads were aligned to the dm3 reference genome. RNA-seq analysis was performed as previously described (134). We defined differentially expressed genes as those having a log CPM greater than 2 in at least one sample and changing by at least 2-fold between pairwise time points. Gene Ontology analysis was performed using DAVID and REViGO (135, 136). FAIRE-seq analysis and peak calling were performed as previously described (24, 131). FAIRE-seq and ChIP-seq data were visualized using IGV (137). Z scores were calculated using the mean and standard deviation per chromosome arm. To focus on a high-confidence set of peaks, we chose a MACS2 $-\log_{10}$ adjusted p value of 40 from the

44hr wild type dataset and selected an equivalent number of peaks (n=7,699) from the remaining datasets. EdgeR was used for differential peak calling, as described previously (24, 138). Briefly, BedTools was used to calculate read depth for each set of peaks (139). FAIRE peaks with an FDR less than 0.05 that changed greater than 2-fold were defined as differentially accessible. We defined E93-dependent peaks as those called as differentially accessible (open or closed) in E93 mutant wings relative to wild type. Heatmaps were generated using Deeptools v2.4.0 (140). Average signal line plots were generated from z-normalized data using the Bioconductor packages rtracklayer v1.32.2, GenomicRanges v1.24.3, and Genomation v1.4.2 along with custom R scripts (available upon request) (141–143). DNA binding motifs used for enrichment analysis were obtained from Fly Factor Survey, and enrichment was measured using the AME tool in MEME by comparing temporally dynamic peaks in each category to static peaks (defined as those changing less than 1.3-fold between consecutive time points) (67, 144, 145). Only motifs with an adjusted p value less than 0.05 were plotted, and only the lowest p value was reported for each transcription factor to remove redundancy. Data are available from GEO under the accession number GSE97956.

Transgenic reporter analysis and immunofluorescence

Candidate enhancers were cloned from wild type *y; cn, bw, sp* genomic DNA based solely on open chromatin data. Gateway (Invitrogen) cloning was used to move candidate enhancers into destination vectors. Injections were performed at BestGene (Chino Hills, CA). The br^{disc} and br^{ade} enhancers were cloned into the pϕUGG GAL-4 destination vector, and integrated into the *attP40* site on chromosome 2; this vector was chosen to allow for different

reporters to be driven by GAL4 (e.g. UAS-destabilized GFP) (146). The *nub*^{vein} and *nub*^{margin} enhancers were cloned into a modified pDEST-HemmarG vector, in which the CD4 transmembrane domain was replaced with an SV40 nuclear-localization signal (PKKKRKV) (147). The *tnc*^{wv} and *tnc*^{blade} enhancers were cloned into a modified pDEST-HemmarR vector, in which the CD4 transmembrane domain was replaced with the SV40 nuclear localization signal; this dsRed vector was chosen to allow for combining the *tnc* reporters with existing GFP-marked GAL4 drivers (147). Each *nub* and *tnc* enhancer were integrated into the *attP2* site on chromosome 3. Integration of each reporter into their respective *attP* sites was confirmed by PCR. Immunostaining and confocal imaging were performed as previously described (131). The following antibodies were used: rabbit anti-GFP (Abcam ab290) 1:1000; mouse anti-phosphoTyrosine (Fisher Scientific, clone 4G10) 1:1000; rabbit anti-E93 (this study) 1:2500. Polyclonal antibodies to E93 were raised in rabbits using amino acid sequences 271–520 of the E93-PA isoform, which is present in all annotated E93 isoforms. In some cases, 30hr wings were used in figure images due to their ease of mounting relative to 24hr wings. In all cases, reporter analysis was also conducted at 24hr, and no significant differences in reporter pattern were observed between 24hr and 30hr. All primers and vectors are available upon request.

Results

Gene expression is temporally dynamic in pupal wings

To examine the mechanisms underlying temporal regulation of gene expression, we focused on the early stages of *Drosophila* pupal wing development. By the end of larval development (Figure 2.1A), the wing disc consists of approximately 50,000 cells, cell fates along the proximal-distal axis have been patterned, and precursors of adult structures such as wing veins and sensory organs are being specified (148). During the next two days of pupal development (Figure 2.1B-C), cell fates continue to be more finely determined while the wing undergoes a final round of cell division (134). This time is also characterized by dramatic morphological changes at both the tissue and cellular levels: changes in cell shape drive eversion of the wing pouch, and changes in cell adhesion allow for the apposed dorsal and ventral surfaces of the wing epithelium to form the upper and lower layers of the wing blade. Cytoskeletal changes also result in extrusion of the cell membrane to produce a single cuticular hair (trichome) from each wing blade epithelial cell (149) (Figure 2.1C**”**). Not surprisingly, these developmental changes are associated with widespread changes in gene expression. To quantify these changes, we performed RNA-seq on wing discs dissected from wandering third instar larvae (Figure 2.1A, “L3”), and wings dissected from flies 24-hours (Figure 2.1B, “24hr”) and 44-hours (Figure 2.1C, “44hr”) after puparium formation (134). Pairwise comparisons between successive time points revealed thousands of genes both increasing and decreasing between each time point (Figure 2.1D, EdgeR FDR < 0.05, fold-change greater than or equal to 2-fold for expressed genes, Table 2.S1). Gene ontology analysis showed enrichment for biological processes known to occur at these times (135, 136). For example, genes increasing between L3 and 24hr include those involved in cell

adhesion (p value $2.4x10^{-5}$), whereas genes increasing between 24hr and 44hr include those involved in actin regulation (p value $6.8x10^{-4}$). Conversely, genes decreasing between L3 and 24hr include those involved in DNA replication (p value $1.7x10^{-34}$), whereas genes decreasing between 24hr and 44hr include those involved in mitosis (p value $3.9x10^{-10}$) (Figure 2.1D, Figure 2.S1). Thus, the first two days of pupal wing development are marked by temporally dynamic changes in gene expression.

Open chromatin profiles are temporally dynamic in pupal wings

We next sought to examine the mechanisms underlying the temporal changes in gene expression that we observed in pupal wings. Due to the competition between transcription factors and nucleosomes for DNA binding, methods that identify nucleosome-depleted regions, also known as open chromatin sites, can be used as a proxy to identify sites of transcription factor binding in the genome. To map open chromatin sites genome wide, we performed FAIRE-seq on L3, 24hr, and 44hr wings (Figure 2.2) (150). We find that open chromatin profiles in early pupal wings are highly dynamic between time points, with changes in open chromatin occurring at genes that change expression between time points (Figure 2.S2B). For example, the *tenectin* gene (*tnc*), which encodes a constituent of the extracellular matrix that binds alpha-PS2 integrin, exhibits multiple open chromatin changes between L3, 24hr, and 44hr wings (Figure 2.2A) (151). These changes coincide with a strong increase in *tnc* expression between L3 and 24hr wings (Figure 2.2A). Similarly, the *expansion* locus, which encodes a protein involved in chitin biosynthesis, contains multiple open chromatin sites that become accessible specifically between 24hr and 44hr (152). The timing of this chromatin opening coincides with an increase in *expansion* RNA levels (Figure

Figure 2.1. Gene expression is temporally dynamic in pupal wings.

(A – C) Immunostaining of wings from three developmental time points. DAPI (top row) and phospho-tyrosine (bottom row) label nuclei and cell membranes, respectively. (D) MA plots of RNA-seq signal in annotated genes for consecutive time points. Differentially expressed genes are colored red. The top two GO terms for differentially expressed genes are indicated with p values in parentheses. Scale bars indicate 50μm.

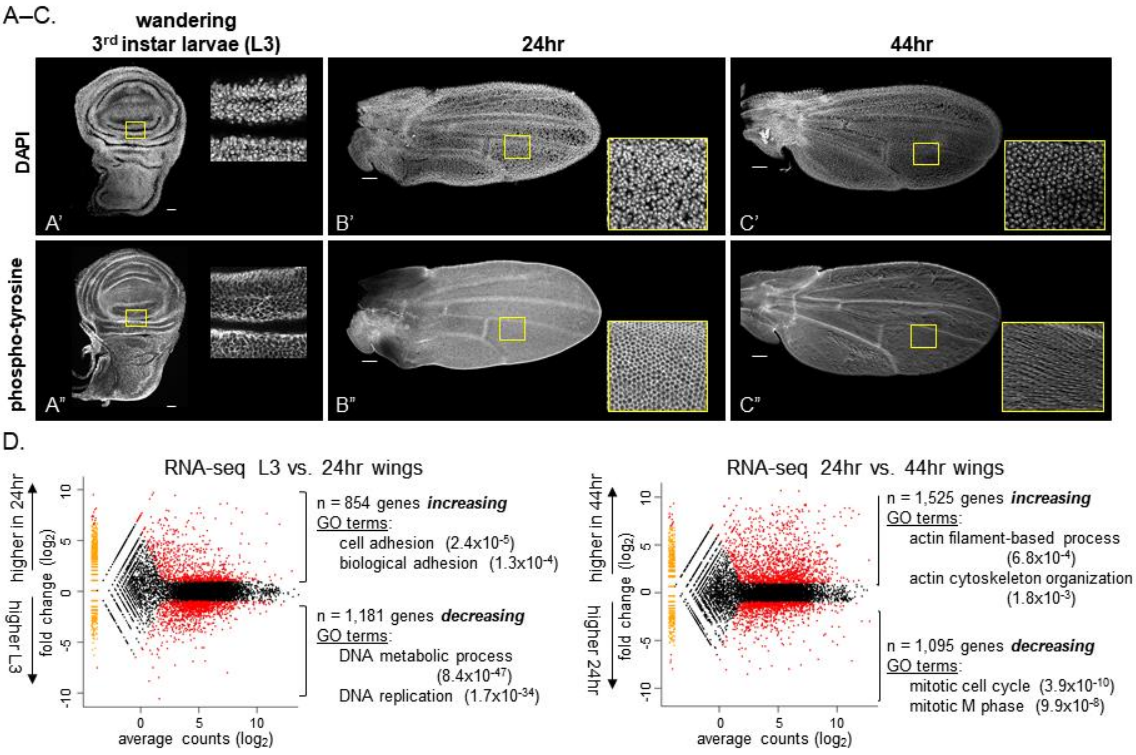
A–C.
wandering
3rd instar larvae (L3)
24hr
44hr
DAPI
phospho-tyrosine
A'
B'
C'
A"
B"
C"
D.
RNA-seq L3 vs. 24hr wings
higher in 24hr
higher L3
fold change (log2)
average counts (log2)
n = 854 genes increasing
GO terms:
cell adhesion (2.4x10-5)
biological adhesion (1.3x10-4)
n = 1,181 genes decreasing
GO terms:
DNA metabolic process (8.4x10-47)
DNA replication (1.7x10-34)
RNA-seq 24hr vs. 44hr wings
higher in 44hr
higher 24hr
n = 1,525 genes increasing
GO terms:
actin filament-based process (6.8x10-4)
actin cytoskeleton organization (1.8x10-3)
n = 1,095 genes decreasing
GO terms:
mitotic cell cycle (3.9x10-10)
mitotic M phase (9.9x10-8)

Figure 2.2. Open chromatin profiles are temporally dynamic in pupal wings.

(A) Browser shots of FAIRE-seq signal (z score) at the *tenectin* and *expansion* loci. Temporally dynamic open chromatin sites are highlighted with gray shading. Bar plots show the RNA-seq signal for each gene over time. (B) Heat map of the Pearson correlation coefficients between FAIRE-seq replicates. The number of differentially accessible FAIRE peaks out of the top 7,699 peaks for each consecutive time point is shown. (C) Line plots of the average FAIRE-seq signal across all categories of differentially accessible FAIRE peaks. The L3 signal is shown in blue, 24hr in red, and 44hr in orange.

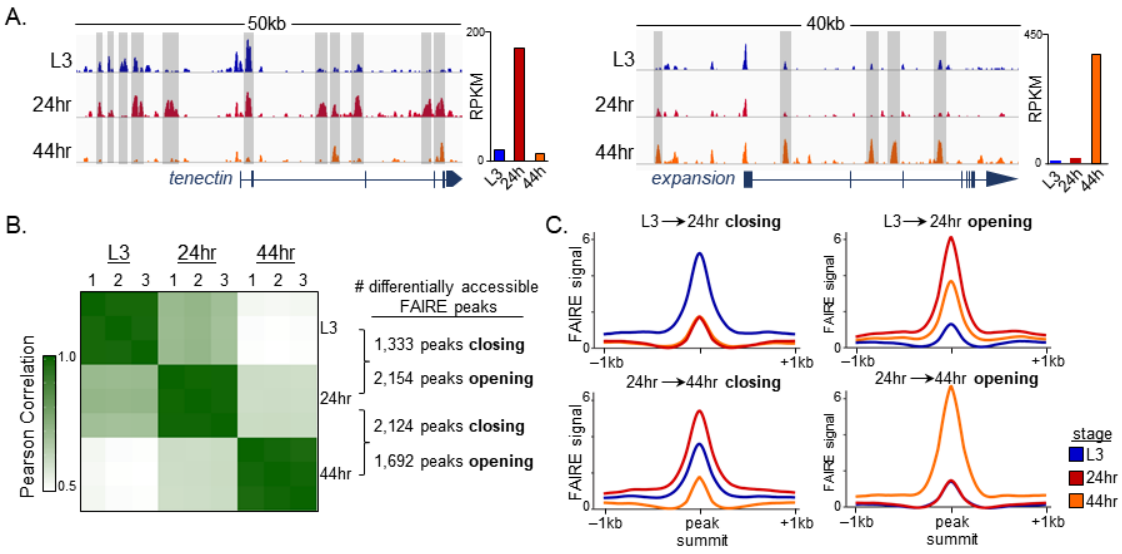

Figure 2.S1. Gene ontology analysis of pupal wing RNA-seq data.

Bar plots of the p value for GO term enrichment (Biological Process) for differentially expressed genes between consecutive time points.

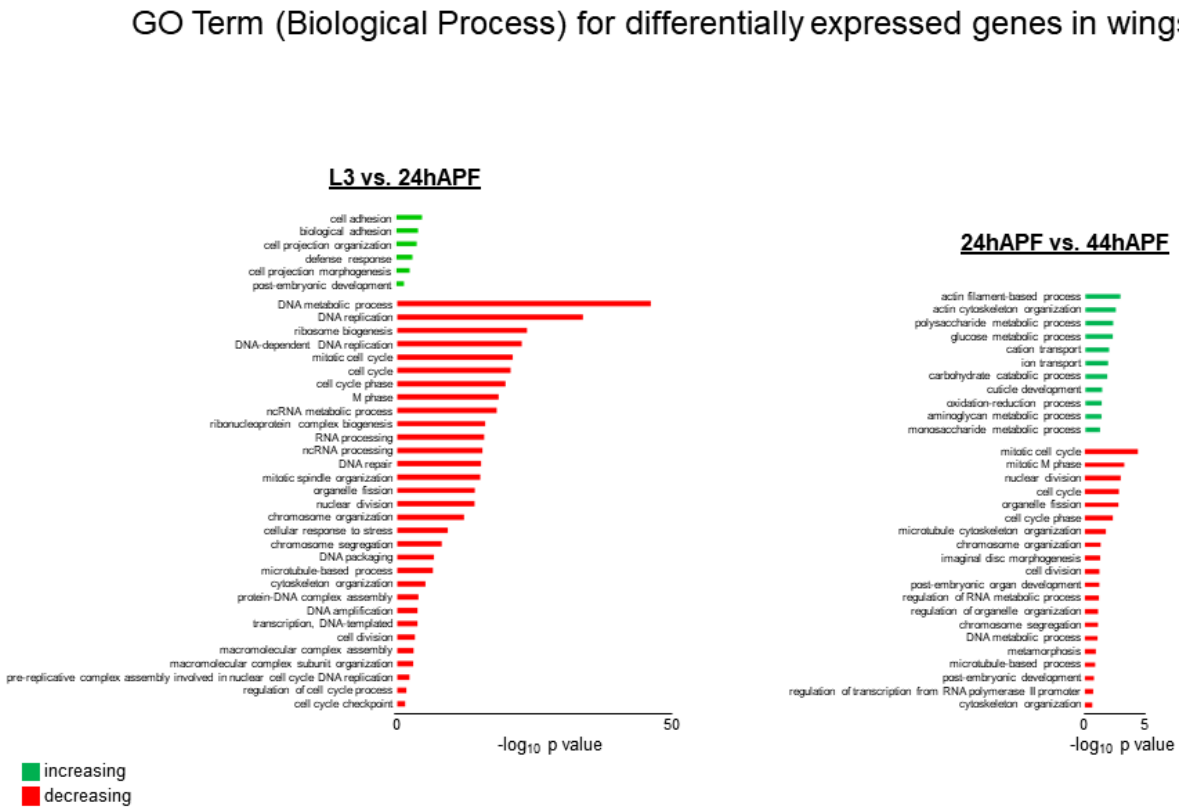

2.2A), and the production of chitin by wing epidermal cells during cuticle secretion at this stage of development (152). At the genome-wide level, we find that approximately one-third of open chromatin sites are temporally dynamic (Figure 2.2B, Figure 2.S2C). Out of the top 7,699 FAIRE peaks from each time point (corresponding to a MACS2 Q-value of 40), 2,154 sites increase, and 1,333 sites decrease in accessibility between L3 and 24hr wings (Figure 2.2B, EdgeR FDR < 0.05, fold change greater than or equal to 2-fold). Similarly, 1,692 peaks increase, and 2,124 peaks decrease in accessibility between 24hr and 44hr wings (Figure 2.2B, Figure 2.S2D). We henceforth refer to sites that decrease in accessibility between successive time points as "closing", and sites that increase in accessibility between successive time points as "opening". We find that the great majority of these temporally dynamic open chromatin sites (78% – 89%) are located distal to gene promoters (Figure 2.S2E). Finally, plots of the average FAIRE signal in temporally dynamic open chromatin indicate that many temporally dynamic open chromatin sites are used transiently in development. For example, sites closing between L3 and 24hr tend to stay closed, and sites opening between 24hr and 44hr tend to be closed at L3 (i.e., prior to 24hr) (Figure 2.2C). Thus, the dynamic gene expression exhibited by early pupal wings coincides with dynamic changes in chromatin accessibility.

Temporally dynamic open chromatin sites correspond to temporal specific transcriptional enhancers

Open chromatin sites are highly correlated with functional DNA regulatory element activity (131). Our findings above suggest that temporally dynamic open chromatin sites may be transiently-used, promoter-distal enhancers in pupal wings. To test this directly, we cloned

open chromatin sites from three genes for use in transgenic reporter assays. These sites were chosen because they exhibit temporally dynamic accessibility, and the neighboring genes are required for proper wing development. Candidate enhancers were cloned into reporter constructs and integrated into the genome as single copies via phiC31-mediated site-specific recombination. Altogether, we cloned six temporally dynamic open chromatin sites. Each of these six sites corresponds to a temporally regulated transcriptional enhancer. We discuss them in turn.

We first examined two candidate enhancers from the *tnc* locus. As mentioned above, *tnc* encodes an extracellular matrix protein involved in cell adhesion. Consistent with a role for *tnc* in mediating adhesion between the dorsal and ventral surfaces of the wing pouch, RNAi-mediated knockdown of tnc results in defects in wing morphology (151). We cloned two temporally dynamic open chromatin sites located approximately 40kb upstream of the *tnc* promoter. Our FAIRE-seq data show that these sites increase in accessibility between the L3 and 24hr time points, and subsequently decrease in accessibility between 24hr and 44hr (Figure 2.3A, Figures S3A, S4A). While neither reporter is active in L3 wing discs, there is activity in 24hr wings. We have termed these the tnc^{blade} (blade) and tnc^{wv} (wing vein) enhancers. Tnc^{blade} is active most strongly in the interveins between the first and second, and the fourth and fifth longitudinal veins, and in cells near the proximal posterior margin. It is also active at lower levels in the intervein between the third and fourth longitudinal veins (Figure 2.3A). Tnc^{wv} is active most strongly near the first, fifth and sixth longitudinal veins, and at lower levels in the third longitudinal vein (Figure 2.S4A). Thus, tnc^{blade} and tnc^{wv} are active in complementary domains of the 24hr pupal wing. Since *tnc* is expressed nearly

ubiquitously at this stage of wing development, these open chromatin sites likely correspond to *bona fide* transcriptional enhancers that interpret different spatial inputs.

We next examined two candidate enhancers from the *nubbin* (*nub*) locus, which encodes a transcription factor required for proximal-distal axis and vein development in wings (153). The cloned candidate enhancers are located approximately 5kb and 6.5kb upstream of the *nub* promoter. Our FAIRE-seq data show that these sites progressively increase in accessibility between the L3 and 44hr time points (Figure 2.3B, Figures 2.S3B, 2.S4B). Immunofluorescence experiments show that a reporter carrying the distal site is not active in L3 wing discs. By 44hr, it shows strong activity in the L3 and L5 wing veins, and weaker activity in the L2 and L4 veins (Figure 2.3B). We have thus designated this as the nub^{vein} enhancer. Consistent with the nub^{vein} activity pattern, hypomorphic *nub* alleles show defects in wing vein development (153). Immunostaining of the more proximal site, which we have named nub^{margin}, shows reporter activity near the wing margin and near the posterior crossvein of 44hr wings (Figure 2.S4B), again consistent with defects observed in *nub* hypomorphic alleles (153). Thus, temporally dynamic open chromatin sites identify functionally relevant enhancers with temporal specific activity.

Lastly, we examined two candidate enhancers from the *broad* (*br*) locus, which encodes a family of transcription factors active in third instar and early prepupal tissues, including the wing (107, 134). Using our FAIRE-seq data, we identified open chromatin sites at the *br* locus that are accessible in L3 wing discs, but which subsequently decrease in accessibility by 24hr and 44hr (Figure 2.3C, Figures 2.S3C, 2.S4C). These candidate enhancers were cloned upstream of GAL4 to allow for flexibility in the reporters used. Crossing these GAL4 drivers to flies containing UAS-GFP revealed that both open chromatin

sites are transcriptional enhancers active in L3 wing discs. The br^{disc} enhancer is located approximately 40kb upstream of the *br* promoter. Similar to Br protein, br^{disc} is active nearly ubiquitously in wing imaginal disc epithelial cells, with higher levels along the anterior-posterior and dorsal-ventral boundaries in the wing pouch (Figure 2.3C). We next sought to determine whether the decrease in accessibility of br^{disc} between L3 and 24hr coincides with a decrease in enhancer activity. Since there are a limited number of cell divisions in pupal wings, GFP signal can persist even after an enhancer turns off. Therefore, we used a destabilized GFP reporter, reasoning that increased GFP degradation may make the reporter more sensitive to the enhancer's activity state, even if GAL4 persists. Consistent with the timing of br^{disc} closing, we found that it shuts off between L3 and 24hr (Figure 2.3C). Thus, the timing of br^{disc} closing coincides with the timing of it turning off. We identified a second *br* enhancer, which we have termed br^{ade} (Figure 2.S4C). This enhancer is located approximately 30kb upstream of the *br* promoter, and it is active in L3 wing discs in a pattern similar to the adepithelial cells located in the notum of the wing. Like the br^{disc} enhancer, there is no sign of br^{ade} reporter activity in the wing blade by 24hr, consistent with expectations since the adepithelial cells remain in the notum to form the indirect flight muscles. Notably, Br is required for proper differentiation of these cells into adult muscles (154). Together, these findings support the premise that temporally dynamic open chromatin sites correspond to temporal specific transcriptional enhancers, and that genes utilize different DNA regulatory elements to control their expression at different stages of development.

Figure 2.3. Temporally dynamic open chromatin corresponds to temporal specific enhancer activity.

(top row) Browser shots of FAIRE-seq signal from the (A) *tenectin*, (B) *nubbin*, and (C) *broad* loci, with cloned regions indicated by grey boxes, and depicted enhancers indicated by green boxes. (middle and bottom rows) Immunostaining of reporter activity in wings at the indicated early and late time points. Enhancer activity in green. Scale bars indicate 50μm. Additional time points shown in Supplemental Figure S3.

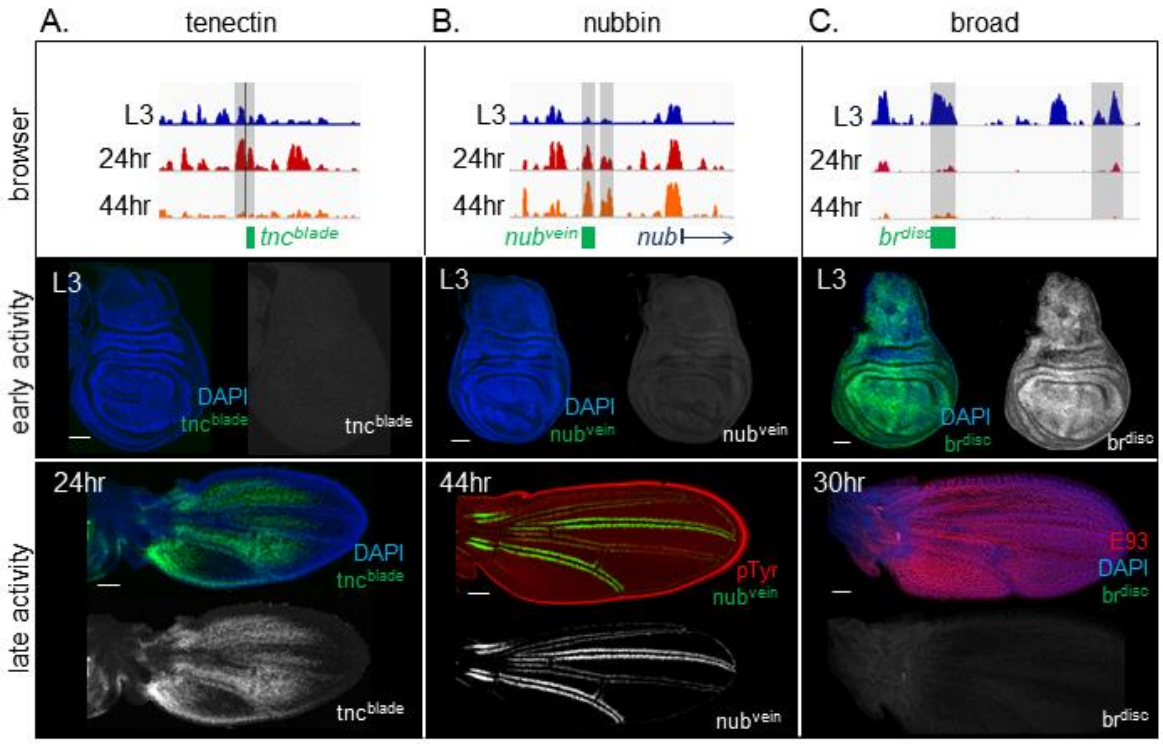

Figure 2.S2. FAIRE-seq profiles show temporally dynamic open chromatin in pupal wings.

(A) Stacked bar plots showing overlap between gene promoters and FAIRE peaks at fixed distances away. Genes that increase in expression are more likely to overlap a nearby FAIRE peak that is opening between the time intervals. Conversely, genes that decrease in expression are more likely to overlap a nearby FAIRE peak that is closing between 24hr to 44hr. However, genes that decrease in expression between L3 and 24hr are not more likely to overlap a nearby FAIRE peak that is closing. It is not clear why this happens. (B) MA plots showing FAIRE-seq signal in the union set of FAIRE peaks for consecutive time points in wing development. Differentially accessible peaks are colored red (EdgeR FDR < 0.05, fold change > 2). (C) Stacked bar plots showing the fraction of FAIRE peaks that change between consecutive time points. (D) Pie charts showing the overlap of dynamic FAIRE peaks with proximal promoter sequences (+/- 500bp transcription start sites) for each category of dynamic FAIRE peak.

Open chromatin profiles are temporally dynamic in pupal wings

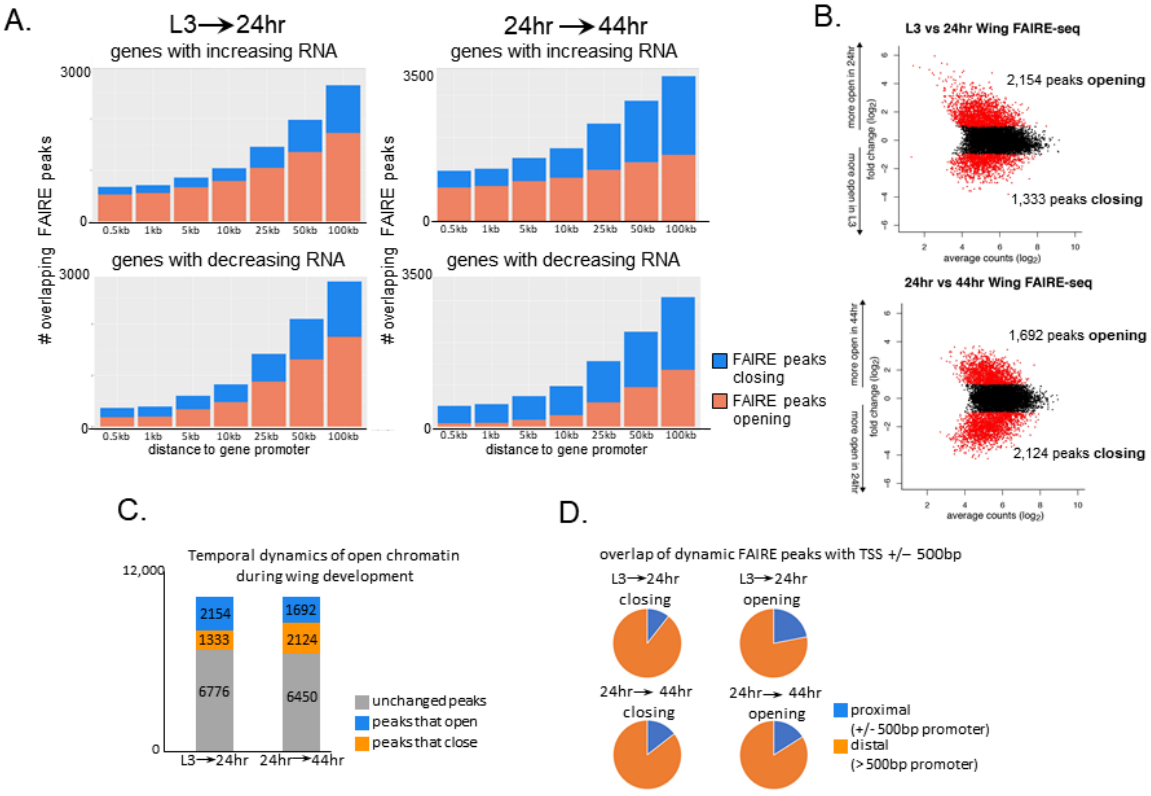

Figure 2.S3. Additional time points for the enhancers depicted in Figure 2.3.

(top row) Browser shots of FAIRE-seq signal from the *tnc* (A), *nub* (B), and *br* (C) loci. (remaining rows) Confocal images of wings at time points approximately coinciding with the FAIRE-seq time course. Persistent tnc^{blade} reporter activity at 44hr (A) is likely a consequence of perdurance of tdTomato protein (green), since there are no cell divisions between 24hr and 44hr in pupal wings.

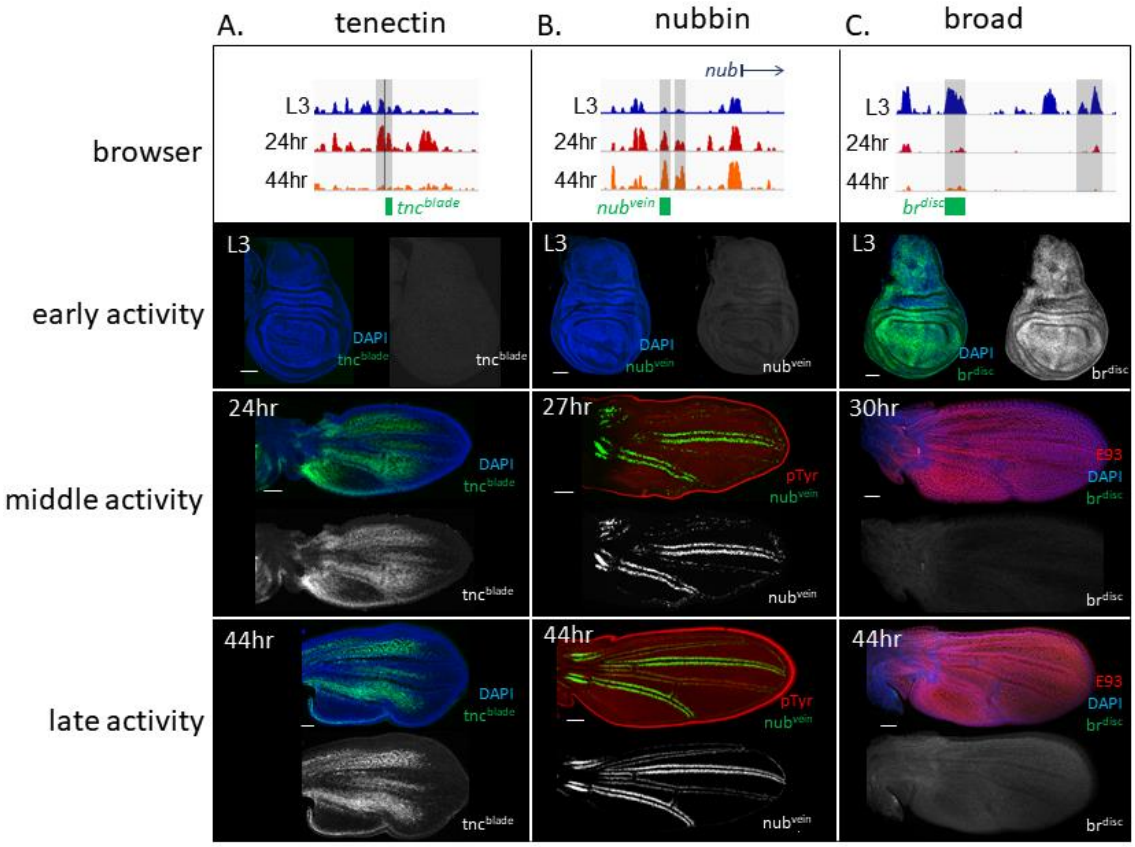

Figure 2.S4. Additional examples of temporally dynamic open chromatin sites corresponding to temporal specific enhancers.

(top row) Browser shots of FAIRE-seq signal from the *tnc* (A), *nub* (B), and *br* (C) loci. (remaining rows) Confocal images of wings at early and late time points for the indicated enhancers. The absence of br^{ade} reporter activity in 30hr wings (C) may be due to the absence of adepithelial cells in the wing blade at this stage of development.

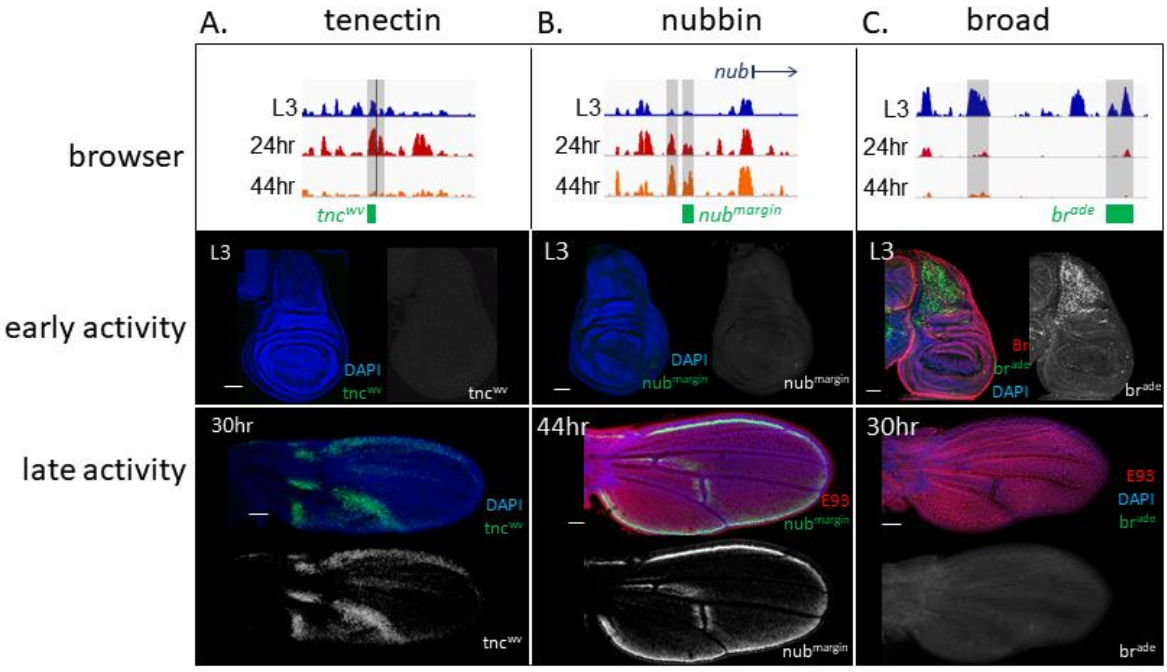

A temporal cascade of ecdysone-induced transcription factors is expressed in pupal wings

The above findings suggest that temporal changes in gene expression are driven by temporal changes in the accessibility of transcriptional enhancers. We next sought to identify factors that could be involved in controlling the accessibility of these enhancers. We reasoned that ecdysone signaling may be involved since it controls developmental transitions in insects and our previous work suggested an extrinsic signal may coordinate temporal changes in chromatin accessibility between the appendages (92, 129, 131). We performed RNA-seq at six time points in pupal wings (134). Consistent with the Ashburner model of ecdysone signaling (Figure 2.4A) we observe a clear temporal cascade of ecdysone-induced transcription factor expression, such that each time point in early pupal wing development can be defined by a distinct combination of these transcription factors (Figure 2.4B, Table 2.S2) (52). Moreover, the timing of each factors' expression coincides with the timing of its requirement in *Drosophila* development. For example, *br* is required for the transition from larval to prepupal stages, and we find it is expressed specifically at the L3 time point in wings (107). Likewise, *ftz-f1* is required for the transition from prepupal to pupal stages, and we find it is expressed specifically at the 6hr time point in wings (98). Finally, the transcription factor E93 is expressed at the 18hr and 24hr time points, when it is required for bract development in pupal legs (155). Thus, a temporal cascade of ecdysone-induced transcription factors occurs in early pupal wings.

If ecdysone-induced transcription factors control chromatin accessibility, one may expect to find their DNA binding motifs to be over-represented in temporally-dynamic open chromatin sites. To ask this question, we looked for enrichment of known DNA binding

Figure 2.4. A temporal cascade of ecdysone-induced transcription factors in pupal wings.

(A) Diagram of the Ashburner model of ecdysone signaling. (B) Heat map of gene expression values for selected ecdysone-induced genes across six stages of wing development, plotted as a fraction of the maximum expression value. Blue shows high expression, grey shows low expression. (C) Heat maps of DNA binding site motif enrichment in dynamic FAIRE peaks for selected transcription factors. (D) DAPI stain of L3 wing discs (top) and bright field images of 96hr wings (bottom) from wild type (left) and E93 mutants (right). Scale bars: 75μm (top), 500μm (bottom).

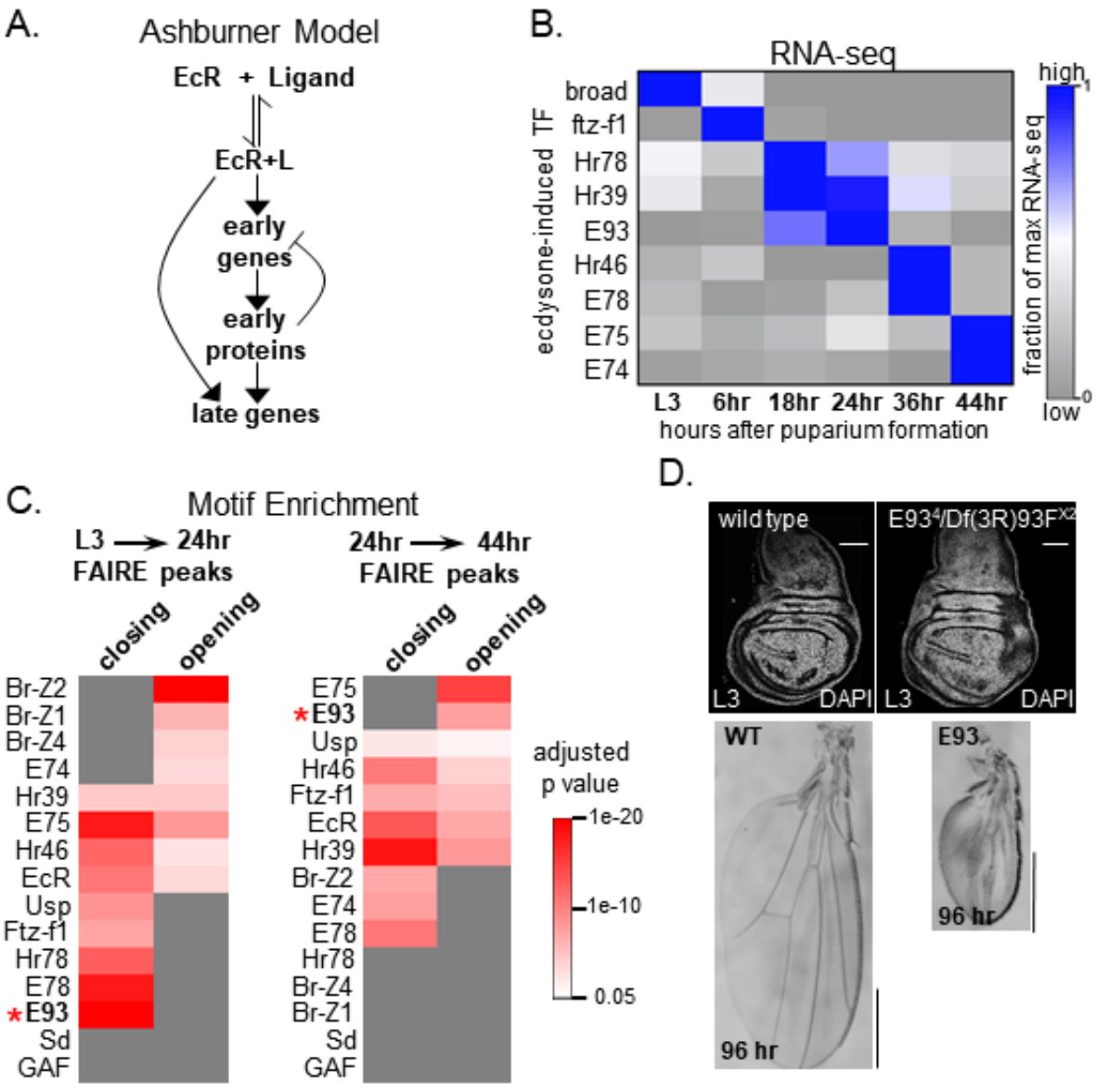
A.
Ashburner Model
EcR + Ligand
EcR+L
early genes
early proteins
late genes
B.
RNA-seq
ecdysone-induced TF
broad
ftz-f1
Hr78
Hr39
E93
Hr46
E78
E75
E74
L3
6hr
18hr
24hr
36hr
44hr
hours after puparium formation
high
fraction of max RNA-seq
low
C.
Motif Enrichment
L3 → 24hr FAIRE peaks
24hr → 44hr FAIRE peaks
closing
opening
Br-Z2
Br-Z1
Br-Z4
E74
Hr39
E75
Hr46
EcR
Usp
Ftz-f1
Hr78
E78
*E93
Sd
GAF
adjusted p value
1e-20
1e-10
0.05
D.
wild type
E93[4]/Df(3R)93F[X2]
L3
DAPI
WT
E93
96 hr

motifs for a set of ecdysone-induced transcription factors (Table 2.S3) in temporally dynamic FAIRE peaks relative to temporally-static FAIRE peaks (67). We observed significant enrichment ($p < 0.05$) for multiple motifs in FAIRE peaks that open or close between successive time points (Figure 2.4C). By contrast, we did not find any enrichment in temporally dynamic peaks for the motif of Scalloped (Sd), the DNA binding partner of the wing master transcription factor Vestigial (133). We also looked for enrichment of the motif for GAGA Factor (GAF), a transcription factor often associated with transcriptional enhancers and open chromatin sites (156). We found the GAF motif was enriched in both dynamic and static FAIRE peaks, suggesting that GAF is not responsible for the temporal dynamics. Together, these findings are consistent with a role for ecdysone-induced transcription factors in regulating temporally dynamic open chromatin sites.

The motif for the ecdysone-induced transcription factor E93 was strongly over-represented in open chromatin sites that close between L3 and 24hr, as well as those that open between 24hr and 44hr (Figure 2.4C). We therefore sought to determine if E93 plays a role in wing development. E93 encodes a pipsqueak domain-containing transcription factor that was first identified as an ecdysone target required for autophagy of the larval salivary gland (100, 101). More recently, E93 was shown to act as a competence factor for temporal specific gene regulation in the pupal leg (155). Our RNA-seq data show that E93 is transcribed at high levels in pupal wings at the 18hr and 24hr time points (Figure 24B). To ask if E93 is required for normal wing development, we compared the morphology of wild type and E93 mutant wings. At the L3 stage, wild type and E93 mutant wings are indistinguishable (Figure 2.4D), consistent with expectations since E93 is not expressed at this time. At 24hr, when E93 is expressed at high levels, E93 mutant wings display defects in

cell adhesion between the dorsal and ventral surfaces of the wing epithelium (not shown). Later at 96hr, following the period of E93 expression, E93 mutant wings are dramatically smaller than wild type wings, with significant defects in vein development (Figure 2.4D). Thus, E93 is essential for proper wing development, and the appearance of defects in E93 mutants is commensurate with the timing of its expression in pupal wings.

ChIP-seq reveals that E93 binds open chromatin sites in pupal wings

The above findings reveal that the temporal changes in gene expression that occur during pupal wing development coincide with temporal changes in the accessibility of thousands of open chromatin sites, many of which could be transcriptional enhancers. We next sought to examine the role of E93 in this process. As a first step, we performed ChIP-seq to identify sites in the genome to which E93 binds. We utilized an E93 protein-trap fly strain generated by the *Drosophila* Gene Disruption Project (157). In this strain, the endogenous *E93* gene has a transposon inserted within an intron that is shared by all annotated E93 isoforms. The transposon carries an "artificial exon" cassette with the coding sequence for GFP and other epitope tags in the same reading frame as E93, flanked by splice acceptor and donor sites. Upon transcription and translation, an E93 fusion protein is expressed (hereafter, $E93^{GFSTF}$) that can be immuno-precipitated with antibodies to GFP. Importantly, the $E93^{GFSTF}$ chromosome complements a deletion encompassing the *E93* locus ($Df(3R)93F^{X2}$), demonstrating that the fusion protein is functional. Supporting this functionality, immunostaining of $E93^{GFSTF}$ flies shows clear fusion protein expression in 24hr and 44hr wings (Figure 2.S5).

We performed ChIP-seq for E93 on dissected 24hr pupal wings (Figure 2.5A). Peak calling with MACS2 identified 8,477 significantly bound sites genome-wide. *De novo* motif discovery analysis identified a sequence enriched in E93 ChIP peaks that is very similar to an E93 motif derived from a bacterial one-hybrid screen for *Drosophila* transcription factors (Figure 2.5B), supporting the quality of the data (67, 158). Overall, E93 binding corresponds well with 24hr open chromatin in pupal wings (Figure 2.5C-D); 50% of E93 ChIP peaks are contained within the top 6,225 24hr FAIRE peaks, and 96% of E93 ChIP peaks are contained within all 24hr FAIRE peaks (Figure 2.5C). While there is good correspondence between E93 binding and open chromatin, not all 24hr FAIRE peaks are bound by E93 (Figure 2.S6A), demonstrating that the E93 ChIP signal is specific and not simply an indirect consequence of open chromatin. This is further supported by differences in the distribution of E93 ChIP and 24hr FAIRE peak locations across the genome: E93 preferentially binds to promoter-distal sites in the genome, whereas FAIRE peaks overlap proximal promoter regions with greater frequency (Figure 2.S6B). We next examined the relationship between E93 binding and temporally dynamic open chromatin in pupal wings. 51% of FAIRE peaks that change in accessibility between L3 and 24hr are directly bound by E93 at 24hr. Likewise, 51% of FAIRE peaks that change in accessibility between 24hr and 44hr are directly bound by E93 at 24hr (Figure 2.5E). By contrast, only 14% of temporally dynamic FAIRE peaks in early embryos are bound by E93 in 24hr pupal wings (131). Thus, E93 directly binds a significant majority of open chromatin sites that change accessibility (opening or closing) between L3 and 44hr.

Figure 2.S5. The E93 protein trap recapitulates E93 expression in pupal wings.

(top) Immunostaining of three stages of wing development. DAPI in blue, GFP in green, E93 antibodies in red. White squares indicate zoomed regions. (bottom) Table indicating the number of progeny from a cross between flies bearing the $E93^{GFSTF}$ protein trap chromosome and flies bearing a deficiency that deletes the *E93* locus. Because E93 loss of function mutants are recessive lethal, the viability of $E93^{GFSTF}/Df(3R)93F^{X2}$ progeny indicates that the E93 protein trap is functional.

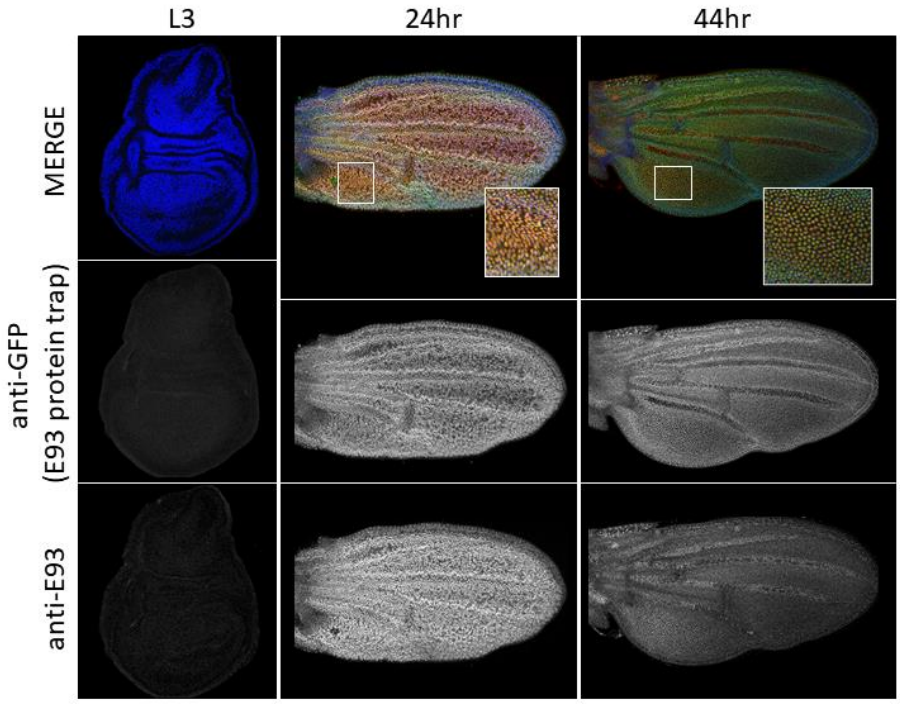

cross: $\frac{E93^{GFSTF}}{TM3} \times \frac{Df(3R)93F^{X2}}{TM6B}$

# progeny:	*Df(3R)93F^{X2}*	*TM6B, tb*
E93^{GFSTF}	212	265
TM3, sb	251	157

Figure 2.5. E93 binds temporally dynamic open chromatin.

(A) Browser shot from the *fringe* locus showing FAIRE-seq and E93 ChIP-seq signals (z score) from pupal wings. (B) Position weight matrices comparing the E93 motif discovered in ChIP peaks with the known E93 motif. (C) Cumulative distribution plot of E93 ChIP peak overlap with 24hr FAIRE peaks (red line), relative to randomly shuffled FAIRE peaks (gray line). (D) Heat maps plotting E93 ChIP-seq and FAIRE-seq signals (z score) in E93 ChIP peaks from 24hr pupal wings. (E) Stacked bar plots showing the fraction of temporally dynamic FAIRE peaks (opening and closing) that overlap an E93 ChIP peak (* overlap p value < 2.2×10^{-16} relative to temporally dynamic FAIRE peaks in embryos, Fisher's exact test).

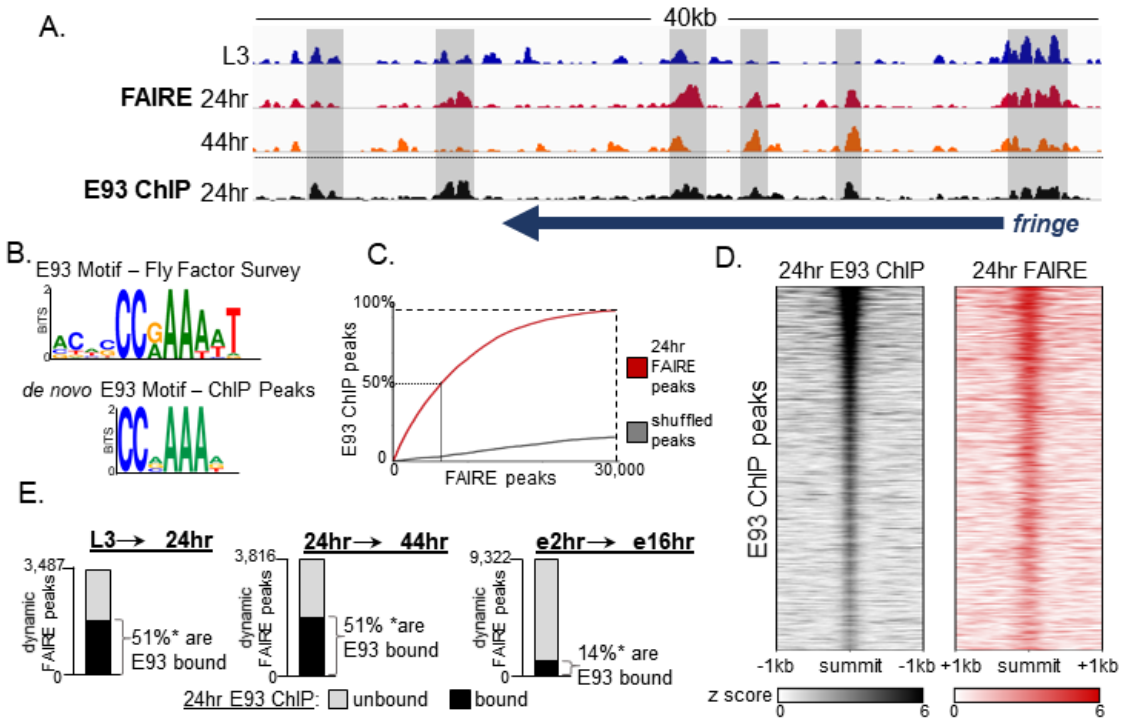

Figure 2.S6. E93 ChIP-seq signal is correlated with, but distinct from, 24hr FAIRE-seq signal.

(A) Scatterplot of E93 ChIP-seq and 24hr FAIRE-seq signals for all 24hr FAIRE peaks. FAIRE peaks that overlap an E93 ChIP peak (>50%) are colored red. (B) Pie charts showing overlap of E93 ChIP-seq and 24hr FAIRE-seq peaks with transcription start sites of annotated genes (+/- 500bp).

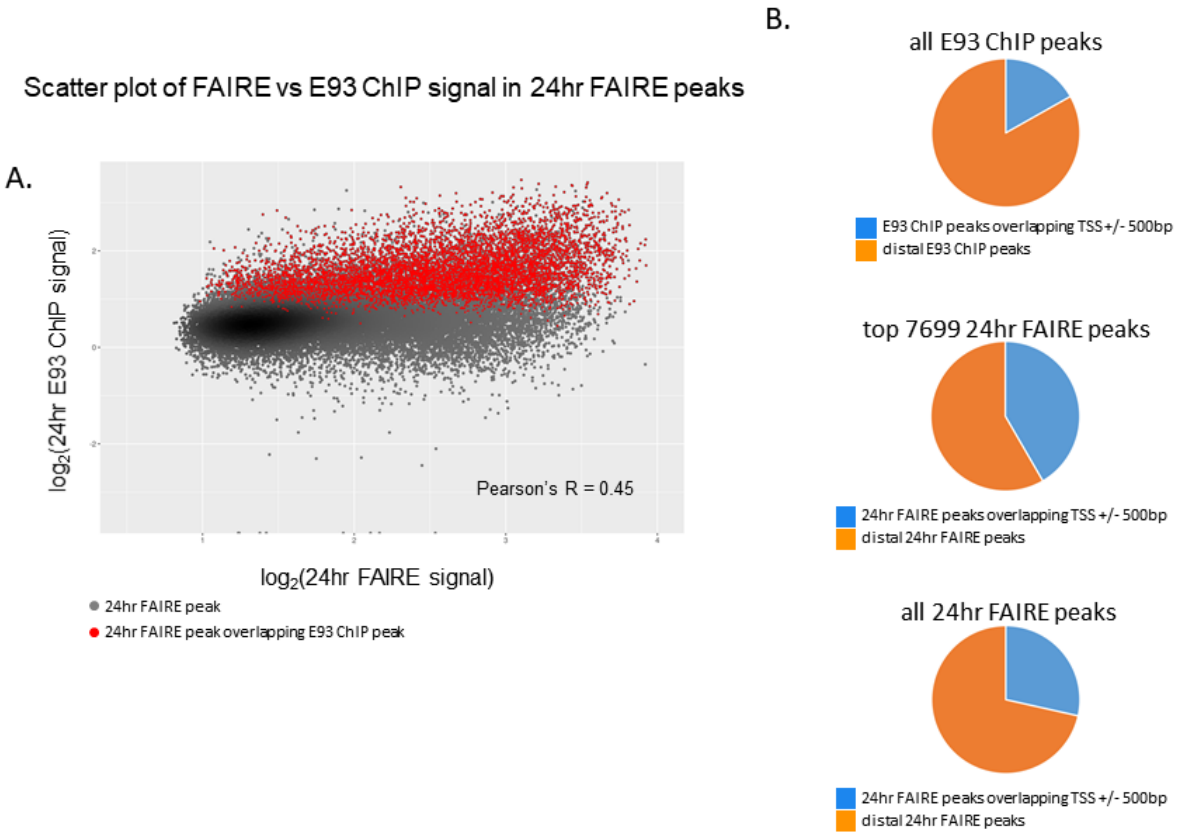

E93 binding is required for temporally dynamic open chromatin changes

The high degree of overlap between E93 binding and temporally dynamic open chromatin sites suggests that E93 may play a direct role in controlling chromatin accessibility during pupal wing development. To test this hypothesis, we performed FAIRE-seq in E93 mutant wings at L3, 24hr, and 44hr (Figure 2.6A). In L3 wings, we observed very few changes in open chromatin between wild type and E93 mutants (Figure 2.6B), consistent with expectations since E93 is not yet expressed at this time. By contrast, we observed thousands of changes in open chromatin between wild type and E93 mutant wings at 24hr and at 44hr. For example, 1,508 FAIRE peaks out of the top 7,699 peaks from each pair of datasets are more open in wild type wings than in E93 mutants at 24hr (Figure 2.6B), demonstrating that E93 is required for accessibility at these sites. Surprisingly, 659 FAIRE peaks are more open in E93 mutant wings than in wild type at 24hr, indicating that E93 is not required to promote accessibility at these sites; instead, it is required for the opposite: promoting nucleosome occupancy. Thus, loss of E93 not only results in the loss of accessibility at thousands of sites in the genome, it also results in the inappropriate presence of accessible chromatin at hundreds of additional sites.

We next asked whether sites that depend on E93 for proper chromatin accessibility correspond to temporally dynamic FAIRE peaks. Indeed, 70% of E93-dependent FAIRE peaks are temporally dynamic between L3 and 24hr in wild type wings (Figure 2.6C). This includes 53% of sites that normally open between L3 and 24hr in wild type wings, but which fail to open in E93 mutants, and 27% sites that normally close between L3 and 24hr in wild type wings, but which fail to close in E93 mutants (Figure 2.6D, Figure 2.S7A). By contrast, only 4% of sites that change in accessibility during embryogenesis overlap an E93-dependent

Figure 2.6. E93 binding is required for temporally dynamic open chromatin changes

(A) Browser shot showing FAIRE-seq signal from wild type (WT) and E93 mutant wings. E93 ChIP-seq signal from wild type 24hr wings is shown in black. The *nub*^{vein} and *nub*^{margin} enhancers are shown in green. (B) MA plots of FAIRE-seq signal in top 7,699 FAIRE peaks from each wild type and E93 mutant wing dataset. Differentially accessible peaks are colored red. (C) Stacked bar plots of the fraction of E93-dependent FAIRE peaks that overlap a temporally dynamic FAIRE peak. (D) Line plots of the average FAIRE-seq signal in FAIRE peaks that close, open, or remain unchanged between consecutive time points. The percentage of FAIRE peaks in each category that are E93-dependent is shown. Solid lines show wild type FAIRE-seq signal. Dashed lines show E93 mutant FAIRE-seq signal. (E) Stacked bar plot showing the fraction of E93-dependent FAIRE peaks that overlap an E93 ChIP peak.

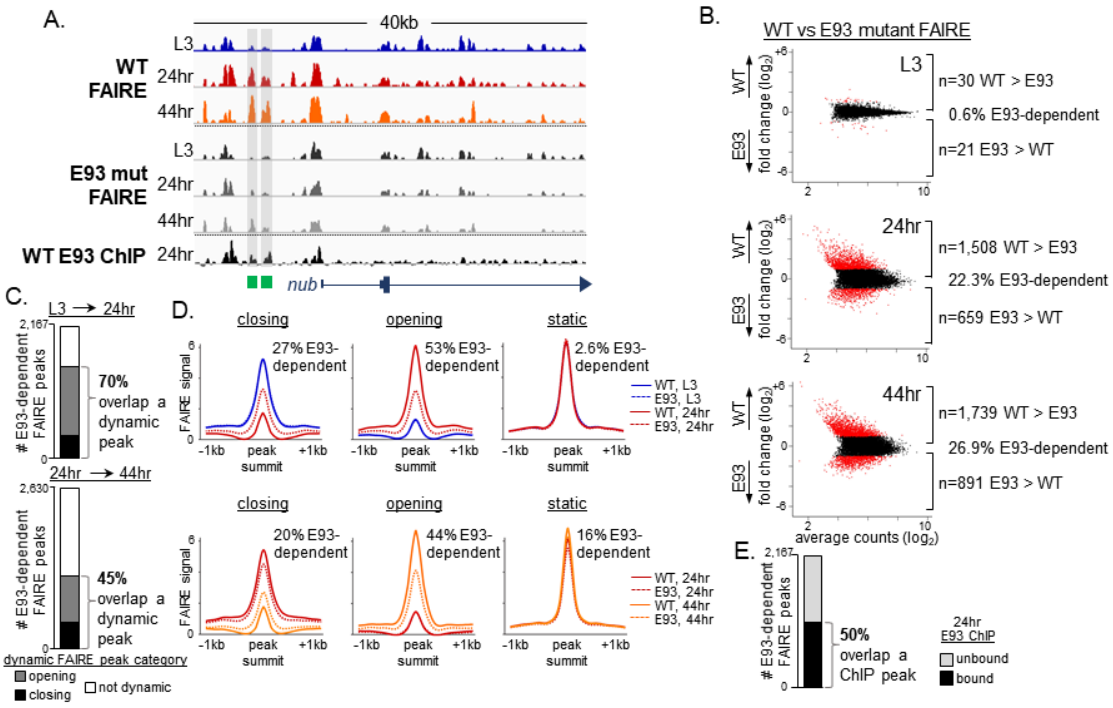

Figure 2.S7. E93-dependent peaks exhibit temporally-dynamic changes in wild type wings.

(A) Line plots of the average FAIRE-seq signal in FAIRE peaks that close, open, or remain unchanged between L3 and 24hr, separated into E93-bound and E93-unbound categories, as determined by E93 ChIP-seq. (B) Same as in A, but with 24hr to 44hr data. (C, D) Stacked bar plot of the fraction of temporally dynamic FAIRE peaks between L3 and 24hr (C) and between 24hr and 44hr (D) that overlap an E93-dependent FAIRE peak, as compared to the fraction of temporally dynamic FAIRE peaks across two stages of embryogenesis (e2-4hr to e16-18hr) (p values from Fisher's exact test).

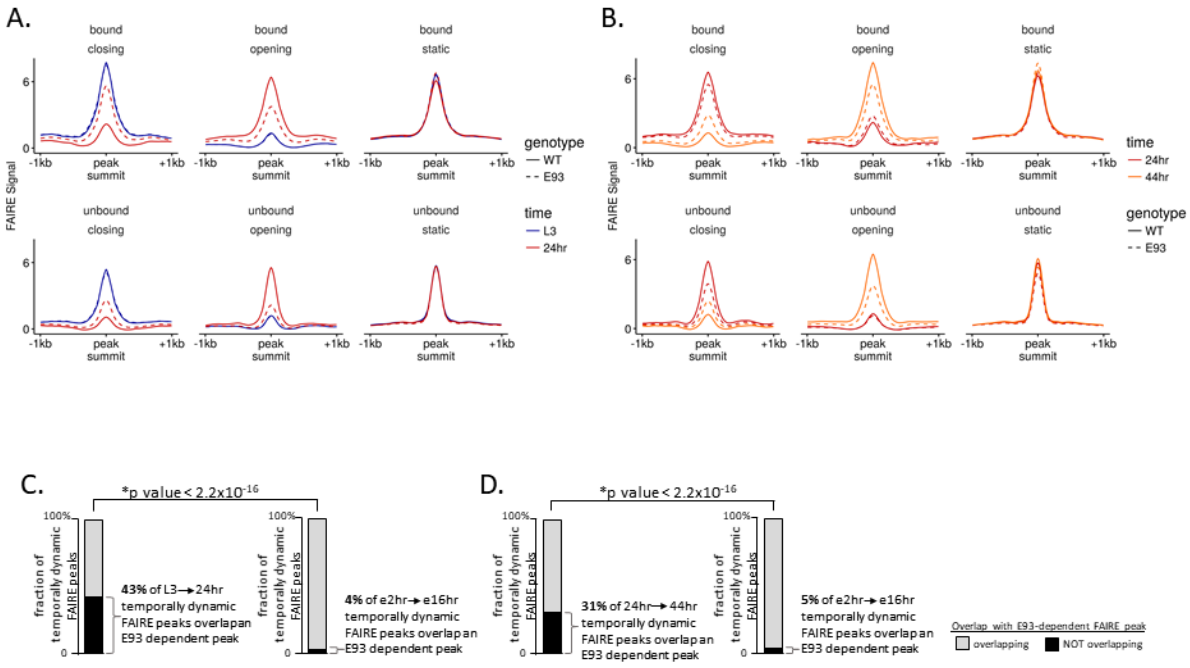

FAIRE peak (Fisher's exact test p value < $2.2x10^{-16}$) (Figure 2.S7C). FAIRE peaks that don't change in accessibility between L3 and 24hr in wild type wings exhibit no change in accessibility in E93 mutants (Figure 2.6D, "static" peaks). We obtained similar results for the 24hr to 44hr interval. The lower number of E93-dependent FAIRE peaks that overlap a dynamic FAIRE peak at this later time interval (Figure 2.6C, Figure 2.S7D) is possibly due to a persistent failure in chromatin accessibility from the earlier time point, such as sites that fail to open in E93 mutants at 24hr, and which stay closed at 44hr (e.g., highlighted region in Figure 2.6A). Similarly, these indirect effects likely explain the increase in the fraction of static peaks that exhibit E93-dependence during this time interval (Figure 2.6D). Importantly, we found that 50% of FAIRE peaks that are dependent on E93 for accessibility at 24hr are directly bound by E93 (Figure 2.6E). Together, these findings demonstrate that E93 controls temporal progression of development by directly and indirectly regulating the accessibility of thousands of sites in the genome. In the absence of E93, nearly half of the expected open chromatin changes fail to occur. One consequence of this failure is that E93 mutants exhibit a heterochronic open chromatin defect: open chromatin profiles of E93 mutant wings at 24hr are as similar to those of wild type wings at 0hr as they are to those of wild type wings at 24hr (Figure 2.S8).

E93 controls temporal specific enhancer activity through three distinct mechanisms

The results described above suggest that the developmental defects observed in E93 mutants are due to a failure to make temporally required changes in the accessibility of DNA regulatory elements genome wide. To directly test this hypothesis, we examined the consequences of E93 loss of function on the activity of the temporally dynamic

Figure 2.S8. E93 mutant wings show heterochronic open chromatin defects.

Heat map of Pearson correlation coefficients for each wild type and E93 mutant FAIRE-seq replicate. Note the increased similarity of E93 mutant open chromatin profiles relative to wild type open chromatin profiles of earlier developmental stages, indicating that the failure to change over time results in chronologically later mutant wings resembling those of an earlier developmental stage.

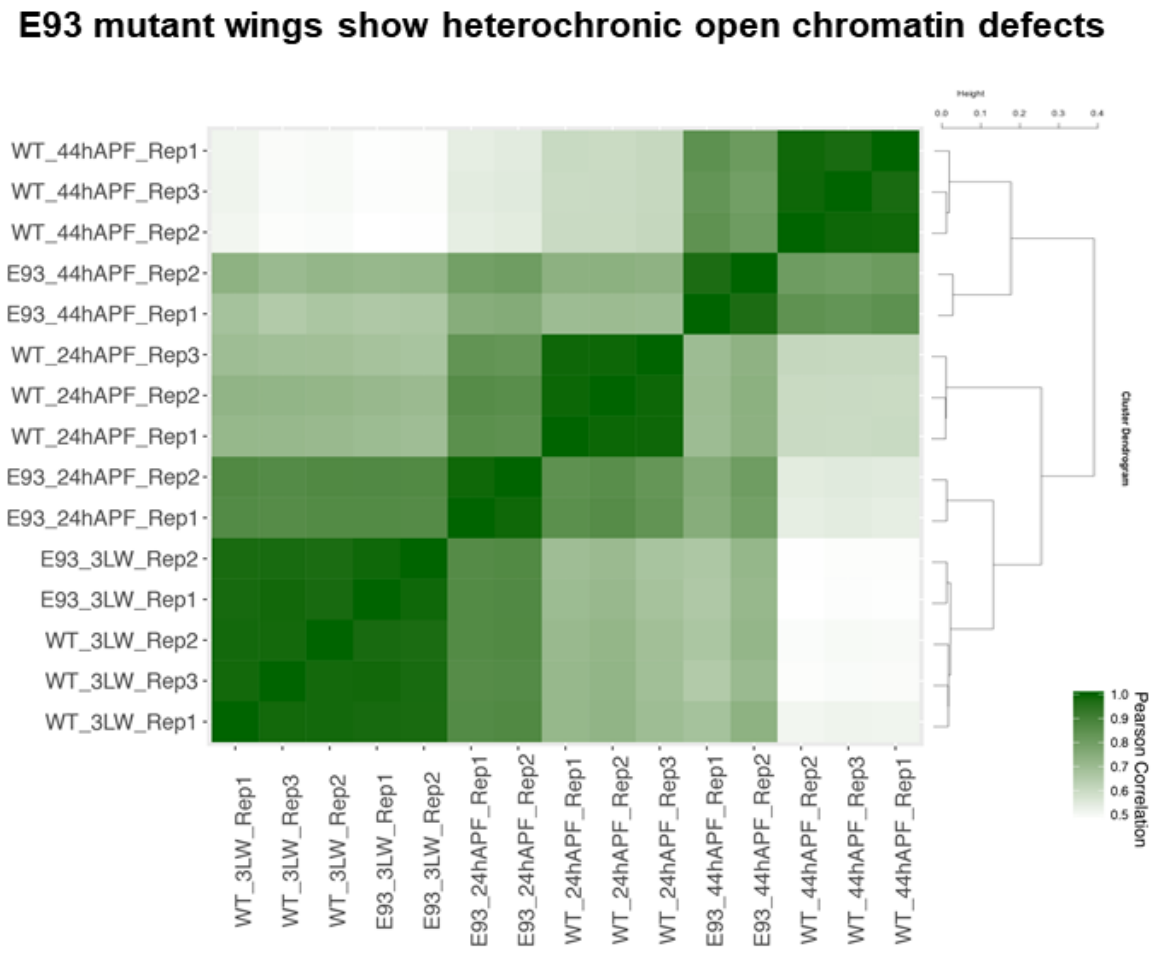

transcriptional enhancers we identified above. ChIP-seq shows that the *nub*^{vein} enhancer is directly bound by E93 at 24hr, and FAIRE-seq in wild type wings shows that *nub*^{vein} progressively opens after the L3 stage (Figure 2.7). The timing of this accessibility coincides with increasing *nub*^{vein} enhancer activity in wing veins (Figure 2.4). FAIRE-seq from E93 mutant wings reveals that this enhancer is dependent on E93 for its accessibility: it fails to open at 24hr, and it remains closed at 44hr in the absence of E93 (Figure 2.7). Using the GAL4-UAS system to drive an E93 RNAi construct specifically in the posterior compartment of the wing with *En-GAL4*, we observed a strong loss of *nub*^{vein} activity upon E93 knockdown specifically in the regions where the RNAi was expressed (Figure 2.7). The enhancer remains active only in a few cells in the proximal wing after E93 knockdown, and most RNAi-expressing cells show complete loss of GFP. Thus, the failure to open the *nub*^{vein} enhancer in E93 mutant flies correlates with a failure to activate the enhancer in transgenic reporter assays.

We next examined the *br*^{disc} enhancer, which is open and active in L3 wings, but which is closed and inactive in 24hr and 44hr wings (Figure 2.4). ChIP-seq reveals that E93 is directly bound to this enhancer, and FAIRE-seq shows that it remains persistently open at 24hr and 44hr in E93 mutant wings (Figure 2.7). Consistent with this persistent accessibility, *br*^{disc} is expressed in E93 mutants at 24hrs, when it would normally be off in wild type wings (Figure 2.7). The *br*^{disc} pattern in 24hr E93 mutant wings is nearly ubiquitous, similar to its pattern earlier in L3 wings. Thus, E93 is required to close this enhancer after the L3 stage, and failure to do so results in its aberrant expression at later developmental stages.

Finally, we examined the *tnc*^{blade} enhancer, which is open and active in 24hr wings (Figure 2.4). ChIP-seq shows that E93 is directly bound to *tnc*^{blade} (Figure 2.7). However,

despite this binding, *tnc*^{blade} does not significantly change in accessibility in E93 mutant wings, demonstrating that E93 is not required for promoting the accessibility of this enhancer. Nevertheless, RNAi-mediated knockdown of E93 in the anterior compartment of the wing using *Ci-GAL4* results in loss of *tnc*^{blade} activity in RNAi-expressing cells. Thus, while the *tnc*^{blade} enhancer is not dependent on E93 for its accessibility, it is still dependent on E93 for its activity. Importantly, the mutual dependence of the *nub*^{vein} and *tnc*^{blade} enhancers on E93 for transcriptional activity, combined with the specific dependence of *nub*^{vein} on E93 for accessibility, suggests distinct biochemical mechanisms underlie E93 function at these enhancers.

Figure 2.7. E93 controls temporal specific enhancer activity through three distinct modalities.

(A, top row) Browser shots of FAIRE-seq and ChIP-seq signal from wild type and E93 mutant wings at the indicated loci. (B – C) Immunostaining of reporter activity for each indicated enhancer. (B, middle row) Reporter activity in control or wild type wings. (C, bottom row) Reporter activity (green) in wings expressing E93 RNAi under control of Ci-GAL4 (tnc^{blade}), or En-GAL4 (nub^{vein}), or in E93 mutant wings (br^{disc}). The dotted lines indicate the boundary between RNAi-expressing and non-expressing cells. Arrows indicate loss of reporter activity. Scale bars indicate 50μm.

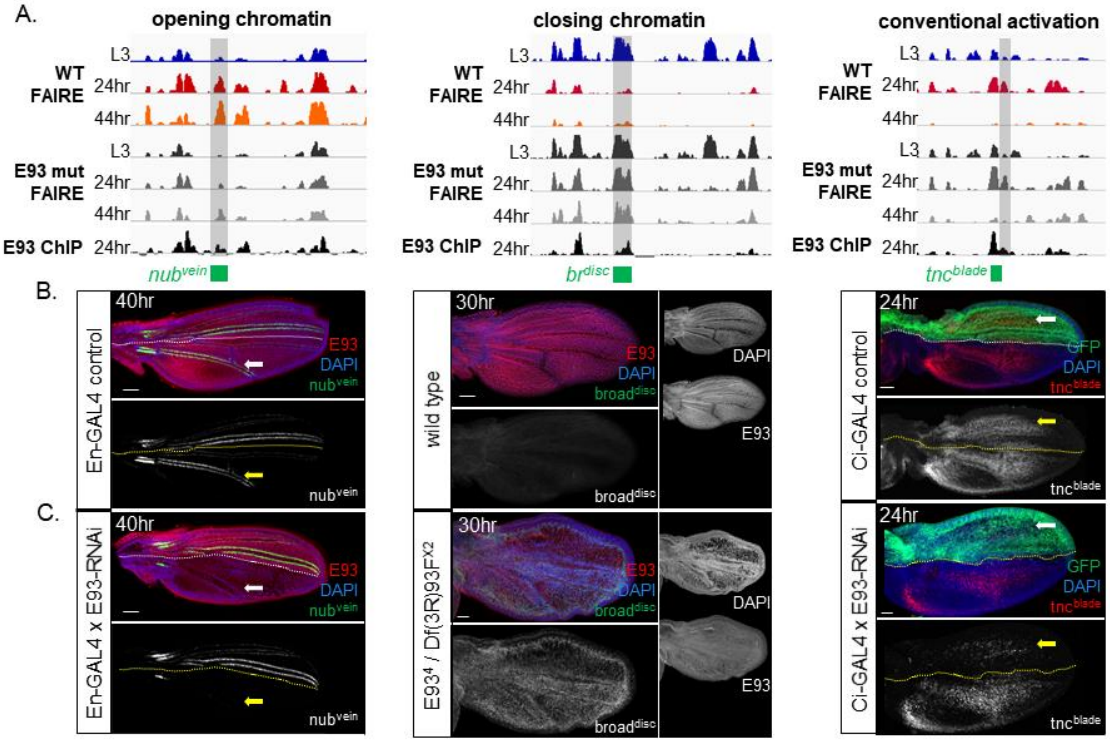

Discussion

The mechanisms controlling transcription factor targeting in the genome are incompletely understood, particularly in the context of animal development. Here, we show that the hormone-induced transcription factor E93 plays a direct role in controlling temporal changes in chromatin accessibility in the developing *Drosophila* wing. Together with our previous findings, this work supports a model in which two axes of information regulate enhancer activity in developing appendages: temporal information is provided by hormone-induced transcription factors that regulate accessibility of transcriptional enhancers, and spatial information is provided by the appendage master transcription factors that differentially regulate the activity of these enhancers.

Transcription factor targeting and temporal gene regulation

The importance of master transcription factors in specifying spatial identity during development suggests they may control where other transcription factors bind in the genome. One prediction of this model is that tissues whose identities are determined by different master transcription factors would exhibit different genome wide DNA binding profiles. However, we recently found that the *Drosophila* appendages (wing, leg, haltere), which utilize different transcription factors to determine their identities, share nearly identical open chromatin profiles. Moreover, these shared open chromatin profiles change coordinately over developmental time. There are two possible explanations for these findings. Either (1) different transcription factors produce the same open chromatin profiles in different appendages, or (2) transcription factors shared by each appendage control open chromatin profiles, instead of the master transcription factors of appendage identity. We favor the

second model for several reasons. Since the appendage master transcription factors possess different DNA binding domains with distinct DNA binding specificities, it is unlikely for them to bind the same sites in the genome. Supporting this expectation, ChIP for *scalloped* and *Homothorax*, two transcription factors important for appendage identity, shows clear tissue-specific binding in both the wing and eye-antennal imaginal discs (159). We also prefer the second model because it provides a relatively straightforward mechanism for the observed temporal changes in open chromatin: by changing the expression of the shared temporal transcription factor over time, the open chromatin profiles it controls would change as well. By contrast, appendage master transcription factor expression is relatively stable over time, making it unlikely for them to be sufficient for temporal changes in open chromatin.

We propose that control of chromatin accessibility in the appendages is mediated at least in part by transcription factors downstream of ecdysone signaling. According to this model, a systemic pulse of ecdysone initiates a temporal cascade of hormone induced transcription factor expression in each of the appendages. We thus refer to these as "temporal" transcription factors. Temporal transcription factors can directly regulate accessibility of transcriptional enhancers by opening or closing them, thereby conferring temporal specificity to their activity and driving development forward in time. Master transcription factors then bind accessible enhancers depending on their DNA binding preferences (or other means of binding DNA) and differentially regulate the activity of these enhancers to control spatial patterns of gene expression, thus shaping the unique identities of individual appendages.

Our experiments with E93 provide direct support for this model. In wild type wings, thousands of changes in open chromatin occur after the large pulse of ecdysone that triggers the end of larval development. In E93 mutants, approximately 40% of these open chromatin changes fail to occur. Importantly, nearly three-quarters of sites that depend on E93 for accessibility correspond to temporally dynamic sites in wild type wings. Thus, chromatin accessibility is not grossly defective across the genome; instead, defects occur specifically in sites that change in accessibility over time. This finding, combined with the large fraction of temporally dynamic sites that depend on E93 for accessibility, indicate that E93 controls a genome-wide shift in the availability of temporal specific transcriptional enhancers. Supporting this hypothesis, we show that temporal specific enhancers depend on E93 both for accessibility and for activity. Since we propose that the response to ecdysone is shared across the appendages, we predict that similar defects occur in appendages besides the wing. It remains to be seen whether other ecdysone-induced transcription factors besides E93 control accessibility of enhancers at different developmental times. It also remains to be seen how the temporal transcription factors work with the appendage master transcription factors to control appendage specific enhancer activity.

Mechanisms of temporal transcription factor function

Our findings suggest that E93 controls temporal specific gene expression through three different modalities that potentially rely on three distinct biochemical activities. The enrichment of E93 motifs in these sites and binding of E93 according to ChIP-seq data indicate that it contributes to this regulation directly. We propose these combined activities

drive development forward in time by turning off early acting enhancers and simultaneously turning on late acting enhancers.

First, as in the case of the *tnc*^{blade} enhancer, E93 appears to function as a conventional activator. In the absence of E93, *tnc*^{blade} fails to express at high levels, but the accessibility of the enhancer does not measurably change. This suggests that binding of E93 to *tnc*^{blade} is required to recruit an essential co-activator. Importantly, this finding demonstrates that E93 is not solely a regulator of chromatin accessibility. E93 binds many open chromatin sites in the genome without regulating their accessibility, and thus it may regulate the temporal specific activity of many other enhancers. In addition, since the *tnc*^{blade} enhancer opens between L3 and 24hr even in the absence of E93 (Figure 2.7A), there must be other factors that control its accessibility, perhaps for example, transcription factors induced by ecdysone earlier in the temporal cascade.

Second, as in the case of the *nub*^{vein} enhancer, E93 is required to promote chromatin accessibility. In this capacity, E93 may function as a pioneer transcription factor to open previously inaccessible chromatin. Alternatively, E93 may combine with other transcription factors, such as the wing master transcription factors, to compete nucleosomes off DNA. Testing the ability of E93 to bind nucleosomal DNA will help to discriminate between these two alternatives. In either case, we propose this function of E93 is necessary to activate late-acting enhancers across the genome. Since only half of E93-dependent enhancers are directly bound by E93 at 24hr (Figure 2.6E), it is also possible that E93 regulates the expression of other transcription factors that control chromatin accessibility. Alternatively, if E93 uses a hit-and-run mechanism to open these enhancers, our ChIP time point may have been too late to capture E93 binding at these sites.

Finally, as in the case of the *br*^{disc} enhancer, E93 is required to decrease chromatin accessibility. We propose this function of E93 is necessary to inactivate early-acting enhancers across the genome. Current models of gene regulation do not adequately explain how sites of open chromatin are rendered inaccessible, but the ability to turn off early-acting enhancers is clearly an important requirement in developmental gene regulation. It may also be an important contributor to diseases such as cancer, which exhibits widespread changes in chromatin accessibility relative to matched normal cells (160). Thus, this role of E93 may represent a new functional class of transcription factor ("reverse-pioneer"), or it may represent conventional transcriptional repressor activity. Additional work is required to decipher the underlying mechanisms. Notably, recent work on the temporal dynamics of iPS reprogramming suggest a similar role for Oct4, Sox2, and Klf4 in closing open chromatin to inactivate somatic enhancers (11).

Acknowledgements

Transgenic fly stocks were obtained from the Vienna Drosophila Resource Center (VDRC, www.vdrc.at). Stocks obtained from the Bloomington Drosophila Stock Center (NIH P40OD018537) were used in this study. This work was supported by startup funds provided by The University of North Carolina at Chapel Hill to DJM. CMU was supported in part by NIH grant T32GM007092.

CHAPTER 3: A DIRECT AND WIDESPREAD ROLE FOR THE NUCLEAR RECEPTOR ECR IN MEDIATING THE RESPONSE TO ECDYSONE IN DROSOPHILA[2]

Introduction

Hormones function as critical regulators of a diverse set of physiological and developmental processes, including reproduction, immune system function, and metabolism. During development, hormones act as long-range signals to coordinate the timing of events between distant tissues. The effects of hormone signaling are mediated by nuclear receptors, which function as transcription factors that differentially regulate gene expression in a hormone-dependent manner. Whereas many of the co-regulators that contribute to nuclear receptor function have been identified, the mechanisms used by these factors to generate distinct, yet appropriate, transcriptional responses in different target tissues are incompletely understood.

Ecdysone signaling has long served as a paradigm to understand how hormones generate spatial and temporal-specific biological responses. In Drosophila, ecdysone is produced by the ring gland and secreted into the hemolymph, where it is converted into its active form, 20-hydroxyecdysone (20E), before reaching target tissues (33, 92). Pulses of ecdysone are required for transitions between developmental stages, such as the larval molts.

[2] This chapter originally appeared as an article in Proceedings of the National Academy of Sciences. The original citation is as follows:
C. M. Uyehara, D. J. McKay, Direct and widespread role for the nuclear receptor EcR in mediating the response to ecdysone in Drosophila. *Proc Natl Acad Sci U S A* **116**, 9893–9902 (2019).

A high titer pulse of ecdysone triggers the end of larval development and the beginning of metamorphosis (33, 92). Ecdysone effects transcriptional changes through binding to its receptor, a heterodimer of the proteins EcR (Ecdysone receptor, homolog of the mammalian Farnesoid X Receptor) and Usp (ultraspiracle, homolog of mammalian RXR)(61). In the absence of ecdysone, EcR/Usp is nuclear-localized and bound to DNA where it is thought to act as a transcriptional repressor (80, 161). Upon ecdysone binding, EcR/Usp switches to a transcriptional activator (161). Consistent with the dual regulatory capacity of EcR/Usp, a variety of co-activator and co-repressor complexes have been shown to function with this heterodimer to regulate gene expression (80, 82, 162, 163).

Understanding how ecdysone exerts its effects on the genome has been heavily influenced by the work of Ashburner and colleagues in the 1970's. By culturing larval salivary glands in vitro, Ashburner described a sequence of visible puffs that appear in the giant polytene chromosomes upon addition of ecdysone (52). A small number of puffs appeared immediately after ecdysone addition, followed by the appearance of more than one hundred additional puffs over the next several hours (52). The appearance of early puffs was found to be independent of protein synthesis, suggesting direct action by EcR/Usp, whereas the appearance of late puffs was not, suggesting they require the protein products of early genes for activation (52). These findings, and decades of subsequent work elucidating the molecular and genetic details, have led to a hierarchical model of ecdysone signaling in which EcR/Usp directly induces expression of a small number of early response genes. Many of these early response genes encode transcription factors, such as the zinc finger protein Broad, the nuclear receptor Ftz-f1, and the pipsqueak domain factor E93 (33). The early response transcription factors are required, in turn, to induce expression of the late response

genes, which encode proteins that impart temporal and tissue-specific responses in target tissues.

Although the framework of the ecdysone pathway was established through work in salivary glands, additional studies affirmed an essential role for ecdysone signaling in many other tissues. Similar to other hormones, the physiological response to ecdysone is often profoundly specific to each target tissue. For example, ecdysone signaling triggers proliferation, changes in cell and tissue morphology, and eventual differentiation of larval tissues fated to become part of the adult fly, such as the imaginal discs (33, 85). By contrast, ecdysone signaling initiates the wholesale elimination of obsolete tissues, such as the larval midgut and salivary glands through programmed cell death (33, 85, 92). Ecdysone is also essential for remodeling larval neurons that persist until adulthood and specifying the temporal identity of neural stem cell progeny born during this time (164). While it is clear that ecdysone signaling triggers the gene expression cascades that underlie these events, the molecular mechanisms by which ecdysone elicits diverse transcriptional responses in target tissues remains poorly understood.

A key step in delineating the mechanisms by which ecdysone signaling regulates target gene expression involves identification of EcR/Usp DNA binding sites. Given the hierarchical structure of the ecdysone pathway, it is unclear if EcR acts primarily at the top of the transcriptional cascade, or if it also acts directly on downstream effector genes. Several early response genes such as br, Eip74EF, and the glue genes have been shown to be directly bound by EcR in vivo (112, 165). At the genome-wide level, polytene chromosome staining revealed approximately 100 sites bound by EcR in larval salivary glands (166). DamID and ChIP-seq experiments have identified roughly 500 sites directly bound by EcR in Drosophila

cell lines (90, 130). Thus, the available evidence, albeit limited, indicates that EcR binds to a limited number of target genes, consistent with hierarchical models wherein the response to ecdysone is largely driven by early response genes and other downstream factors.

We recently identified the ecdysone-induced transcription factor E93 as being essential for the proper temporal sequence of enhancer activation during pupal wing development (167). In the absence of E93, early-acting enhancers fail to turn off, and late-acting enhancers fail to turn on. Moreover, ChIP-seq identified thousands of E93 binding sites across the genome. These data support the hierarchical model of ecdysone signaling in which early response transcription factors like E93 directly regulate a significant fraction of ecdysone-responsive genes in target tissues.

Here, we sought to determine the role that EcR performs in temporal gene regulation during the larval-to-prepupal transition of the wing. Using wing-specific RNAi, we find that EcR is required for proper morphogenesis of prepupal wings, although it is largely dispensable for wing disc patterning at earlier stages of development. RNA-seq profiling reveals that EcR functions as both a temporal gate to prevent the precocious transition to prepupal development as well as a temporal trigger to promote progression to next stage. Using CUT&RUN, we map binding sites for EcR genome wide before and after the larval-to-prepupal transition. Remarkably, we find that EcR binds extensively throughout the genome, including at many genes with wing-specific functions that are not part of the canonical ecdysone signaling cascade. Moreover, EcR binding is highly dynamic, with thousands of binding sites gained and lost over time. Finally, transgenic reporter analyses demonstrate that EcR is required not only for temporal regulation of enhancer activity, but also for spatial regulation of target enhancers. Together, these findings indicate that EcR does

not control gene expression solely through induction of a small number of downstream transcription factors, but instead plays a direct and widespread role in regulating tissue-specific transcriptional programs.

Materials and Methods

Western Blots

For each sample, 40 wings were lysed directly in Laemmli sample buffer preheated to 95C. Samples were run on a BioRad 7.5% Mini-Protean TGX gel at 90V for 60m and then transferred to a nitrocellulose membrane at 100V for 60m. Membranes were block in 5% carnation instant milk for 30m at room temperature (RT) or overnight at 4C. Primary and secondary antibodies were incubated for 2hr at RT using four washes with 1XTBST between incubations. The following antibody concentrations were used to probe blots: 1:1000 mouse anti-EcR (DSHB DDA2.7, concentrate); 1:1000 anti-EcR-A (DSHB 15G1a, concentrate), 1:1000 anti-EcR-B1 (DSHB AD4.4, concentrate); 1:5000 rabbit anti-GFP (Abcam ab290); 1:30000 mouse anti-alpha Tubulin (Sigma T6074); 1:5000 goat anti-mouse IgG, HRP-conjugated (Fisher 31430); 1:5000 donkey anti-rabbit, HRP-conjugated (GE Healthcare NA934). Membranes were imaged on a GE Amersham Imager 600.

Transgenic Reporter Construction

Candidate enhancers were cloned into the pΦUGG destination vector (146) and integrated into the attP2 site. Primer sequences are available upon request.

Immunofluorescence

Immunostaining was performed as described previously (131). For mitotic clones, *usp3 FRT19A / Ubi-RFP, hs-FLP, FRT19A; Enhancer-GAL4 / UAS-dsGFP* animals were heat-shocked at 24-48hrs AEL. The following antibody concentrations were used: 1:750 mouse anti-EcR (DSHB DDA2.7, concentrate), 1:4000 rabbit anti-GFP (Abcam ab290),

1:3500 mouse anti-Dl (DSHB C594.9b, concentrate), 1:200 mouse anti-FLAG M2 (Sigma F1804), 1:10 mouse anti-Achaete (DSHB anti-Achaete, supernatant), 1:1000 anti-Br (DSHB 25E9.D7, concentrate). Samples were imaged on a Leica Sp5 confocal microscope.

Sample preparation for RNAseq

A minimum of 60 wings were prepared as previously described (131) from either Oregon R (WT) or *yw; vg-GAL4, tub>CD2>GAL4, UAS-GFP, UAS-FLP / UAS-EcR-RNAi*^{104} (EcR-RNAi). For library construction, 50-100ng RNA was used as input to the Ovation Drosophila RNA-Seq System. Single-end, 1x50 sequencing was performed on an Illumina HiSeq 2500 at the UNC High Throughput Sequencing Facility.

Sample preparation for CUT&RUN

A minimum of 100 wings from *w; EcR*^{GFSTF}*/Df(2R)BSC313* were dissected in 1XPBS. Samples were centrifuged at 800rcf for 5minutes at 4C and washed twice with dig-wash buffer (20mM HEPES-NaOH, 150mM NaCl, 2mM EDTA, 0.5mM Spermidine, 10mM PMSF, 0.05% digitonin) and incubated in primary antibody for 2hrs at 4C. Samples were washed as before and incubated in secondary antibody for 2hrs. Samples were washed and incubated for 1hr with protein A MNase. Samples were washed twice in dig-wash buffer without EDTA and then resuspended in 150uL dig-wash buffer without EDTA. Following this, samples were equilibrated to 0C in an ice bath. 2uL CaCl2 (100mM) was added to activate MNase and digestion allowed to proceed for 45s before treating with 150uL 2XRSTOP+ buffer (200mM NaCl, 20mM EDTA, 4mM EGTA, 50ug/ml RNase, 40ug/ml glycogen, 2pg/ml yeast spike-in DNA). Soluble fragments were released by incubating at

37C for 10m. Samples were spun twice at 800g, 5m at 4C and the aqueous phase removed. The rest of the protocol was performed as described in Skene et al., 2018. For library preparation, the Rubicon Thruplex 12s DNA-seq kit was used following the manufacturer's protocol until the amplification step. For amplification, after the addition of indexes, 16-21 cycles of 98C, 20s; 67C, 10s were run. A 1.2x SPRI bead cleanup was performed (Agencourt Ampure XP). Libraries were sequenced on an Illumina MiSeq. The following antibody concentrations were used: 1:300 mouse anti-FLAG M2; 1:200 rabbit anti-Mouse (Abcam ab46450); 1:400 Batch#6 protein A-MNase (from Steven Henikoff).

RNA Sequencing Analysis

Reads were aligned with STAR (2.5.1b) (168). Indexes for STAR were generated with parameter --sjdbOverhang 49 using genome files for the dm3 reference genome. The STAR aligner was run with parameters --alignIntronMax 50000 --alignMatesGapMax 50000. Subread (v1.24.2) was used to count reads mapping to features (169). DESeq2 (v1.14.1) was used to identify differentially expressed genes using the lfcShrink function to shrink log-fold changes (170). Differentially expressed genes were defined as genes with an adjusted p-value less than 0.05 and a log2 fold change greater than 2. Normalized counts were generated using the counts function in DESeq2. For k-medoids clustering, normalized counts were first converted into the fraction of maximum WT counts and clustering was performed using the cluster package in R. Optimal cluster number was determined by minimizing the cluster silhouette. Heatmaps were generated using pheatmap (v1.0.10) in R. Gene Ontology analysis was performed using Bioconductor packages TopGO (v2.26.0) and GenomicFeatures (v1.26.4) using expressed genes as a background set with parameters: algorithm = 'elim' and

statistic = ‘fisher’ (141, 171). Expressed genes were defined as genes that remained after DESeq2 performed independent filtering to remove genes with low counts.

CUT&RUN Sequencing Analysis

Technical replicates were merged by concatenating fastq files. Reads were trimmed using bbmap (v37.50) with parameters ktrim=4 ref=adapters rcomp=t tpe=t tbo=t hdist=1 mink=11. Trimmed reads were aligned to the dm3 reference genome using Bowtie2 (v2.2.8) with parameters --local --very-sensitive-local --no-unal --no-mixed --no-discordant --phred33 -I 10 -X 700 (172). Reads with a quality score less than 5 were removed with samtools (v1.3.1) (173). PCR duplicates were marked with Picard (v2.2.4) and then removed with samtools. Bam files were converted to bed files with bedtools (v2.25.0) with parameter -bedpe and split into different fragment size categories using awk (139). Bedgraphs were generated with bedtools and then converted into bigwigs with ucsctools (v320) (174). Data was z-normalized using a custom R script. MACS (v2016-02-15) was used to call peaks on individual replicates and merged files using a control genomic DNA file from sonicated genomic DNA using parameters -g 121400000 --nomodel --seed 123 (175). A final peak set was obtained by using peaks that were called in the merged file that overlapped with a peak called in at least one replicate. Heatmaps and average signal plots were generated from z-normalized data using the Bioconductor package Seqplots (v1.18.0). ChIPpeakAnno (v3.14.0) was used to calculate distance of peaks to their nearest gene (176, 177). Gene ontology analysis was performed as described for RNA-seq data, except that all genes were used as a background set. To identify clusters of EcR binding sites, the EcR peaks were resized to 5000bp, assigned to clusters, and the furthest start and end coordinate of the

original peaks were used. To shuffle clusters, bedtools shuffle was used using –seed 100, including (-incl) peaks from WT FAIRE (131).

Motif Analysis

De novo motif analysis was performed using DREME (v4.12.0) using parameters -maxk 13 -t 18000 -e 0.05 (158). As background sequences, FAIRE peaks from -6hAPF or +6hAPF were used. To identify occurrences of the EcR motif in the genome, PWMs for the EcR and Usp motifs identified by a bacterial 1-hybrid were obtained from Fly Factor Survey (67). For the palindromic, Usp/EcR motif, the PWMs for EcR and Usp were concatenated together and the probabilities for the central, overlapping base were averaged. FIMO (v4.12.0) was run on the dm3 reference genome using parameters –max-stored-scores 10000000 --max-strand --no-qvalue --parse-genomic-coord --verbosity 4 --thresh 0.01 (178). Motif density plots were generated by counting the number of motifs from peak summits (10bp bins) and normalizing by the number of input peaks.

Drosophila culture and genetics

Flies were grown at 25C under standard culture conditions. Late wandering larvae were used as the –6hAPF timepoint. White prepupae were used as the 0h time point for staging +6hAPF animals. For 96hAEL, apple juice plates with embryos were cleared of any larvae and then four hours later any animals that had hatched were transferred to vials. The following genotypes were used:

yw; vg-GAL4, UAS-FLP, UAS-GFP, Tub>CD2>GAL4 / CyO (179).

w1118; P{UAS-EcR-RNAi}104 (BDSC#9327)

yw; EcR^{GFSTF} (BDSC#59823)

w1118; Df(2R)BSC889/CyO (BDSC#32253)

UAS-dsGFP (gift of Brian McCabe)

usp3, w, P{neoFRT}19A/FM7c (BDSC#64295)*

P{Ubi-mRFP.nls}1, w, P{hsFLP}12 P{neoFRT}19A (BDSC#31418)*

w; UAS-EcR.B2.W650A (BDSC#9449)

Results

Temporal changes in gene expression during the larval-to-prepupal transition

In Drosophila, the end of larval development marks the beginning of metamorphosis. Over a five-day period, larval tissues are destroyed, and the progenitors of adult tissues, such as wing imaginal discs, undergo a series of progressive morphological and cell differentiation events to acquire their final shapes and sizes. By the end of larval development, the wing disc is comprised of a largely undifferentiated array of columnar epithelial cells (134, 180). The first 12 hours after puparium formation (APF) is termed the prepupal stage. During this period, cell division is arrested, and the pouch of the wing disc everts outward, causing the dorsal and ventral surfaces of the wing to appose one another, forming the presumptive wing blade (Figure 3.1A-B) (134, 180). At the same time, the notum of the wing disc extends dorso-laterally, and eventually fuses with the contralateral wing disc to form the back of the adult fly (Figure 3.1A-B). Additional events occurring during this time period include secretion of the prepupal cuticle and migration of muscle progenitor cells.

To understand EcR's role in promoting the larval-to-prepupal transition, we began by identifying global changes in gene expression that occur in wild type wings before and after the onset of pupariation. We collected wing tissue from wandering, third instar larvae, approximately six hours prior to puparium formation (hereafter, –6hAPF) and from prepupae, approximately six hours after puparium formation (hereafter, +6hAPF), and performed RNAseq, aligning our reads to the dm3 reference sequence. As described previously (19), wildtype gene expression is highly dynamic during this time period. Using a conservative definition for differential expression (FDR < 0.05, >= 2-fold change in expression), we identified over 1300 genes increasing in expression and nearly 800 genes

decreasing in expression (Figure 3.1C). The observed gene expression changes are consistent with developmental events occurring at this time. For example, genes that increase over time are involved in cuticle deposition, cellular metabolism and muscle development (Figure 3.1C). By contrast, genes that decrease over time are involved in cell cycle regulation and DNA replication. Thus, the morphological changes that define the larval-to-prepupal transition are rooted in thousands of changes in gene expression.

EcR is required for the larval-to-prepupal transition in wings

The onset of pupariation is induced by a high titer ecdysone pulse. At the genetic level, ecdysone acts through its receptor, EcR. Null mutations in EcR are embryonic lethal. Therefore, 0in combination with an RNAi construct to knockdown EcR expression throughout wing development (181). EcR-RNAi driven in wing discs diminished protein levels by approximately 95% (Figure 3.S1A-C).

In agreement with previous work suggesting that EcR does not appear to be required for wing development during the 1st and 2nd instar stages (182, 183), EcR-RNAi wings appear morphologically similar to wild type (WT) wing imaginal discs at –6hAPF (Figure 3.1B). However, EcR-RNAi wing discs are noticeably larger than WT wing discs, consistent with the proposed role for ecdysone signaling in cell cycle inhibition in 3rd instar larvae (182, 183). By contrast, EcR-RNAi wings at +6hAPF appear morphologically dissimilar to both –6hAPF EcR-RNAi wings and to WT wings at +6hAPF. The pouch fails to properly evert, and larval folds remain visible. Similarly, the notum fails to extend appropriately, and appears more similar to the larval notum than the notum at +6hAPF (Figure 3.1B). These findings suggest that wings fail to properly progress through the larval-to-prepupal transition

in the absence of EcR. Notably, this failure is likely not due to a systemic developmental arrest because legs isolated from larvae and pupae expressing EcR-RNAi in the wing exhibit no morphological defects (Figure 3.S1D) We conclude that EcR is required tissue-specifically for progression through the larval-to-prepupal transition.

To identify genes impacted by the loss of EcR, we performed RNA-seq on EcR-RNAi wings at –6hAPF and +6hAPF. Knockdown of EcR results in widespread changes in gene expression (Figure 3.1D). At –6hAPF, 453 genes are differentially expressed in EcR-RNAi wings relative to wildtype wing imaginal discs. Remarkably, 85% of these genes (n=383, "–6hAPF EcRi > WT") are expressed at higher levels in EcR-RNAi wings relative to WT, suggesting that EcR is primarily required to repress gene expression at –6hAPF. To determine the expression profiles of these genes during WT development, we performed cluster analysis (Figure 3.1E) and found that 72% of these –6hAPF EcRi UP genes normally increase in expression between –6hAPF and +6hAPF (Figure 3.1E). Genes in this category include those involved in cuticle development as well as multiple canonical ecdysone response genes (Table 3.S1). Thus, a major role of EcR at –6hAPF is to keep genes involved in the prepupal program from being precociously activated during larval stages.

We next examined the impact of EcR knockdown in +6hAPF wings. In contrast to the effect at –6hAPF, wherein genes primarily increased in the absence of EcR, we observed approximately equal numbers of up- and down-regulated genes relative to WT wings at +6hAPF (Figure 3.1F). Clustering of EcR-RNAi and WT RNA-seq data revealed distinct differences in the inferred regulatory role of EcR at +6hAPF relative to –6hAPF (Figure 3.1G). 74% of the genes expressed at higher levels in EcR-RNAi wings relative to WT normally decrease in expression between –6hAPF and +6hAPF (Figure 3.1G). Genes in this

category include factors that promote sensory organ development and cell cycle genes (Table 3.S2). The increased levels of these "+6hAPF EcRi > WT" genes suggest that in addition to preventing precocious activation of the prepupal gene expression program, EcR is also required to shut down the larval gene expression program. However, we also observe a role for EcR in gene activation. For genes that are expressed at lower levels in EcR-RNAi wings (n=619, "+6hAPF WT > EcRi"), 96% of these genes normally increase between –6hAPF and +6hAPF. Genes in this category include those involved in muscle development, metabolic genes and regulators of cell and tissue morphology (Table 3.S2). We conclude that EcR is required not only for gene repression but also for gene activation, consistent with the demonstrated interaction of EcR with both activating and repressing gene regulatory complexes (80, 82, 162, 163). Collectively, these data demonstrate that the failure of EcR-RNAi wings to progress through the larval-to-prepupal transition coincides with widespread failures in temporal gene expression changes.

The transcriptional response to ecdysone has recently been examined in a set of 41 different Drosophila cell lines (86), including several wing disc-derived cell lines. To determine the extent to which these responses mirror ecdysone-triggered gene expression changes in a developing tissue, we compared them to our EcR-RNAi wings (Figure 3.S2). In general, the overlap between differentially-expressed genes for any given cell line and EcR-dependent genes in the wing was low (e.g., median = 3.97% of EcR-dependent genes at -6hAPF overlap an ecdysone responsive gene in cell lines) (Figure 3.S2D). A subset of wing disc-derived cell lines exhibited modestly greater similarity (e.g., median = 8.39% of ecdysone-responsive genes in wing disc-derived cell lines are categorized as EcR-dependent

Figure 3.1: EcR is required to promote global changes in gene expression in wings between –6hAPF and +6hAPF

(A) Cartoon diagram of wildtype (WT) wing eversion between –6hAPF and +6hAPF. (B) Confocal images of *WT* wings and wings expressing *UAS-EcR RNAi* from *vg-tubGAL4* (hereafter EcR-RNAi) at –6hAPF and +6hAPF. The dorsal-ventral (DV) boundary is marked by an orange dotted line. The edge of the pouch is indicated by a blue dotted line. (C) MA plots (top) and gene ontology terms (bottom) of RNAseq comparing gene WT wings at –6hAPF and +6hAPF. (D-E) MA Plots and clustered heatmaps of RNAseq comparing EcR-RNAi wings and WT wings at -6hAPF. (F-G) MA plots and heatmaps of RNAseq comparing EcR-RNAi wings at WT wings at +6hAPF. Scale bars for immunostaining are 100μm. For MA plots, differentially expressed genes (padj < 0.05, absolute $\log_2$ fold change > 1) are colored red and blue. Heatmaps are represented as the fraction of max WT counts. Colored bars to the right denote start and end of each cluster. Line plots are the mean signal for each cluster (solid: WT; dashed: EcR-RNAi, see legend between panels E and G).

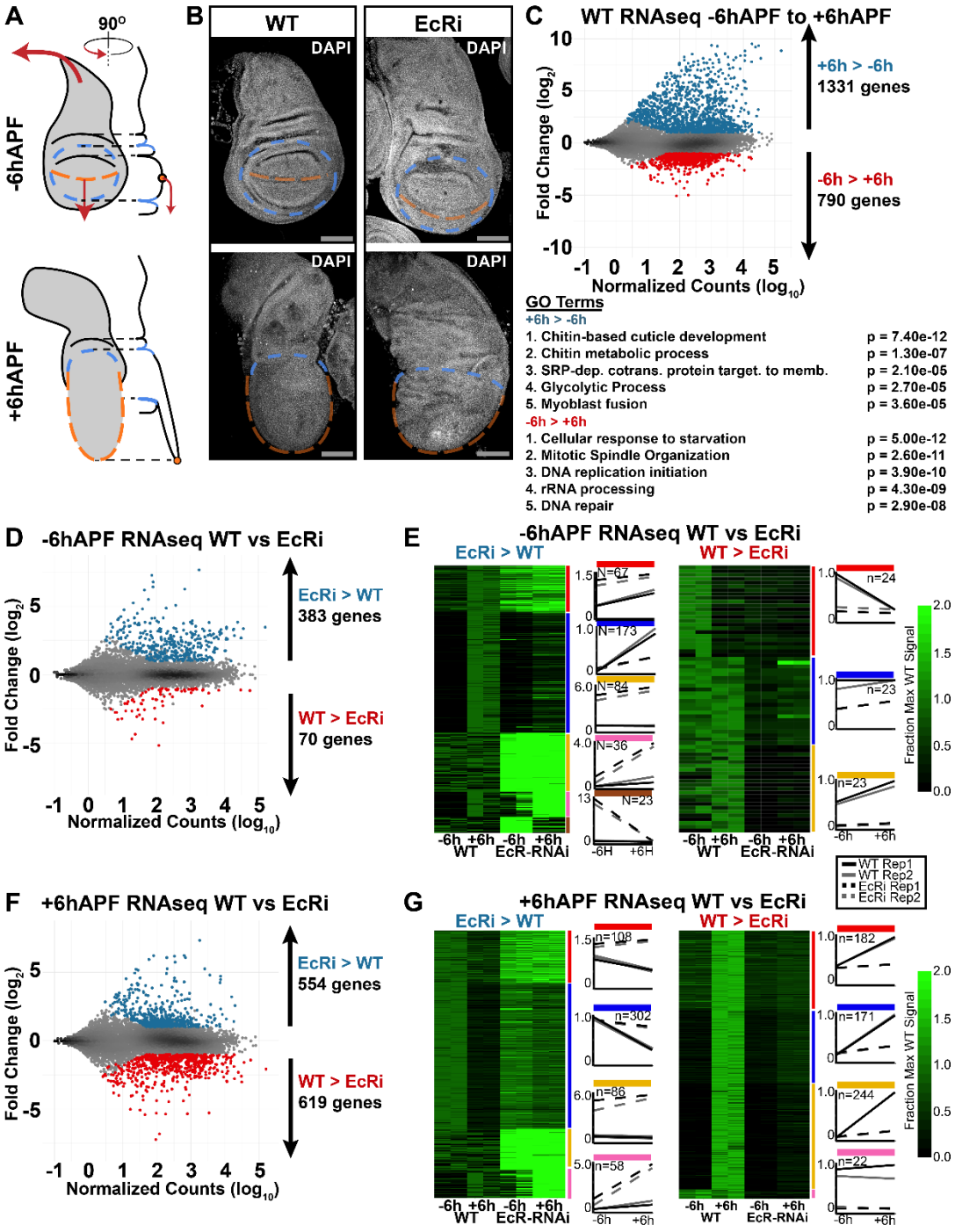
A
90°
-6hAPF
+6hAPF
B
WT
EcRi
DAPI
C
WT RNAseq -6hAPF to +6hAPF
Fold Change (log2)
Normalized Counts (log10)
+6h > -6h
1331 genes
-6h > +6h
790 genes
GO Terms
+6h > -6h
1. Chitin-based cuticle development p = 7.40e-12
2. Chitin metabolic process p = 1.30e-07
3. SRP-dep. cotrans. protein target. to memb. p = 2.10e-05
4. Glycolytic Process p = 2.70e-05
5. Myoblast fusion p = 3.60e-05
-6h > +6h
1. Cellular response to starvation p = 5.00e-12
2. Mitotic Spindle Organization p = 2.60e-11
3. DNA replication initiation p = 3.90e-10
4. rRNA processing p = 4.30e-09
5. DNA repair p = 2.90e-08
D
-6hAPF RNAseq WT vs EcRi
EcRi > WT
383 genes
WT > EcRi
70 genes
E
-6hAPF RNAseq WT vs EcRi
EcRi > WT
WT > EcRi
-6h +6h -6h +6h
WT EcR-RNAi
Fraction Max WT Signal
WT Rep1
WT Rep2
EcRi Rep1
EcRi Rep2
F
+6hAPF RNAseq WT vs EcRi
EcRi > WT
554 genes
WT > EcRi
619 genes
G
+6hAPF RNAseq WT vs EcRi
EcRi > WT
WT > EcRi

Figure 3.S1: EcR-RNAi knock down is effective and does not result in systemic developmental arrest

(A) WT and *vg-GAL4, UAS-FLP, tub>>STOP>>GAL4, UAS-GFP; UAS-EcR-RNAi* (hereafter EcR-RNAi) wings at –6hAPF. Activity of vg-GAL4 throughout the wing primordia causes flip-out of the STOP cassette, resulting in persistent GAL4 expression throughout the wing. Location of insets is indicated by dashed boxes. (B) Western blots of EcR and alpha-tubulin levels in WT and EcR-RNAi wings from a serial dilution of wing tissue. (C) Quantification of western blots normalized to alpha-tubulin expressed as the fraction of WT signal. (D) Legs from WT and EcR-RNAi legs at –6hAPF and +6hAPF. Scale bars are 100μm.

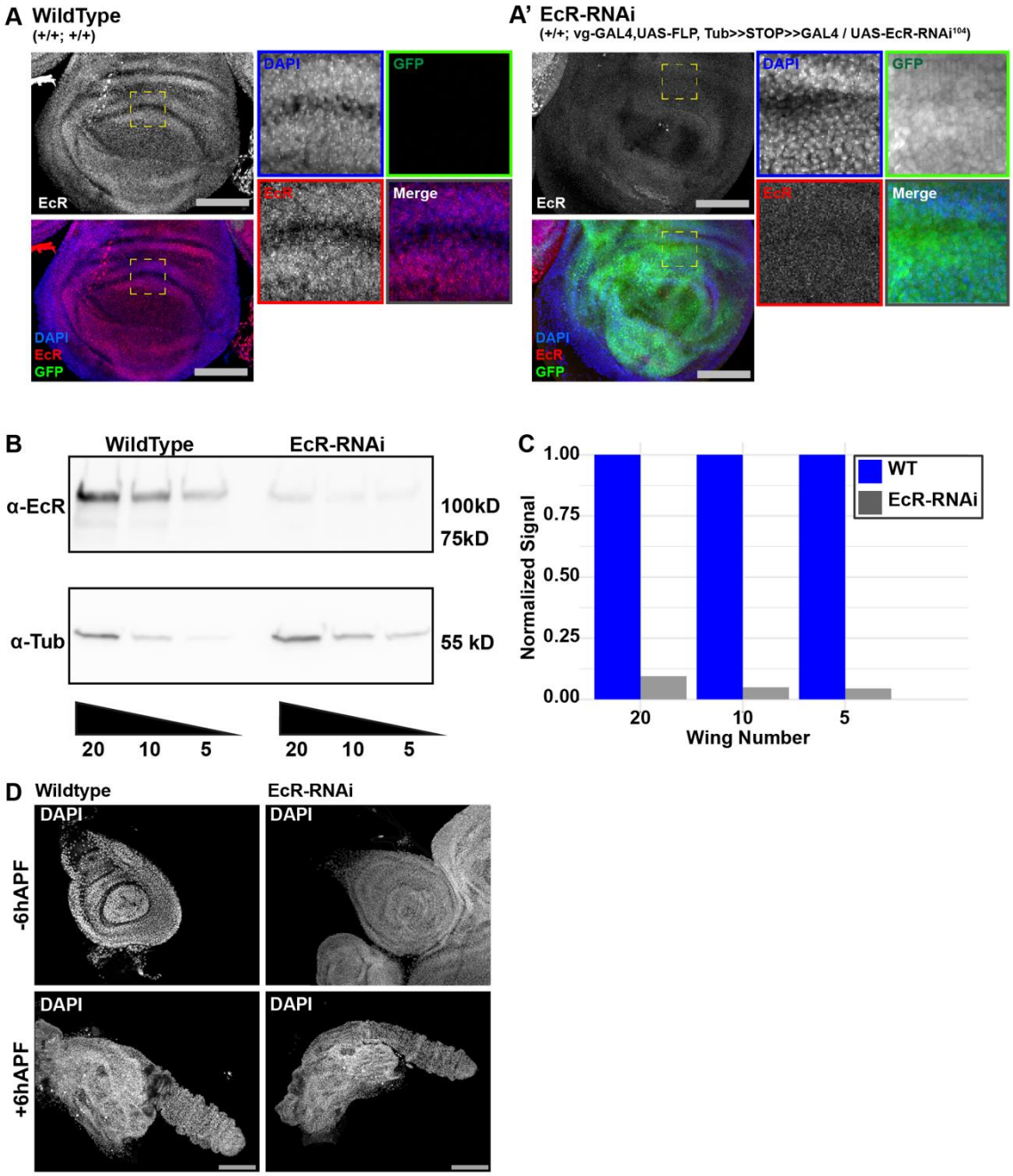
A WildType
(+/+; +/+)
A' EcR-RNAi
(+/+; vg-GAL4,UAS-FLP, Tub>>STOP>>GAL4 / UAS-EcR-RNAi104)
DAPI
GFP
EcR
Merge
B
WildType
EcR-RNAi
α-EcR
100kD
75kD
α-Tub
55 kD
20 10 5
20 10 5
C
Normalized Signal
1.00
0.75
0.50
0.25
0.00
WT
EcR-RNAi
20
10
5
Wing Number
D
Wildtype
EcR-RNAi
-6hAPF
+6hAPF
DAPI

Figure 3.S2: Comparison with Stoiber et al., 2016 (86).

(A) Venn diagrams depicting the overlap between WT –6hAPF to +6hAPF differentially expressed (DE) genes and those that respond to ecdysone in any cell line (left) or in any wing-derived cell line (right). Wing-derived cell lines are highlighted in blue in the bar plots. (B) Bar plot of the fraction of DE genes in WT wings between –6hAPF and +6hAPF that overlap a gene differentially expressed in response to ecdysone in each indicated cell line. (C-D) Venn diagrams and bar plots as in A-B for –6hAPF WT vs EcRi DE genes (D-E) Venn diagrams and bar plots as in A-B for +6hAPF WT vs EcRi DE genes.

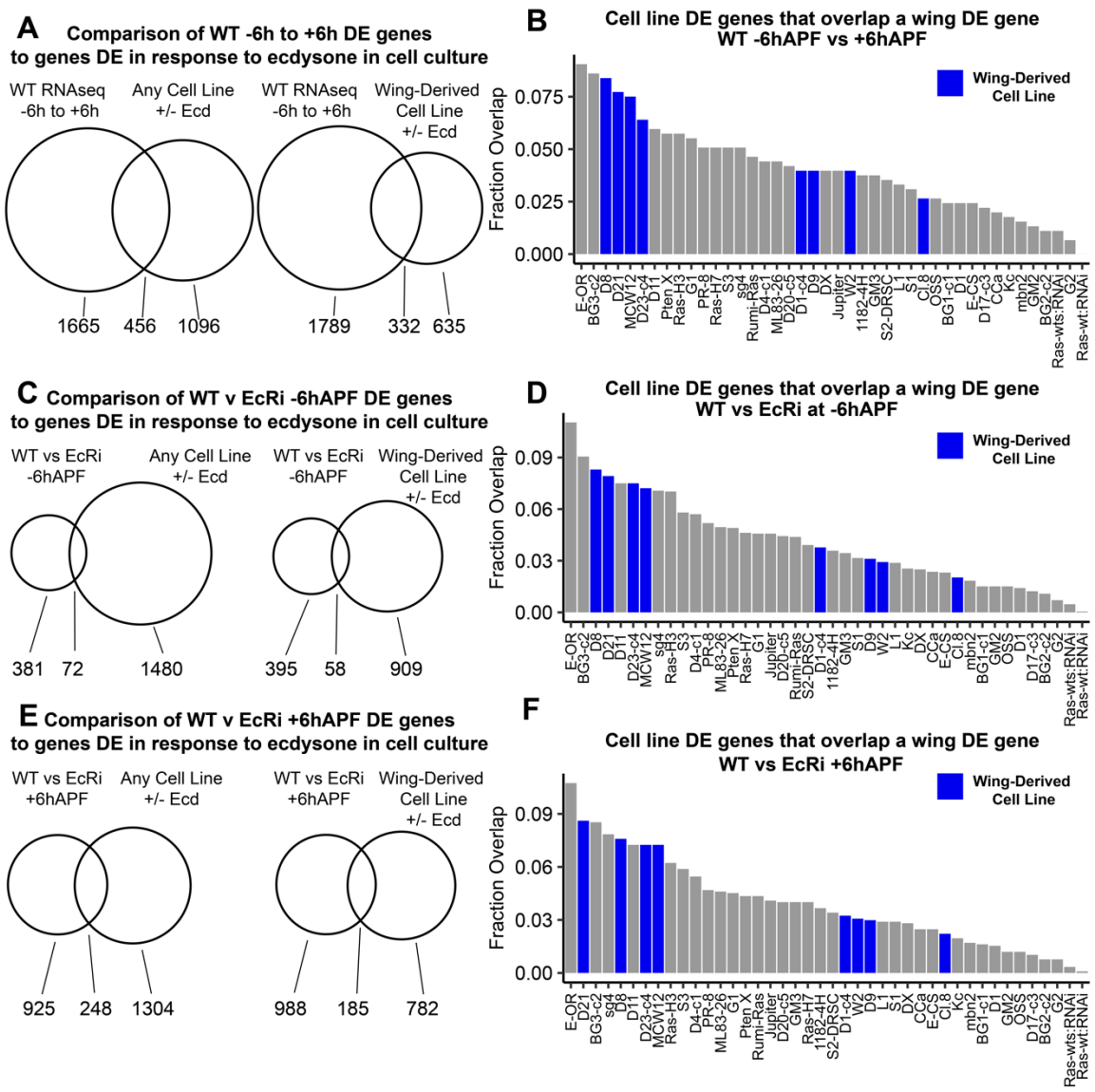
A
Comparison of WT -6h to +6h DE genes
to genes DE in response to ecdysone in cell culture
WT RNAseq
-6h to +6h
Any Cell Line
+/- Ecd
WT RNAseq
-6h to +6h
Wing-Derived
Cell Line
+/- Ecd
1665
456
1096
1789
332
635
B
Cell line DE genes that overlap a wing DE gene
WT -6hAPF vs +6hAPF
Wing-Derived
Cell Line
Fraction Overlap
0.075
0.050
0.025
0.000
E-OR
BG3-c2
D8
D21
MCW12
D23-c4
D11
Pten X
Ras-H3
G1
PR-8
Ras-H7
S3
sg4
Rumi-Ras
D4-c1
ML83-26
D20-c5
D1-c4
D9
DX
Jupiter
W2
1182-4H
GM3
S2-DRSC
L1
S1
Cl.8
OSS
BG1-c1
D1
E-CS
D17-c3
CCa
Kc
mbn2
GM2
BG2-c2
G2
Ras-wts:RNAi
Ras-wt:RNAi
C
Comparison of WT v EcRi -6hAPF DE genes
to genes DE in response to ecdysone in cell culture
WT vs EcRi
-6hAPF
Any Cell Line
+/- Ecd
WT vs EcRi
-6hAPF
Wing-Derived
Cell Line
+/- Ecd
381
72
1480
395
58
909
D
Cell line DE genes that overlap a wing DE gene
WT vs EcRi at -6hAPF
Wing-Derived
Cell Line
Fraction Overlap
0.09
0.06
0.03
0.00
E-OR
BG3-c2
D8
D21
D11
D23-c4
MCW12
sg4
Ras-H3
S3
D4-c1
PR-8
ML83-26
Pten X
Ras-H7
G1
Jupiter
D20-c5
Rumi-Ras
S2-DRSC
D1-c4
1182-4H
GM3
S1
D9
W2
L1
Kc
DX
CCa
E-CS
Cl.8
mbn2
BG1-c1
GM2
OSS
D1
D17-c3
BG2-c2
G2
Ras-wts:RNAi
Ras-wt:RNAi
E
Comparison of WT v EcRi +6hAPF DE genes
to genes DE in response to ecdysone in cell culture
WT vs EcRi
+6hAPF
Any Cell Line
+/- Ecd
WT vs EcRi
+6hAPF
Wing-Derived
Cell Line
+/- Ecd
925
248
1304
988
185
782
F
Cell line DE genes that overlap a wing DE gene
WT vs EcRi +6hAPF
Wing-Derived
Cell Line
Fraction Overlap
0.09
0.06
0.03
0.00
E-OR
D21
BG3-c2
sg4
D8
D11
D23-c4
MCW12
Ras-H3
S3
D4-c1
PR-8
ML83-26
G1
Pten X
Rumi-Ras
Jupiter
D20-c5
GM3
Ras-H7
1182-4H
S2-DRSC
D1-c4
W2
D9
L1
S1
DX
CCa
E-CS
Cl.8
Kc
mbn2
BG1-c1
D1
GM2
OSS
D17-c3
BG2-c2
G2
Ras-wts:RNAi
Ras-wt:RNAi

in–6hAPF wings); however, the overlap remained low overall. Cumulatively, only 16-21% of EcR-dependent genes in the wing were identified as ecdysone-responsive in any given cell line (Figure 3.S2C, E). Conversely, only 6-16% of ecdysone-responsive genes in any given cell line were identified as EcR-dependent in the wing (Figure 3.S2C, E). Thus, the transcriptional response to ecdysone is highly specific to both cell and developmental state.

EcR directly binds thousands of sites genome-wide

The experiments described above reveal that ecdysone triggers thousands of gene expression changes in wings during the larval-to-prepupal transition. Because ecdysone signaling initiates a cascade of transcription factor expression, it is unclear which of these changes are mediated directly by EcR. Therefore, we sought to determine the genome-wide DNA binding profiles of EcR in developing wings. For these experiments, we utilized a fly strain in which the endogenous EcR gene product has been epitope-tagged by a transposon inserted into an intron of EcR (184). This epitope tag is predicted to be incorporated into all EcR protein isoforms (hereafter EcR^{GFSTF}) (Figure 3.S3A). Genetic complementation tests determined that EcR^{GFSTF} flies are viable at the expected frequency (Figure 3.S3B), indicating that epitope-tagged EcR proteins are fully functional. Supporting this interpretation, western blotting demonstrated that EcR^{GFSTF} protein levels are equivalent to untagged EcR, and immunofluorescence experiments revealed nuclear localization of EcR^{GFSTF} as well as binding of EcR^{GFSTF} to DNA in polytene chromosome spreads (Figure 3.S3C-E).

To generate genome-wide DNA binding profiles for EcR, we performed CUT&RUN on –6hAPF wings (Figure 3.2A) from EcR^{GFSTF} flies. CUT&RUN provides similar genome-

wide DNA binding information for transcription factors as ChIP-seq, but requires fewer cells as input material (185), making it useful for experiments with limiting amounts of tissue. Our EcR CUT&RUN data exhibit features that are similar to those previously reported for other transcription factors, including greater DNA-binding site resolution relative to ChIP-seq (Figure 3.S4, S8). Wing CUT&RUN profiles at –6hAPF reveal that EcR binds extensively throughout the genome (Figure 3.2). Many EcR binding sites localize to canonical ecdysone target genes, including broad, Eip93F, Hr3, Hr4 and Eip75B (Figure 3.2A). Surprisingly, we also observed EcR binding to many genes that have not previously been categorized as ecdysone targets, including homothorax, Delta, Actin 5C, Stubble and crossveinless-c (Figure 3.2B). Thus, EcR binds widely across the genome in wing imaginal discs. The widespread binding of EcR observed here contrasts with previous genome-wide DNA binding profiles obtained for EcR. For example, ChIP-seq profiles from S2 cells and DamID profiles from Kc167 cells identified 500-1000 binding sites (90, 130). By contrast, our findings demonstrate that EcR binds both canonical and non-canonical ecdysone-target genes, raising the question as to whether EcR directly contributes to a wing-specific transcriptional program.

In addition to widespread DNA binding, we also observed clustering of EcR binding sites in the genome. EcR peaks are significantly closer to one another than expected by chance (Figure 3.S5A-C), and a large fraction of peaks are located within 5kb of an adjacent peak (Figure 3.S5D). In particular, canonical ecdysone target genes often exhibit clusters of EcR binding (Figure 3.S5E-F). These findings suggest that EcR often binds multiple cis-regulatory elements across target gene loci, consistent with the observed clustering of ecdysone-responsive enhancers in S2 cells (130).

Figure 3.S3: The EcR^{GFSTF} tag does not impair EcR function

(A) Schematic of the *EcR*^{GFSTF} line generated by the *Drosophila* Gene Disruption Project (157, 184, 186). The line was generated through integration of a *Minos* transposon into a coding intron of the *EcR* locus. Subsequently, recombination-mediated cassette exchange was used to create an EcR protein trap containing the GFSTF tag (184, 186). The structure and size of the tag is indicated below the gene models. The insertion point is upstream of all exons shared between EcR isoforms and downstream of all isoform-specific exons. (B) Viability assay of *EcR*^{GFSTF} animals crossed to a deficiency spanning the EcR locus. Statistical significance was determined using a chi-squared test with an expected ratio of 1:2 homozygous to heterozygous animals. (C) Western blots of wings from *EcR*^{GFSTF} or *WT* animals stained for EcR or EcR^{GFSTF} (anti-GFP). EcR isoforms A/B1 and B2 are predicted to be ~150kD and ~125kD when the EcR^{GFSTF} tag is incorporated, respectively. The western blot indicates both the 150kD and 125kD isoforms are trapped, and relative isoform abundance is maintained. (D) Immunostaining for EcR^{GFSTF} (anti-FLAG) shows nuclear localization in wings. Scale bars are 50µm (E) Polytene squashes from *WT* or *EcR*^{GFSTF} indicate EcR^{GFSTF} binds DNA. Scale bars are 25µm. Dashed boxes indicate the location of insets.

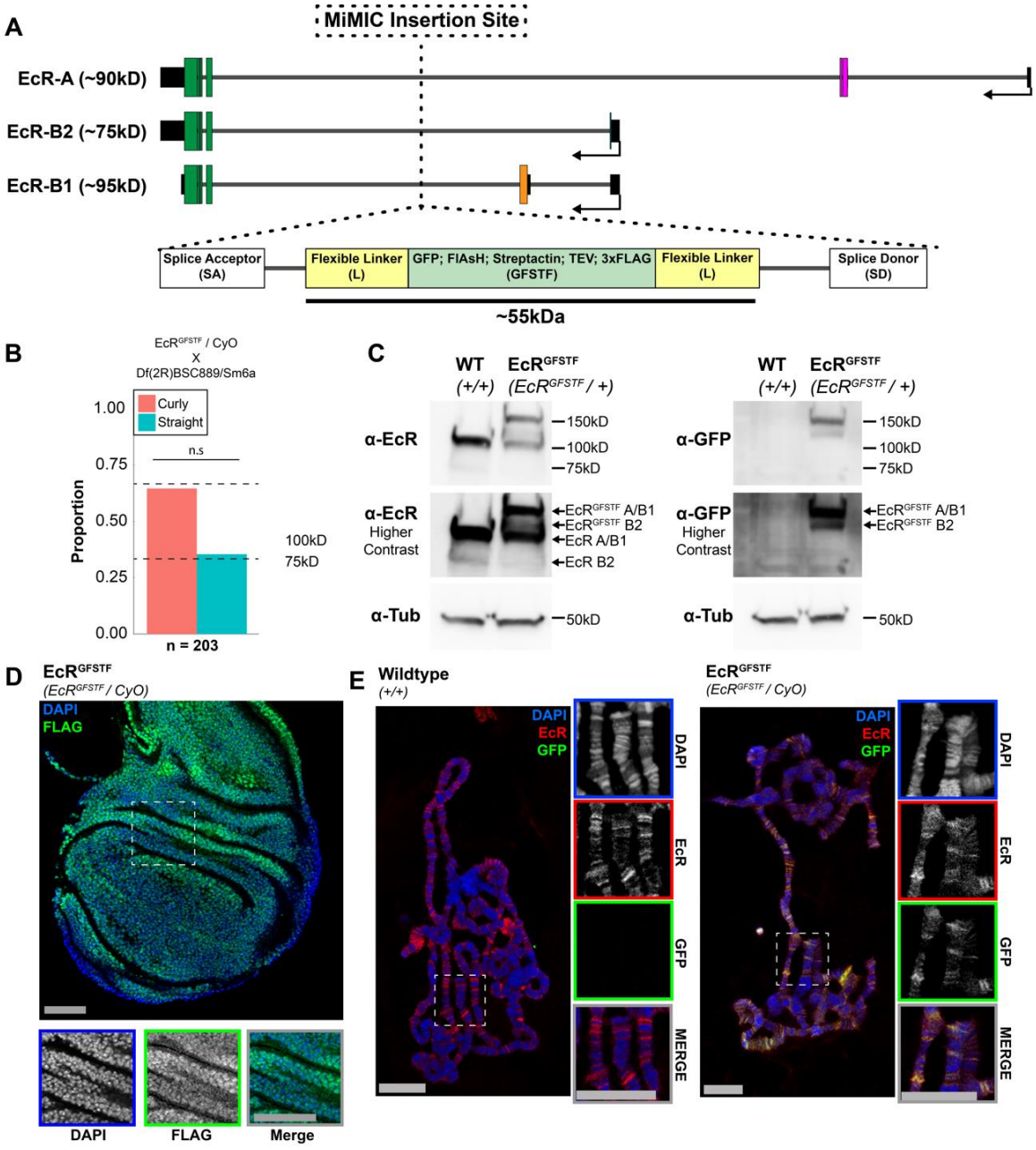
A
MiMIC Insertion Site
EcR-A (~90kD)
EcR-B2 (~75kD)
EcR-B1 (~95kD)
Splice Acceptor (SA)
Flexible Linker (L)
GFP; FlAsH; Streptactin; TEV; 3xFLAG (GFSTF)
Flexible Linker (L)
Splice Donor (SD)
~55kDa
B
EcRGFSTF / CyO
X
Df(2R)BSC889/Sm6a
Curly
Straight
n.s
Proportion
1.00
0.75
0.50
0.25
0.00
n = 203
100kD
75kD
C
WT (+/+)
EcRGFSTF (EcRGFSTF / +)
α-EcR
150kD
100kD
75kD
α-EcR Higher Contrast
EcRGFSTF A/B1
EcRGFSTF B2
EcR A/B1
EcR B2
α-Tub
50kD
α-GFP
D
EcRGFSTF
(EcRGFSTF / CyO)
DAPI
FLAG
DAPI
FLAG
Merge
E
Wildtype
(+/+)
EcRGFSTF
(EcRGFSTF / CyO)
DAPI
EcR
GFP
MERGE

Figure 3.S4: EcR CUT&RUN exhibits similar properties to those that have been previously reported

(A) Histograms of fragment sizes from EcR CUT&RUN. (B) Cumulative distribution plot of fragment sizes. (C) Representative browser shots comparing EcR C&R signal from 20-120bp fragments and 150-700bp. (D) Average signal plots of EcR C&R signal split by overlap with annotated promoters and fragment size.

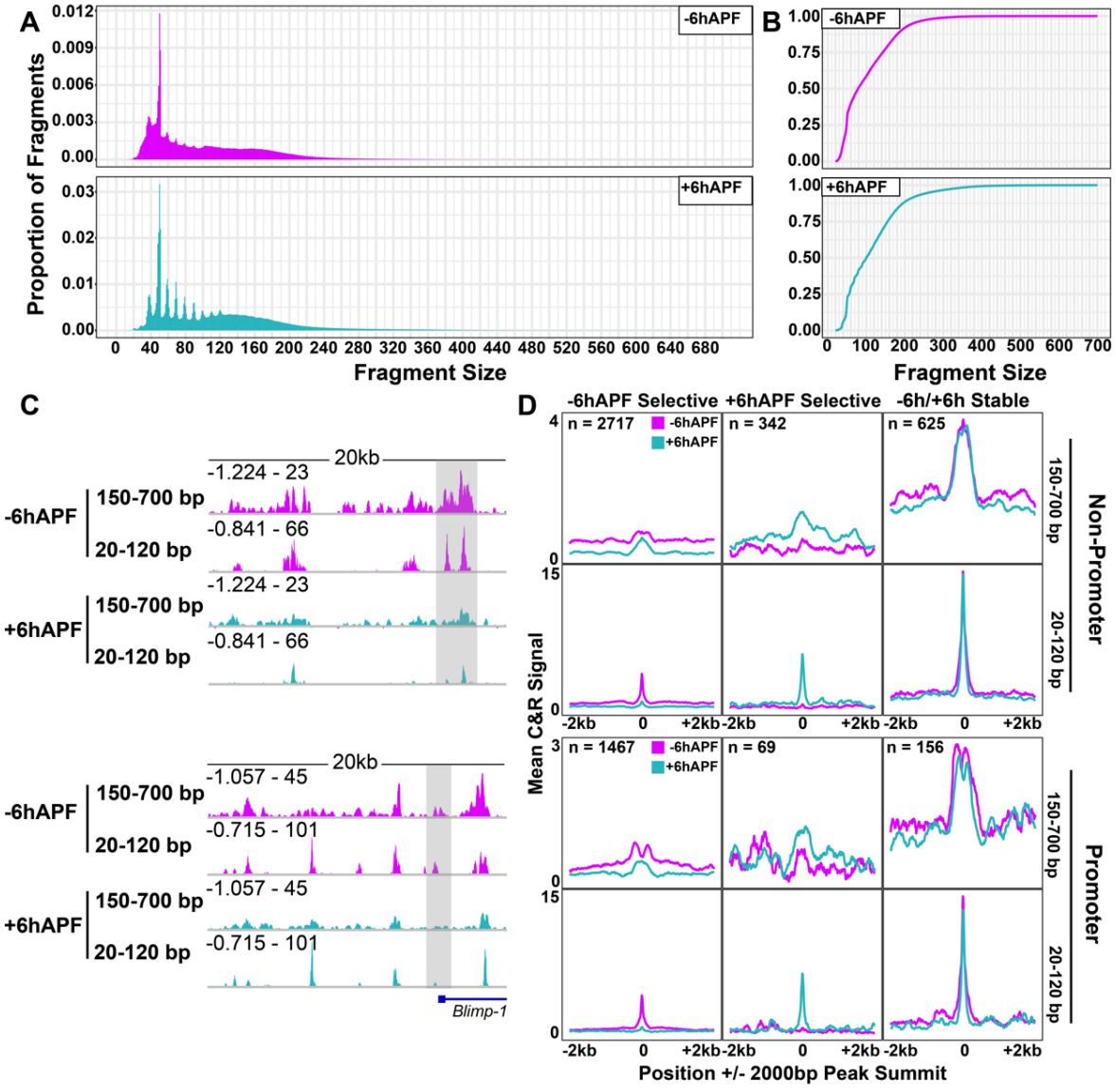

Figure 3.2: EcR binds extensively throughout the genome

Browser shots of EcR CUT&RUN signal (z-score) at –6hAPF and +6hAPF at (A) canonical and (B) non-canonical ecdysone response genes. Signal range is indicated in top-left corner. Shaded areas correspond to EcR peaks.

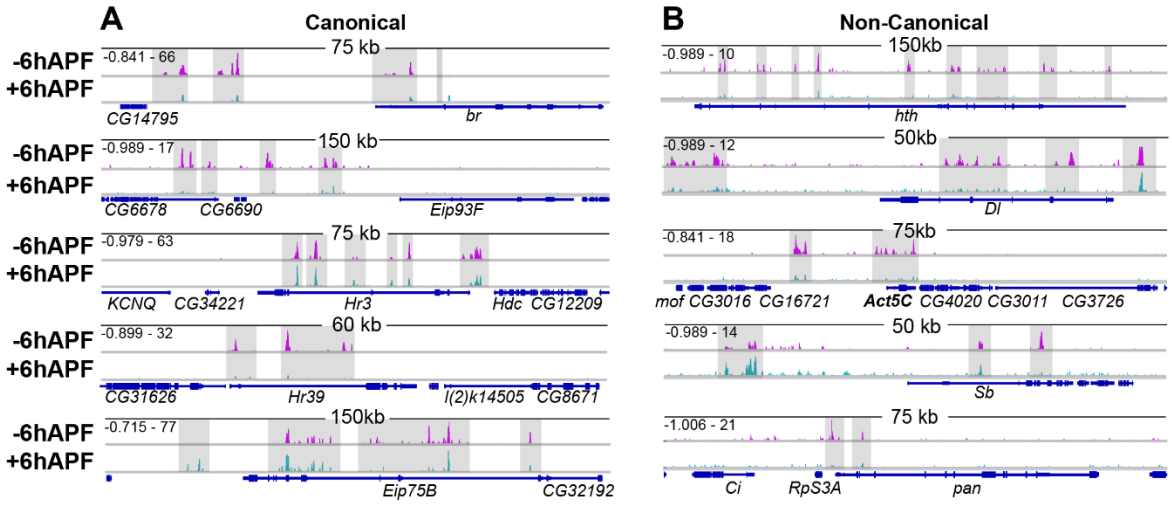

Figure 3.S5: EcR peaks are clustered genome-wide

(A) Histograms of distance of each EcR peak to its nearest neighbor compared to a peak set shuffled over FAIRE peaks. (B) Cumulative distribution plots of the distance of each EcR peak to its nearest neighbor compared to shuffled peaks. Distributions were compared with a KS-test. (C) The mean number of peaks that overlap at least one other peak using different sizes of EcR peak. Peaks within 5kb (arrow) of each other were merged into a single cluster for subsequent analyses. (D) Numbers of EcR peaks that fall into a cluster at –6hAPF and +6hAPF. (E) Examples of EcR clusters. (F) Numbers of canonical ecdysone-response genes that overlap an EcR cluster and those that only overlap an EcR singleton (i.e., non-clustered peak) compared to clusters or singletons shuffled over open chromatin peaks. A list of canonical ecdysone response genes was generated by taking the union set of genes in gene ontology terms: Cellular response to ecdysone (GO:0071390); Steroid hormone mediated signaling pathway (GO:0043401) and appending all “Eip” (ecdysone induce protein) and “Imp” genes (40 total, see Table 3.S3).

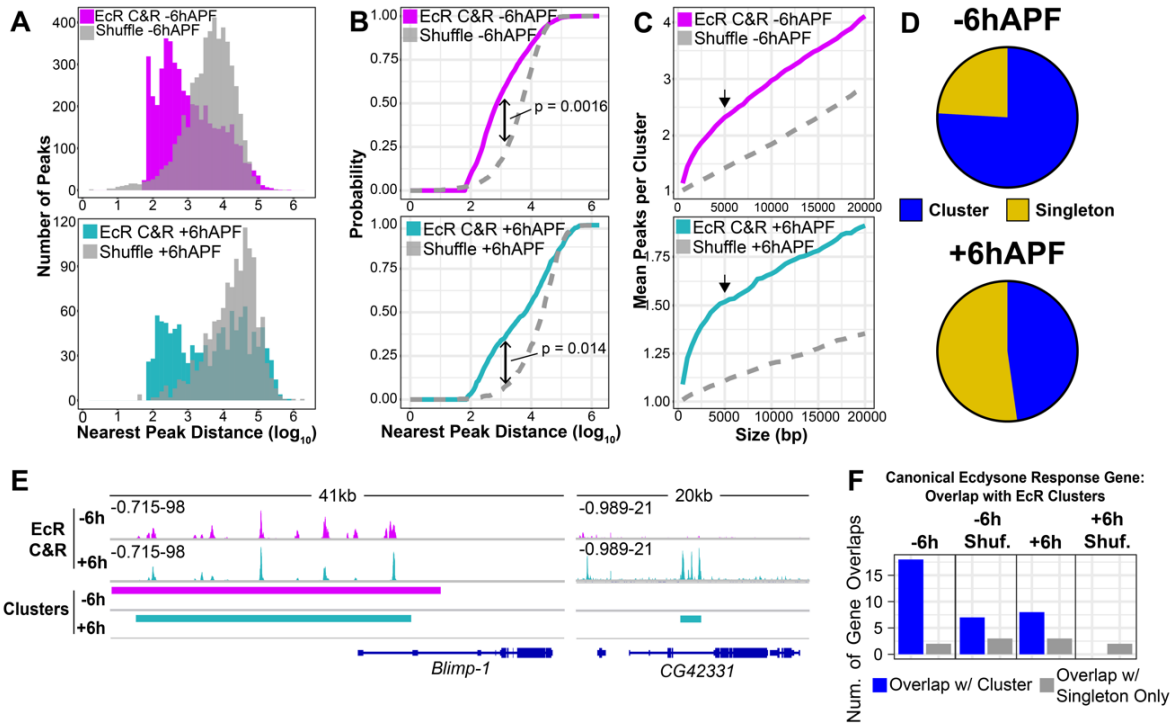
A
EcR C&R -6hAPF
Shuffle -6hAPF
EcR C&R +6hAPF
Shuffle +6hAPF
Number of Peaks
Nearest Peak Distance (log10)
B
Probability
p = 0.0016
p = 0.014
C
Mean Peaks per Cluster
Size (bp)
D
-6hAPF
Cluster
Singleton
+6hAPF
E
41kb
20kb
-0.715-98
-0.989-21
EcR C&R
-6h
+6h
Clusters
Blimp-1
CG42331
F
Canonical Ecdysone Response Gene:
Overlap with EcR Clusters
-6h
-6h Shuf.
+6h
+6h Shuf.
Num. of Gene Overlaps
Overlap w/ Cluster
Overlap w/ Singleton Only

EcR binding is temporally-dynamic

To understand the role of EcR binding in temporal progression of wing development, we performed CUT&RUN on +6hAPF wings (Figure 3.2, 3A). Similar to our findings from –6hAPF wings, we found that EcR binds widely across the genome at +6hAPF. Interestingly, there is a global decrease in the number of sites occupied by EcR over time: a total of 4,967 EcR peaks are called at –6hAPF, whereas 1,174 EcR peaks are called at +6hAPF (Figure 3.3B). While many of

the +6hAPF binding sites overlap with –6hAPF binding sites (763 peaks, 65%) (hereafter –6h/+6h stable binding sites), we also identified 411 peaks that are specific to the +6hAPF time. Similar to –6hAPF peaks, +6hAPF EcR peaks are clustered genome-wide (Figure 3.S5). Thus, the larval-to-prepupal transition in wings is marked by both a decrease in EcR occupancy at the majority of its –6hAPF binding sites, as well as an increase in EcR occupancy at hundreds of new binding sites. It is notable that many differences in EcR binding between –6hAPF and +6hAPF reflect quantitative rather than binary changes in CUT&RUN signal. Many peaks specific to –6hAPF exhibit low-level CUT&RUN signal at +6hAPF (and vice versa). Among other explanations, this suggests the propensity of EcR to occupy target DNAs is modulated over developmental time.

To investigate the potential biological significance of temporal changes in EcR occupancy, we separated EcR peaks into three categories: –6hAPF-selective, +6hAPF-selective, and –6h/+6h stable. Gene annotation enrichment analysis identified genes involved in imaginal disc-derived wing morphogenesis as the top term for each binding site category (Table 3.S4), indicating that EcR may directly regulate genes involved in wing development at both of these developmental stages. Interestingly, we found that the amplitude of EcR

CUT&RUN signal is greater at –6h/+6h stable binding sites relative to temporal-selective binding sites (Figure 3.3C). To investigate the potential basis for the difference in binding intensity, we examined the DNA sequence within each class of EcR binding site. Nuclear receptors such as EcR/Usp bind palindromic motifs, with each binding partner recognizing a nearly identical 7-bp half-site (76) (Figure 3.S6). For some nuclear receptors, the orientation and spacing of these half-sites can vary. De novo motif discovery analysis revealed the presence of the EcR half-site in each of the three peak categories (Figure 3.3D, Figure 3.S6A). De novo searches for longer motifs identified the palindromic motif in –6h/+6h stable and +6hAPF-selective peaks (Figure 3.3D, 3.S6A-B). We did not detect variations in the orientation or spacing of half-sites, indicating that when the full palindrome is present, it preferentially exists in a 13-bp inverted repeat conformation. To determine if differences in signal amplitude between –6h/+6h stable EcR binding sites could be caused by differences in motif content, we examined motif density around peak summits within each of the three binding site categories for the EcR and Usp half-sites, as well as for the EcR/Usp palindromic motif. On average, we observed a positive correlation between motif density and CUT&RUN signal amplitude, with –6hAPF temporal-selective binding sites having both the lowest motif density and lowest signal amplitude, and –6h/+6h stable binding sites having both the highest motif density and highest signal amplitude (Figure 3.3E, 3.S6C). Furthermore, the average motif strength (i.e., the extent to which the motif matches the consensus EcR half-site) in –6h/+6h stable binding sites was also significantly higher (Figure 3.3F). We observed a similar relationship in the +6hAPF-selective binding sites, which exhibit both intermediate CUT&RUN signal and intermediate motif content (Figure 3.3E, 3.S6C). These data are consistent with a model in which EcR remains stably bound to target

Figure 3.3: EcR binding is temporally-dynamic

(A) Browser shots of EcR CUT&RUN data from –6hAPF and +6hAPF wings, with examples of –6hAPF-selective, +6hAPF-selective and –6h/+6h stable peaks highlighted by colored boxes. (B) Venn diagrams showing the number of peaks in each category. (C) Heatmaps and average signal plots of EcR C&R signal (z-score). (D) Sequence logos comparing the canonical EcR/Usp binding motif to the EcR half-site PWM and EcR motifs identified through *de novo* motif analysis. (E) Motif density plots of the number of EcR motifs around the peak summit using the EcR half-site PWM. For –6h/+6h stable peaks, the peak summit for +6h was used. (F) Violin plots showing the average motif strength ($-\log_{10}$ p-value) of motifs within EcR peaks (*** p-value < 0.001, students t-test).

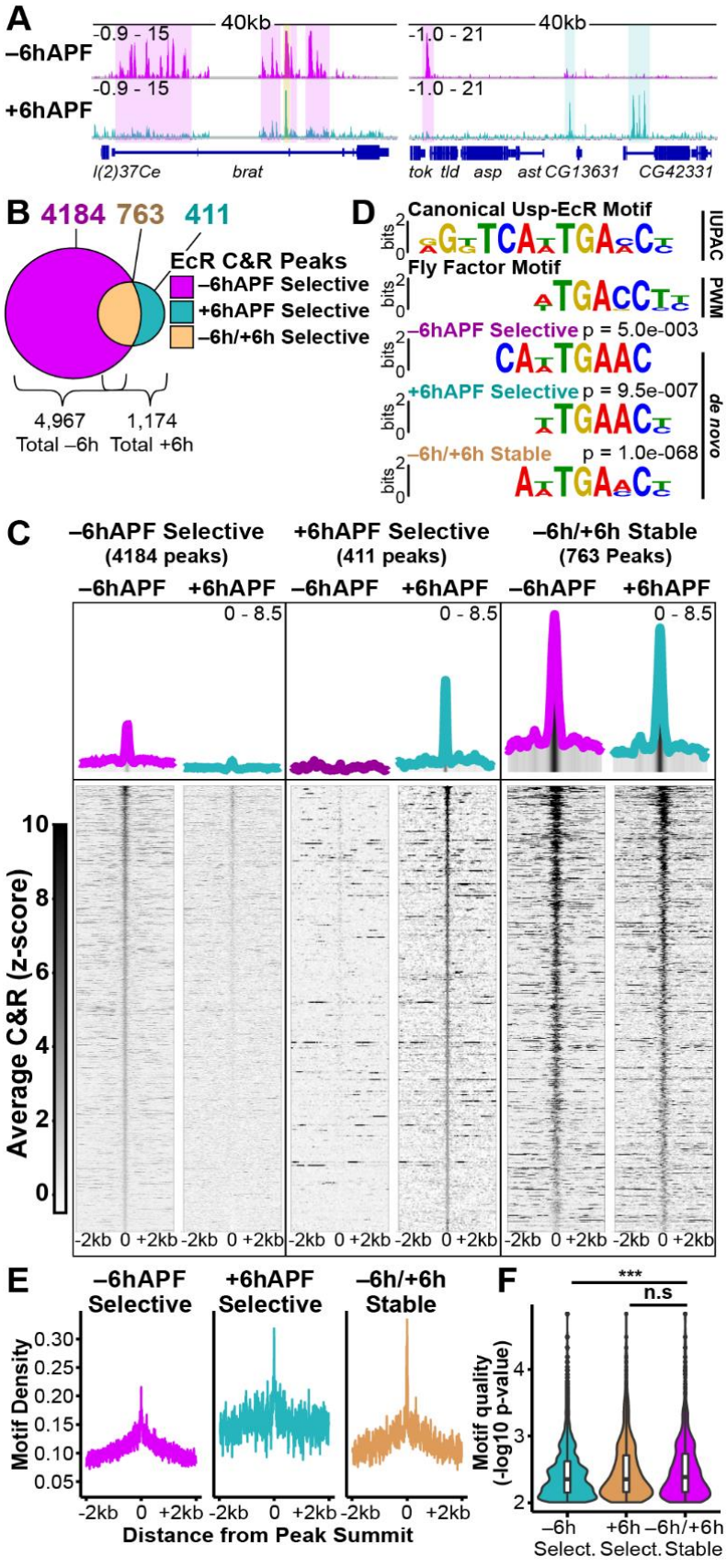
A
–6hAPF
+6hAPF
-0.9 - 15
-0.9 - 15
40kb
-1.0 - 21
-1.0 - 21
40kb
l(2)37Ce
brat
tok tld asp ast CG13631 CG42331
B 4184 763 411
EcR C&R Peaks
–6hAPF Selective
+6hAPF Selective
–6h/+6h Selective
4,967
Total –6h
1,174
Total +6h
D
Canonical Usp-EcR Motif
IUPAC
Fly Factor Motif
PWM
–6hAPF Selective p = 5.0e-003
+6hAPF Selective p = 9.5e-007
–6h/+6h Stable p = 1.0e-068
de novo
bits
C
–6hAPF Selective
(4184 peaks)
+6hAPF Selective
(411 peaks)
–6h/+6h Stable
(763 Peaks)
–6hAPF +6hAPF –6hAPF +6hAPF –6hAPF +6hAPF
0 - 8.5
Average C&R (z-score)
10
8
6
4
2
0
-2kb 0 +2kb
E
–6hAPF Selective
+6hAPF Selective
–6h/+6h Stable
Motif Density
0.30
0.25
0.20
0.15
0.10
0.05
Distance from Peak Summit
F
***
n.s
Motif quality (-log10 p-value)
–6h Select.
+6h Select.
–6h/+6h Stable

Figure 3.S6: Motifs identified in EcR binding sites

(A) A full list of *de novo* motifs identified by DREME. (B) The top seven *de novo* motifs identified by MEME. For *de novo* motif identification, +/- 200bp from peak summit was used (see methods for details). Stars denote matches to the EcR motif or the EcR/Usp palindrome. (C) Motif density plots around the summits of EcR binding sites using motifs identified by bacterial 1-hybrid (67).The canonical motif was generated by combining the EcR and Usp PWMs together.

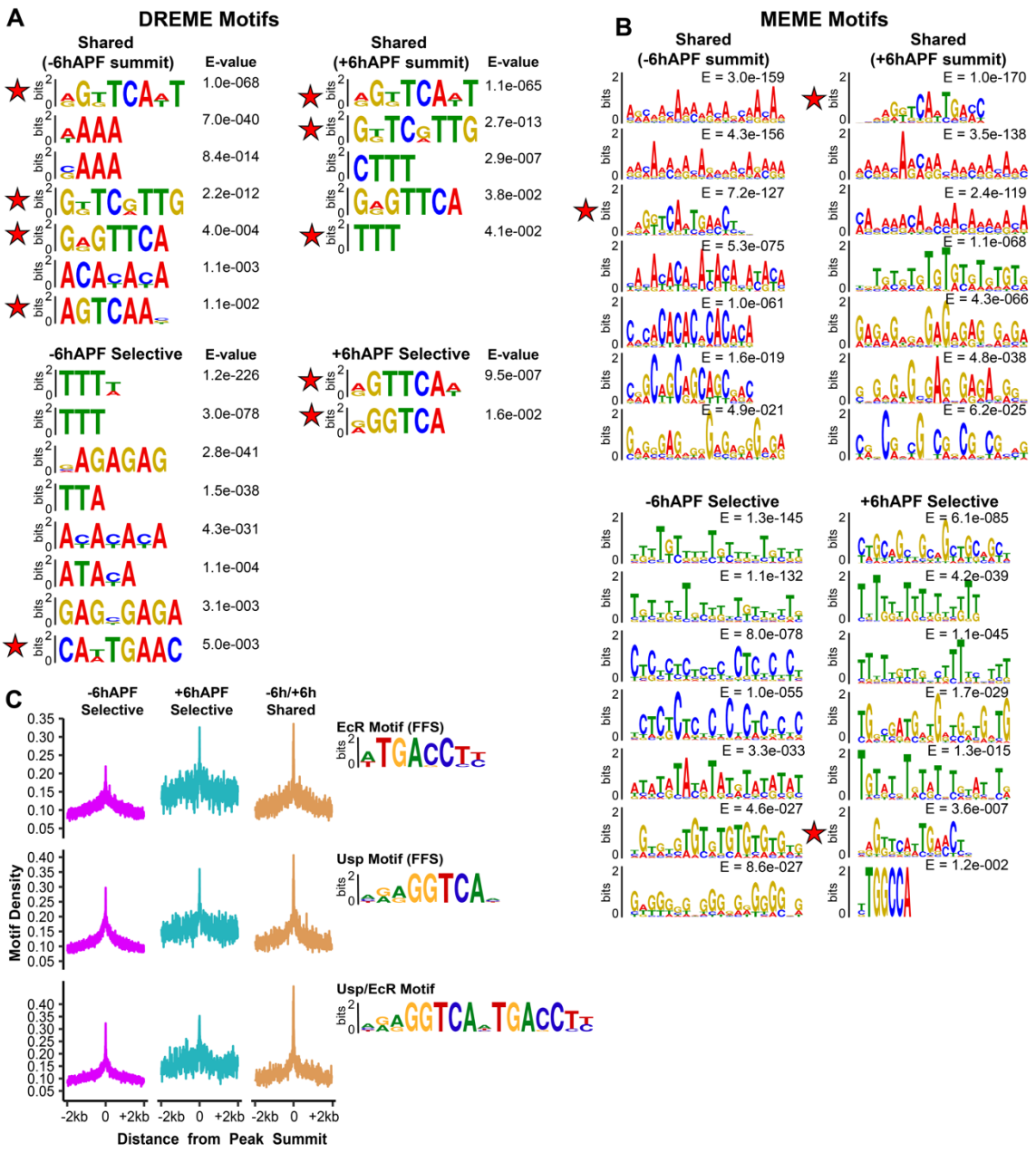
A
DREME Motifs
Shared (-6hAPF summit)
E-value
1.0e-068
7.0e-040
8.4e-014
2.2e-012
4.0e-004
1.1e-003
1.1e-002
Shared (+6hAPF summit)
E-value
1.1e-065
2.7e-013
2.9e-007
3.8e-002
4.1e-002
-6hAPF Selective
E-value
1.2e-226
3.0e-078
2.8e-041
1.5e-038
4.3e-031
1.1e-004
3.1e-003
5.0e-003
+6hAPF Selective
E-value
9.5e-007
1.6e-002
B
MEME Motifs
Shared (-6hAPF summit)
E = 3.0e-159
E = 4.3e-156
E = 7.2e-127
E = 5.3e-075
E = 1.0e-061
E = 1.6e-019
E = 4.9e-021
Shared (+6hAPF summit)
E = 1.0e-170
E = 3.5e-138
E = 2.4e-119
E = 1.1e-068
E = 4.3e-066
E = 4.8e-038
E = 6.2e-025
-6hAPF Selective
E = 1.3e-145
E = 1.1e-132
E = 8.0e-078
E = 1.0e-055
E = 3.3e-033
E = 4.6e-027
E = 8.6e-027
+6hAPF Selective
E = 6.1e-085
E = 4.2e-039
E = 1.1e-045
E = 1.7e-029
E = 1.3e-015
E = 3.6e-007
E = 1.2e-002
C
-6hAPF Selective
+6hAPF Selective
-6h/+6h Shared
EcR Motif (FFS)
Usp Motif (FFS)
Usp/EcR Motif
Motif Density
-2kb 0 +2kb
Distance from Peak Summit

sites with high motif density and strength. Conversely, the lower motif content within temporal-selective peaks suggests EcR may rely on cooperative interactions with other transcription factors to assist binding at these sites.

In addition to motif content, we considered the possibility that temporal changes in EcR DNA-binding profiles may be a consequence of temporal changes in EcR protein isoform expression. There are three EcR protein isoforms which share the same DNA-binding domain but differ in their N-terminal domains, allowing them to differentially interact with cofactors (85, 94). The relative isoform abundance varies between tissues and developmental stages. To investigate whether changes in EcR isoform abundance could explain temporal changes in EcR DNA binding, we performed western blots using isoform-specific antibodies. Consistent with prior studies (96), we found that EcR-A is the predominant isoform expressed in wing imaginal discs (Figure 3.S3, 3.S7A). EcR-B1 is also detected, and EcR-B2 is expressed at low levels. Importantly, we observed no relative changes in EcR isoform abundance between –6hAPF and +6hAPF, nor did we observe a change in the overall levels of EcR over time (Figure 3.S7A). Therefore, we conclude that changes in EcR isoform expression are not responsible for the observed changes in EcR binding profiles between –6hAPF and +6hAPF in the wing.

EcR binding is tissue-specific

The results described above indicate that EcR binds extensively across the genome, including to many genes with wing-specific function, thus raising the question as to whether EcR binding is tissue-specific. To address this question, we first examined loci that had been previously determined to contain functional EcR binding sites by in vitro DNA binding and

in vivo reporter assays (65, 69, 112). Many of these sites, including the glue genes Sgs3, Sgs7 and Sgs8, the fat body protein Fbp1, and the oxidative response gene Eip71CD, show no evidence of EcR binding in wings (Figure 3.S8), supporting the finding that EcR binds target sites in a tissue-specific manner. To examine this question more globally, we compared our wing CUT&RUN data to EcR ChIP-seq data from Drosophila S2 cells (Figure 3.4A). Overall, a small fraction of wing EcR binding sites overlap an EcR binding site in S2 cells (Figure 3.4B, C). However, among the sites that are shared between wings and S2 cells, there is marked enrichment of overlap with –6h/+6h stable wing binding sites. Whereas only 0.1% of –6hAPF-selective binding sites (41 peaks) and 2% of +6hAPF-selective binding sites (9 peaks) overlap an S2 cell EcR binding site, 16% of –6h/+6h stable binding sites (122 peaks) overlap an S2 cell EcR binding site. Thus, binding sites to which EcR is stably bound over time in developing wings are more likely to be shared with EcR binding sites in other cell types, relative to temporal-selective EcR binding sites in the wing.

To investigate potential differences in target gene function between wing-specific binding sites and those shared with S2 cells, we performed gene annotation enrichment analysis on genes near EcR binding sites. This analysis revealed steroid hormone-mediated signaling pathway as the most significant term for genes overlapping an EcR peak in both wings and S2 cells (Figure 3.4D). Genes annotated with this term include canonical ecdysone-responsive genes, such as Eip78C, Hr39 and usp. By contrast, imaginal disc-derived wing morphogenesis was identified as the top term for genes near wing-specific EcR binding sites, similar to our findings from above. These data indicate that EcR binding sites that are shared by wings and S2 cells tend to occur at canonical ecdysone target genes, whereas wing-specific EcR binding sites tend to occur at genes with wing-specific functions.

Together, these data suggest EcR plays a direct role in mediating the distinct gene expression responses to ecdysone exhibited by different cell types (86).

EcR regulates the temporal activity of an enhancer for broad, a canonical ecdysone target gene

The results described above indicate that EcR binds to both canonical and non-canonical ecdysone target genes in the wing, and that EcR is required for temporal progression of wing transcriptional programs. We next sought to examine the relationship between EcR binding in the genome and regulation of gene expression. Because EcR both activates and represses target gene expression, we grouped all differentially expressed genes together and counted the proportion of genes that overlap an EcR binding cluster Figure 3.S9A-C). We observed an enrichment of EcR binding sites near genes that are differentially expressed in EcR-RNAi wing at both –6hAPF and +6hAPF and a depletion of EcR binding sites near genes that are either temporally-static or not expressed (Figure 3.S9A-C). These correlations support a direct role for EcR in regulating temporal changes in gene expression during the larval-to-prepupal transition.

To obtain a more direct readout of EcR's role in target gene regulation, we investigated whether EcR binding contributes to control of enhancer activity. We first examined the potential regulation of a canonical ecdysone target gene. The broad complex (br) encodes a transcription factor required for the larval-to-prepupal transition in wings and other tissues (Figure 3.5A) (99, 107). Br has been characterized as a canonical ecdysone target gene that is induced early in the transcriptional response upon release of hormone (99,

187). In wing imaginal discs, Br protein levels are uniformly low in early 3rd instar larvae, and by

Figure 3.S7: EcR isoforms levels over time

(A) Western blots depicting levels of EcR levels at –6hAPF and +6hAPF using isoform specific antibodies (EcR-A and EcR-B1) and an antibody that recognizes all EcR isoforms (EcR-core). Quantification of the core was performed by separately quantifying the top band, corresponding to EcR-A/B1, and the bottom band, corresponding to EcR-B2. The signal was normalized to tubulin. (B) Schematic of the EcR locus indicating exons shared between all isoforms (grey), exons specific to EcR-B1 (green), exons shared between EcR-B1 and EcR-B2 (yellow) and exons specific to EcR-A (pink). Note that EcR-A contains alternative 5'UTRs that do not affect the protein coding sequence. (C) Proportion of each exon type present at each time point. Exon counts were normalized to length.

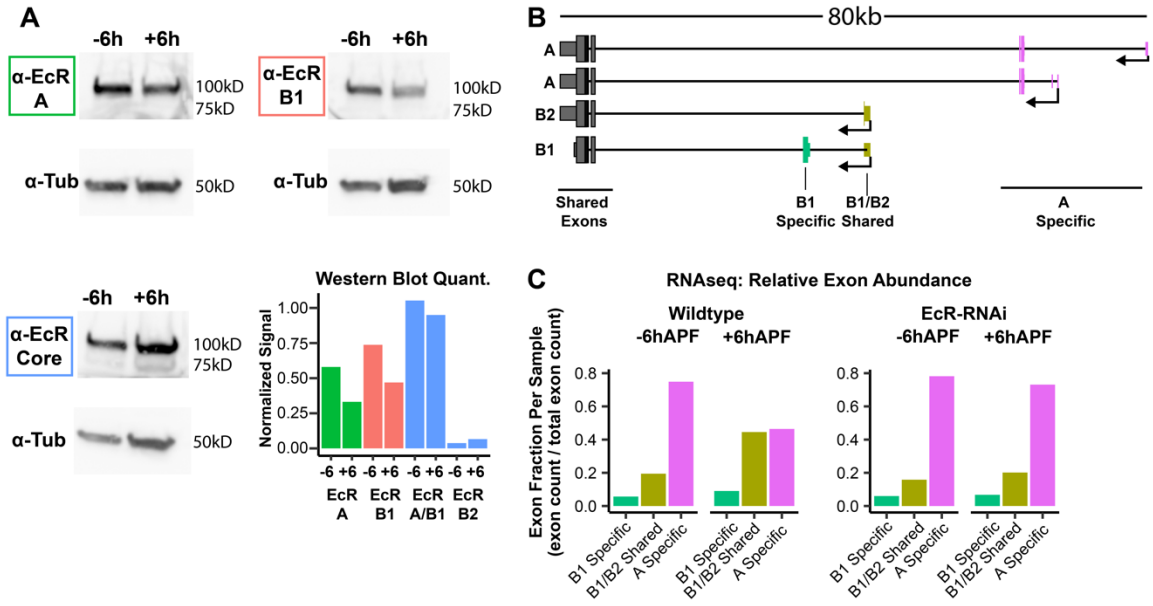

Figure 3.S8: EcR binding is absent in wings and S2 cells from many sites previously identified as functional EcR binding sites in other tissues

(A) Browser shots showing EcR C&R signal and S2 ChIPseq (130) at previously identified EcR binding sites. (B) Browser shots comparing precision of EcR binding between EcR and S2 cells.

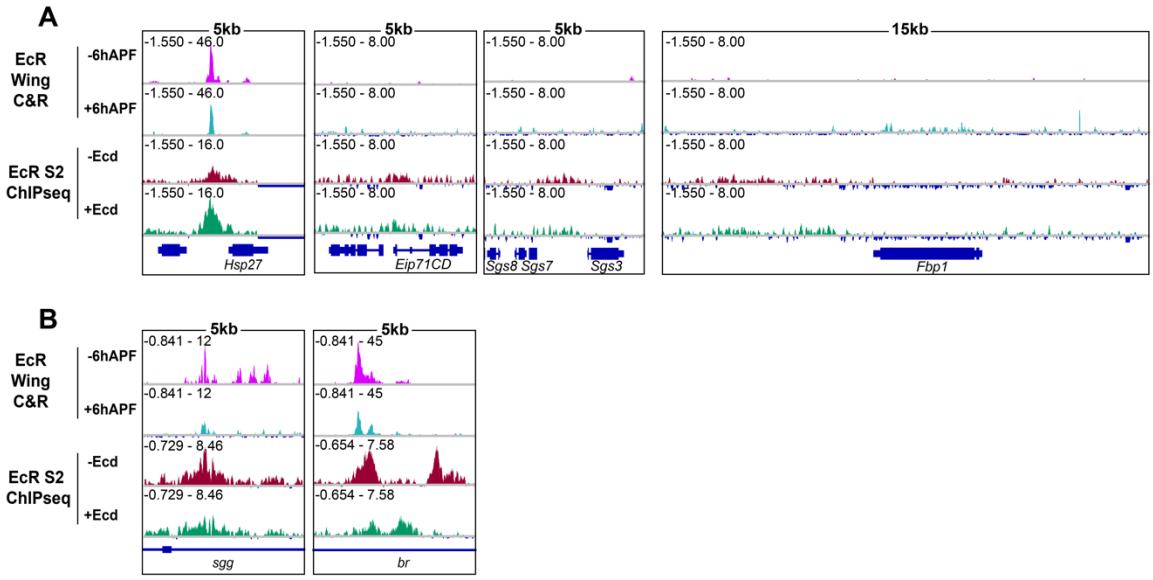

Figure 3.4: EcR binding is tissue-specific

(A) Browser shots comparing EcR CUT&RUN to EcR ChIPseq in S2 cells (130). Colored boxes highlight examples of shared (red), S2-specific (yellow) and wing-specific peaks (grey). (B) Bar plots showing the proportion of EcR C&R peaks that overlap an S2 ChIP peak in each category. (C) A comparison of the average signal within EcR C&R peaks colored by how they behave temporally (left) and whether they overlap an S2 ChIP peak (right). (D) GO terms of the closest gene to a wing EcR peak stratified by whether they overlap an S2 ChIP peak.

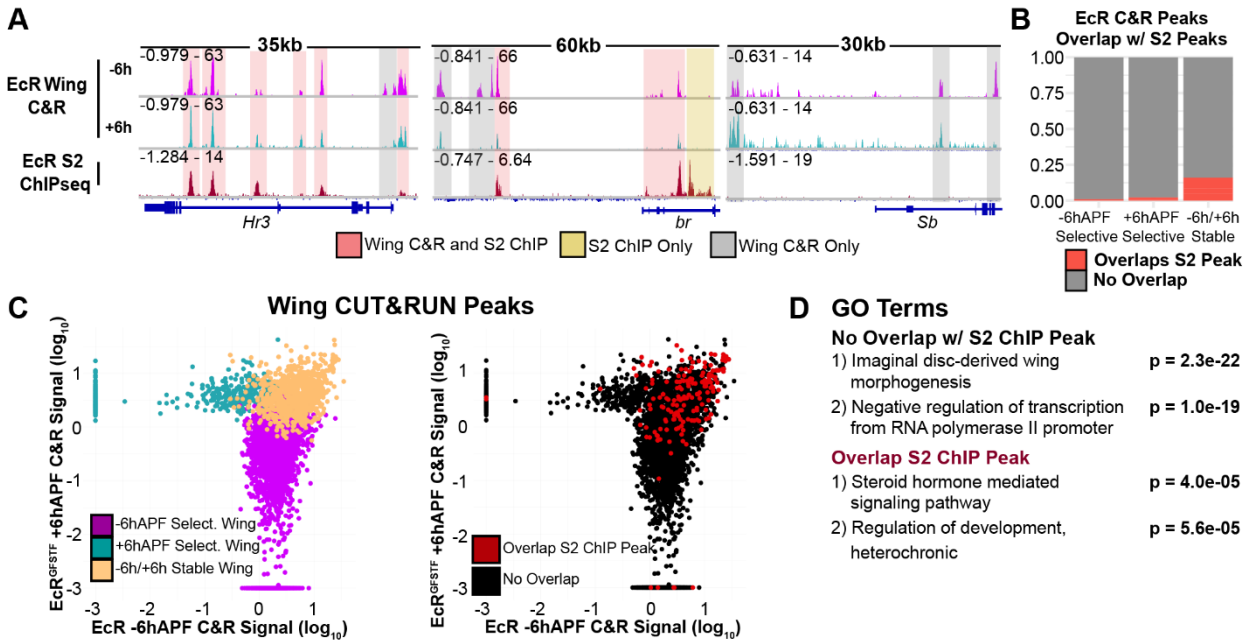

Figure 3.S9: EcR binding is enriched at genes that are affected by EcR knockdown

Percentage of EcR clusters that overlap (barplots, left), or fall within some distance of (cumulative distribution plots, right), a differentially expressed (D.E.), static, or not-expressed (N.E.) gene in RNAseq comparing (A) WT to EcR-RNAi wings at –6hAPF, (B) WT –6hAPF to +6hAPF, (C) WT to EcR-RNAi at +6hAPF. EcR peaks were compared to peaks randomly shuffled over FAIRE peaks. Differentially expressed genes were defined as genes with an adjusted p-value < 0.05. Not expressed genes were defined as genes that were filtered out by DESeq2 (padj = NA). Overlapping genes were defined as genes that overlapped a CUT&RUN peak by at least a single base pair. Note that separately examining up- and down-regulated genes in EcRi wings at either time point did not result in a statistically significant correlation between EcR binding and differential gene expression.

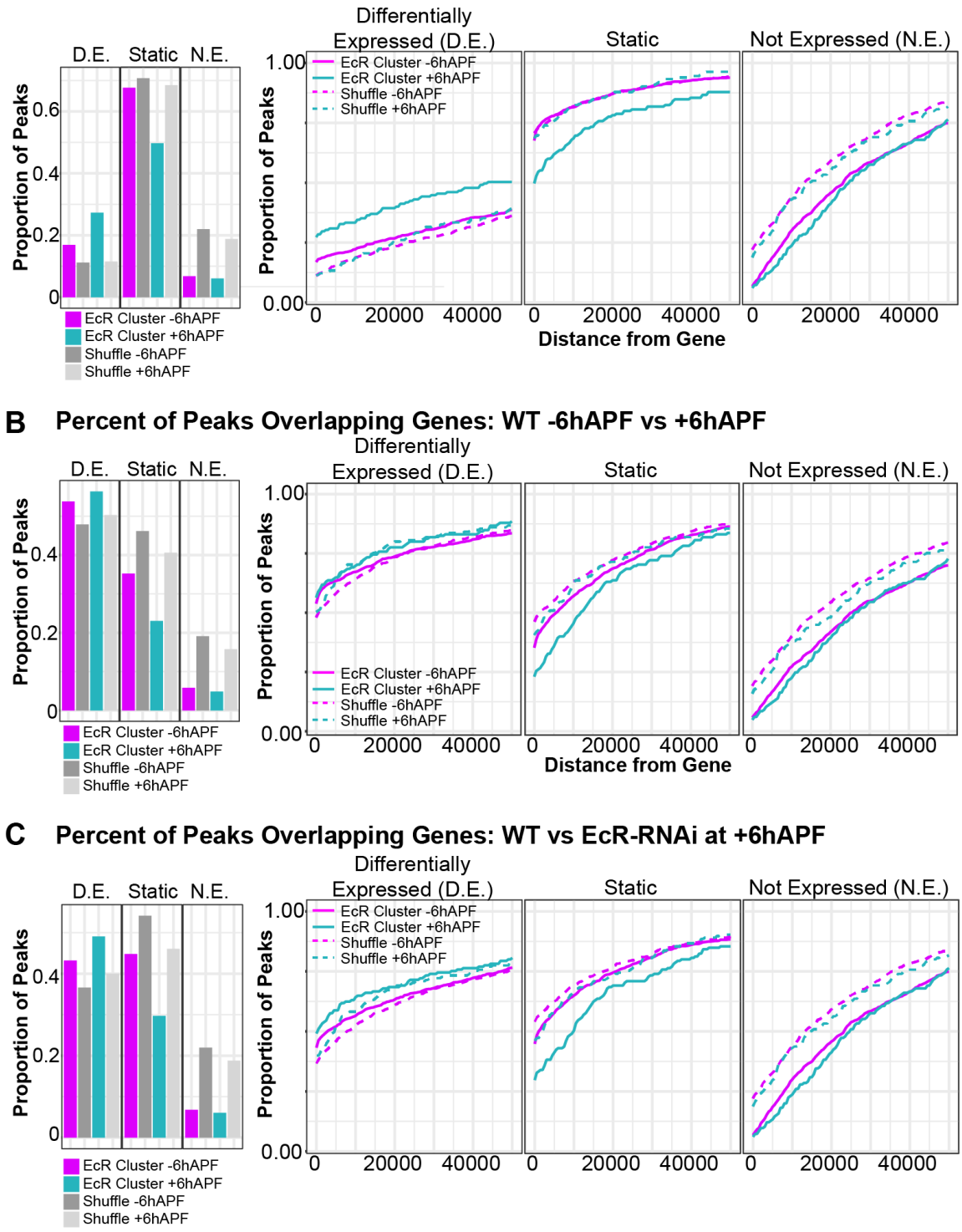
A
Percent of Peaks Overlapping Genes: WT vs EcR-RNAi at -6hAPF
D.E.
Static
N.E.
Proportion of Peaks
0
0.2
0.4
0.6
EcR Cluster -6hAPF
EcR Cluster +6hAPF
Shuffle -6hAPF
Shuffle +6hAPF
Differentially Expressed (D.E.)
Static
Not Expressed (N.E.)
1.00
0.00
0
20000
40000
Distance from Gene
B
Percent of Peaks Overlapping Genes: WT -6hAPF vs +6hAPF
C
Percent of Peaks Overlapping Genes: WT vs EcR-RNAi at +6hAPF

late 3rd instar, Br levels have increased (Figure 3.S10A). Ecdysone signaling has been proposed to contribute to this increase in Br expression in wings over time (182, 183).

Our CUT&RUN data identify multiple EcR binding sites across the br locus at both –6hAPF and +6hAPF (Figure 3.5A, 3.S11). One of these binding sites corresponds to an enhancer (br^{disc}) we previously identified that recapitulates br activity in the wing epithelium at –6hAPF (167). Consistent with the observed increase in Br protein levels during 3rd instar wing development, the activity of br^{disc} increases with time (Figure 3.5B). To investigate the potential role of EcR in controlling the activity of br^{disc}, we ectopically expressed an isoform of EcR with a point mutation in the ligand-binding domain that prevents it from binding ecdysone and thus functions as a constitutive repressor (EcR^{DN}) (188). EcR^{DN} expression in the anterior compartment of the wing results in decreased br^{disc} activity in both early and late-stage wing discs (Figure 3.5C), indicating that EcR^{DN} represses br^{disc}. We further examined the role of EcR in regulating br^{disc} by knocking down EcR via RNAi, which would eliminate both activating and repressing functions of EcR. EcR knockdown resulted in a modest increase in the activity of br^{disc} in early wing discs compared to WT wings (Figure 3.5D-E), demonstrating that EcR is required to repress br^{disc} at this stage. We also observed a slight increase in br^{disc} activity in late wing discs (Figure 3.5D-E). Together, these findings indicate that EcR is required to keep br^{disc} activity low in early 3rd instar wing discs, but it is not required for br^{disc} activation in late 3rd instar wing discs. Additionally, the observation that br^{disc} is active in the absence of EcR, and continues to increase in activity over time, suggests that br requires other unknown activators which themselves may be temporally dynamic. Because the levels of Br increase with time, we conclude that release of repression by EcR

functions as a temporal switch to control Br expression during the larval-to-prepupal transition.

EcR binds to enhancers with spatially-restricted activity patterns in the wing

EcR's role in controlling the timing of br transcription through the br^{disc} enhancer supports conventional models of ecdysone signaling in coordinating temporal gene expression. To determine whether EcR plays a similar role at non-canonical ecdysone target genes, we focused on the Delta (Dl) gene, which encodes the ligand for the Notch (N) receptor. Notch-Delta signaling is required for multiple cell fate decisions in the wing (189, 190). In late third instar wing discs, Dl is expressed at high levels in cells adjacent to the dorsal-ventral boundary, along each of the four presumptive wing veins, and in proneural clusters throughout the wing (190). Remarkably, despite the requirement of Notch-Delta signaling in each of these areas, no enhancers active in wing discs have been described for the Dl gene. The Dl locus contains multiple sites of EcR binding (Figure 3.6A, 3.S11). Using open chromatin data from wing imaginal discs to identify potential Dl enhancers (131), we cloned two EcR-bound regions for use in transgenic reporter assays. The first of these enhancers exhibits a spatially-restricted activity pattern in late third instar wing discs that is highly reminiscent of sensory organ precursors (SOPs) (Figure 3.6B). Immunostaining for the proneural factor Achaete (Ac) revealed that cells in which this Dl enhancer is active co-localize with proneural clusters (Figure 3.6B). Immunostaining also confirmed these cells express Dl (Figure 3.6C). We therefore refer to this enhancer as Dl^{SOP}. Notably, using Dl^{SOP} to drive expression of a destabilized GFP reporter, its activity pattern refines from a cluster of cells to a single cell (Figure 3.6C), consistent with models of SOP specification in which

feedback loops between N and Dl result in high levels of N signaling in the cells surrounding the SOP, and high levels of Dl expression in the SOP itself. By +6hAPF, the pattern of Dl^{SOP} activity does not change, and it remains spatially restricted to cells along the D/V boundary and proneural clusters in the notum. The second Dl enhancer bound by EcR is also active in late 3rd instar wing discs (Figure 3.6A). This enhancer is most strongly active in Dl-expressing cells of the tegula, lateral notum, and hinge (Figure 3.6D-E) (191). In the pouch, it is active in cells that comprise the L3 and L4 proveins, which require Dl for proper development (192) although overlap with Dl in each of these regions is less precise (Figure 3.6D-E). We refer to this enhancer as Dl^{teg}. Collectively, these data demonstrate that, in contrast to the widespread activity of br^{disc}, the EcR-bound enhancers in the Dl locus exhibit spatially-restricted activity, raising the possibility that EcR binding may serve a different function at these binding sites.

Ultraspiracle clones display changes in the spatial pattern of enhancer activity

We next sought to determine if EcR regulates the activity of these enhancers. Since the Dl enhancers drive GAL4 expression, we could not use the EcR^{DN} and EcR-RNAi lines employed above. Therefore, we generated loss of function clones of Usp, the DNA binding partner of EcR. Clones of usp were induced at 48-60 hours and enhancer activity was assayed at –6hAPF. Surprisingly, usp loss of function results in an increased number of cells in which Dl^{SOP} is active in the pouch of wing discs (Figure 3.6F, inset i), suggesting that EcR/Usp are required to repress Dl^{SOP} activation. Notably, clones of usp in other regions of the wing (Figure 3.6F, inset ii) do not activate Dl^{SOP}, indicating that EcR/Usp are not necessary for repression of Dl^{SOP} in all cells of the wing. We also note that regions exhibiting ectopic Dl^{SOP}

activity in usp clones tend to be near regions of existing *Dl*^{SOP} activity, suggesting that localized activating inputs are required to switch the *Dl*^{SOP} enhancer on, and that EcR/Usp binding to *Dl*^{SOP} acts as a countervailing force to restrict its activation to certain cells within these regions. Because the pattern of *Dl*^{SOP} activity does not expand between –6hAPF and +6hAPF in WT wings, the ectopic activation of this enhancer in usp clones supports the conclusion that EcR/Usp regulate the spatial pattern of *Dl*^{SOP} activation rather than its temporal activity pattern, as in the case of the br^{disc} enhancer.

We observed a similar effect of usp loss of function on activity of the *Dl*^{teg} enhancer. *Dl*^{teg} activity expands in usp clones adjacent to regions in which *Dl*^{teg} is active in WT cells (Figure 3.6G). As with *Dl*^{SOP}, however, loss of usp function does not appear to be sufficient to cause ectopic *Dl*^{teg} activity, as clones that are not adjacent to existing *Dl*^{teg} activity do not ectopically activate the enhancer. Notably, we did not observe expanded expression of Ac within usp clones, suggesting that the expanded activity pattern of the clones is not due to an expanded proneural domain (Figure 3.S12). These results suggest that EcR primarily functions to repress these enhancers at –6hAPF in order to spatially restrict their activity. The observation that usp loss of function is not sufficient to cause ectopic enhancer activity may be because the activation of these enhancers requires other inputs.

Figure 3.S10: Broad protein levels increase with time.

(A) Changes in Br protein (red) levels over time in WT wings between 96hrs after egg laying (96AEL) and 120AEL (-6hAPF). Scale bars are 100um. DAPI was used to stain nuclei.

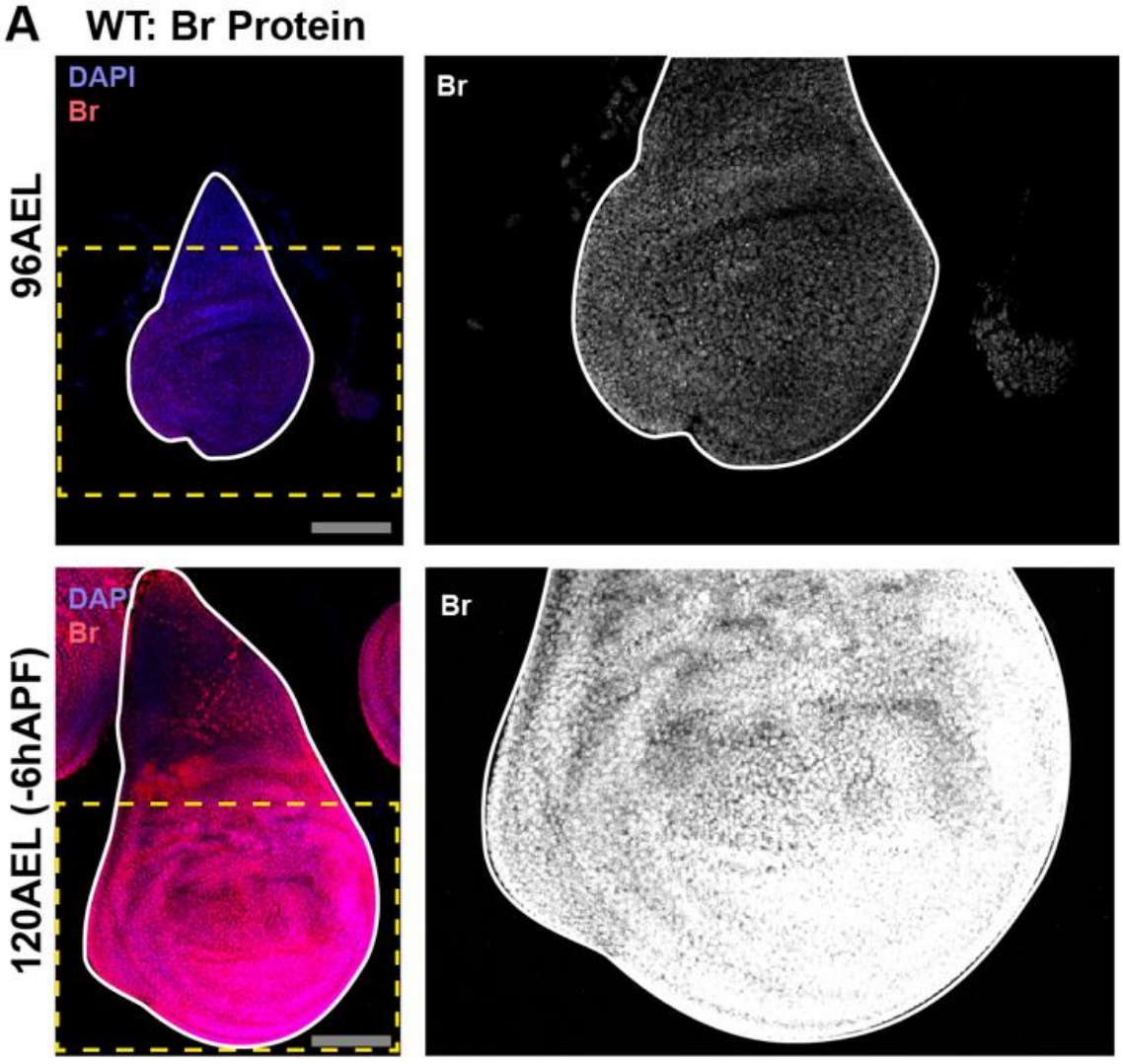

Figure 3.5: EcR regulates the temporal activity of an enhancer for the gene *broad*

(A) Browser shots of the *br* locus, with the location of the br^{disc} highlighted by a shaded gray region. (B) br^{disc} activity in WT wings (red) at 96hrs after egg laying (96AEL) and 120AEL (–6hAPF). (C) The effect expressing EcR-B2^{W650A} (EcR^{DN}) in the anterior compartment of the wing marked by GFP (green) on br^{disc} activity. (D) Comparison of br^{disc} activity between the anterior (Ant) and posterior (Pos) compartments of the wing in WT and EcR-RNAi wings (* $p < 0.05$; *** $p < 0.005$, paired student's t-test). Dotted yellow boxes indicate the location of insets. Scale bars are 100uM.

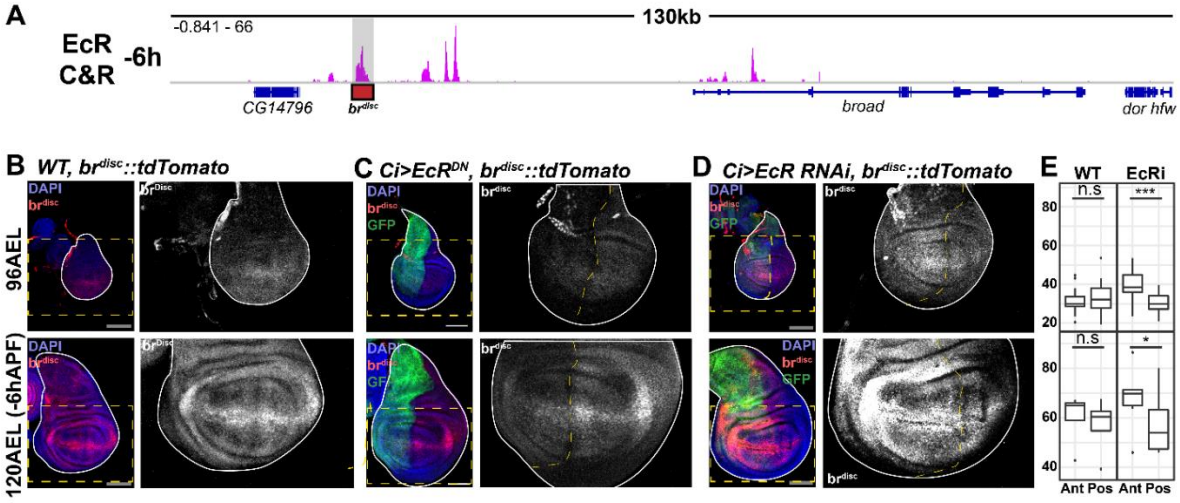

Figure 3.6: EcR regulates the spatial activity of enhancers for the gene *Dl*

(A) Browser shots of the *Dl* locus, with the location of the Dl^{SOP} and Dl^{teg} highlighted by a gray box. (B-C) Enhancer activity of Dl^{SOP} (green) showing overlap with Ac and Dl. (D-E) Enhancer activity of Dl^{teg} showing overlap with Dl and Ac. (F-G) Enhancer activity of $Dl^{SOP}$and Dl^{teg} in usp^{3} mitotic clones which are marked by the absence of RFP. Dotted yellow boxes indicate the location of insets. Scale bars are 100µm.

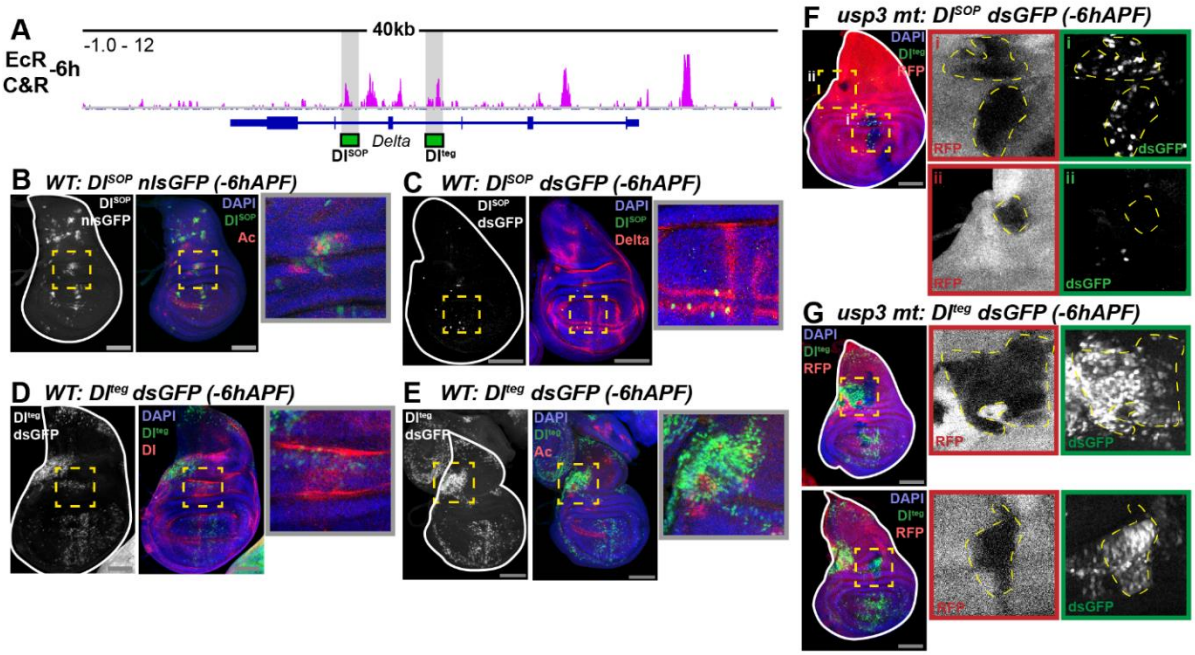

Figure 3.S11: Motif content inside br and Dl enhancers.

(A) Browser shots of the three enhancers examined in this study. The width of each browser corresponds to the enhancer boundaries. The locations of EcR motifs are indicated with dashed lines. (B-D) Enhancer sequences for *br*^{Disc}, *Dl*^{SOP}, and *Dl*^{teg}. EcR motifs are indicated by coloring the bases. The EcR motif from Fly Factor Survey (67) was used.

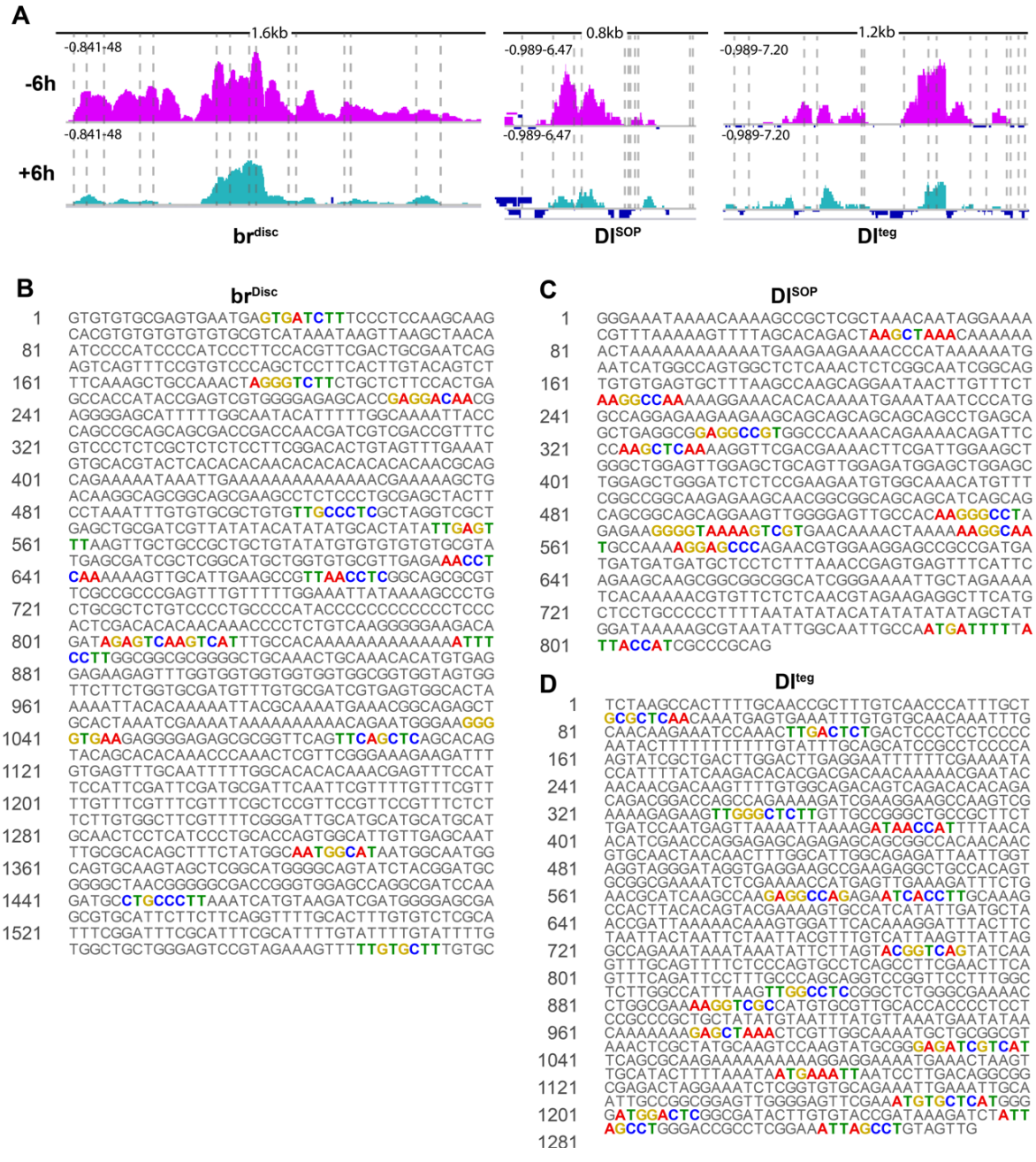

Figure 3.S12: usp^3 clones to not result in cell fate changes

(A) –6hAPF wings showing usp^3 mitotic clones stained for Ac. Clones are marked by the absence of RFP. Scale bars are 100um. DAPI was used to stain nuclei.

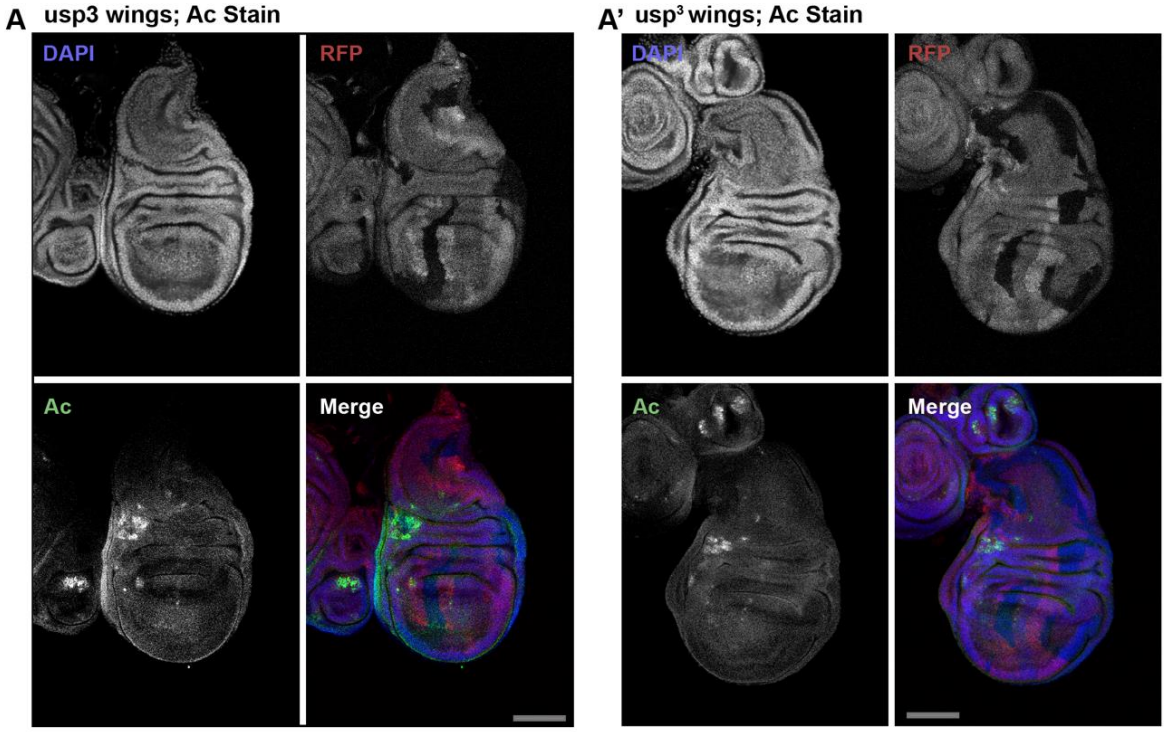

Discussion

Decades of work have established the central role that ecdysone signaling, acting through its nuclear receptor, EcR/Usp, plays in promoting developmental transitions in insects. In this study, we investigate the genome-wide role of EcR during the larval-to-prepupal transition in *Drosophila* wings. Our findings validate existing models of ecdysone pathway function, and they extend understanding of the direct role played by EcR in coordinating dynamic gene expression programs.

The role of EcR in promoting gene expression changes during developmental transitions

Our RNA-seq data reveal that EcR controls the larval-to-prepupal transition by activating and repressing distinct sets of target genes. In larval wing imaginal discs, we find that EcR is primarily required to prevent precocious activation of the prepupal gene expression program. This finding is consistent with previous work which demonstrated precocious differentiation of sensory neurons in the absence of ecdysone receptor function (193). Since ecdysone titers remain low during most of the 3rd larval instar, these data are also consistent with prior work which demonstrated that EcR functions as a transcriptional repressor in the absence of hormone (65, 161). Later in prepupal wings, we find that loss of EcR results in failure to activate the prepupal gene expression program. Indeed, many of the genes that become precociously activated in wing discs fail to reach their maximum level in prepupae. Since rising ecdysone titers at the end of 3rd larval instar trigger the transition to the prepupal stage, this finding is consistent with a hormone-induced switch in EcR from a repressor to an activator (65, 161). We also find that loss of EcR results in persistent

activation of the larval gene expression program in prepupal wings. This finding is not clearly explained by a hormone-induced switch in EcR's regulatory activity. However, it is possible that EcR activates a downstream transcription factor, which represses genes involved in larval wing development. Overall, these findings indicate that EcR functions both as a temporal gate to ensure accurate timing of the larval-to-prepupal transition and as a temporal switch to simultaneously shut down the preceding developmental program and initiate the subsequent program. Finally, it is of particular note that these genome-wide results fit remarkably well with the model of ecdysone pathway function predicted by Ashburner forty-five years ago (52).

Widespread binding of EcR across the genome

Existing models describe EcR as functioning at the top of a transcriptional cascade, in which it binds a relatively small number of primary-response genes. These factors then activate downstream effectors that mediate the physiological response to ecdysone. Consistent with this model, attempts to assay EcR binding genome-wide in S2 cells and Kc167 cells identified relatively few EcR binding sites. However, this model does not adequately explain how ecdysone elicits distinct transcriptional responses from different target tissues. Our data reveal that EcR binds to thousands of sites genome-wide. While many genes bound by EcR have been previously identified as direct targets, the majority of EcR binding we observe occurs near genes with essential roles in wing development. These data support a model in which EcR directly mediates the response to ecdysone both at the top of the hierarchy and at many of the downstream effectors. Interestingly, comparison of our wing binding profiles with ChIP-seq from S2 cells revealed that shared EcR binding sites are

enriched in canonical ecdysone-response genes, suggesting that the top tier of genes in the ecdysone hierarchy are direct targets of EcR across multiple tissues, while the downstream effectors are direct EcR targets only in specific tissues. These data neatly account for the observation that parts of the canonical ecdysone transcriptional response are shared between tissues, even as many other responses are tissue-specific. Aside from assay-specific issues, it is possible that the greater number of EcR binding sites identified in the wing relative to cell lines is due to the presence of multiple cell types in the wing that possess distinct EcR binding profiles. Additionally, the extent of EcR binding may directly scale with the magnitude of the physiological response to ecdysone, which in wing imaginal discs is arguably greater (i.e. transformation into pupal wings) than in Kc167 cells (i.e. change in cell shape) (134). In any case, it will be important to identify the factors that contribute to EcR's tissue-specific DNA targeting in future work. It is possible that tissue-specific transcription factors facilitate EcR binding, as suggested by recent DNA-binding motif analysis of ecdysone-responsive enhancers in S2 and OSC cell lines (130).

Temporally-dynamic binding of EcR

Pulses of ecdysone mediate distinct transcriptional responses at different times in development. Some of this temporal-selectivity is mediated by the sequential activation of transcription factors that form the core of the ecdysone cascade (99, 104, 105). Our data suggest that changes in EcR binding over time may also be involved. The mechanisms responsible for these changes remain unclear. One potential explanation is that changes in the expression of EcR isoforms could allow recruitment to new sites in the genome. However, we do not observe changes in protein isoform abundance, indicating that this is unlikely to

account for changes in EcR DNA-binding profiles. An alternative possibility is that ecdysone titers could induce ligand-dependent changes in EcR structure or affect ligand-dependent interactions with co-regulator proteins that influence EcR's DNA-binding. It is also possible that overall EcR levels or the nuclear-to-cytoplasmic ratio of EcR changes with time, as has been previously proposed (194). However, we do not observe changes in EcR protein levels, and while nuclear export of EcR could explain the global reduction in the number of EcR binding sites, it cannot explain the appearance of new EcR binding sites at +6hAPF. For this reason, it is notable that temporal-selective binding sites contain lower motif content on average relative to temporally-stable EcR binding sites. This suggests that temporal-selective binding may be more dependent on external factors. An intriguing possibility is that stage-specific transcription factors activated as part of the canonical ecdysone cascade may contribute to recruitment or inhibition of EcR binding at temporal-selective sites.

EcR controls both temporal and spatial patterns of gene expression.

EcR has been shown to act as both a transcriptional activator and repressor. This dual functionality confounded our attempts to draw genome-wide correlations between EcR binding and changes in gene expression. Therefore, we sought to examine the effect of EcR binding on individual target enhancers. We find that EcR regulates the temporal activity of an enhancer for the early-response gene, *br*. In wild type wings, the activity of this enhancer increases between early and late third instar stages, as do Br protein levels. Ectopic expression of a dominant-repressor isoform of EcR decreased activity of br^{disc}. Surprisingly, RNAi-knockdown of EcR increased br^{disc} activity, indicating that EcR is not required for br^{disc} activation. Instead, these findings indicate that EcR represses br^{disc} in early third instar

wings, consistent with our RNA-seq data which demonstrated that EcR prevents precocious activation of the prepupal gene expression program prior to the developmental transition. It is not known what factors activate *br* or other prepupal genes.

Temporal control of gene expression by EcR is expected given its role in governing developmental transitions. However, our examination of EcR-bound enhancers from the *Dl* locus demonstrates that it also directly controls spatial patterns of gene expression. Loss-of-function clones for EcR's DNA binding partner Usp exhibited ectopic activation of two *Dl* enhancers. However, we did not detect ectopic enhancer activity in all *usp* mutant clones, indicating that EcR is required to restrict activity of target enhancers only at certain locations within the wing. Examination of +6hAPF wings revealed no changes in the spatial pattern of *Dl* enhancer activity relative to –6hAPF, indicating that ectopic enhancer activation in *usp* clones does not reflect incipient changes in enhancer activity. Recently, EcR binding sites were shown to overlap with those for the *Notch* regulator, Hairless, supporting a potential role of EcR in regulating spatial patterns of gene expression (14). We conclude that EcR regulates both temporal and spatial patterns of gene expression. Given the widespread binding of EcR across the genome, our findings suggest that EcR plays a direct role in temporal and spatial patterning of many genes.

Hormones and other small molecules act through nuclear receptors to initiate transcriptional cascades that continue for extended periods of time. For example, thyroid hormone triggers metamorphosis in frogs and other chordates, a process that can take weeks for completion. Our work raises the possibility that nuclear receptors play a direct role in regulating the activity of many response genes. In particular, the widespread and temporally-

dynamic binding of EcR that we observed over a short interval of wing development suggests that the complete repertoire of EcR targets is vastly larger than previously appreciated.

Table 3.S1: Gene Ontology Terms for EcR Clusters at -6hAPF (top five)

Behavior	Cluster	GO.ID	Term	p-value (-log10)
ECRi3LW > WT3LW	1	GO:0015833	peptide transport	2.508638306
ECRi3LW > WT3LW	1	GO:0035848	oviduct morphogenesis	2.356547324
ECRi3LW > WT3LW	1	GO:0010898	positive regulation of triglyceride catabolic process	2.356547324
ECRi3LW > WT3LW	1	GO:0010716	negative regulation of extracellular matrix disassembly	2.356547324
ECRi3LW > WT3LW	1	GO:0048621	post-embryonic digestive tract morphogenesis	2.356547324
ECRi3LW > WT3LW	2	GO:0008063	Toll signaling pathway	4.886056648
ECRi3LW > WT3LW	2	GO:0040003	chitin-based cuticle development	3.744727495
ECRi3LW > WT3LW	2	GO:0035074	pupation	3.148741651
ECRi3LW > WT3LW	2	GO:0006965	positive regulation of biosynthetic process of antibacterial peptides active against Gram-positive bacteria	2.928117993
ECRi3LW > WT3LW	2	GO:0016045	detection of bacterium	2.928117993
ECRi3LW > WT3LW	3	GO:0002028	regulation of sodium ion transport	3.443697499
ECRi3LW > WT3LW	3	GO:0045479	vesicle targeting to fusome	2.301899454
ECRi3LW > WT3LW	3	GO:0042554	superoxide anion generation	2.301899454
ECRi3LW > WT3LW	3	GO:0070731	cGMP transport	2.301899454
ECRi3LW > WT3LW	3	GO:0051597	response to methylmercury	2.301899454
ECRi3LW > WT3LW	4	GO:0040003	chitin-based cuticle development	18.95860731
ECRi3LW > WT3LW	4	GO:0003383	apical constriction	1.455931956
ECRi3LW > WT3LW	4	GO:0008362	chitin-based embryonic cuticle biosynthetic process	1.387216143
ECRi3LW > WT3LW	4	GO:0070252	actin-mediated cell contraction	1.387216143
ECRi3LW > WT3LW	4	GO:0042335	cuticle development	1.356547324
ECRi3LW > WT3LW	5	GO:0031427	response to methotrexate	3.958607315
ECRi3LW > WT3LW	5	GO:0007218	neuropeptide signaling pathway	3.244125144
ECRi3LW > WT3LW	5	GO:0006094	gluconeogenesis	2.36552273
ECRi3LW > WT3LW	5	GO:0009408	response to heat	2.191789027
ECRi3LW > WT3LW	5	GO:0035079	polytene chromosome puffing	1.998699067
WT3LW > ECRi3LW	1	GO:0071390	cellular response to ecdysone	3.602059991
WT3LW > ECRi3LW	1	GO:0009597	detection of virus	2.872895202
WT3LW > ECRi3LW	1	GO:0006833	water transport	2.571865206

WT3LW > ECRi3LW	1	GO:0071329	cellular response to sucrose stimulus	2.395773947
WT3LW > ECRi3LW	1	GO:0007610	behavior	2.381951903
WT3LW > ECRi3LW	2	GO:0043401	steroid hormone mediated signaling pathway	3.214670165
WT3LW > ECRi3LW	2	GO:0045200	establishment of neuroblast polarity	2.302770657
WT3LW > ECRi3LW	2	GO:0090163	establishment of epithelial cell planar polarity	2.302770657
WT3LW > ECRi3LW	2	GO:0072697	protein localization to cell cortex	2.302770657
WT3LW > ECRi3LW	2	GO:0016336	establishment or maintenance of polarity of larval imaginal disc epithelium	2.206209615
WT3LW > ECRi3LW	3	GO:0035320	imaginal disc-derived wing hair site selection	2.187086643
WT3LW > ECRi3LW	3	GO:0071632	optomotor response	2.187086643
WT3LW > ECRi3LW	3	GO:0019752	carboxylic acid metabolic process	2.173925197
WT3LW > ECRi3LW	3	GO:0009408	response to heat	2.086186148
WT3LW > ECRi3LW	3	GO:0001676	long-chain fatty acid metabolic process	1.943095149

Table 3.S2: Gene Ontology Terms for EcR Clusters at +6hAPF (top five)

Behavior	Cluster	GO.ID	Term	p-value (-log10)
ECRi6hAPF > WT6hAPF	1	GO:0006030	chitin metabolic process	2.853871964
ECRi6hAPF > WT6hAPF	1	GO:0090100	positive regulation of transmembrane receptor protein serine/threonine kinase signaling pathway	2.13076828
ECRi6hAPF > WT6hAPF	1	GO:0006784	heme a biosynthetic process	1.991399828
ECRi6hAPF > WT6hAPF	1	GO:0046160	heme a metabolic process	1.991399828
ECRi6hAPF > WT6hAPF	1	GO:0001837	epithelial to mesenchymal transition	1.991399828
ECRi6hAPF > WT6hAPF	2	GO:0007052	mitotic spindle organization	11.32790214
ECRi6hAPF > WT6hAPF	2	GO:0009267	cellular response to starvation	10.85387196
ECRi6hAPF > WT6hAPF	2	GO:0006364	rRNA processing	8.721246399
ECRi6hAPF > WT6hAPF	2	GO:0022008	neurogenesis	6.958607315
ECRi6hAPF > WT6hAPF	2	GO:0042254	ribosome biogenesis	6.522878745
ECRi6hAPF > WT6hAPF	3	GO:0002028	regulation of sodium ion transport	3.408935393
ECRi6hAPF > WT6hAPF	3	GO:0055072	iron ion homeostasis	2.747146969
ECRi6hAPF > WT6hAPF	3	GO:0034605	cellular response to heat	2.385102784
ECRi6hAPF > WT6hAPF	3	GO:0042335	cuticle development	2.12090412
ECRi6hAPF > WT6hAPF	3	GO:0045479	vesicle targeting to fusome	2.086716098
ECRi6hAPF > WT6hAPF	4	GO:0040003	chitin-based cuticle development	17.04095861
ECRi6hAPF > WT6hAPF	4	GO:0048082	regulation of adult chitin-containing cuticle pigmentation	2.920818754
ECRi6hAPF > WT6hAPF	4	GO:0045187	regulation of circadian sleep/wake cycle, sleep	2.537602002
ECRi6hAPF > WT6hAPF	4	GO:0048066	developmental pigmentation	2.283996656
ECRi6hAPF > WT6hAPF	4	GO:0001692	histamine metabolic process	2.229147988
WT6hAPF > ECRi6hAPF	1	GO:0045214	sarcomere organization	3.366531544
WT6hAPF > ECRi6hAPF	1	GO:0007525	somatic muscle development	2.950781977
WT6hAPF > ECRi6hAPF	1	GO:0060402	calcium ion transport into cytosol	2.850780887
WT6hAPF > ECRi6hAPF	1	GO:0006869	lipid transport	2.705533774
WT6hAPF > ECRi6hAPF	1	GO:0010888	negative regulation of lipid storage	2.554395797
WT6hAPF > ECRi6hAPF	2	GO:0055085	transmembrane transport	3.251811973
WT6hAPF > ECRi6hAPF	2	GO:0010025	wax biosynthetic process	2.954677021
WT6hAPF > ECRi6hAPF	2	GO:0007320	insemination	2.657577319
WT6hAPF > ECRi6hAPF	2	GO:0006508	proteolysis	2.345823458

WT6hAPF > ECRi6hAPF	2	GO:0042752	regulation of circadian rhythm	2.301899454
WT6hAPF > ECRi6hAPF	3	GO:0008299	isoprenoid biosynthetic process	7.113509275
WT6hAPF > ECRi6hAPF	3	GO:0051923	sulfation	3.698970004
WT6hAPF > ECRi6hAPF	3	GO:0006805	xenobiotic metabolic process	3.408935393
WT6hAPF > ECRi6hAPF	3	GO:0003383	apical constriction	3.107905397
WT6hAPF > ECRi6hAPF	3	GO:0006030	chitin metabolic process	2.728158393
WT6hAPF > ECRi6hAPF	4	GO:0071329	cellular response to sucrose stimulus	2.431798276
WT6hAPF > ECRi6hAPF	4	GO:0050709	negative regulation of protein secretion	2.251811973
WT6hAPF > ECRi6hAPF	4	GO:0001676	long-chain fatty acid metabolic process	1.954677021
WT6hAPF > ECRi6hAPF	4	GO:0009651	response to salt stress	1.829738285
WT6hAPF > ECRi6hAPF	4	GO:0006970	response to osmotic stress	1.655607726

Table 3.S3: Canonical Ecdysone Response Genes

Category	Gene ID
GO:0043401 (Steroid Hormone Mediated Signaling Pathway)	dsf
GO:0043401 (Steroid Hormone Mediated Signaling Pathway)	eg
GO:0043401 (Steroid Hormone Mediated Signaling Pathway)	Eip75B
GO:0043401 (Steroid Hormone Mediated Signaling Pathway)	Eip78C
GO:0043401 (Steroid Hormone Mediated Signaling Pathway)	ERR
GO:0043401 (Steroid Hormone Mediated Signaling Pathway)	ftz-f1
GO:0043401 (Steroid Hormone Mediated Signaling Pathway)	Hnf4
GO:0043401 (Steroid Hormone Mediated Signaling Pathway)	Hr38
GO:0043401 (Steroid Hormone Mediated Signaling Pathway)	Hr39
GO:0043401 (Steroid Hormone Mediated Signaling Pathway)	Hr3
GO:0043401 (Steroid Hormone Mediated Signaling Pathway)	Hr51
GO:0043401 (Steroid Hormone Mediated Signaling Pathway)	Hr78
GO:0043401 (Steroid Hormone Mediated Signaling Pathway)	Hr83
GO:0043401 (Steroid Hormone Mediated Signaling Pathway)	Hr96
GO:0043401 (Steroid Hormone Mediated Signaling Pathway)	knrl
GO:0043401 (Steroid Hormone Mediated Signaling Pathway)	svp
GO:0043401 (Steroid Hormone Mediated Signaling Pathway)	tll
GO:0043401 (Steroid Hormone Mediated Signaling Pathway)	usp
GO:0071390 (Cellular Response to Ecdysone)	Blimp-1
GO:0071390 (Cellular Response to Ecdysone)	br
GO:0071390 (Cellular Response to Ecdysone)	Eip93F
GO:0071390 (Cellular Response to Ecdysone)	let-7-C
GO:0071390 (Cellular Response to Ecdysone)	Lpt
GO:0071390 (Cellular Response to Ecdysone)	MED27
GO:0071390 (Cellular Response to Ecdysone)	Sgs3
GO:0071390 (Cellular Response to Ecdysone)	usp
GO:0071390 (Cellular Response to Ecdysone)	Utx
Other Ecdysone Response Genes	Eip55E

Other Ecdysone Response Genes	Eip63E
Other Ecdysone Response Genes	Eip63F-1
Other Ecdysone Response Genes	Eip63F-2
Other Ecdysone Response Genes	Eip71CD
Other Ecdysone Response Genes	Eip74EF
Other Ecdysone Response Genes	Imp
Other Ecdysone Response Genes	ImpE1
Other Ecdysone Response Genes	ImpE2
Other Ecdysone Response Genes	ImpE3
Other Ecdysone Response Genes	ImpL1
Other Ecdysone Response Genes	ImpL2
Other Ecdysone Response Genes	ImpL3

Table 3.S4: Gene Ontology Terms for EcR Binding Sites (top five)

Overlap Type	GO.ID	Term	p-value (-log10)
+6hAPF Unique	GO:0007476	imaginal disc-derived wing morphogenesis	4.040958608
+6hAPF Unique	GO:0002009	morphogenesis of an epithelium	3.420216403
+6hAPF Unique	GO:0035152	regulation of tube architecture, open tracheal system	3.366531544
+6hAPF Unique	GO:0018107	peptidyl-threonine phosphorylation	3.236572006
+6hAPF Unique	GO:0007370	ventral furrow formation	3.207608311
-6h/+6h Stable	GO:0007476	imaginal disc-derived wing morphogenesis	8.142667504
-6h/+6h Stable	GO:0048190	wing disc dorsal/ventral pattern formation	6.259637311
-6h/+6h Stable	GO:0007156	homophilic cell adhesion via plasma membrane adhesion molecules	5.15490196
-6h/+6h Stable	GO:0007411	axon guidance	4.853871964
-6h/+6h Stable	GO:0016318	ommatidial rotation	4.769551079
-6hAPF Unique	GO:0000122	negative regulation of transcription from RNA polymerase II promoter	20.92081875
-6hAPF Unique	GO:0007476	imaginal disc-derived wing morphogenesis	20.76955108
-6hAPF Unique	GO:0007411	axon guidance	15.38721614
-6hAPF Unique	GO:0045944	positive regulation of transcription from RNA polymerase II promoter	14.88605665
-6hAPF Unique	GO:0035277	spiracle morphogenesis, open tracheal system	12.18045606

Acknowledgements

We thank Peter J. Skene and Steven Henikoff for reagents and advice on the CUT&RUN protocol. Stocks obtained from the Bloomington Drosophila Stock Center (NIH P40OD018537) were used in this study. CMU was supported in part by NIH grant T32GM007092. This work was supported in part by Research Scholar Grant RSG-17-164-01-DDC to DJM from the American Cancer Society, and in part by grant R35-GM128851 to DJM from the National Institute of General Medical Sciences of the NIH (https://www.nigms.nih.gov/).

CHAPTER 4: COORDINATION OF TISSUE-SPECIFIC GENE EXPRESSION PROFILES BY DYNAMIC ECR BINDING AND CHROMATIN ACCESSIBILITY

Introduction

A central feature of metazoan development is that a single, undifferentiated progenitor gives rise to a diverse array of specialized cell types. During this process, individual tissues develop transcriptional profiles that are specific to each lineage and stage of development. Genetically, this specificity in achieved, in part, through differences in the complement of transcription factors (TFs) found within each cell. TFs effect changes in transcription by binding specific DNA motifs found within cis-regulatory modules (CRMs) and recruiting protein complexes that either enhance or repress transcription. The packaging of DNA into nucleosomes plays an important role in shaping how regulatory information is accessed genome wide. For most TFs, nucleosome-associated DNA (closed) is refractory to TF binding, while nucleosome-free DNA (open) is free to be bound. The accessibility of enhancers is dictated by a special class of TFs, called "pioneer" TFs, which have the ability to bind nucleosome-associated DNA (27). Once bound, pioneers can open CRMs either by directly evicting nucleosomes or by recruiting ATP-dependent chromatin remodeling complexes, rendering them competent to be bound by other, non-pioneer TFs (20, 195, 196). The pattern of accessible and inaccessible DNA throughout the genome is called the "open chromatin" pattern. In addition to the open chromatin pattern, TF binding is also influenced by TF-TF interactions – TFs can both stabilize and disrupt each other's binding. Collectively,

the open chromatin pattern, TF-TF interactions, as well as whether TFs function as activators or repressors, dictate the gene expression profile of each cell type.

In the fruit fly *Drosophila melanogaster*, the precursors to the adult appendages, imaginal discs, are an attractive model for studying how gene expression changes are controlled in a developing organism. The imaginal discs are originally specified during embryonic development, which then grow and undergo a series of gene patterning events during larval stages. By the end of larval development, the imaginal discs are comprised of a sheet of columnar epithelia which differentiate into the multitude of different cell types that comprise the adult appendage over the course of the pupal stage of development (134, 180). The differentiation of the imaginal discs into adult appendages involves extensive remodeling of the open chromatin landscape, as well as changes in the complement of TFs that are expressed (131, 134, 197).

In a series of experiments to determine the contribution that tissue-identity ("master regulator") TFs in directing chromatin accessibility, McKay and Lieb investigated open chromatin differences in the wing, leg, and haltere over time (131). They found that the accessibility profiles of the imaginal discs change coordinately over time – the open chromatin profiles of each tissue were more similar to one another at each time point, than they were to the same tissue at a later time point (131). Their data suggested that the master regulators specified tissue-specific gene expression profiles by modulating the activity of enhancers with shared accessibility across the three tissues (131). However, the observation that accessibility profiles changed in register with one another over time raised the question of how this coordination occurred. Since the leg, wing, and haltere are spatially-isolated, it suggested that an extrinsic signal might be responsible.

Decades of work have established the central role that the steroid hormone ecdysone plays coordinating *Drosophila* development. Ecdysone is secreted from the prothoracic gland at discrete times in development ("pulses") to initiate major transitions throughout the *Drosophila* life cycle (33, 34). The transcriptional response to ecdysone was originally characterized in work done by Michael Ashburner and colleagues on studies on the large, polyploid cells of the *Drosophila* salivary gland (52). Polytene spreads of salivary contain decondensed regions of DNA called, "puffs" that appeared and disappeared in a stereotypical manner in response to ecdysone (52). By culturing salivary glands *ex vivo* under different conditions, they developed the "Ashburner Model" in which ecdysone initiates a series of early puffs, whose protein products activate the late puffs, as well as inhibit their own expression (52, 92).

The initial genetic response to ecdysone occurs through its receptor, the ecdysone receptor (EcR), which, in combination with its binding partner, ultraspiracle (usp) forms a heterodimeric transcription factor (58, 61). Similar to other nuclear receptors, EcR / Usp heterodimers recognize a canonical, palindromic nuclear receptor motif (an Ecdysone Response Element, ECRE), found in both promoters and distal regulatory elements (66, 71, 198). During periods of low ecdysone titer, EcR is nuclear-localized where it functions as a transcriptional-repressor (80, 161, 193, 199). During periods of high-ecdysone titer, EcR undergoes a ligand-dependent conformational change and becomes a transcriptional activator (82, 193). The switch between repressive and activator modalities is thought to involve changes in EcR's binding partners (33, 82, 163). EcR has previously been shown to interact with a variety of repressor and activator complexes in a ligand-dependent manner, including

the SMRTER repressor, members of the NURF and NURD ATP-dependent chromatin remodeling complexes, and many others (80, 82, 162, 163, 200–206).

The genetic response to ecdysone is both temporally and spatially diverse. Each successive pulse of ecdysone acts on tissues throughout the animal that respond differently both from one another, and over time. This is perhaps most strikingly demonstrated by the divergence in the response of larval tissues that do not persist into adulthood, including the salivary gland, midgut, and fat body, which respond to the late-3rd instar ecdysone pulse by undergoing cell death, and the imaginal tissues which respond by beginning metamorphosis into the adult appendages (85, 93, 94, 207). This diversity has been recapitulated in cell culture. The ModENCODE project assayed the gene expression profiles of 41 cell lines before and after treatment with ecdysone, and found that their response varied considerably, and that a large fraction of the genome was responsive to ecdysone (86). Similarly, transcriptomic profiling of larval wings, salivary glands and midgut over time have identified many genes with temporal- and tissue-specificity (87, 91, 208).

Specificity to the ecdysone response is achieved in different ways. Some of this information is encoded in the progression of EcR's primary response transcription factors. For instance, in the fat body, larval induction of *Blimp-1* represses the expression of *ftz-f1* rendering it insensitive to the larval ecdysone pulses (43, 104). During pre-pupal development, Ftz-f1 activates targets specific to that time point (98). More recently, our lab showed that E93 which is expressed during pupal development provides temporal-specificity, in part, by altering the chromatin landscape to potentiate the wing to respond differently to extrinsic signals over time.

In addition to interactions amongst EcR's primary response transcription factors, changes in EcR binding itself appear to play a role in providing specificity to the ecdysone response. Recently, our lab found that EcR binding in the wing is temporally-dynamic – a subset of its binding sites is specific to each timepoint – even over a relatively short, ~12hr developmental window (209). Additionally, there is evidence that suggests that changes in EcR binding may also provide spatial-specificity to the ecdysone response. Several genes have been identified with tissue-specific expression that contain functional ECREs, including the fat body protein, *Fbp1*, the salivary gland glue genes, and the methionine sulfoxide reductase, *MsrA* (formerly *Eip28/29* and *Eip71CD*) (112–114). *MsrA*, in particular, has a complex expression pattern governed by ECREs active in different tissues (114). However, the genome-wide DNA binding profile of EcR across multiple tissues at the same point has never been profiled. Consequently, the extent to which tissue-specific binding of EcR mediates the response to ecdysone, as well as what promotes this specificity, remains unclear.

In this work, we investigated the role that tissue-specific EcR binding plays in mediating tissue-specific gene expression responses. We focused on two tissues that undergo divergent developmental responses to an identical pulse of ecdysone – the larval salivary gland and wing. In response to rising ecdysone titers during 3rd instar, the salivary gland produces glue gene products prior to undergoing programmed cell death (101, 109, 210, 211). In contrast, in response to the same ecdysone pulse, the wing completes the final stages of tissue-growth and patterning, prior to initiating metamorphosis (134, 212). We used RNAseq to profile the gene expression profiles of developing wing and salivary glands and found that the temporal dynamics of their gene expression changes were exquisitely tissue-

specific. Knockdown of EcR demonstrated that most temporal changes were dependent on EcR, including at many primary response genes. To investigate the direct contribution of EcR to promoting these changes, we assayed its binding and found that EcR binding was highly tissue-specific and associated with tissue-specific gene activation and repression in a temporal- and tissue-specific manner. Because the accessibility of enhancers genome-wide plays an important role in dictating tissue-specific gene expression profiles, we used FAIREseq to assay the open chromatin landscape in wings and salivary glands. The open chromatin profiles in wings and salivary glands were highly tissue-specific and associated with differences in EcR binding – tissue-specific binding sites were more likely to be differentially-accessible. We investigated what role EcR played in directing these changes and found that it functions as a passive factor whose binding is primarily dictated by the accessibility landscape. Collectively, this work has shed light on one means by which specificity to the ecdysone response is achieved and further highlighted the central, and direct role that EcR plays in this process.

Materials and Methods

Immunofluorescence

Individual larvae were inverted at RT in 1XPBS and then transferred to a 9-well dissecting dish on ice. Animals were dissected in batches of 5-20. Samples were then fixed using 4% paraformaldehyde (Electron Microscopy Services) in 1XPBS for 25m at RT on an orbital shaker. Fix was removed and samples were washed twice, briefly, with 1XPBS + 0.15% triton (PBT), and then underwent three, 20m washes in PBT at RT. Antibodies were incubated either for 1.5 – 2hrs at RT or overnight at 4C. After secondary antibody incubation, samples were washed once with PBT, once with PBT + 0.2µg / ml DAPI, and once with PBT. The following antibody concentrations were used: 1:750 mouse anti-EcR (DSHB DDA2.7, concentrate), 1:4000 rabbit anti-GFP (Abcam ab290), 1:3500 mouse anti-Dl (DSHB C594.9b, concentrate), 1:200 mouse anti-FLAG M2 (Sigma F1804), 1:1000 anti-Br (DSHB 25E9.D7, concentrate). Secondary antibodies were: 1:1000 goat anti-rabbit, or goat anti-mouse, conjugated with either Alexa-488 or Alexa-594 (ThermoFisher A11037, A11034). Samples were imaged on a Leica Sp5 or Leica Sp8 confocal microscope.

Sample preparation for RNAseq

A minimum of 60 wings or salivary glands were prepared as previously described (131) from either *Oregon R (WT)* or *yw; vg-GAL4, tub>CD2>GAL4, UAS-GFP, UAS-FLP / UAS-EcR-RNAi^{104} (EcR-RNAi)*. For library construction, 50-100ng RNA was used as input to the Tecan Genomics Universal RNA-Seq with NuQuant, Drosophila. Library preparation followed the manufacturer's instructions with the following modifications: 1) after second-strand cDNA synthesis, samples were sonicated 5x20s (30s rest between cycles) on high

power in a BioRupter bath sonicator; 2) qPCR was performed to determine the optimal cycle number using manufacturer's recommendations; 3) after library amplification, an additional, 1.2:1 SPRI bead-cleanup was performed. Paired-end, 2x75 sequencing was performed on an Illumina HiSeq X using Novogene Co.

Sample preparation for CUT&RUN

A minimum of 75 wings or 50 salivary glands from w; EcR^{GFSTF}/Df(2R)BSC313 were dissected in wash buffer (20mM HEPES-NaOH, 150mM NaCl, 2mM EDTA, 0.5mM Spermidine, 10mM PMSF). The rest of the protocol was performed as described in Ahmad, 2018, protocols.io (213).For library preparation, the Takara ThruPLEX DNA-seq kit with unique dual-indexes was used following the manufacturer's protocol until the amplification step. For amplification, after the addition of indexes, 16-21 cycles of 98C, 20s; 67C, 10s were run. A 1.2x SPRI bead cleanup was performed (Agencourt Ampure XP). Libraries were sequenced on an Illumina HiSeq 4000 with 2x75 read . The following antibody concentrations were used: 1:300 mouse anti-FLAG M2; 1:200 rabbit anti-Mouse (Abcam ab46450); 1:400 Batch#6 protein A-MNase (from Steven Henikoff).

Sample preparation for FAIREseq

Larvae from either *Oregon R (WT)* or *yw; vg-GAL4, tub>CD2>GAL4, UAS-GFP, UAS-FLP / UAS-EcR-RNAi^{104} (EcR-RNAi).* were dissected in 1XPBS in batches of 5-10 then fixed at RT for 10m in 4% paraformaldehyde, 50mM HEPES (pH 8.0), 100mM NaCl, 1mM EDTA (pH 8.0), 0.5mM EGTA (pH 8.0). Fixation was quenched by incubation for 5m in 1xPBS, 125mM Glycine, 0.01% Triton X-100 and then transferred to 10mM HEPES (pH

8.0), 10mM EDTA (pH 8.0), 0.5mM EGTA (pH 8.0), 0.25% Triton X-100, 1mM PMSF. Wings or salivary glands were dissected off cuticles and snap frozen in liquid nitrogen. Samples were lysed in 2% Triton X-100, 1% SDS, 100mM NaCl, 10mM Tris (pH 8.0), 1mM EDTA. Following lysis, a minimum of 40 wings or salivary glands were pooled together and homogenized using 2.38mm tungsten beads with 6 cycles of 1min on and 2min off and then sonicated using a Branson Sonifier with 5 cycles of 30s (1s on, 0.5s off) while letting the samples rest for at least 2m on ice between cycles. An aliquot was removed as an input fraction. The remaining samples were subjected to phenol-chloroform and chloroform extractions and then precipitated with ethanol. Input and experimental samples were heated overnight at 65C to reverse cross links and then treated with RNase A for 1hr at 37C. DNA was purified with a Qiagen QIAquick PCR Purification Kit eluting in nuclease free water. Samples were used as input into the Takara ThruPLEX DNA-seq kit following manufacturer's instructions.

RNA Sequencing Analysis

Reads were trimmed using bbmap (v38.75) with parameters ktrim=r ref=adapters rcomp=t tpe=t tbo=t hdist=1 mink=11. Reads were aligned with STAR (2.7.3a) (168). Indexes for STAR were generated with parameter --sjdbOverhang 74 using genome files for the dm6 reference genome. The STAR aligner was run with parameters --alignIntronMax 50000 --alignMatesGapMax 50000. Samtools (v1.9) was used to filter reads to those with a q-score greater than 2. RSubread (v2.0.1) was used to count reads mapping to genes using a gtf file from flybase.org (r6.32) using parameters: annot.ext = gtfPath, isGTFAnnotationFile = T, isPairedEnd = T, strandSpecific = 1, nthreads = 4, GTF.featureType = 'exon',

allowMultiOverlap = F (169). DESeq2 (v1.26.0) was used to identify differentially expressed genes using the lfcShrink function to shrink log-fold changes and with each genotype and time-point as a separate contrast (170). Differentially expressed genes were defined as genes with an adjusted p-value less than 0.05 and an absolute log2 fold change greater than 1. Normalized counts were generated using the counts function in DESeq2. For c-means clustering, normalized counts were first converted into the fraction of maximum normalized counts across all tissues and conditions and c-means clustering was performed using the ppclust package (v1.1.0) (214). MA Plots were made with ggplot2 and points were shaded using kernel density estimates calculated using the MASS (v7.3-51.4) package (215). Heatmaps were generated using ggplot2 (v3.3.2) and patchwork (v1.1.0) in R (216–218). Gene Ontology (GO) analysis was performed using Bioconductor packages TopGO (v2.38.1) and GenomicFeatures (v1.38.2) using expressed genes as a background set with parameters: algorithm = ‘elim’ and statistic = ‘fisher’(141, 171). Similar GO terms were collapsed based on semantic similarity using the rrvgo package in R and only the parent term was used (v1.1.1) (219). Expressed genes were defined as genes with a normalized count value >= 10.

CUT&RUN Sequencing Analysis

Technical replicates were merged by concatenating fastq files. Reads were trimmed using bbmap (v38.75) with parameters ktrim=r ref=adapters rcomp=t tpe=t tbo=t hdist=1 mink=11. Trimmed reads were aligned to the dm6 reference genome using Bowtie2 (v2.2.8) with parameters --local --very-sensitive-local --no-unal --no-mixed --no-discordant --phred33 -I 10 -X 700 (172). Reads with a quality score less than 5 were removed with samtools (v1.9) (173). PCR duplicates were marked with Picard (v2.21) and then removed with samtools.

Fragments between 20 and 120bp were isolated using a custom awk script and used for downstream analyses as recommended in Skene and Henikoff, 2017 (220). Bam files were converted to bed files with bedtools (v2.29) with parameter -bedpe (139). Bedgraphs were generated with bedtools and then converted into bigwigs with ucsctools (v320) (174). Data was z-normalized using a custom R script. MACS (v2.1.2) was used to call peaks on individual replicates and merged files using parameters -g 137547960--nomodel --seed 123 (175). As a control for peak calling, supernatant or pellet samples from a wing IgG control was used. Wing IgG controls were *yw* CUT&RUN samples in which the primary antibody was omitted and only the mouse anti-Rabbit IgG secondary was used. To identify differentially-bound regions, a union peak set was generated and RSubread (v2.0.1) was used to assign to features using parameters strandSpecific = 0, allowMultiOverlap = T and then used as input for DESeq2 (v1.26.0) (170, 221). For pairwise comparisons, union peaks were subsequently filtered to contain peaks that overlapped a peak found in either sample by at least one base pair. MA plots were made as described for RNAseq. Heatmaps and average signal plots were generated from z-normalized data using the Bioconductor package Seqplots (v1.24.0) and plotted using ggplot2 (176). ChIPpeakAnno (v3.20.0) was used to calculate distance of peaks to their nearest gene (176, 177). To identify clusters of EcR binding sites, the EcR peaks were resized to 5000bp, assigned to clusters, and the furthest start and end coordinate of the original peaks were used.

FAIRE sequencing analysis

Technical replicates were merged by concatenating fastq files. Reads were trimmed using bbmap (v38.75) with parameters ktrim=r ref=adapters rcomp=t tpe=t tbo=t hdist=1

mink=11. Trimmed reads were aligned to the dm6 reference genome using Bowtie2 (v2.2.8) with parameters --phred33 --seed 123 -x (172). Reads with a quality score less than 5 were removed with samtools (v1.9) (173). PCR duplicates were marked with Picard (v2.21) and then removed with samtools. The remaining processing and analysis steps were performed as described for CUT&RUN.

Motif Analysis

To identify occurrences of the EcR motif in the genome, PWMs for the EcR and Usp motifs identified by a bacterial 1-hybrid were obtained from Fly Factor Survey (67). For the palindromic, Usp/EcR motif, the PWMs for EcR and Usp were concatenated together and the probabilities for the central, overlapping base were averaged. FIMO (v4.12.0) was run on the dm6 reference genome using parameters –max-stored-scores 10000000 --max-strand --no-qvalue --parse-genomic-coord --verbosity 4 --thresh 0.01 (178). Motif density plots were generated by counting the number of motifs from peak summits (10bp bins) and normalizing by the number of input peaks.

EcR knockdown in the wing and salivary gland

To knockdown EcR in the wing and salivary gland in parallel, we made use of the previously published line: *yw; vg-GAL4, UAS-FLP, Tub>>STOP>>GAL4, UAS-GFP / CyO* (179). Early activation of *vg-GAL4* throughout the wing primordia results in flip-out of the stop-cassette and persistent expression of *Tub-GAL4* throughout wing development. This construct is also active in the salivary gland, which may be a consequence of the *vg-GAL4* p-

element vector which has been previously reported to have a minimal promoter active in the salivary gland (78, 222–224).

Drosophila culture and genetics

Flies were grown at 25C under standard culture conditions. Late wandering larvae were used as the –6hAPF timepoint. White prepupae were used as the 0h time point for staging +6hAPF animals. For -30hAPF, apple juice plates with embryos were cleared of any larvae and then four hours later any animals that had hatched were transferred to vials. The following genotypes were used:

yw; vg-GAL4, UAS-FLP, UAS-GFP, Tub>CD2>GAL4 / CyO (179).

w1118; P{UAS-EcR-RNAi}104 (BDSC#9327)

yw; EcR^{GFSTF} (BDSC#59823)

w1118; Df(2R)BSC889/CyO (BDSC#32253)

yw; + / + ; br^{disc}::tdTomato / TM6B

Results

The gene expression profiles of wings and salivary glands are temporally dynamic and tissue-specific

During mid-3rd instar in *Drosophila*, rising ecdysone titers initiate developmental events that prepare the larvae to metamorphose into an adult fly. The response to ecdysone during this time was originally extensively characterized in the developing salivary gland, a secretory tissue that helps to prepare the animal for pupal development (109, 111). The proximal response to rising ecdysone titers involves that activation of a set of early, canonical ecdysone targets, many of which include other transcription factors, which then activate additional downstream targets (35, 52, 92). In the salivary gland, this involves the production and packaging of glue gene products into exosome in preparation for their eventual secretion at the onset of the larval-to-adult transition (pupariation) (109, 210). Shortly after pupariation, the secretory portion of the salivary gland – a strictly larval tissue – undergoes programmed cell death in an ecdysone-dependent manner (101, 225). In contrast to the salivary gland, the imaginal discs, tissues that form that precursors to adult appendages, including the progenitors to the adult wing, respond differently to the same change in ecdysone. The wing undergoes a final series of cell divisions, gene patterning events, and cytoskeletal rearrangements that alter the gross morphology of the discs (134, 183, 212). At the onset of pupariation, the wing begins its transformation into an adult appendage – a process that will continue for the next 5 days. However, although the global response to ecdysone in the wing is highly divergent from the salivary gland, genes that are part of the core ecdysone cascade have been shown to activated and are required for development events that occur during this time period (183).

Because members of the core ecdysone pathway are involved in promoting the response to ecdysone in both tissues, one possibility was that the response to ecdysone involved the activation of a core, shared transcriptional program, as well as a tissue-specific one. Therefore, to investigate the extent to which temporal gene expression responses in wing and salivary gland were shared or tissue-specific, we performed RNAseq at three stages surrounding the larval-to-pupal transition: approximately 30hrs prior to the onset of pupariation (-30hAPF), at the wandering stage about 6hs prior to pupariation (-6hAPF), and 6hrs after the onset of pupariation (+6hAPF). To identify categories of differentially expressed genes, we used DESeq2 to generate normalized RNAseq counts, and then performed c-means clustering on all genes expressed in either tissue (DESeq2 normalized count >= 10).

The gene expression profiles of the wing and salivary gland are both tissue-specific and highly temporally dynamic. Although we identified a cluster of genes that was expressed constitutively in both the wing and salivary gland (clusters 12,13), somewhat unexpectedly, we did not identify a cluster of genes that were tissue-specific and not temporally-dynamic – that is expressed in one tissue constitutively over all three time-points, but not expressed in the other (Fig 4.4.1A). Instead, the vast majority of genes were temporally-dynamic in a pattern specific to each tissue. Consistent with the translation and packaging of glue gene products that occurs in the salivary gland during this time period, genes that decreased between -30hAPF and -6hAPF (clusters 5,6) were enriched in gene ontology (GO) terms for metabolic and biosynthetic processes (Fig 4.4.1B). In contrast, SG genes that increased between -30hAPF and -6hAPF (clusters 9,10,11), were enriched for GO terms involved in vesicle transport and fusion. In contrast to the salivary gland, at -30hAPF the wing is actively

dividing, but becomes less proliferative at -6hAPF and +6hAPF. Consistent with this, we identified two clusters (clusters 1,2) that progressively decrease in expression between -30hAPF and +6hAPF, one of which was enriched with genes involved in cell division. Genes that increased in expression over time (clusters 3,4) were enriched for genes involved in cytoskeletal processes, chitin-deposition, and extracellular matrix remodeling.

These data demonstrate that the majority of genes expressed in the wing and salivary gland exhibit different temporal-behavior. However, the highly multidimensional nature of the data made quantifying whether there was a shared set of co-regulated targets challenging. To identify these targets, and as more broadly quantify the tissue-specificity of the response, we used DESeq2 to identify differentially-expressed genes between each tissue. Consistent with our clustering approach, we found that the majority of genes that were dynamic over time were specific to each tissue (Fig 4.4.1C). Between -30hAPF and -6hAPF, we found that there were 760 genes that changed over time in the wing, and 3449 genes that changed over time in the salivary gland. Of these, however, only 351 were shared between the two tissues (46% of wing genes; 10% of SG genes). At the next developmental state, between, -6hAPF and +6hAPF, we found that there were 1636 genes that changed over time in the wing, and 2911 genes that changed over time in the salivary gland. Of these, only 789 genes were shared between the two tissues (49% of wing genes; 27% of SG genes). Notably, this analysis indicated that there were a higher number of temporally-dynamic genes in the salivary gland than in the wing. This was unexpected because the wing is a complex tissue, comprised of many cell types. However, it has been previously demonstrated that there are many changes in gene patterning that occur during this time, which involve changes in which cells express individual genes. Since our RNAseq was generated from whole tissue, it may be

insufficiently sensitive to detect these changes. To investigate the functional significance of genes that were shared between each time-point, we performed GO analysis. Shared genes were enriched for terms involved in a variety of difference processes, including toll signaling, various metabolic categories, as well as ecdysone-signaling genes (Fig 4.4.1D). Genes in the lattermost categories, which were found in genes that decreased between -30hAPF and -6hAPF, included *br, Hr4,* and *Eip75B*, which are canonical ecdysone targets, and is consistent with a hypothesis that there may be a set of core, ecdysone-responsive genes (Table S1).

The majority of temporal gene expression changes require ecdysone signaling.

Although ecdysone plays an important role in regulating developmental transitions, it is one of multiple inputs that regulate wing and salivary gland development. Therefore, to examine the requirement of EcR to promote tissue development in the wing and salivary gland in parallel, we used RNAi to knockdown EcR in the wing and salivary gland constitutively (see methods). During mid-3rd instar, a series of low amplitude ecdysone pulses precede a larger pulse that initiates the onset of pupariation. In the salivary gland, these pulses initiate the beginning of the canonical puffing cascade, in which a subset of pre-existing intermolt puffs containing the glue genes are activated and then regress, while puffs comprising the early genes are form. During this same period, the wing undergoes a period of tissue growth, and tissue-patterning events that spatially define various structures, including that dorsal/ventral (D/V) boundary, and wing veins. At -30hAPF, knockdown of the wing and salivary gland has little effect on the morphology of either the wing or salivary gland compared to their wildtype counterparts (Fig 4.2A-B). By contrast, at -6hAPF, EcR-RNAi

salivary glands were smaller than WT salivary glands, while EcR-RNAi wings were slightly enlarged. In the salivary gland, enlargement of the cytoplasmic lumen is a consequence of the production of glue gene products which are packaged into extracellular vesicles. In EcR-RNAi salivary glands, the glue genes are inactive, potentially providing an explanation for this size difference (Fig 4.2E, see *Sgs* genes).

The majority of genes that typically change in expression in WT wings and salivary glands fail-to-change in EcR-RNAi. In wings, we observed 318 genes increase in expression and 442 gene decrease in expression between -6hAPF. In EcR-RNAi wings, however, only 241 genes increased and 74 genes decreased (Fig 4.2A). By contrast, in WT salivary glands, 1943 genes increased and 1506 gene decreased. However, strikingly, only 182 genes increased in expression in EcR-RNAi salivary glands and 105 genes decreased (Fig 4.2B). In our previous work, we observed that EcR had a bimodal function developmentally. It initially acts as a break to prevent the transition to the next stage and development, and, subsequently, acts to push it forward as a "trigger". Consistent with this, we saw many genes were already differentially-expressed at -30hAPF EcR-RNAi wings and salivary glands (Fig 4.S1). Therefore, to more precisely quantify the number of genes that were affected by EcR-RNAi, we asked what fraction of genes that change in WT were called as differentially expressed between WT at either -30hAPF or -6hAPF. Using this definition, we found that, in WT wings, 29% of genes that increase over time and 52% of genes that decreased were affected by EcR-RNAi (Fig 4.2D). In the salivary gland, we found that 61% of the genes that increase, and 67% of genes that decrease were affected. Consequently, we do observe a greater aggregate requirement for EcR in promoting changes in gene expression in the salivary gland than in the wing. Additionally, in the wing it appears that EcR has a greater

requirement to repress genes than activate them, which is consistent with work from our lab and others that has found that EcR appears to primary act as a repressor during this time period. In the salivary gland, on the other hand, it appears to be required to both activate and repress genes.

The expression of canonical ecdysone response genes is also tissue-specific

Ecdysone is posited to regulate a core set of ecdysone-responsive genes that were originally identified by observing the puffing pattern in larval salivary glands (48, 52). By reviewing the literature, we identified 20 genes that were originally characterized as part of the core puffing cascade in salivary glands (55–57, 88, 100, 114, 128, 226). We divided these, broadly, into four categories: 1) intermolt puffs, which contain the glue genes and first activated, and then regress upon ecdysone addition; 2) early puffs which are immediately induced upon ecdysone addition; 3) late puffs which are activated after early puffs, though still during larval stages, by ecdysone; and 4) pre-pupal puffs, which are only activated after the onset of pupariation (Fig 4.2E). Our RNAseq data recapitulate the temporal progression of the puffing cascade in the salivary gland. Consistent with their role as primary ecdysone response genes, all the genes we identified were expressed in the salivary gland and affected by EcR knockdown. Strikingly, however, many of these were not active in the wing at the same time point, and were, similarly, unaffected by EcR knockdown. A notable exception to this was the transcription factor, *broad*, which was active in both wing and salivary gland. Broad plays an essential, and well-characterized, role in promoting wing development during this time. was down-regulated in the salivary gland at -30hAPF, while, in the wing, it was slightly up-regulated at -30hAPF. This is consistent with previous work by others that

demonstrated that EcR represses *br* during this time-point, as well our previous work in which we identified an enhancer directly bound by EcR which was precociously activated at -30hAPF upon EcR knockdown. To determine whether these genes became active later in wing development, we looked at previously published data from an RNAseq time-course from -6hAPF to 44hAPF. We found that, indeed, many of these canonical ecdysone response genes became active later in wing development (Fig 4.S1). These data demonstrate that ecdysone primary response genes also exhibit divergent responses across tissue and underscored the extent to which the response to ecdysone differs between the wing and salivary gland.

EcR binding in the wing and salivary gland is tissue-specific

Many ecdysone primary response genes are transcription factors that may direct changes in gene expression in an EcR-dependent manner. Therefore, to identify direct targets of EcR and understand to what extent its binding was tissue-specific, we performed CUT&RUN on –6hAPF wings and salivary glands (Fig 4.3A). We focused on this time-point because our RNAseq data indicated that there were many differentially-expressed genes between the wing and salivary gland, including at many primary response genes. We found that the properties of EcR binding were broadly similar to data we had previously collected. Relative to the whole genome, EcR binding is enriched in promoters and introns, and relatively depleted in exons and UTRs (Fig 4.S2A). Additionally, we also found that EcR binding events were clustered throughout the genome, with approximately half of EcR peaks found within 5000bp of another peak in the same tissue (Fig 4.S2B-C). We found that EcR binding was a mixture of tissue-specific and shared binding sites (Fig 4.3A). We used

DESeq2 to quantify the number of sites that were differentially-bound by EcR between the wing and salivary gland (adjusted p-value < 0.05 and absolute log2 fold change > 1) (Fig 4.2B). We identified 862 regions that were bound more highly in the wing (wing-enriched) and 844 peaks that were more highly bound in the salivary gland (SG-Enriched), and 1644 peaks that were not called as differentially-bound (shared).

To determine the functional significance of these binding sites, we our RNAseq data from EcR-RNAi wings at -30hAPF and -6hAPF. We assigned peaks to the nearest gene and asked what fraction of genes differentially-expressed or static genes in EcR-RNAi were associated with an EcR binding site in each tissue (Fig 4.2C). In the wing, we found that EcR bound a higher proportion of genes that were up-regulated in EcR-RNAi at both -30hAPF and -6hAPF, than genes that were static or down-regulated. These data are consistent with EcR functioning as a repressor during this time-point in the wing. Notably, we observed a stronger relationship between EcR binding and up-regulated genes in EcR-RNAi at -30hAPF than at -6hAPF. In our previous work, we observed that EcR-RNAi resulted in the precocious activity of an enhancer for the *br* locus (br^{disc}). This was more pronounced at -30hAPF than -6hAPF, but we did not have RNAseq data to determine if this effect was seen more broadly. Consequently, these data expand upon these findings and support a model in which EcR acts as a strong repressor in the wing at mid-3rd instar, which is relieved by rising titers that occur prior to -6hAPF. In the salivary gland, we observed as similar association between EcR binding and genes that were up-regulated upon loss of EcR at -30hAPF. However, at -6hAPF, this relationship was inverted – genes that were down-regulated in EcR-RNAi were more likely to be associated with EcR binding sites. This is consistent with the observation that canonical, primary response genes are down-regulated upon loss of EcR (Fig 4.2E).

Consequently, in contrast to the wing, this indicates that EcR may act as an activator in the salivary gland at -6hAPF. EcR is predicted to switch from a repressor to an activator as ecdysone titers rise. This switch may occur earlier in the salivary gland than in the wing, although why this would be is unclear.

When looking throughout the genome, we visually observed many genes with mixtures of tissue-specific and shared binding sites, but also many genes that had only tissue-specific binding sites. To explore this property of EcR binding, we assigned EcR peaks to the nearest gene, and grouped genes into different categories depending on what types of EcR binding sites were associated with them (Fig 4.3D). Strikingly, we observed that approximately half of genes were only associated with tissue-specific binding sites (Fig 4.3D), with the remainder associated with either shared, or mixtures of shared and tissue-specific binding sites (Fig 4.3D). The specific combination of binding sites at each gene was predictive of its relative expression in each tissue – genes that only had tissue-specific binding sites were more highly expressed in that tissue, while genes with only shared, or mixtures of shared and tissue-specific binding sites, were expressed at more equivalent levels (Fig 4.3E). The largest category we identified were genes that only contained SG-enriched binding sites, and, overall, there were more genes associated with SG binding sites than wing binding sites. Consistent with this, SG binding sites were less clustered genome-wide (Fig 4.S2B-C) and were more strongly-enriched in promoter regions (Fig 4.S2A). Overall, EcR's regulation of target genes appears to occur through a mixture of tissue-specific and shared binding, with many genes containing mixtures of binding sites, indicating a complex regulatory architecture. Compared to other genes, EcR's primary response genes appeared exceptional. Primary response genes often contained mixtures of wing-enriched, SG-

enriched, and shared binding sites (Fig 4.S3A-D). They were also associated with a high number of binding sites in each category (Fig 4.S3E).

To determine if tissue-specific binding sites exhibited different properties than shared binding sites, we looked at the amplitude of EcR's binding. Previously, we had found that temporally-dynamic binding sites were lower-amplitude than sites that were static, and that these amplitude differences corresponded to differences in motif content – high amplitude, static binding sites had more motifs, than tissue-specific ones. To determine if this was true of tissue-specific binding, we performed this analysis for wing- and salivary-enriched binding sites (Fig 4.3F). We found that while binding sites that were specific to either tissue were lower amplitude than binding sites shared between the two tissues, we did not observe a difference in EcR motif number or quality across the three categories (Fig 4.3G, Fig 4.S2E-F).

Tissue-specific binding is associated with tissue-specific open chromatin

To gain insight into the function of genomic regions bound by EcR, we performed FAIREseq on wings and salivary glands at -6hAPF (Fig 4.4A). FAIRE enriches for regions of DNA that are locally depleted of nucleosomes, and thus it can be used as a proxy for identifying *cis*-regulatory elements genome wide (150). We found that wings and salivary glands exhibit tissue-specific open chromatin profiles, with many differentially accessible sites found in each tissue, as well as a subset that were shared between the two tissues (Fig 4.4A). Overall, we observed 2405 sites that were more accessible in the wing, 2151 peaks that were more accessible in the salivary gland, and 6216 peaks that were not differentially accessible (Fig 4.4B). To determine whether the differences in open chromatin we observed

were associated with differences in gene expression, we performed assigned FAIRE peaks to the nearest gene and asked what proportion of genes that were differentially-expressed between WT wings and salivary glands were associated with a tissue-specific or shared FAIRE peak. We found a strong association between differences in open chromatin and genes that were more active in each tissue. 20% of genes that are more highly expressed in the wing were associated with a wing-specific FAIRE peak, and 25% of genes more highly expressed in the SG were associated a SG-specific FAIRE peak (Fig 4.4C). This relationship is consistent with most open chromatin sites functioning as transcriptional activators. Despite this, however, most differentially-expressed genes were not associated with a tissue-specific open chromatin site, underscoring that while tissue-specific open chromatin plays an important role in regulating gene expression, it is one of many inputs.

To examine the relationship between open chromatin and EcR binding, we calculated the difference in open chromatin signal between wings and salivary glands over tissue-specific and shared EcR binding sites. We found that wing-enriched EcR binding sites were more accessible in the wing than in the salivary gland, while salivary gland-enriched binding sites were more accessible in the salivary gland (Fig 4.4D). To test whether differentially-accessible sites corresponded to enhancers differentially-active in each tissue, we assayed the activity of two elements. The br^{disc} enhancer is an element we have previously identified which is bound by EcR and accessible only in the wing (167). In the wing, it is active throughout the wing imaginal disc, with slightly higher activity in cells adjacent to the dorsal-ventral boundary (Fig 4.4F). By contrast, the br^{disc} enhancer was inactive in the secretory cells of the salivary gland, where it is not accessible and unoccupied by EcR, though we observed some br^{disc} activity in the cells of the tubule and imaginal ring (Fig

4.4F). These cells represent a small fraction of salivary gland cells, and in contrast to the polyploid secretory cells, they have a diploid genome copy number, possibly explaining why br^{disc} is not detected as accessible in the salivary gland. The GMR79E07 site is found within the CG9650 gene and is both more accessible and bound in the salivary gland. Immunofluorescence analysis revealed that it is active throughout the secretory tissue of the salivary gland, and inactive in the tubule and imaginal ring cells. By contrast, GMR79E07 is inactive in the wing. Thus, we conclude that the association between tissue-specific open chromatin and EcR binding corresponds to functional differences in the cis-regulatory architecture within these genes.

EcR knockdown in the wing does not result in global changes in open chromatin

Our data suggests that tissue-specific EcR binding, and tissue-specific open chromatin seem to play an important role in dictating the transcriptional response to ecdysone. Nucleosome-associated DNA is refractory to most transcription factor binding (20, 27). A special class of transcription factors, called “pioneers”, have the ability to bind nucleosome-occupied DNA and evict nucleosomes, either by directly displacing them, or by recruiting ATP-dependent chromatin remodeling complexes (20, 227). We therefore hypothesized that the association between EcR binding and chromatin accessibility could result from two alternative models. In the first, EcR have pioneer-like activity and be direct changes in chromatin accessibility at target DNAs. Alternatively, EcR could be functioning as a passive factor, and, instead, the open chromatin profile could dictate which motifs it was able to access throughout the genome.

To distinguish between these two models, we performed FAIREseq in EcR-RNAi wings at -6hAPF. Our RNAseq and CUT&RUN data demonstrate that EcR is bound and functionally regulating gene expression at this time point. If EcR directs differences in chromatin accessibility, then EcR-bound sites are predicted to decrease in accessibility in EcR-RNAi wings. If, instead, EcR acts as a passive factor that does not play a role in altering the accessibility landscape, the accessibility of its binding sites should be unaffected by loss of EcR. We observed few differences in open chromatin upon knockdown of EcR (Fig 4.5A-B). Overall, there were only 132 peaks that were more accessible in EcR-RNAi wings than WT, and only 150 peaks that were more accessible in WT wings. Consistent with this, the global FAIREseq signal over EcR binding sites was not different between WT and EcR-RNAi wings (Fig 4.5C).

EcR's ability to both activate and repress genes has been shown to occur through its recruitment of ATP-dependent chromatin remodeling complexes. However, in addition to acting with pioneer transcription factors, ATP-dependent remodeling complexes can also act with factors that are not thought to be pioneers to increase gene expression. This activity can cause increases or decreases in accessibility that might be more subtle than a pioneer. To investigate whether EcR effected changes in accessibility in a more modest way, we looked the distribution of DESeq2-computed fold changes over FAIRE peaks that did or did not overlap EcR binding sites (Fig 4.5D). In aggregate, we observed a modest reduction in the accessibility of EcR-bound FAIRE peaks relative to unbound sites (Fig 4.5D). Some of these sites were identified as statistically significant changes by DESeq2 but did not meet our log fold cutoff (i.e., they had an adjusted p-value < 0.05, but log2 fold changes $-1 < x < 0$). Collectively, these data are consistent with a model in which EcR does not function as a

pioneer transcription factor, but instead, acts as a passive factor. It's previously identified association with nucleosome-remodeling complexes may facilitate its ability to activate or repress gene expression through modest changes in accessibility.

EcR binding in the leg imaginal disc is identical to the wing imaginal disc

Thus far, our data supports a model in which different metamorphic responses to ecdysone are achieved, in part, through tissue-specific open chromatin sites that dictate where EcR can bind. However, this raises the question of where EcR might bind in tissues with similar open chromatin profiles. The wing, leg, and haltere are a means provide a system that can answer this question. The open chromatin profiles in these tissues change coordinately with one another over time. At any given stage, the open chromatin profiles across the three tissues are more similar to one another then they are to themselves are an earlier or later developmental stage (131). However, a subset of transcription factors in each tissue are different, providing one means by which differences in gene expression could be achieved (131). Additionally, although all three tissues respond to ecdysone, they are ultimately fated to become different appendages. Consequently, one possibility is that different metamorphic responses to ecdysone could be achieved through differential recruitment of EcR throughout the genome by transcription factors that vary between tissues. Alternatively, if, instead, open chromatin is the primary determinant of EcR binding then we would predict that EcR binding would be more similar across tissues.

To discriminate between these possibilities, we therefore performed FAIREseq and CUT&RUN for EcR in the leg at -6hAPF (Fig 4.6A-B). Consistent with prior findings, the open chromatin profiles at -6hAPF in the leg and wing were highly similar to one another

and more similar to one another than the SG (Fig 4.6B). Overall, there were only 247 FAIRE peaks that were more accessible in the wing than in the leg and 277 FAIRE peaks that were more accessible in the leg (Fig 4.S4C). We next asked how similar EcR's binding profile. Strikingly, in contrast the SG, in which hundreds of sites were differentially bound, only 16 peaks were more strongly bound in the wing and 30 peaks were highly bound in the leg, compared to 2432 peaks that were shared across the two tissues (Fig 4.6C). Of note, this was not affected by using a log-fold cut-off to define differentially-bound regions, because there were only 3 peaks that were called as

statistically significant that did not meet our log fold cutoff. The signal in a union set of wing, leg, and salivary gland binding sites was also much more highly correlated between the wing and leg than between either the wing and salivary gland, or leg and salivary gland. The small number of differentially-bound sites in the wing and leg appear, in some cases, to be meaningful and overlap the small number of differentially-accessible FAIRE peaks (Fig 4.S4A-B). Sites that were enriched in the wing were more accessible in the wing and vice versa.

The similarity between EcR binding in the wing and leg supports a model in which the tissue-specific differences in open chromatin play a central in dictating EcR's binding profile (Fig 4.6E). In this model, tissue-specific pioneer factors in the imaginal discs alter the accessibility of EcR's binding sites throughout the genome and dictate which enhancers and genes EcR can act on. The similarity between EcR binding in the wing and leg indicates that the contribution of tissue-specific, non-pioneer transcription factors in promoting EcR binding may be relatively minimal. However, we cannot rule out a possible role for non-

pioneer transcription factors that are expressed in both that wing and leg that may perform this function.

Figure 4.1: The temporal gene expression profiles in the wing and salivary gland are tissue-specific

A) C-means clustering of all expressed genes in the wing and salivary glands (SG) over time represented as fraction of max expression. Expressed genes were defined as genes with a DESeq2 normalized count value > 10, and fraction of max was calculated using normalized counts across all conditions. B) Gene ontology (GO) terms for genes found in each cluster. C) Number of genes that increase and decrease over time in WT wings and salivary glands, and the number of genes that overlap. Differentially-expressed genes were defined as genes with an adjusted p-value <0.05 and an absolute $\log_2$ fold change > 1 as called by DESeq2.

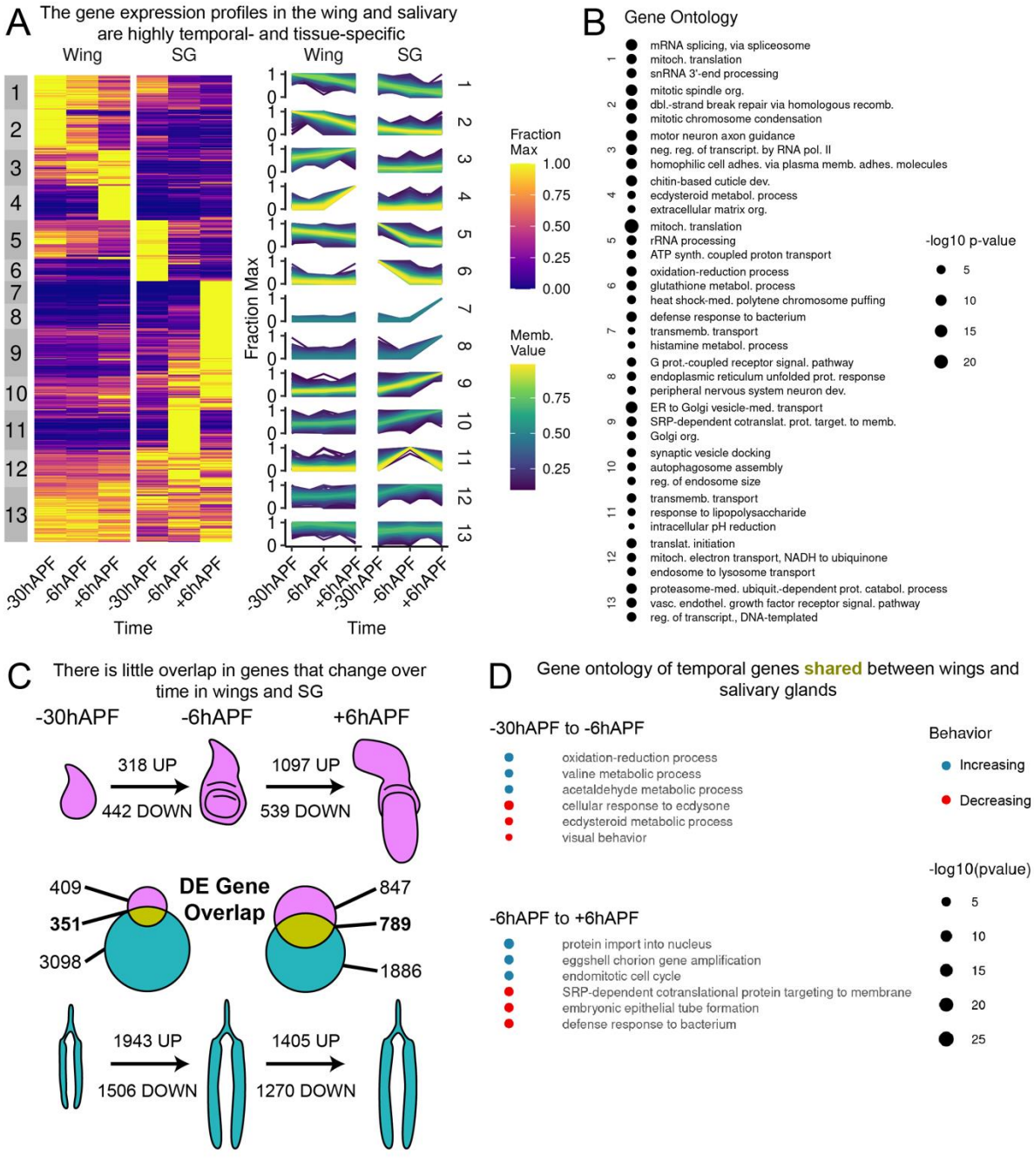
A
The gene expression profiles in the wing and salivary are highly temporal- and tissue-specific
Wing
SG
Wing
SG
Fraction Max
Time
Time
B
Gene Ontology
mRNA splicing, via spliceosome
mitoch. translation
snRNA 3'-end processing
mitotic spindle org.
dbl.-strand break repair via homologous recomb.
mitotic chromosome condensation
motor neuron axon guidance
neg. reg. of transcript. by RNA pol. II
homophilic cell adhes. via plasma memb. adhes. molecules
chitin-based cuticle dev.
ecdysteroid metabol. process
extracellular matrix org.
mitoch. translation
rRNA processing
ATP synth. coupled proton transport
oxidation-reduction process
glutathione metabol. process
heat shock-med. polytene chromosome puffing
defense response to bacterium
transmemb. transport
histamine metabol. process
G prot.-coupled receptor signal. pathway
endoplasmic reticulum unfolded prot. response
peripheral nervous system neuron dev.
ER to Golgi vesicle-med. transport
SRP-dependent cotranslat. prot. target. to memb.
Golgi org.
synaptic vesicle docking
autophagosome assembly
reg. of endosome size
transmemb. transport
response to lipopolysaccharide
intracellular pH reduction
translat. initiation
mitoch. electron transport, NADH to ubiquinone
endosome to lysosome transport
proteasome-med. ubiquit.-dependent prot. catabol. process
vasc. endothel. growth factor receptor signal. pathway
reg. of transcript., DNA-templated
Fraction Max
Memb. Value
-log10 p-value
C
There is little overlap in genes that change over time in wings and SG
-30hAPF
-6hAPF
+6hAPF
318 UP
442 DOWN
1097 UP
539 DOWN
DE Gene Overlap
409
351
3098
847
789
1886
1943 UP
1506 DOWN
1405 UP
1270 DOWN
D
Gene ontology of temporal genes shared between wings and salivary glands
-30hAPF to -6hAPF
oxidation-reduction process
valine metabolic process
acetaldehyde metabolic process
cellular response to ecdysone
ecdysteroid metabolic process
visual behavior
Behavior
Increasing
Decreasing
-log10(pvalue)
-6hAPF to +6hAPF
protein import into nucleus
eggshell chorion gene amplification
endomitotic cell cycle
SRP-dependent cotranslational protein targeting to membrane
embryonic epithelial tube formation
defense response to bacterium

Figure 4.2: Ecdysone is required to promote genome-wide changes in gene expression over time

Immunofluorescence of A) wings and B) salivary glands in WT and EcR-RNAi at -30hAPF and -6hAPF stained with anti-EcR (red) and DAPI (blue). GFP (green) indicates expression of the RNAi construct. A'-B') MA Plots showing numbers of differentially expressed (DE) genes over time. DE genes were defined as p-adj < 0.05 and absolute $\log_2$ fold change > 1. C) Proportion of differentially expressed genes that change in WT between -6hAPF and -30APF that do not change in EcR-RNAi. E) Gene expression of WT and EcR-RNAi wings and salivary glands of genes corresponding to different salivary gland puffs. Genes are split by puff category. Expression is represented as the fraction of maximum normalized expression across all conditions. For immunofluorescence, scale bars are 100μm.

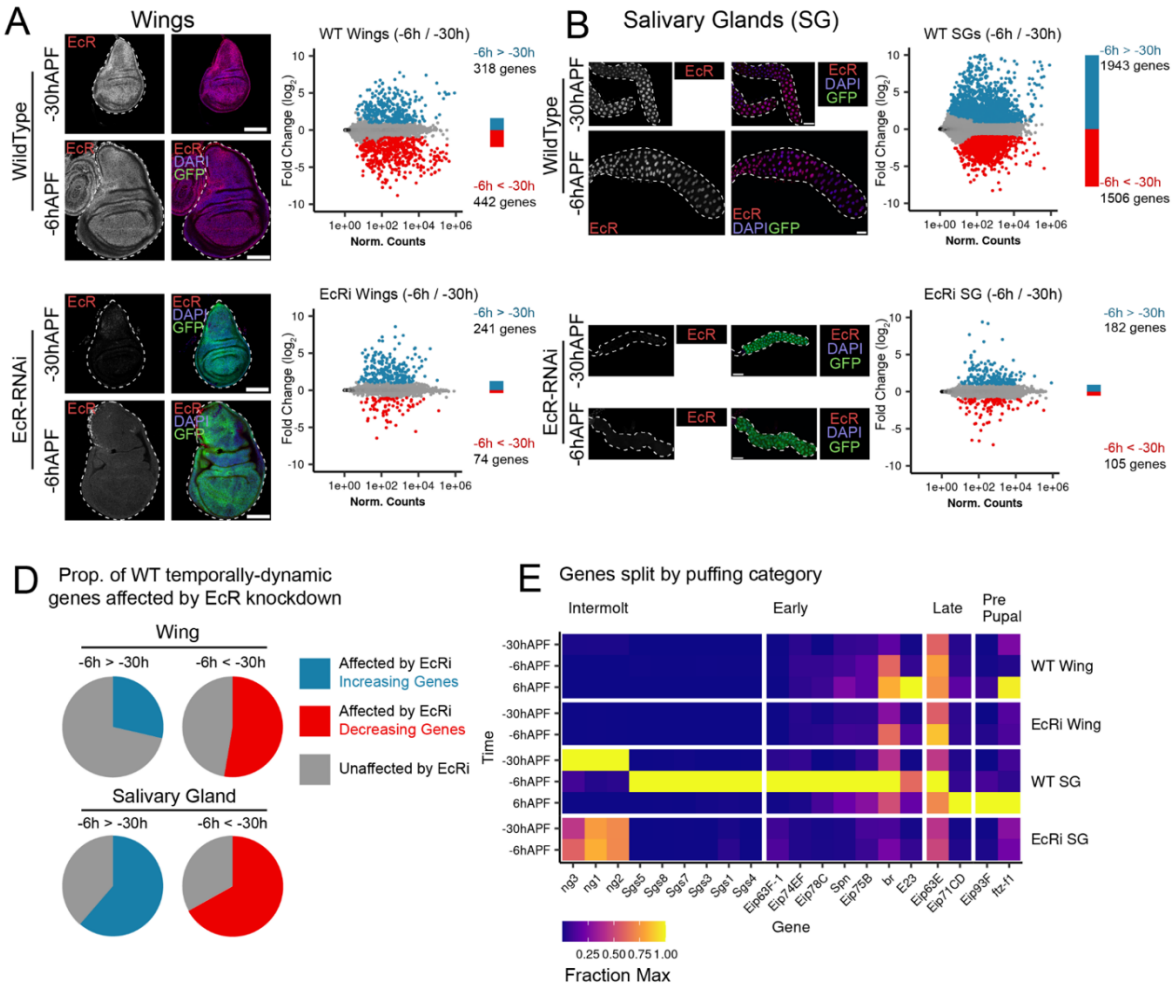
A
Wings
WildType
-30hAPF
-6hAPF
EcR
EcR DAPI GFP
WT Wings (-6h / -30h)
-6h > -30h
318 genes
-6h < -30h
442 genes
Fold Change (log2)
Norm. Counts
B
Salivary Glands (SG)
WT SGs (-6h / -30h)
-6h > -30h
1943 genes
-6h < -30h
1506 genes
EcR-RNAi
EcRi Wings (-6h / -30h)
-6h > -30h
241 genes
-6h < -30h
74 genes
EcRi SG (-6h / -30h)
-6h > -30h
182 genes
-6h < -30h
105 genes
D
Prop. of WT temporally-dynamic genes affected by EcR knockdown
Wing
-6h > -30h
-6h < -30h
Salivary Gland
Affected by EcRi Increasing Genes
Affected by EcRi Decreasing Genes
Unaffected by EcRi
E
Genes split by puffing category
Intermolt
Early
Late
Pre Pupal
Time
WT Wing
EcRi Wing
WT SG
EcRi SG
ng3
ng1
ng2
Sgs5
Sgs8
Sgs7
Sgs3
Sgs1
Sgs4
Eip93F-1
Eip74EF
Eip78C
Spn
Eip75B
br
E23
Eip63E
Eip71CD
Eip93F
ftz-f1
Gene
0.25 0.50 0.75 1.00
Fraction Max

Figure 4.S1: Expression of puffing genes in WT wings

Gene expression from a previously published dataset over wing development (134). B) Gene expression from this study of WT and EcR-RNAi wings and salivary glands as in Figure 4.2. Genes are split by puff category. Expression is represented as the fraction of maximum normalized expression across all conditions.

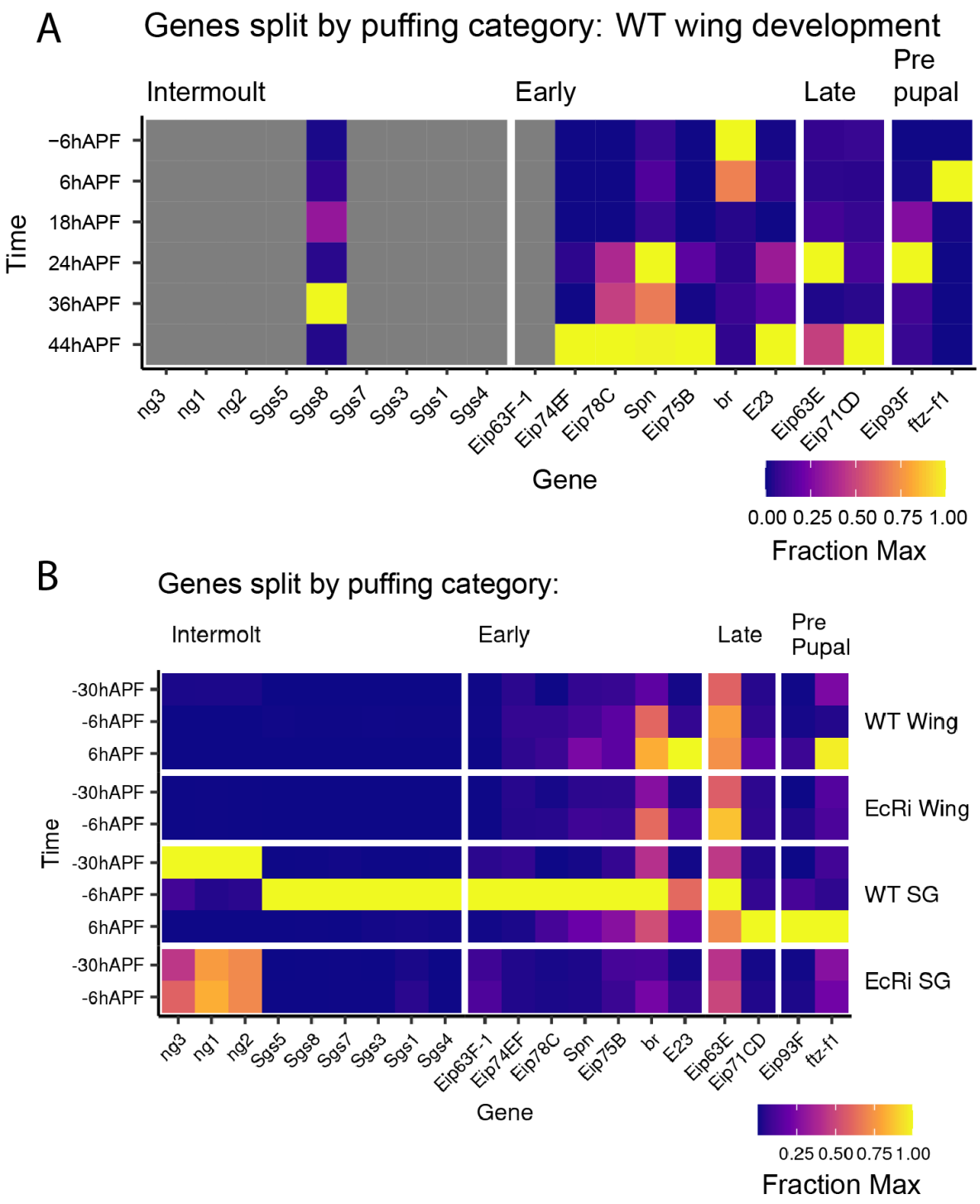
A
Genes split by puffing category: WT wing development
Intermoult
Early
Late
Pre pupal
Time
−6hAPF
6hAPF
18hAPF
24hAPF
36hAPF
44hAPF
ng3
ng1
ng2
Sgs5
Sgs8
Sgs7
Sgs3
Sgs1
Sgs4
Eip63F-1
Eip74EF
Eip78C
Spn
Eip75B
br
E23
Eip63E
Eip71CD
Eip93F
ftz-f1
Gene
0.00 0.25 0.50 0.75 1.00
Fraction Max
B
Genes split by puffing category:
Intermolt
Early
Late
Pre Pupal
Time
-30hAPF
-6hAPF
6hAPF
WT Wing
EcRi Wing
WT SG
EcRi SG
Gene
0.25 0.50 0.75 1.00
Fraction Max

Figure 4.3: EcR binding is tissue-specific

A) Browser shot showing wing and salivary gland (SG) CUT&RUN (C&R) data with different categories of peaks highlighted. B) MA Plots showing the numbers of differentially-bound sites in wings and salivary glands. C) Fraction of genes up- or down-regulated in EcR-RNAi wings and salivary glands that are associated with an EcR C&R peak. H0 (dotted lines) indicate the expected proportion if genes were randomly sampled. D) Upset plot of the number of genes associated with at least one EcR peak in each tissue split by different peak categories. Gene lists mutually exclusive between categories and each gene is only represented once. E) Fraction of maximum RNAseq expression of genes associated with an EcR C&R peak in at least one tissue using the same categories in D. Statistics were performed pairwise between wings and salivary glands in each category (*$P < 0.05$; **$P < 0.01$; *** $P < 0.001$; ****$P < 0.0001$; n.s. not significant, Wilcoxon rank sum test with Bonferroni correction). F) Heatmaps and average signal plots of wing-enriched, shared, and SG-enriched binding sites. G) EcR motif density +/- 1kb around EcR peak summits binned at 10bp. The motif used was a EcR/Usp hybrid motif made by combining EcR and Usp motifs from Fly Factor Survey (67).

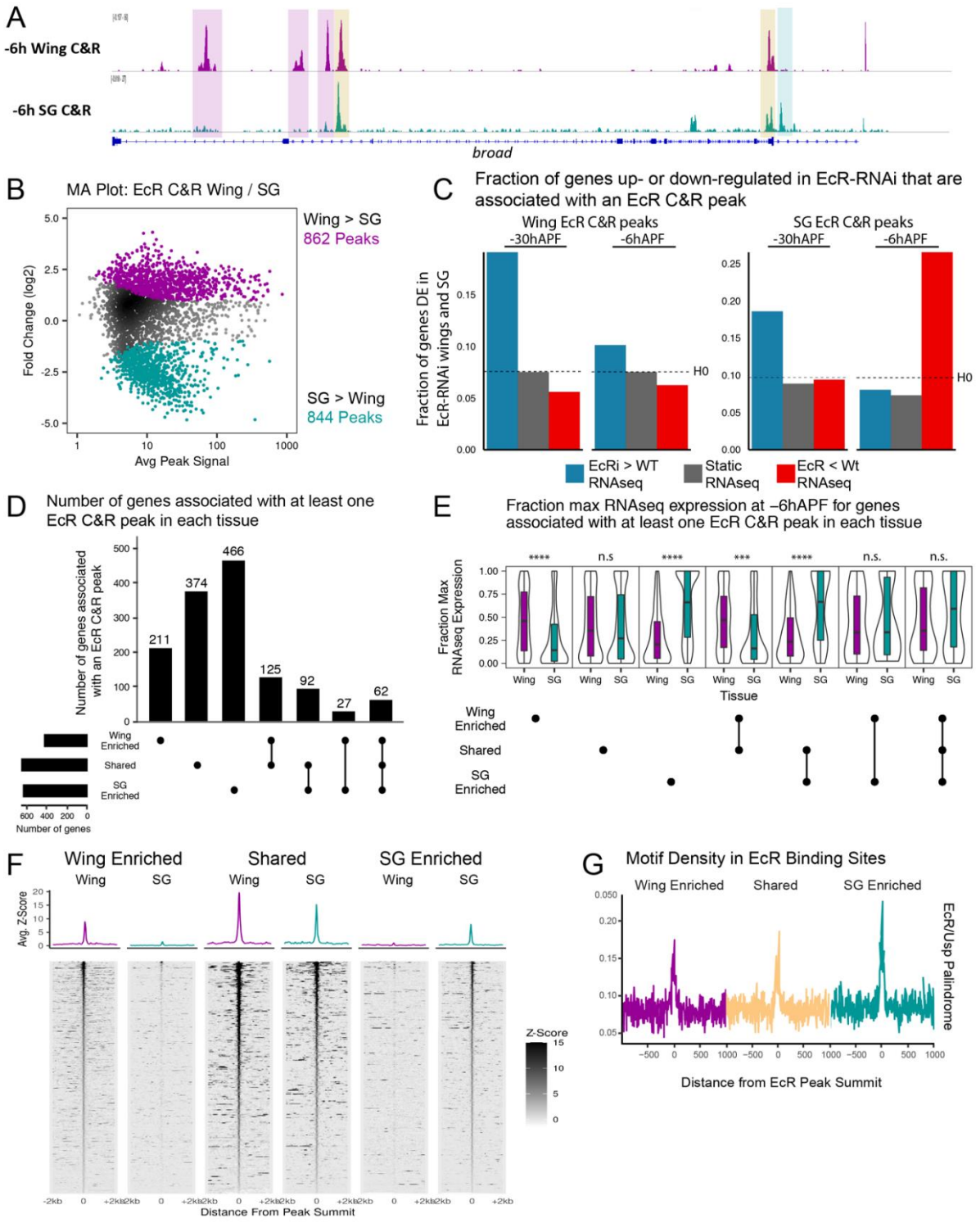
A
-6h Wing C&R
-6h SG C&R
broad
B
MA Plot: EcR C&R Wing / SG
Wing > SG
862 Peaks
SG > Wing
844 Peaks
Fold Change (log2)
Avg Peak Signal
C
Fraction of genes up- or down-regulated in EcR-RNAi that are associated with an EcR C&R peak
Wing EcR C&R peaks
SG EcR C&R peaks
-30hAPF
-6hAPF
Fraction of genes DE in EcR-RNAi wings and SG
H0
EcRi > WT RNAseq
Static RNAseq
EcR < Wt RNAseq
D
Number of genes associated with at least one EcR C&R peak in each tissue
Number of genes associated with an EcR C&R peak
211
374
466
125
92
27
62
Wing Enriched
Shared
SG Enriched
Number of genes
E
Fraction max RNAseq expression at –6hAPF for genes associated with at least one EcR C&R peak in each tissue
Fraction Max RNAseq Expression
Tissue
Wing
SG
F
Wing Enriched
Shared
SG Enriched
Avg. Z-Score
Z-Score
Distance From Peak Summit
G
Motif Density in EcR Binding Sites
EcR/Usp Palindrome
Distance from EcR Peak Summit

Figure 4.S2: Additional properties of EcR binding sites

A) Genome-wide distribution of EcR binding sites. B-C) Histogram and cumulative distribution plots of the distance of each EcR peak to its nearest neighbor. Dotted line indicates 5kb, the definition of an EcR cluster we used in a previous publication (209). D) Fraction of EcR peaks between supernatant and pellet fractions that overlap with one another. E) Motif density of EcR and Usp individual motifs around the peak summit. F) Motif quality of EcR and Usp individual motifs around the peak summit. Motifs were from Fly Factor Survey. The EcR/Usp palindrome was generated by combining the EcR and Usp motifs (67).

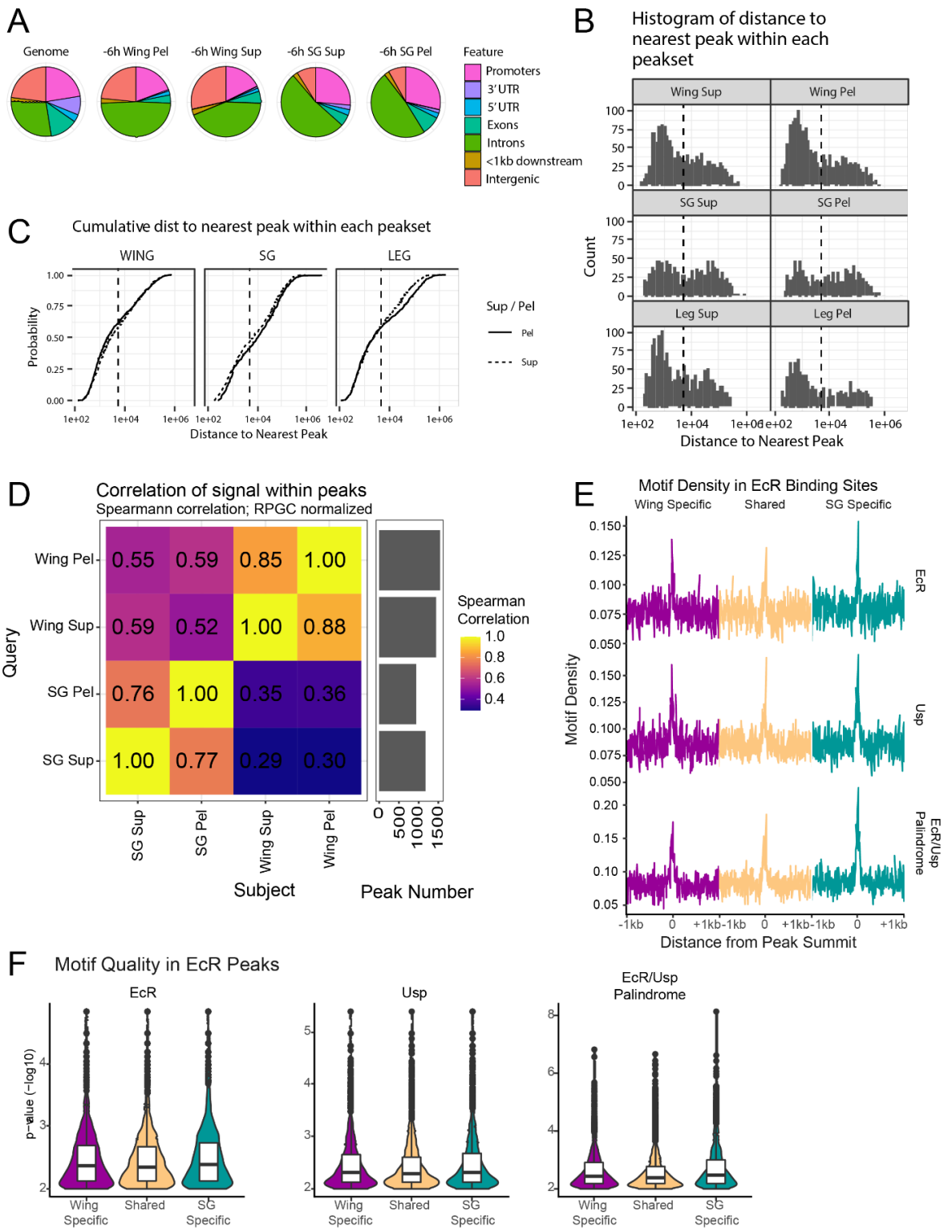
A
Genome
-6h Wing Pel
-6h Wing Sup
-6h SG Sup
-6h SG Pel
Feature
Promoters
3'UTR
5'UTR
Exons
Introns
<1kb downstream
Intergenic
B
Histogram of distance to nearest peak within each peakset
Wing Sup
Wing Pel
SG Sup
SG Pel
Leg Sup
Leg Pel
Count
Distance to Nearest Peak
C
Cumulative dist to nearest peak within each peakset
WING
SG
LEG
Probability
Distance to Nearest Peak
Sup / Pel
Pel
Sup
D
Correlation of signal within peaks
Spearmann correlation; RPGC normalized
Wing Pel
Wing Sup
SG Pel
SG Sup
0.55 0.59 0.85 1.00
0.59 0.52 1.00 0.88
0.76 1.00 0.35 0.36
1.00 0.77 0.29 0.30
Query
Subject
Peak Number
Spearman Correlation
E
Motif Density in EcR Binding Sites
Wing Specific
Shared
SG Specific
Motif Density
EcR
Usp
EcR/Usp Palindrome
Distance from Peak Summit
F
Motif Quality in EcR Peaks
EcR
Usp
EcR/Usp Palindrome
p-value (−log10)
Wing Specific
Shared
SG Specific

Figure 4.S3: EcR binds extensively near canonical ecdysone response genes using a mix of tissue-specific and shared binding sites.

A – D) EcR binding in the wing and salivary glands at sites of salivary glands as previously identified in figure 4.2 and 4.S1. E) Number of EcR binding sites in different categories associated with each gene. Puffing genes are colored red and highlighted.

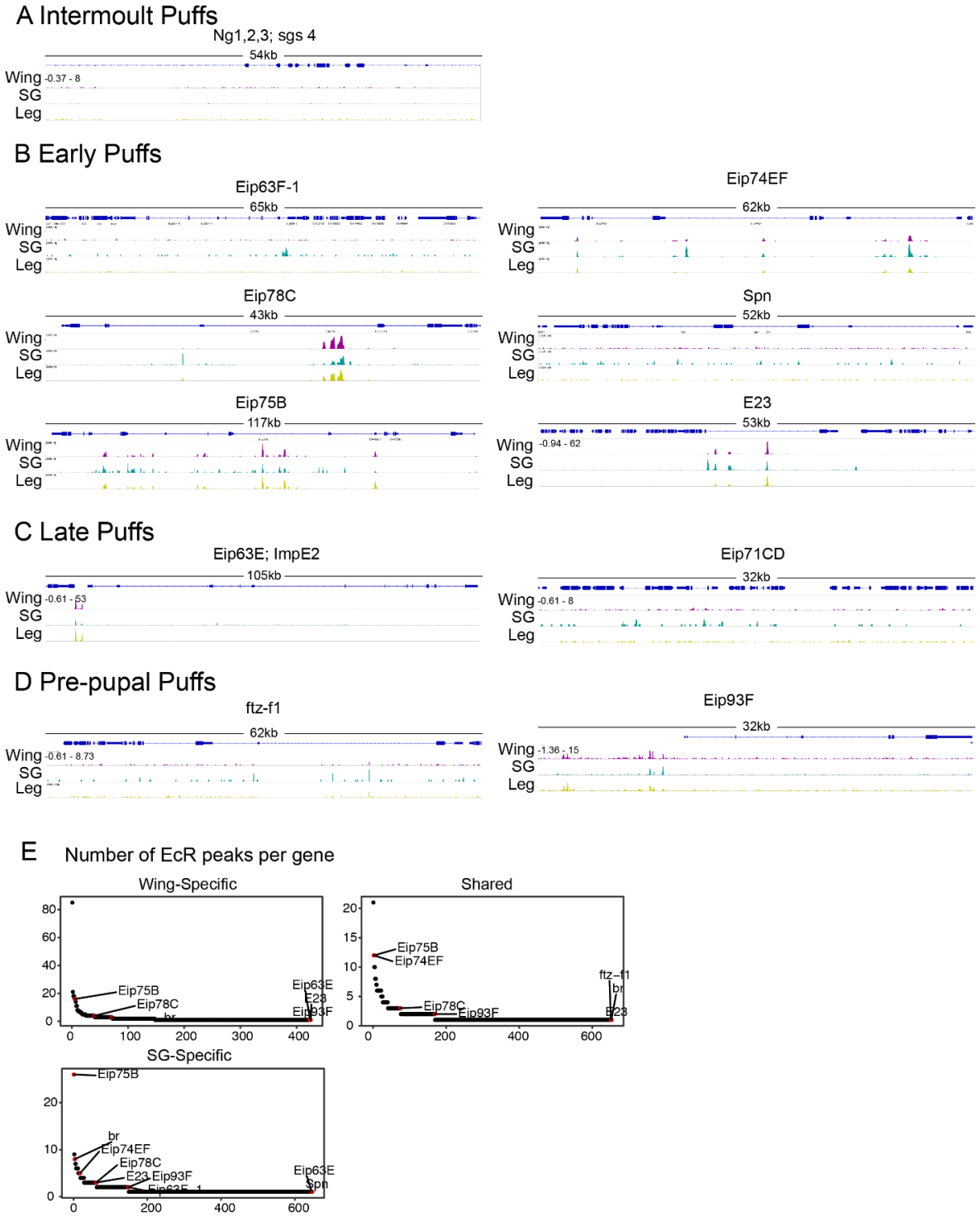
A Intermoult Puffs
Ng1,2,3; sgs 4
54kb
Wing
SG
Leg
-0.37 - 8
B Early Puffs
Eip63F-1
65kb
Eip74EF
62kb
Eip78C
43kb
Spn
52kb
Eip75B
117kb
E23
53kb
-0.94 - 62
C Late Puffs
Eip63E; ImpE2
105kb
-0.61 - 53
Eip71CD
32kb
-0.61 - 8
D Pre-pupal Puffs
ftz-f1
62kb
-0.61 - 8.73
Eip93F
32kb
-1.36 - 15
E
Number of EcR peaks per gene
Wing-Specific
Shared
SG-Specific
Eip75B
Eip78C
Eip63E
E23
Eip93F
br
Eip74EF
ftz-f1
Spn

Figure 4.4: Tissue-specific EcR binding is associated with tissue-specific open chromatin

A) Browser shots of FAIRE and CUT&RUN in WT Wings and SG. B) MA Plots showing numbers of differentially accessible open chromatin sites between WT wings and salivary glands at -6hAPF. C) Proportion of that genes DE by RNAseq between wings and salivary glands that overlap at least one FAIRE peak in different categories. Dotted line indicates the proportion expected by random chance. D) Average FAIRE signal over different categories of EcR C&R peaks. F-G) Activity patterns of differentially-bound and accessible enhancers in the wing and salivary gland. Location of enhancers is indicated in panel A. Scale bars are 100uM.

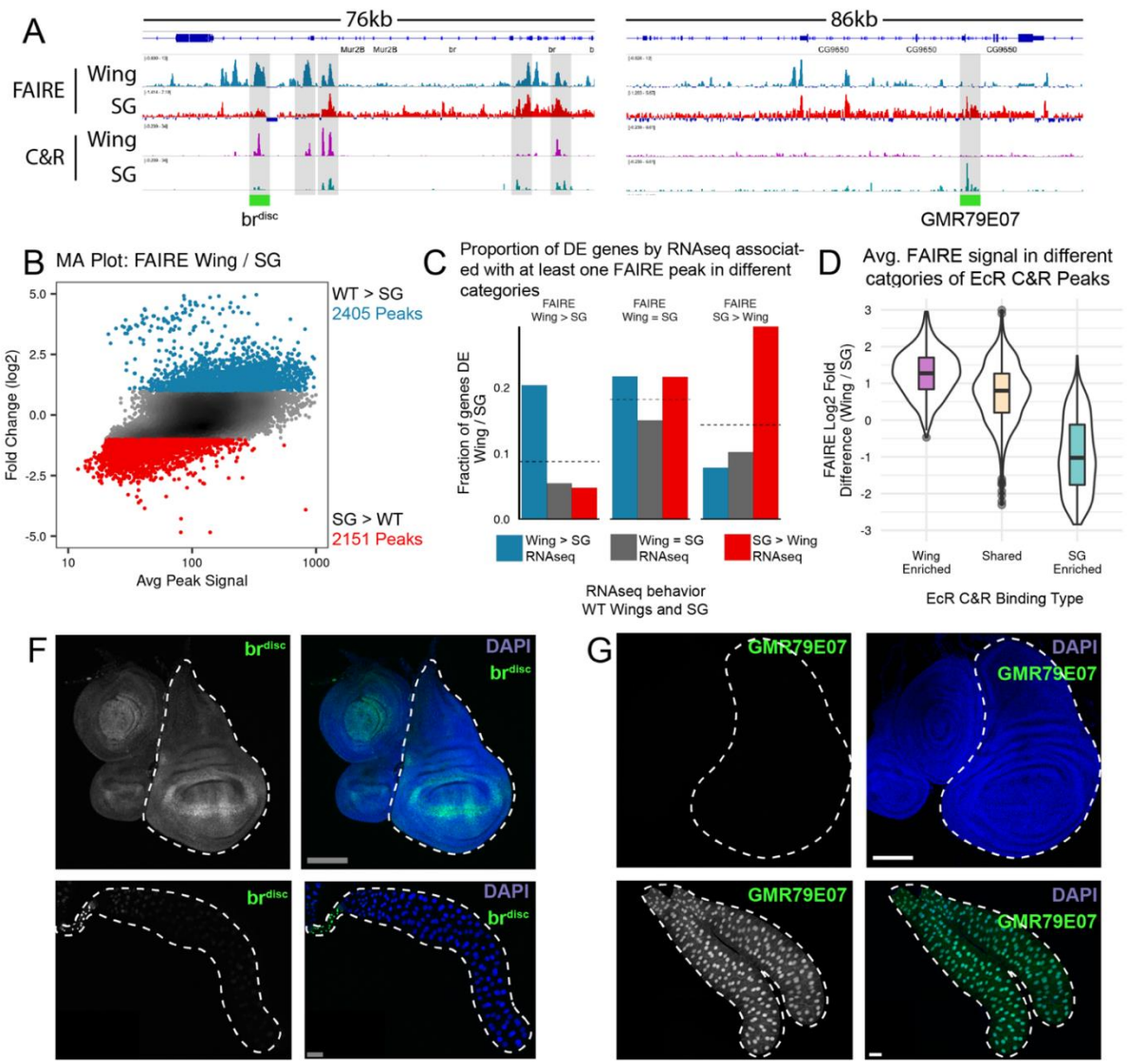
A
76kb
86kb
FAIRE
Wing
SG
C&R
Wing
SG
br^disc
GMR79E07
B
MA Plot: FAIRE Wing / SG
WT > SG
2405 Peaks
SG > WT
2151 Peaks
Fold Change (log2)
Avg Peak Signal
C
Proportion of DE genes by RNAseq associated with at least one FAIRE peak in different categories
FAIRE Wing > SG
FAIRE Wing = SG
FAIRE SG > Wing
Fraction of genes DE Wing / SG
Wing > SG RNAseq
Wing = SG RNAseq
SG > Wing RNAseq
RNAseq behavior WT Wings and SG
D
Avg. FAIRE signal in different catgories of EcR C&R Peaks
FAIRE Log2 Fold Difference (Wing / SG)
Wing Enriched
Shared
SG Enriched
EcR C&R Binding Type
F
br^disc
DAPI
br^disc
G
GMR79E07
DAPI
GMR79E07

Figure 4.5: Knockdown of EcR has little effect on the chromatin landscape

A) Browser shot of FAIRE data from WT and EcR-RNAi wings at -6hAPF and EcR C&R from -6h wings. B) MA Plots showing differences in chromatin accessibility between WT and EcR-RNAi wings. Differential peaks were defined as peaks with an absolute log2 fold change > 1, and an adjusted p-value < 0.05 as identified by DESeq2. C) Heatmaps and average signal of FAIRE over EcR binding sites ranked by strength of EcR binding. D) FAIRE fold-changes (EcR-RNAi / WT) split by whether they do (Bound) or do not overlap (UnBound) an EcR C&R peak. E) Proportion of FAIRE peaks in different categories for all FAIRE peaks, and peaks that overlap an EcR C&R peak. In this analysis, peaks that were called as statistically significant (p-adj < 0.05) but did not meet a log-fold cut-off are identified, as well.

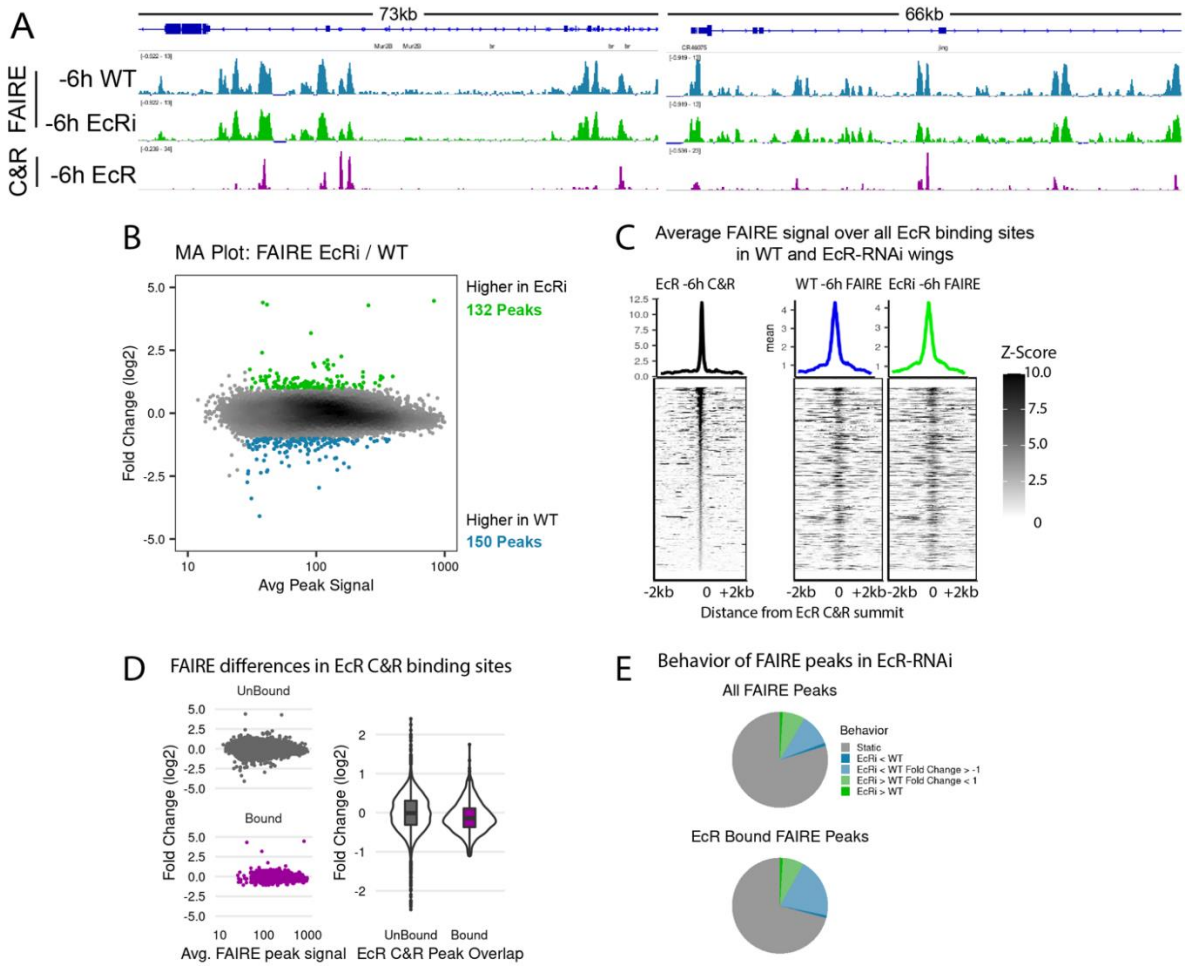
A
73kb
66kb
FAIRE
-6h WT
-6h EcRi
C&R
-6h EcR
B
MA Plot: FAIRE EcRi / WT
Higher in EcRi
132 Peaks
Higher in WT
150 Peaks
Fold Change (log2)
Avg Peak Signal
C
Average FAIRE signal over all EcR binding sites
in WT and EcR-RNAi wings
EcR -6h C&R
WT -6h FAIRE
EcRi -6h FAIRE
mean
Z-Score
-2kb
0
+2kb
Distance from EcR C&R summit
D
FAIRE differences in EcR C&R binding sites
UnBound
Bound
Fold Change (log2)
Avg. FAIRE peak signal
EcR C&R Peak Overlap
E
Behavior of FAIRE peaks in EcR-RNAi
All FAIRE Peaks
Behavior
Static
EcRi < WT
EcRi < WT Fold Change > -1
EcRi > WT Fold Change < 1
EcRi > WT
EcR Bound FAIRE Peaks

Figure 4.6: EcR binding in the leg and wing is more similar than in the salivary gland

A) Browser shot of EcR CUT&RUN in the wing, leg, and salivary gland. B) Correlation between FAIRE signal in the wing, leg and salivary gland. C) MA Plots of C&R signal from wings and legs. Differential peaks were defined as peaks with an absolute log2 fold change > 1, and an adjusted p-value < 0.05 as identified by DESeq2. D) Scatter plots showing average CUT&RUN signal comparing wings, legs, and salivary glands. E) Model for how tissue-specific open chromatin potentiates EcR binding genome-wide.

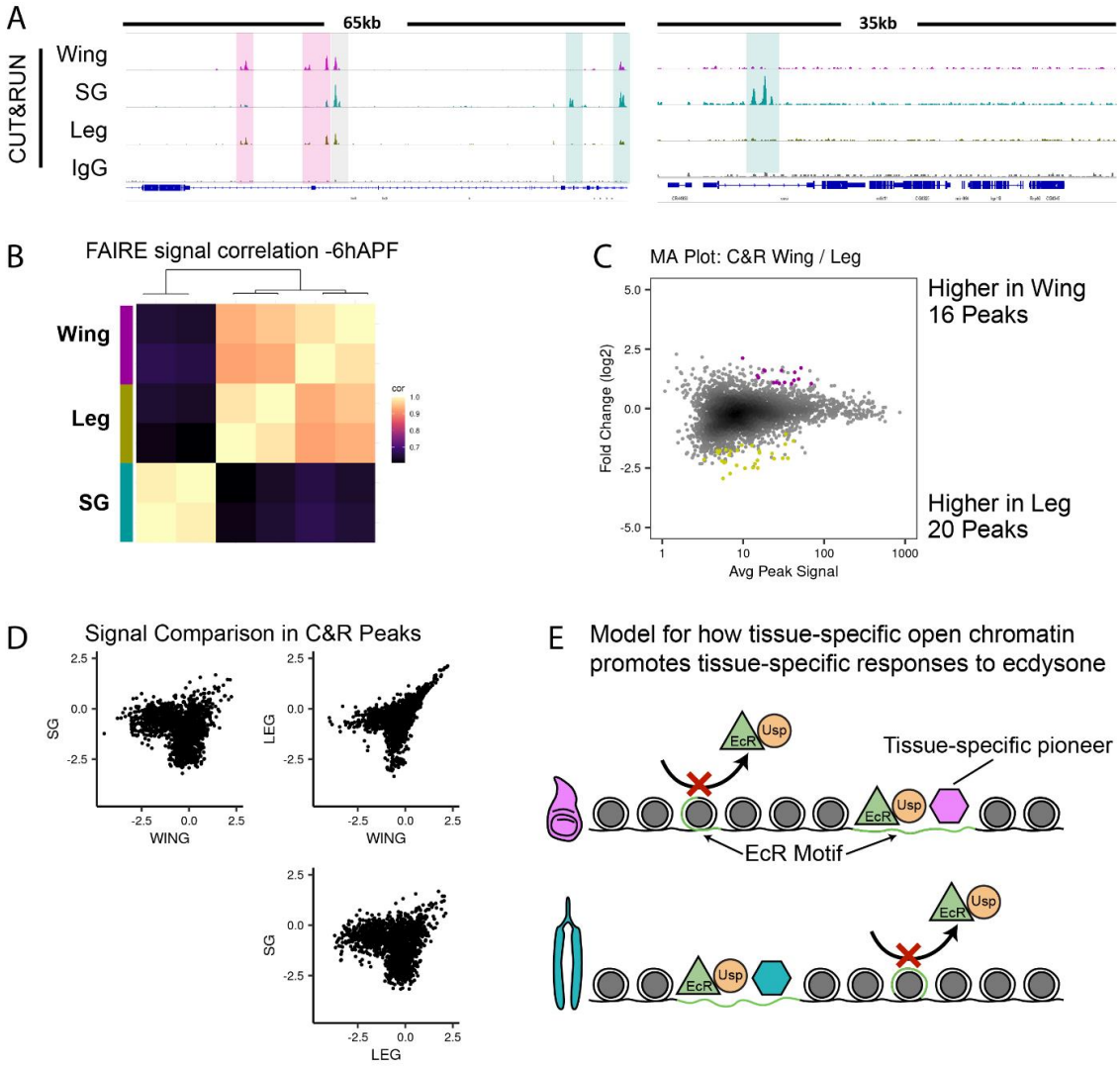

Figure 4.S4: Differential EcR binding sites in the wing and leg overlap sites of differential accessibility

Browser shots of EcR CUT&RUN and FAIREseq in the wing and leg highlighting A) wing enriched binding sites and B) leg-enriched binding sites. B) MA Plot comparing FAIREseq signal in the wing and leg. Differential peaks were defined as peaks with an absolute log2 fold change > 1, and an adjusted p-value < 0.05 as identified by DESeq2

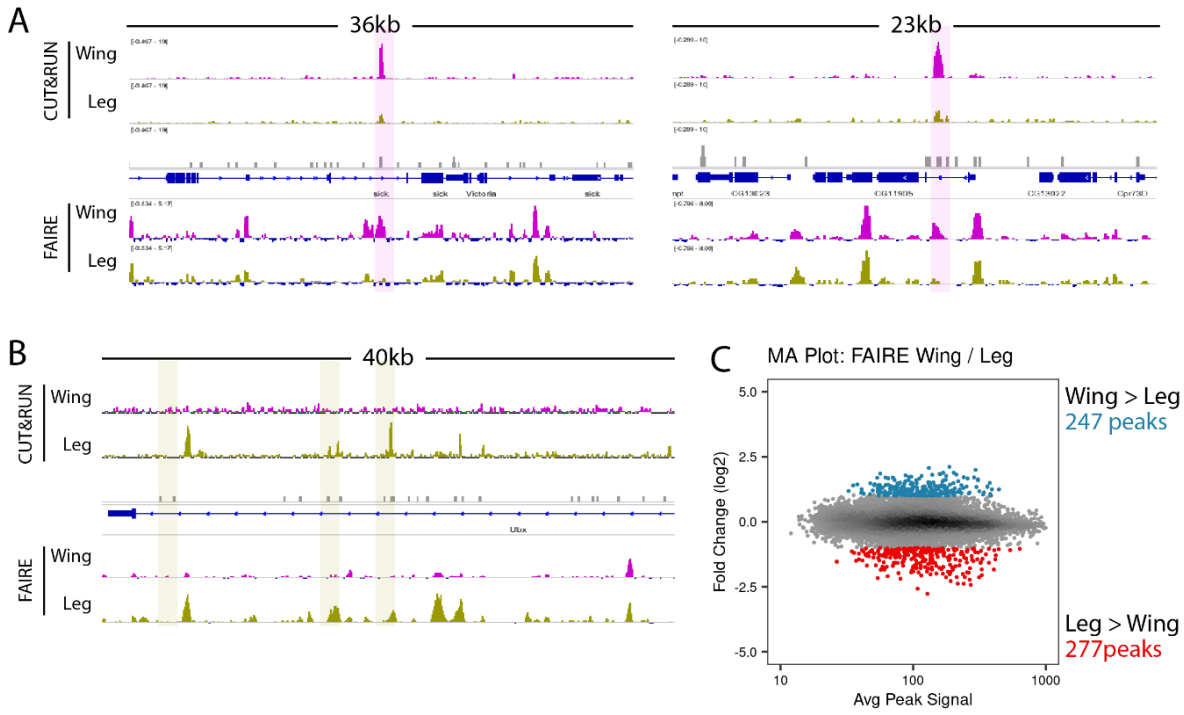

Discussion

The response to ecdysone is both widespread and transcriptionally diverse – tissues throughout the animal respond to identical pulses of ecdysone in different ways. However, the means by which this specificity is achieved remains incompletely understood. In this work, we demonstrated that the response to the mid- and late- larval pulses of ecdysone in the wing and salivary gland are mediated by both shared and tissue-specific EcR binding. The identity of tissue-specific EcR binding sites is dictated, in part, through differences in chromatin accessibility genome-wide.

Tissue- and temporal-specific gene expression profiles in the wing and salivary gland

The end of larval development marks a period of widespread change in the salivary gland and wing. The former begins the production and storage of glue gene products, prior to secreting them and, ultimately, undergoing programmed cell death (101, 109, 210, 211). The latter completes tissue-patterning and growth, and then begins the process of metamorphosis into an adult appendage (134, 212). Our RNAseq data reflect this – the majority of the genes in the wing and salivary gland are dynamic over time, with a broad range of temporal patterns. Most genes that change over time in the wing and salivary gland do so only in one tissue. Additionally, clustering the genes reveals that, even for genes differentially expressed in both the wing and salivary gland between any two time-points, many undergo a broader range of temporal-patterns when the full time-course is considered.

The magnitude of the gene expression response was notably different between the wing and salivary gland. We identified many more differentially expressed genes in the salivary gland than in the wing. This may be a consequence of the heterogeneous nature of

the wing. The end of larval development is marked by changes in the spatial expression pattern of many genes throughout the wing. For any given gene, patterning changes only involve a subset of the overall tissue, and, in some cases, may simply result in different cells expressing the gene, without a strong, aggregate change. For instance, at mid-L3, Delta, is expressed ubiquitously throughout the wing, and at elevated levels in the notum and in a single-stripe along dorsal-ventral (D/V) boundary (189, 190). Prior to wandering, it undergoes additional patterning changes; its expression becomes higher in two stripes adjacent to the D/V boundary, and along each of the presumptive veins (212). This effect is too subtle for our RNAseq data to detect. In contrast, although some gene expression differences occur along the proximal-distal (P/D) axis of the salivary gland, it's a more homogenous tissue. Consequently, we have more sensitivity to detect gene expression changes in the salivary gland than the wing. In the wing we are probably preferentially capturing gene expression changes that occur across relatively large numbers of cells and are underestimating the extent to which the wing's gene expression profile is temporally-dynamic, and, by extension, tissue-specific.

Not all temporal changes in gene expression are necessarily dependent on ecdysone. To determine how many of the gene expression changes we observed were dependent on ecdysone, we assayed gene expression in EcR-RNAi. We found that the majority of genes change over time in WT fail-to-change in EcR-RNAi in both the wing and salivary gland. However, there was a greater requirement for EcR in the salivary gland than in the wing – nearly all the genes that changed in WT salivary glands between -30hAPF and -6hAPF were dependent on EcR, while only slightly more than half were dependent in the wing. Although it's possible that this is still a consequence of not having enough sensitivity to capture

patterning changes, this problem should affect WT and EcR-RNAi equally. Additionally, this result comports well with our previous paper, in which we found only a small number of differentially expressed genes at -6hAPF (209). Consequently, this may reflect a real, differential requirement for ecdysone to promote gene expression changes in the salivary gland at an earlier stage in larval development. Because many of the patterning changes in the wing occur through interactions between other cell-signaling pathways, it's possible this is a consequence of a greater reliance on these other pathways in the wing (153, 189, 228).

Tissue-specific EcR binding mediates gene expression differences between the wing and salivary gland

The possibility that EcR binding might vary across tissues was first indicated by the observation that the puffing cascade differed between the larval fat body and salivary gland (229). Since then, several examples of cis-regulatory elements have been found with functional ECREs that act on genes whose expression is restricted to specific tissues throughout the animal (69, 112–114). Our CUT&RUN data in wings and salivary glands both validates and extends these findings. We find that EcR exhibits both shared and tissue-specific binding sites – a subset of its binding is specific to either the wing or salivary gland. We find both many examples of genes that contain EcR binding sites only in one tissue, indicating that their regulation is wholly tissue-specific, as well many examples of genes that contain both shared and tissue-specific binding sites. A notable example of this is the broad locus, a canonical EcR primary response gene that plays a central role in mediating the response to ecdysone. Our RNAseq data find that temporal kinetics of broad regulation vary between the wing and salivary gland – its expression peaks at -6hAPF in the wing before

decreasing while, in the wing, it appears to continue to increase through +6hAPF. Additionally, one of the wing-specific binding sites we identified corresponds to an enhancer that is active throughout the wing and inactive in the salivary gland. Consequently, our data demonstrate that the response to ecdysone, even at primary response genes, is additively regulated by partially-overlapping regulatory information. One intriguing possibility is that this type of regulation acts as a rheostat to fine-tune the ecdysone response's duration or magnitude. Additionally, recent work has suggested that EcR binding sites shared across tissues may initially be established during embryogenesis and maintained throughout development (205). Consequently, it would be interesting to determine whether the shared binding sites we observe are also found in embryos.

Associating EcR binding sites with genes affected by loss of EcR revealed several interesting properties. In both the wing and salivary gland, EcR binding is associated with affected genes, however this relationship is stronger in the salivary gland than in the wing. This is consistent with our previous work which found that there was only a modest association with gene expression differences in the wing (209). In that paper, we found that EcR regulated both the temporal and spatial activity patterns of target enhancers. It's possible that the stronger association we observe in the salivary gland is because it's a more homogenous tissue, with fewer spatially-restricted genes, or patterning changes, providing us with better sensitivity to detect the effects of EcR loss. The directionality of gene expression changes in EcR-RNAi also revealed differences between the wing and salivary gland. In the wing, EcR binding was associated with genes that were up-regulated in EcR-RNAi wings at both -30hAPF and -6hAPF which is consistent with both our own and others' work showing that EcR functions as a repressor during these time periods (182, 183, 209). In contrast, in the

salivary gland, EcR binding was associated genes that were up-regulated at -30APF in EcR-RNAi salivary glands, and down-regulated at -6hAPF. This relationship indicates EcR acts as a repressor at -30hAPF, and an activator at -6hAPF. Because EcR acts as a repressor during periods of low ecdysone, and as an activator during periods of high ecdysone, this might indicate that the salivary gland is more sensitive to ecdysone than the wing (78, 208).

The open chromatin landscape potentiates EcR binding throughout the genome

The accessibility of cis-regulatory elements genome-wide plays an important role in establishing tissue-specific gene expression profiles by dictating where transcription factors can bind (20, 27, 230). We investigated the interaction between EcR and chromatin accessibility and found that tissue-specific EcR-binding is associated with tissue-specific open chromatin. However, constitutive expression of an EcR-RNAi in the wing resulted in only few changes in chromatin accessibility that were not associated with EcR binding. This indicates that EcR acts as a passive factor whose binding is potentiated by differences in chromatin accessibility. This underscores the important role that the open chromatin landscape plays in shaping the ability of tissues to respond appropriately to extrinsic signaling pathways. Furthermore, previous work has found that response to ecdysone is highly heterogenous across cell types in both in vivo experiments on tissues, as well as in vitro experiments using cell culture (86, 87, 114). It's possible that much of this variability is actually a consequence of differences in open chromatin profiles.

Although EcR acts as a passive factor, other work from our lab has found that temporal changes in open chromatin in the wing are promoted, in part, though the transcription factor E93, an EcR primary response gene expressed maximally at +6hAPF in

the salivary gland and +24hAPF in the wing (105, 155, 167, 231, 232). Loss of E93 causes hundreds of open chromatin sites genome-wide to fail-to-open and fail-to-close (167). These changes are thought to render the tissue competent to respond appropriately to extrinsic signaling pathways, including Dpp and EGFR (155, 231, 232). The potentiation of EcR binding by differences in open chromatin raises the intriguing possibility that E93 may redirect EcR binding throughout the genome by altering the accessibility of its binding sites.

EcR does not exhibit tissue-specific binding between the wing and leg

The leg and wing imaginal discs have similar open chromatin profiles that change coordinately with one another over time. The few differences that exist are enriched around so-called "master regulator" transcription factors which play an important role in specifying tissue-identity (115, 116). In order to test our model that EcR primarily acted as a passive factor that responded the open chromatin landscape, rather than directing it, we assayed its binding profile in the leg imaginal disc. We found that EcR's binding profile was nearly identical to the wing, with a small number of differences that mostly corresponded to the relatively small number of sites that are differentially accessible between the wing and leg. In addition to supporting our model, this result suggests that the contribution of master-regulator transcription factors is relatively minimal. It's believed that master regulators generate differences in the gene expression profiles of the leg and wing by modulating the activity, rather than the accessibility, of enhancers (131). One model by which this might occur is by altering how other transcription factors bind throughout the genome. Our data indicate that the modulation of EcR's binding by master regulators is not a means by which diversity to the ecdysone response is achieved. It's possible that master regulators and EcR

bind non-overlapping sets of enhancers, and that the ecdysone-induced program is largely separate from regulation by tissue-identity factors. Alternatively, and more intriguingly, it may be that master regulators alter the activity enhancers in an additive way, or facilitate recruitment of other activators or repressors, to EcR-bound enhancers without directly affecting EcR's binding.

Table 4.S1: Gene Ontology of Shared Genes

Time	Gene Type	Behavior	GO.ID	Term	Gene	Enrichment	p-value
-30hAPF vs -6hAPF	shared	higher	GO:0055114	oxidation-reduction process	D2hgdh	3.157894737	6.20E-05
-30hAPF vs -6hAPF	shared	higher	GO:0055114	oxidation-reduction process	su(r)	3.157894737	6.20E-05
-30hAPF vs -6hAPF	shared	higher	GO:0055114	oxidation-reduction process	FASN1	3.157894737	6.20E-05
-30hAPF vs -6hAPF	shared	higher	GO:0055114	oxidation-reduction process	Aldh	3.157894737	6.20E-05
-30hAPF vs -6hAPF	shared	higher	GO:0055114	oxidation-reduction process	Cyp6w1	3.157894737	6.20E-05
-30hAPF vs -6hAPF	shared	higher	GO:0055114	oxidation-reduction process	Cyp9b2	3.157894737	6.20E-05
-30hAPF vs -6hAPF	shared	higher	GO:0055114	oxidation-reduction process	CG15093	3.157894737	6.20E-05
-30hAPF vs -6hAPF	shared	higher	GO:0055114	oxidation-reduction process	Acox57D-d	3.157894737	6.20E-05
-30hAPF vs -6hAPF	shared	higher	GO:0055114	oxidation-reduction process	CG10512	3.157894737	6.20E-05
-30hAPF vs -6hAPF	shared	higher	GO:0055114	oxidation-reduction process	Sodh-2	3.157894737	6.20E-05
-30hAPF vs -6hAPF	shared	higher	GO:0055114	oxidation-reduction process	AOX1	3.157894737	6.20E-05
-30hAPF vs -6hAPF	shared	higher	GO:0055114	oxidation-reduction process	PH4alphaSG2	3.157894737	6.20E-05
-30hAPF vs -6hAPF	shared	higher	GO:0055114	oxidation-reduction process	Men	3.157894737	6.20E-05
-30hAPF vs -6hAPF	shared	higher	GO:0055114	oxidation-reduction process	Gpo1	3.157894737	6.20E-05
-30hAPF vs -6hAPF	shared	higher	GO:0055114	oxidation-reduction process	PH4alphaSG1	3.157894737	6.20E-05
-30hAPF vs -6hAPF	shared	higher	GO:0006117	acetaldehyde metabolic process	Aldh	66.66666667	0.0003
-30hAPF vs -6hAPF	shared	higher	GO:0006117	acetaldehyde metabolic process	CrzR	66.66666667	0.0003
-30hAPF vs -6hAPF	shared	higher	GO:0006573	valine metabolic process	CG1673	66.66666667	0.0003
-30hAPF vs -6hAPF	shared	higher	GO:0006573	valine metabolic process	CG15093	66.66666667	0.0003
-30hAPF vs -6hAPF	shared	lower	GO:0071390	cellular resp. to ecdysone	Hr4	18.51851852	5.10E-06
-30hAPF vs -6hAPF	shared	lower	GO:0071390	cellular resp. to ecdysone	Blimp-1	18.51851852	5.10E-06
-30hAPF vs -6hAPF	shared	lower	GO:0071390	cellular resp. to ecdysone	Sgs3	18.51851852	5.10E-06
-30hAPF vs -6hAPF	shared	lower	GO:0071390	cellular resp. to ecdysone	br	18.51851852	5.10E-06
-30hAPF vs -6hAPF	shared	lower	GO:0071390	cellular resp. to ecdysone	lncRNA: let7C	18.51851852	5.10E-06
-30hAPF vs -6hAPF	shared	lower	GO:0045455	ecdysteroid metabolic process	CG12539	9.523809524	0.00074
-30hAPF vs -6hAPF	shared	lower	GO:0045455	ecdysteroid metabolic process	fiz	9.523809524	0.00074
-30hAPF vs -6hAPF	shared	lower	GO:0045455	ecdysteroid metabolic process	shd	9.523809524	0.00074
-30hAPF vs -6hAPF	shared	lower	GO:0045455	ecdysteroid metabolic process	Eip75B	9.523809524	0.00074
-30hAPF vs -6hAPF	shared	lower	GO:0007632	visual behavior	b	11.11111111	0.00221
-30hAPF vs -6hAPF	shared	lower	GO:0007632	visual behavior	Syn	11.11111111	0.00221
-30hAPF vs -6hAPF	shared	lower	GO:0007632	visual behavior	ogre	11.11111111	0.00221

-6hAPF vs +6hAPF	shared	higher	GO:0006606	prot. import into nucleus	Nup205	11.62790698	4.10E-07
-6hAPF vs +6hAPF	shared	higher	GO:0006606	prot. import into nucleus	Nup154	11.62790698	4.10E-07
-6hAPF vs +6hAPF	shared	higher	GO:0006606	prot. import into nucleus	Nup160	11.62790698	4.10E-07
-6hAPF vs +6hAPF	shared	higher	GO:0006606	prot. import into nucleus	Cse1	11.62790698	4.10E-07
-6hAPF vs +6hAPF	shared	higher	GO:0006606	prot. import into nucleus	Gp210	11.62790698	4.10E-07
-6hAPF vs +6hAPF	shared	higher	GO:0006606	prot. import into nucleus	Nup50	11.62790698	4.10E-07
-6hAPF vs +6hAPF	shared	higher	GO:0006606	prot. import into nucleus	Rcc1	11.62790698	4.10E-07
-6hAPF vs +6hAPF	shared	higher	GO:0006606	prot. import into nucleus	CG10286	11.62790698	4.10E-07
-6hAPF vs +6hAPF	shared	higher	GO:0006606	prot. import into nucleus	Ranbp9	11.62790698	4.10E-07
-6hAPF vs +6hAPF	shared	higher	GO:0006606	prot. import into nucleus	Nup358	11.62790698	4.10E-07
-6hAPF vs +6hAPF	shared	higher	GO:0007307	eggshell chorion gene amp.	Mcm6	14.70588235	1.80E-05
-6hAPF vs +6hAPF	shared	higher	GO:0007307	eggshell chorion gene amp.	geminin	14.70588235	1.80E-05
-6hAPF vs +6hAPF	shared	higher	GO:0007307	eggshell chorion gene amp.	PCNA	14.70588235	1.80E-05
-6hAPF vs +6hAPF	shared	higher	GO:0007307	eggshell chorion gene amp.	Caf1-55	14.70588235	1.80E-05
-6hAPF vs +6hAPF	shared	higher	GO:0007307	eggshell chorion gene amp.	RecQ4	14.70588235	1.80E-05
-6hAPF vs +6hAPF	shared	lower	GO:0006614	SRP-dep. cotrans. prot. target. to memb.	TRAM	12.90322581	1.70E-05
-6hAPF vs +6hAPF	shared	lower	GO:0006614	SRP-dep. cotrans. prot. target. to memb.	Sec61alpha	12.90322581	1.70E-05
-6hAPF vs +6hAPF	shared	lower	GO:0006614	SRP-dep. cotrans. prot. target. to memb.	CG5885	12.90322581	1.70E-05
-6hAPF vs +6hAPF	shared	lower	GO:0006614	SRP-dep. cotrans. prot. target. to memb.	Srp9	12.90322581	1.70E-05
-6hAPF vs +6hAPF	shared	lower	GO:0006614	SRP-dep. cotrans. prot. target. to memb.	Srp68	12.90322581	1.70E-05
-6hAPF vs +6hAPF	shared	lower	GO:0006614	SRP-dep. cotrans. prot. target. to memb.	Srp72	12.90322581	1.70E-05
-6hAPF vs +6hAPF	shared	lower	GO:0006614	SRP-dep. cotrans. prot. target. to memb.	Sec61beta	12.90322581	1.70E-05
-6hAPF vs +6hAPF	shared	lower	GO:0006614	SRP-dep. cotrans. prot. target. to memb.	Gtp-bp	12.90322581	1.70E-05
-6hAPF vs +6hAPF	shared	lower	GO:0042742	defense resp. to bacter.	GlyP	2.580645161	1.80E-05
-6hAPF vs +6hAPF	shared	lower	GO:0042742	defense resp. to bacter.	Tep2	2.580645161	1.80E-05
-6hAPF vs +6hAPF	shared	lower	GO:0042742	defense resp. to bacter.	Tep3	2.580645161	1.80E-05
-6hAPF vs +6hAPF	shared	lower	GO:0042742	defense resp. to bacter.	sick	2.580645161	1.80E-05
-6hAPF vs +6hAPF	shared	lower	GO:0042742	defense resp. to bacter.	Dro	2.580645161	1.80E-05
-6hAPF vs +6hAPF	shared	lower	GO:0042742	defense resp. to bacter.	CG7798	2.580645161	1.80E-05
-6hAPF vs +6hAPF	shared	lower	GO:0042742	defense resp. to bacter.	Gbp1	2.580645161	1.80E-05
-6hAPF vs +6hAPF	shared	lower	GO:0042742	defense resp. to bacter.	St3	2.580645161	1.80E-05
-6hAPF vs +6hAPF	shared	lower	GO:0042742	defense resp. to bacter.	drpr	2.580645161	1.80E-05
-6hAPF vs +6hAPF	shared	lower	GO:0042742	defense resp. to bacter.	PGRP-LA	2.580645161	1.80E-05
-6hAPF vs +6hAPF	shared	lower	GO:0042742	defense resp. to bacter.	PGRP-LC	2.580645161	1.80E-05

-6hAPF vs +6hAPF	shared	lower	GO:0042742	defense resp. to bacter.	PGRP-LF	2.580645161	1.80E-05
-6hAPF vs +6hAPF	shared	lower	GO:0042742	defense resp. to bacter.	Eig71Ea	2.580645161	1.80E-05
-6hAPF vs +6hAPF	shared	lower	GO:0042742	defense resp. to bacter.	Eig71Eb	2.580645161	1.80E-05
-6hAPF vs +6hAPF	shared	lower	GO:0042742	defense resp. to bacter.	Eig71Ec	2.580645161	1.80E-05
-6hAPF vs +6hAPF	shared	lower	GO:0042742	defense resp. to bacter.	Eig71Ed	2.580645161	1.80E-05
-6hAPF vs +6hAPF	shared	lower	GO:0042742	defense resp. to bacter.	Eig71Ef	2.580645161	1.80E-05
-6hAPF vs +6hAPF	shared	lower	GO:0042742	defense resp. to bacter.	Eig71Eg	2.580645161	1.80E-05
-6hAPF vs +6hAPF	shared	lower	GO:0042742	defense resp. to bacter.	Eig71Eh	2.580645161	1.80E-05
-6hAPF vs +6hAPF	shared	lower	GO:0042742	defense resp. to bacter.	Eig71Ei	2.580645161	1.80E-05
-6hAPF vs +6hAPF	shared	lower	GO:0042742	defense resp. to bacter.	Eig71Ej	2.580645161	1.80E-05
-6hAPF vs +6hAPF	shared	lower	GO:0042742	defense resp. to bacter.	Eig71Ek	2.580645161	1.80E-05
-6hAPF vs +6hAPF	shared	lower	GO:0042742	defense resp. to bacter.	NUCB1	2.580645161	1.80E-05
-6hAPF vs +6hAPF	shared	lower	GO:0042742	defense resp. to bacter.	Npc2e	2.580645161	1.80E-05
-6hAPF vs +6hAPF	shared	lower	GO:0001838	embryo. epith. tube formation	mmy	18.18181818	1.80E-05
-6hAPF vs +6hAPF	shared	lower	GO:0001838	embryo. epith. tube formation	Mmp2	18.18181818	1.80E-05
-6hAPF vs +6hAPF	shared	lower	GO:0001838	embryo. epith. tube formation	kkv	18.18181818	1.80E-05
-6hAPF vs +6hAPF	shared	lower	GO:0001838	embryo. epith. tube formation	knk	18.18181818	1.80E-05

CHAPTER 5: DISCUSSION AND FUTURE DIRECTIONS

Contrasting roles of EcR and E93 in directing changes in open chromatin

In this work, we found that differences in chromatin accessibility between tissues and across time are a central means by which temporal- and tissue-specificity is achieved in response to ecdysone. The ecdysone response gene, E93, is active during an ~24h window of wing development and had been previously shown to be a specificity factor that distinguishes early and late ecdysone pulses. has a temporally-restricted pattern of expression and have previously been shown to temporal-specific responses ecdysone. We found that expression of E93 is required to both open and close open chromatin sites throughout the genome; in the absence of E93, many of the sites it binds to fail-to-open and many fail-to-close. By cloning target enhancers into reporter constructs, we demonstrated that E93 binds to functional enhancers whose activity corresponds to their accessibility. In E93 mutants, in which these sites fail-to-open and fail-to-close, these enhancers had aberrant activity patterns – they failed to turn-on or off in a manner that corresponded to their accessibility in E93 mutants. These data indicate that a central means by which E93 directs temporal-specific responses to ecdysone is by promoting changes in accessibility.

We also assayed the role of the ecdysone receptor, EcR, in directing changes in open chromatin. In contrast to E93, EcR does not appear to direct changes in chromatin accessibility. Instead, it appears to respond to them. Tissue-specific EcR binding in the wing and salivary gland was associated with tissue-specific open chromatin differences – sites that

were bound more strongly in the wing and salivary gland were also more accessible in those tissues. However, loss of EcR did not affect the accessibility of its binding sites. Consequently, in contrast to E93, EcR does not appear to direct changes in accessibility, but, instead, it appears that differences in accessibility potentiate EcR binding.

A puzzling aspect of this result is that EcR has previously been shown to interact with the ATP-dependent chromatin remodeling complexes NURF and NURD in a ligand-dependent manner (82, 163). The former has been shown to be important for EcR's ability to activate genes; while the latter has been shown for its ability to repress them (82, 163). One possibility is that these associations facilitate EcR's ability to modulate the transcriptional response in a more subtle way, either by altering their accessibility, or by more precisely positioning nucleosomes, both of which are means by which ATP-dependent chromatin remodeling complexes can modulate gene expression (233, 234). Our inability to detect these differences may be a technical consequence of using FAIRE, which has a lower signal-to-noise ratio than other methods of profiling accessibility like ATACseq (235). Alternatively, it may be that EcR's regulation of accessibility is spatially or temporally limited and that we simply assayed the wrong time point. In the future, it would be interesting to assay accessibility using the most recent ATAC protocols to improve signal-to-noise (235, 236). Additionally, directly assaying the binding of NURF and NURD at multiple time points to determine to what role they play in mediating the ecdysone response, and whether this role is spatially- or temporally-restricted, could be an interesting extension of this work.

Extending the Ashburner Model

A clear possibility that arises from this work is that temporal-specificity to the ecdysone response is achieved by the sequential activation of primary response genes with pioneer-like activity that alter the accessibility of EcR's binding sites genome-wide. In this model, some of EcR's primary response transcription factors, like E93, Ftz-f1, and Hr39, would open EcR's binding sites near genes expressed at the next stage of development and close its binding sites near genes expressed at the current stage of development. This would essentially recontextualize the canonical Ashburner model as a model of sequential changes in chromatin accessibility: EcR activates early genes, some of which are transcription factors that act to open EcR binding sites near mid- and late-genes while also closing their own binding sites.

In the above model, changes in EcR binding would simply be a consequence of changes in chromatin accessibility without any direct interaction between EcR and its downstream transcription factors. However, a fundamental precept of the Ashburner model is that EcR and early response genes co-regulate late genes, which has been demonstrated in a number of different contexts (52, 92, 237). There is also ample evidence that EcR may physically interact with a subset of its own primary response transcription factors. In the fat body of the mosquito, *Aedes aegypti,* for instance, the ecdysone primary response transcription factor, *ftz-f1,* forms a complex with EcR and the p160 coactivator, FISC, where it renders competence to the *Vg* gene to respond to ecdysone (203). Similarly, in the silk moth, *Bombyx mori,* E93 has been immunoprecipitated with EcR/Usp – an interaction hypothesized to occur through a canonical LXXLL nuclear-receptor interaction motif found in E93 (238, 239). In contrast to Ftz-f1, however, the interaction of EcR and E93 appeared to

attenuate the ability of E93 to activate transcription (238). Although these studies have demonstrated this effect on individual EcR binding sites, no one has performed these experiments genome-wide. Additionally, whether these interactions control the open chromatin landscape, as well as how they might do so, is unknown. It's possible that there are two means by which EcR binding is redirected throughout the genome: 1) changes in accessibility could cause EcR to be passively re-directed to newly-accessible sites, and 2) ecdysone-response transcription factors could physically interact with EcR and actively recruit it to new sites independently of accessibility changes.

Moving forward, it would be interesting to directly study how EcR interacts with its own primary response transcription factors. Because the response to ecdysone is tissue-specific, these experiments would, ideally, be performed in single-tissues across different timepoints. Historically, the ability to assay tissue-specific binding of transcription factors in *Drosophila* has been difficult due to the large amount of input tissue required for ChIPseq. However, the recent development of low-input methods to assay transcription factors with CUT&RUN and CUT&TAG, the former of which was successfully used to assay EcR binding in this work, has rendered these experiments much more feasible (185, 220, 240). Consequently, it is now possible to assay EcR's binding profile, as well as the binding profiles of ecdysone-response transcription factors, at multiple stages of development and compare these data to open chromatin profiles. Additional experiments might involve assaying EcR binding and open chromatin in mutant tissue and performing the reciprocal experiments of assaying the binding of putative EcR-interacting partners. The transcription factors ftz-f1, which is active at +6hAPF, and E93, active at 24hAPF, would be ideal

candidates for these experiments as they have both been shown to be temporal-competence factors, and the former has already been shown to potentiate EcR binding (98, 105, 203).

Cell-type specific regulation of target enhancers

Drosophila wing development is characterized by dramatic changes in the spatial pattern of genes over time. This is sometimes presented as occurring through a processive series of events driven by the cooperation and antagonism of cell-signaling pathways acting throughout the wing (189, 190, 212, 228). However, several studies have demonstrated that, during third instar, patterning of the wing is subject to at least two independent checkpoints – the minimal viable and post-critical weight checkpoints – that are both regulated by ecdysone signaling (39, 182, 183). Manipulation of ecdysone signaling, either through changes in the titer of ecdysone, knockdown of EcR, or over-expression of a constitutive repressor form of EcR (EcR dominant-negative) can cause patterning of the wing to delay or advance precociously (183, 241). All these data indicate that ecdysone signaling plays an important role in regulating the timing of wing patterning. However, it was not clear at what level in the transcriptional hierarchy this regulation occurred – whether patterned genes were directly regulated by EcR, its primary response transcription factors, or genes further downstream.

Our data demonstrate that EcR plays a direct and widespread role in mediating the response to ecdysone. Using CUT&RUN to assay EcR binding in the wing, we identified thousands of EcR binding sites throughout the genome. Many of these genes were spatially-restricted to subpopulations of cells throughout the wing and were temporally-dynamic over time. The gene *Delta (Dl)*, for example, is expressed in a single stripe at the dorsal/ventral boundary (D/V) boundary and in cells the notum at the onset of third instar (189, 190, 212).

Over the course of third instar, it becomes expressed in cells directly adjacent to cells at the D/V boundary, in cells in the hinge, each of the presumptive wing veins, and in proneural cells (189, 190, 212).

We cloned candidate binding sites from the *Dl* locus and found that, as expected, the activity of each enhancer was only active in specific subpopulations of cells that corresponded to specific cell fates. The Dl^{SOP} enhancer was active only a dozen cells that appeared to be the sensory organ precursors (SOPs), while Dl^{teg}, was active more broadly in cells that we believe correspond to the presumptive tegula. Mitotic clones that were mutant for EcR's binding partner, *ultraspiracle (usp)*, caused ectopic enhancer activity for both Dl^{SOP} and Dl^{Teg}. However, presence of a clone was not sufficient for ectopic enhancer activity. Instead, the enhancers appeared to become active in cells near where they were already active.

These observations raise the question of how a ubiquitously expressed transcription factor, responding to a ubiquitous signal, could cause de-repression in a spatially-restricted manner. One straightforward model is that EcR-mediated repression antagonizes local activation signals to restrict and refine the spatial pattern. In the absence of EcR, activation signals may breach some threshold of signaling causing the enhancer to become active in a larger number of cells. Although it's possible that EcR performs this function alone, there is some evidence that it may interact with other repressor complexes. ChIP-chip experiments that assayed the binding of the Hairless repressor, an antagonist of Notch signaling, found that many of its binding overlapped with EcR binding sites (14). However, whether EcR directly interacts with Hairless, and other effectors of cell-signaling pathways, as well as whether its repression is additive, synergistic, or antagonistic, remains unknown. Since EcR

acts at the top of a transcriptional hierarchy that regulates widespread developmental events, exploring these questions has proved challenging. It's difficult to disentangle a direct role for EcR from a downstream effect. These experiments would likely have to be done by dissecting the grammar of individual enhancers by identifying and mutation binding sites for Hairless or other repressors. Alternatively, a biochemical approach might involve investigating whether EcR physically interacts with repressor complexes. Recently, BioID, which makes use of a promiscuous biotin-ligase, was recently used to identify novel EcR interactors in S2 cells(242). Repeating these experiments in individual tissues would prove challenging but should be technically feasible.

An intriguing alternative possibility is that the cell-type specific de-repression in *usp* mutants reflects cell-type specific binding of EcR within the wing disc which could occur through cooperative interactions with cell-type specific transcription factors. SOP selection in the wing, for instance, involves a negative-feedback loop in which a single-cell within a group of cells expresses progressively higher levels of Notch and up-regulates SOP genes (243). Cells adjacent to it express higher levels of Dl and down-regulate SOP genes (243). Consequently, EcR could cooperatively interact with other TFs to facilitate repression of SOPs. It's easy to imagine similar processes happening throughout the wing disc.

In addition to cooperative interactions, cell-type specific open chromatin could result from cell-type specific EcR binding events. Within the last five years, a plethora of single-cell open chromatin data has demonstrated that many tissues have heterogeneous open chromatin profiles. Recently, single-cell ATACseq on the larval eye-antennal disc found heterogenous open chromatin profiles within this tissue (244, 245). Previous work had found that bulk open chromatin profiles of the eye-antennal disc appeared to be a composite of

open chromatin sites found in the CNS, which is developmentally more similar to the presumptive eye, and the thoracic wing, leg, and haltere, which are more developmentally more similar to the antennae (131). Single-cell ATAC data, however, found that while the dominant division occurred between eye and antenna, the antenna alone was also comprised of a heterogeneous mixture of cell types (244). Additionally, although single-cell ATACseq has not been performed on the wing disc, sorted-cell ATACseq was recently performed that compared the wing pouch to the remainder of the tissue and identified differentially-accessible open chromatin sites across these two populations indicating the wing, too, is likely at least somewhat heterogenous (246). Since EcR binding appears to be potentiated by differences in open chromatin, cell-type specific open chromatin events could render different sites accessible or inaccessible to EcR binding throughout the wing and result in cell-type specific responses to ecdysone. Moving forward, it would be interesting to determine the true extent to which the open chromatin profile of the wing is heterogenous, and whether some of these differences correspond to EcR binding sites. Since CUT&RUN requires low-input, it should be possible to perform sorted-cell CUT&RUN to directly interrogate whether EcR binding is cell-type specific (185).

Additionally, one question that arises from these types of data is how cell-type specific open chromatin profiles are coordinated over time. Previously, we found that E93 acted as a temporal-specific transcription factor to direct global changes in accessibility in the wing (167). However, these experiments were based off the observation that the open chromatin profiles in the wing, leg, and haltere change coordinately over time (131). If the open chromatin profiles in imaginal tissues is heterogeneous, then it would raise the question of how a mixture of shared and tissue-specific open chromatin changes are regulated across

the three tissues such that their aggregate profiles remained similar over time. At a high-level, one possibility is that temporal- and cell-type specific accessibility programs operate in parallel – the former perhaps mediated by ubiquitously-expressed, temporally-dynamic, ecdysone response genes, while the latter mediated by cell-type specific transcription factors – and that the accessibility profile of each cell is a composite of the two.

EcR binding's effect on puff and 3D chromatin architecture

The large polytene salivary gland chromosomes of *Drosophila* have been used to investigate gene regulation for decades. Polytenes are broadly organized into three structures: 1) dark, highly condensed, bands; 2) lighter, more decondensed, interbands; and 3) large, highly decondensed, puffs (49, 94, 247, 248). Bands and interbands are generally thought to map to inactive and active genes, respectively (51). A subset of interbands expand into the polytene puffs and were originally hypothesized to be regions of active transcription (248). However, inhibition of transcription elongation does not result in puff contraction and many interbands map to actively transcribed genes even though they do not appear as puffs indicating that transcription is neither necessary nor sufficient for puff formation (249). Scanning electron microscopy (SEM) of the largest form of puffs, Balbiani Rings, have found that they are comprised of thousands of looped DNA structures, along which RNP complexes are visible (250). Although the molecular determinants of puff formation and contraction are poorly understood, several studies have identified proteins required for their formation. The chromosome looping protein, cohesin, as well as the poly(ADP-ribose) polymerase (PARP) have both been shown to be required for puff formation. In their absence, puffs contract (202, 251).

The Ashburner model was originally developed by examining the sequential expansion and contraction of puffs. Though not all puffs are involved in the ecdysone cascade, many of the primary response genes for EcR are located in puffs and our salivary gland data confirm that EcR directly binds these sites. With the ability to directly interrogate EcR binding, one question that arises is what role EcR plays in the formation of puffs, as well as how it interacts with both PARP and cohesin to promote their formation. Compared to other loci, primary response genes exhibit a higher number of EcR binding sites spread out across their gene bodies. The amplitude of EcR binding sites at these loci are also frequently some of the highest throughout the genome. Additionally, PARP has been shown to biochemically interact with EcR in a ligand-dependent manner and putatively co-occupies an EcR binding site (201, 202, 252). This interaction is particularly intriguing because, recently, recruitment of PARP to the *shh* gene during mammalian limb development was shown to be required for gene activation, but, paradoxically, results in increased distances between enhancers and promoters (253).

Consequently, one model might be that puffs are sites in which a large number of high-affinity EcR binding sites causes repeated looping of enhancers to either the promoter or one another. EcR binding could either promote a looser structure through recruitment of PARP1 and ADP-ribosylation of histones or its binding could be a facilitated by a loose chromatin structure. It's possible that cohesin-mediated looping of the EcR binding sites is completely responsible for the formation of the looped-structures. Alternatively, it could be that cohesin enhances EcR binding across the locus. In that scenario, loss of cohesin may result in decreased occupancy of EcR and its binding partners, including PARP1, resulting in a more contracted chromatin state. However, these models are entirely speculative. In the

future, it would be interesting to investigate the roles of PARP1, cohesin, EcR, and RNA polymerase in promoting puff formation. It would also be interesting to determine whether the polytene puffs are specific to polytene chromosomes, or whether they are, instead, a consequence of a chromatin state found in many cells which manifests as a puff specifically in polytene chromosomes.

REFERENCES

1. Waddington, Conrad H., *The Strategy of Genes* (George Allen & Unwin Ltd, 1957).

2. S. S. Gisselbrecht, *et al.*, Transcriptional Silencers in Drosophila Serve a Dual Role as Transcriptional Enhancers in Alternate Cellular Contexts. *Mol Cell* (2019) https:/doi.org/10.1016/j.molcel.2019.10.004.

3. J. Erceg, *et al.*, Dual functionality of cis-regulatory elements as developmental enhancers and Polycomb response elements. *Genes Dev* **31**, 590–602 (2017).

4. M. Osterwalder, *et al.*, Enhancer redundancy provides phenotypic robustness in mammalian development. *Nature* **554**, 239 (2018).

5. M. J. Borok, D. A. Tran, M. C. W. Ho, R. A. Drewell, Dissecting the regulatory switches of development: lessons from enhancer evolution in Drosophila. *Development* **137**, 5–13 (2010).

6. E. Cannavò, *et al.*, Shadow Enhancers Are Pervasive Features of Developmental Regulatory Networks. *Curr Biol* **26**, 38–51 (2016).

7. J. P. Bothma, *et al.*, Enhancer additivity and non-additivity are determined by enhancer strength in the Drosophila embryo. *Elife* **4** (2015).

8. E. Z. Kvon, R. Waymack, M. G. Elabd, Z. Wunderlich, Enhancer redundancy in development and disease. *Nat Rev Genet* (2021) https:/doi.org/10.1038/s41576-020-00311-x.

9. S. Heinz, *et al.*, Simple Combinations of Lineage-Determining Transcription Factors Prime cis-Regulatory Elements Required for Macrophage and B Cell Identities. *Molecular Cell* **38**, 576–589 (2010).

10. J. B. Carleton, K. C. Berrett, J. Gertz, Multiplex Enhancer Interference Reveals Collaborative Control of Gene Regulation by Estrogen Receptor α-Bound Enhancers. *Cell Syst* **5**, 333-344.e5 (2017).

11. C. Chronis, *et al.*, Cooperative Binding of Transcription Factors Orchestrates Reprogramming. *Cell* **168**, 442-459.e20 (2017).

12. I. K. Nolis, *et al.*, Transcription factors mediate long-range enhancer-promoter interactions. *Proc Natl Acad Sci U S A* **106**, 20222–20227 (2009).

13. S. Barolo, J. W. Posakony, Three habits of highly effective signaling pathways: principles of transcriptional control by developmental cell signaling. *Genes Dev* **16**, 1167–1181 (2002).

14. S. K. K. Chan, *et al.*, Role of co-repressor genomic landscapes in shaping the Notch response. *PLoS Genet.* **13**, e1007096 (2017).

15. A. Tsai, *et al.*, Nuclear microenvironments modulate transcription from low-affinity enhancers. *Elife* **6** (2017).

16. J. Crocker, *et al.*, Low affinity binding site clusters confer hox specificity and regulatory robustness. *Cell* **160**, 191–203 (2015).

17. J. F. Kribelbauer, C. Rastogi, H. J. Bussemaker, R. S. Mann, Low-Affinity Binding Sites and the Transcription Factor Specificity Paradox in Eukaryotes. *Annu Rev Cell Dev Biol* **35**, 357–379 (2019).

18. E. Preger-Ben Noon, *et al.*, Comprehensive Analysis of a cis-Regulatory Region Reveals Pleiotropy in Enhancer Function. *Cell Rep* **22**, 3021–3031 (2018).

19. G. Sabarís, I. Laiker, E. Preger-Ben Noon, N. Frankel, Actors with Multiple Roles: Pleiotropic Enhancers and the Paradigm of Enhancer Modularity. *Trends Genet* **35**, 423–433 (2019).

20. K. S. Zaret, J. S. Carroll, Pioneer transcription factors: establishing competence for gene expression. *Genes Dev.* **25**, 2227–2241 (2011).

21. A. Soufi, *et al.*, Pioneer transcription factors target partial DNA motifs on nucleosomes to initiate reprogramming. *Cell* **161**, 555–568 (2015).

22. Mark Derewicz, A first of its kind tool to study the histone code. *UNC College of Arts & Sciences* (2015) (January 12, 2021).

23. L. de la Torre-Ubieta, *et al.*, The Dynamic Landscape of Open Chromatin during Human Cortical Neurogenesis. *Cell* **172**, 289-304.e18 (2018).

24. K. N. Schulz, *et al.*, Zelda is differentially required for chromatin accessibility, transcription factor binding, and gene expression in the early Drosophila embryo. *Genome Res* **25**, 1715–1726 (2015).

25. K. M. Jozwik, J. S. Carroll, Pioneer factors in hormone-dependent cancers. *Nat Rev Cancer* **12**, 381–385 (2012).

26. M. Iwafuchi-Doi, K. S. Zaret, Pioneer transcription factors in cell reprogramming. *Genes Dev.* **28**, 2679–2692 (2014).

27. K. S. Zaret, S. E. Mango, Pioneer transcription factors, chromatin dynamics, and cell fate control. *Curr. Opin. Genet. Dev.* **37**, 76–81 (2016).

28. M. Fernandez Garcia, *et al.*, Structural Features of Transcription Factors Associating with Nucleosome Binding. *Mol Cell* **75**, 921-932.e6 (2019).

29. S. A. Blythe, E. F. Wieschaus, Establishment and maintenance of heritable chromatin structure during early Drosophila embryogenesis. *eLife* **5**, e20148 (2016).

30. C. E. Hannon, S. A. Blythe, E. F. Wieschaus, Concentration dependent chromatin states induced by the bicoid morphogen gradient. *eLife Sciences* **6**, e28275 (2017).

31. E. E. Swinstead, *et al.*, Steroid Receptors Reprogram FoxA1 Occupancy through Dynamic Chromatin Transitions. *Cell* **165**, 593–605 (2016).

32. A. K. Nagaich, D. A. Walker, R. Wolford, G. L. Hager, Rapid Periodic Binding and Displacement of the Glucocorticoid Receptor during Chromatin Remodeling. *Molecular Cell* **14**, 163–174 (2004).

33. N. Yamanaka, K. F. Rewitz, M. B. O'Connor, Ecdysone Control of Developmental Transitions: Lessons from Drosophila Research. *Annu Rev Entomol* **58**, 497–516 (2013).

34. K. F. Rewitz, N. Yamanaka, M. B. O'Connor, Developmental checkpoints and feedback circuits time insect maturation. *Curr Top Dev Biol* **103**, 1–33 (2013).

35. A. J. Andres, C. S. Thummel, Hormones, puffs and flies: the molecular control of metamorphosis by ecdysone. *Trends in Genetics* **8**, 132–138 (1992).

36. T. Kozlova, C. S. Thummel, Essential roles for ecdysone signaling during Drosophila mid-embryonic development. *Science* **301**, 1911–1914 (2003).

37. J. T. Warren, *et al.*, Discrete pulses of molting hormone, 20-hydroxyecdysone, during late larval development of Drosophila melanogaster: correlations with changes in gene activity. *Dev Dyn* **235**, 315–326 (2006).

38. C. Mirth, J. W. Truman, L. M. Riddiford, The Role of the Prothoracic Gland in Determining Critical Weight for Metamorphosis in Drosophila melanogaster. *Current Biology* **15**, 1796–1807 (2005).

39. Z. McBrayer, *et al.*, Prothoracicotropic hormone regulates developmental timing and body size in Drosophila. *Dev Cell* **13**, 857–871 (2007).

40. S. Layalle, N. Arquier, P. Léopold, The TOR pathway couples nutrition and developmental timing in Drosophila. *Dev Cell* **15**, 568–577 (2008).

41. A. Petryk, *et al.*, Shade is the Drosophila P450 enzyme that mediates the hydroxylation of ecdysone to the steroid insect molting hormone 20-hydroxyecdysone. *Proc Natl Acad Sci U S A* **100**, 13773–13778 (2003).

42. L. I. Gilbert, Halloween genes encode P450 enzymes that mediate steroid hormone biosynthesis in Drosophila melanogaster. *Molecular and Cellular Endocrinology* **215**, 1–10 (2004).

43. K. Akagi, *et al.*, A biological timer in the fat body comprising Blimp-1, betaFtz-f1 and Shade regulates pupation timing in Drosophila melanogaster. *Development* **143**, 2410–2416 (2016).

44. N. Okamoto, *et al.*, A Membrane Transporter Is Required for Steroid Hormone Uptake in Drosophila. *Dev Cell* **47**, 294-305.e7 (2018).

45. N. Okamoto, N. Yamanaka, Steroid Hormone Entry into the Brain Requires a Membrane Transporter in Drosophila. *Curr Biol* **30**, 359-366.e3 (2020).

46. U. Clever, ACTINOMYCIN AND PUROMYCIN: EFFECTS ON SEQUENTIAL GENE ACTIVATION BY ECDYSONE. *Science* **146**, 794–795 (1964).

47. R. J. Hill, I. M. L. Billas, F. Bonneton, L. D. Graham, M. C. Lawrence, Ecdysone receptors: from the Ashburner model to structural biology. *Annu. Rev. Entomol.* **58**, 251–271 (2013).

48. M. Ashburner, Patterns of puffing activity in the salivary gland chromosomes of Drosophila. VI. Induction by ecdysone in salivary glands of D. melanogaster cultured in vitro. *Chromosoma* **38**, 255–281 (1972).

49. K. P. Eagen, T. A. Hartl, R. D. Kornberg, Stable Chromosome Condensation Revealed by Chromosome Conformation Capture. *Cell* **163**, 934–946 (2015).

50. I. F. Zhimulev, D. E. Koryakov, "Polytene Chromosomes" in *ELS*, Major Reference Works., (American Cancer Society, 2009) https:/doi.org/https://doi.org/10.1002/9780470015902.a0001183.pub2 (December 30, 2020).

51. S. A. Demakov, *et al.*, Protein composition of interband regions in polytene and cell line chromosomes of Drosophila melanogaster. *BMC Genomics* **12**, 566 (2011).

52. M. Ashburner, Puffs, genes, and hormones revisited. *Cell* **61**, 1–3 (1990).

53. M. Ashburner, Sequential gene activation by ecdysone in polytene chromosomes of Drosophila melanogaster. II. The effects of inhibitors of protein synthesis. *Dev. Biol.* **39**, 141–157 (1974).

54. M. Ashburner, Sequential gene activation by ecdysone in polytene chromosomes of Drosophila melanogaster. I. Dependence upon ecdysone concentration. *Dev Biol* **35**, 47–61 (1973).

55. M. Ashburner, G. Richards, Sequential gene activation by ecdysone in polytene chromosomes of Drosophila melanogaster. III. Consequences of ecdysone withdrawal. *Dev Biol* **54**, 241–255 (1976).

56. G. Richards, Sequential gene activation by ecdysone in polytene chromosomes of Drosophila melanogaster. V. The late prepupal puffs. *Dev Biol* **54**, 264–275 (1976).

57. G. Richards, Sequential gene activation by ecdysone in polytene chromosomes of Drosophila melanogaster. IV. The mid prepupal period. *Dev Biol* **54**, 256–263 (1976).

58. M. R. Koelle, *et al.*, The Drosophila EcR gene encodes an ecdysone receptor, a new member of the steroid receptor superfamily. *Cell* **67**, 59–77 (1991).

59. T. P. Yao, W. A. Segraves, A. E. Oro, M. McKeown, R. M. Evans, Drosophila ultraspiracle modulates ecdysone receptor function via heterodimer formation. *Cell* **71**, 63–72 (1992).

60. H. E. Thomas, H. G. Stunnenberg, A. F. Stewart, Heterodimerization of the Drosophila ecdysone receptor with retinoid X receptor and ultraspiracle. *Nature* **362**, 471–475 (1993).

61. T. P. Yao, *et al.*, Functional ecdysone receptor is the product of EcR and Ultraspiracle genes. *Nature* **366**, 476–479 (1993).

62. A. Azoitei, M. Spindler-Barth, DNA affects ligand binding of the ecdysone receptor of Drosophila melanogaster. *Molecular and Cellular Endocrinology* **303**, 91–99 (2009).

63. S. Braun, A. Azoitei, M. Spindler-Barth, DNA-binding properties of Drosophila ecdysone receptor isoforms and their modification by the heterodimerization partner ultraspiracle. *Arch. Insect Biochem. Physiol.* **72**, 172–191 (2009).

64. H. Ruff, C. Tremmel, M. Spindler-Barth, Transcriptional activity of ecdysone receptor isoforms is regulated by modulation of receptor stability and interaction with Ab- and C-domains of the heterodimerization partner ultraspiracle. *Arch. Insect Biochem. Physiol.* **72**, 154–171 (2009).

65. L. Cherbas, K. Lee, P. Cherbas, Identification of ecdysone response elements by analysis of the Drosophila Eip28/29 gene. *Genes Dev.* **5**, 120–131 (1991).

66. G. Riddihough, H. R. B. Pelham, An ecdysone response element in the Drosophila hsp27 promoter. *EMBO J* **6**, 3729–3734 (1987).

67. L. J. Zhu, *et al.*, FlyFactorSurvey: a database of Drosophila transcription factor binding specificities determined using the bacterial one-hybrid system. *Nucleic Acids Res* **39**, D111-117 (2011).

68. C. Elke, M. Vögtli, P. Rauch, M. Spindler-Barth, M. Lezzi, Expression of EcR and USP in Escherichia coli: purification and functional studies. *Arch. Insect Biochem. Physiol.* **35**, 59–69 (1997).

69. C. Antoniewski, M. Laval, A. Dahan, J. A. Lepesant, The ecdysone response enhancer of the Fbp1 gene of Drosophila melanogaster is a direct target for the EcR/USP nuclear receptor. *Mol. Cell. Biol.* **14**, 4465–4474 (1994).

70. E. R. Weikum, X. Liu, E. A. Ortlund, The nuclear receptor superfamily: A structural perspective. *Protein Sci* **27**, 1876–1892 (2018).

71. A. Penvose, J. L. Keenan, D. Bray, V. Ramlall, T. Siggers, Comprehensive study of nuclear receptor DNA binding provides a revised framework for understanding receptor specificity. *Nat Commun* **10**, 2514 (2019).

72. F.-J. Shu, N. Sidell, D. Yang, C. B. Kallen, The tri-nucleotide spacer sequence between estrogen response element half-sites is conserved and modulates ERalpha-mediated transcriptional responses. *J Steroid Biochem Mol Biol* **120**, 172–179 (2010).

73. I. M. Billas, L. Moulinier, N. Rochel, D. Moras, Crystal structure of the ligand-binding domain of the ultraspiracle protein USP, the ortholog of retinoid X receptors in insects. *J Biol Chem* **276**, 7465–7474 (2001).

74. S. Devarakonda, J. M. Harp, Y. Kim, A. Ozyhar, F. Rastinejad, Structure of the heterodimeric ecdysone receptor DNA-binding complex. *EMBO J* **22**, 5827–5840 (2003).

75. C. Antoniewski, B. Mugat, F. Delbac, J. A. Lepesant, Direct repeats bind the EcR/USP receptor and mediate ecdysteroid responses in Drosophila melanogaster. *Mol Cell Biol* **16**, 2977–2986 (1996).

76. P. Paolo D'Avino, S. Crispi, L. Cherbas, P. Cherbas, M. Furia, The moulting hormone ecdysone is able to recognize target elements composed of direct repeats. *Molecular and Cellular Endocrinology* **113**, 1–9 (1995).

77. N. Ghbeish, *et al.*, The dual role of ultraspiracle, the Drosophila retinoid X receptor, in the ecdysone response. *Proc. Natl. Acad. Sci. U.S.A.* **98**, 3867–3872 (2001).

78. B. F. B. Costantino, *et al.*, A novel ecdysone receptor mediates steroid-regulated developmental events during the mid-third instar of Drosophila. *PLoS Genet* **4**, e1000102 (2008).

79. G. Lee, R. Sehgal, Z. Wang, J. H. Park, Ultraspiracle-independent anti-apoptotic function of ecdysone receptors is required for the survival of larval peptidergic neurons via suppression of grim expression in Drosophila melanogaster. *Apoptosis* **24**, 256–268 (2019).

80. C.-C. Tsai, H.-Y. Kao, T.-P. Yao, M. McKeown, R. M. Evans, SMRTER, a Drosophila Nuclear Receptor Coregulator, Reveals that EcR-Mediated Repression Is Critical for Development. *Molecular Cell* **4**, 175–186 (1999).

81. E. T. Ables, D. Drummond-Barbosa, The Steroid Hormone Ecdysone Functions with Intrinsic Chromatin Remodeling Factors to Control Female Germline Stem Cells in Drosophila. *Cell Stem Cell* **7**, 581–592 (2010).

82. P. Badenhorst, *et al.*, The Drosophila nucleosome remodeling factor NURF is required for Ecdysteroid signaling and metamorphosis. *Genes Dev.* **19**, 2540–2545 (2005).

83. X. Hu, L. Cherbas, P. Cherbas, Transcription activation by the ecdysone receptor (EcR/USP): identification of activation functions. *Mol Endocrinol* **17**, 716–731 (2003).

84. J.-F. Mouillet, V. C. Henrich, M. Lezzi, M. Vögtli, Differential control of gene activity by isoforms A, B1 and B2 of the Drosophila ecdysone receptor. *European Journal of Biochemistry* **268**, 1811–1819 (2001).

85. W. S. Talbot, E. A. Swyryd, D. S. Hogness, Drosophila tissues with different metamorphic responses to ecdysone express different ecdysone receptor isoforms. *Cell* **73**, 1323–1337 (1993).

86. M. Stoiber, S. Celniker, L. Cherbas, B. Brown, P. Cherbas, Diverse Hormone Response Networks in 41 Independent Drosophila Cell Lines. *G3* **6**, 683–694 (2016).

87. T.-R. Li, K. P. White, Tissue-Specific Gene Expression and Ecdysone-Regulated Genomic Networks in Drosophila. *Developmental Cell* **5**, 59–72 (2003).

88. A. J. Andres, J. C. Fletcher, F. D. Karim, C. S. Thummel, Molecular analysis of the initiation of insect metamorphosis: a comparative study of Drosophila ecdysteroid-regulated transcription. *Dev Biol* **160**, 388–404 (1993).

89. S. E. Gonsalves, S. J. Neal, A. S. Kehoe, J. T. Westwood, Genome-wide examination of the transcriptional response to ecdysteroids 20-hydroxyecdysone and ponasterone A in Drosophila melanogaster. *BMC Genomics* **12**, 475 (2011).

90. Z. Gauhar, *et al.*, Genomic mapping of binding regions for the Ecdysone receptor protein complex. *Genome Res.* **19**, 1006–1013 (2009).

91. R. B. Beckstead, G. Lam, C. S. Thummel, The genomic response to 20-hydroxyecdysone at the onset of Drosophila metamorphosis. *Genome Biology* **6**, R99 (2005).

92. C. S. Thummel, Molecular mechanisms of developmental timing in C. elegans and Drosophila. *Dev. Cell* **1**, 453–465 (2001).

93. M. Bender, F. B. Imam, W. S. Talbot, B. Ganetzky, D. S. Hogness, Drosophila ecdysone receptor mutations reveal functional differences among receptor isoforms. *Cell* **91**, 777–788 (1997).

94. L. Cherbas, X. Hu, I. Zhimulev, E. Belyaeva, P. Cherbas, EcR isoforms in Drosophila: testing tissue-specific requirements by targeted blockade and rescue. *Development* **130**, 271–284 (2003).

95. M. B. Davis, G. E. Carney, A. E. Robertson, M. Bender, Phenotypic analysis of EcR-A mutants suggests that EcR isoforms have unique functions during Drosophila development. *Dev Biol* **282**, 385–396 (2005).

96. M. Schubiger, S. Tomita, C. Sung, S. Robinow, J. W. Truman, Isoform specific control of gene activity in vivo by the Drosophila ecdysone receptor. *Mechanisms of Development* **120**, 909–918 (2003).

97. M. Schubiger, A. A. Wade, G. E. Carney, J. W. Truman, M. Bender, Drosophila EcR-B ecdysone receptor isoforms are required for larval molting and for neuron remodeling during metamorphosis. *Development* **125**, 2053–2062 (1998).

98. J. Broadus, J. R. McCabe, B. Endrizzi, C. S. Thummel, C. T. Woodard, The Drosophila beta FTZ-F1 orphan nuclear receptor provides competence for stage-specific responses to the steroid hormone ecdysone. *Mol Cell* **3**, 143–149 (1999).

99. F. D. Karim, G. M. Guild, C. S. Thummel, The Drosophila Broad-Complex plays a key role in controlling ecdysone-regulated gene expression at the onset of metamorphosis. *Development* **118**, 977–988 (1993).

100. E. H. Baehrecke, C. S. Thummel, The Drosophila E93 gene from the 93F early puff displays stage- and tissue-specific regulation by 20-hydroxyecdysone. *Dev Biol* **171**, 85–97 (1995).

101. C. Y. Lee, *et al.*, E93 directs steroid-triggered programmed cell death in Drosophila. *Mol Cell* **6**, 433–443 (2000).

102. P. Hurban, C. S. Thummel, Isolation and characterization of fifteen ecdysone-inducible Drosophila genes reveal unexpected complexities in ecdysone regulation. *Mol Cell Biol* **13**, 7101–7111 (1993).

103. F. Pecasse, Y. Beck, C. Ruiz, G. Richards, Krüppel-homolog, a stage-specific modulator of the prepupal ecdysone response, is essential for Drosophila metamorphosis. *Dev Biol* **221**, 53–67 (2000).

104. Y. Agawa, *et al.*, Drosophila Blimp-1 is a transient transcriptional repressor that controls timing of the ecdysone-induced developmental pathway. *Mol Cell Biol* **27**, 8739–8747 (2007).

105. C. T. Woodard, E. H. Baehrecke, C. S. Thummel, A molecular mechanism for the stage specificity of the Drosophila prepupal genetic response to ecdysone. *Cell* **79**, 607–615 (1994).

106. J. C. Fletcher, C. S. Thummel, The ecdysone-inducible Broad-complex and E74 early genes interact to regulate target gene transcription and Drosophila metamorphosis. *Genetics* **141**, 1025–1035 (1995).

107. I. Kiss, A. H. Beaton, J. Tardiff, D. Fristrom, J. W. Fristrom, Interactions and developmental effects of mutations in the Broad-Complex of Drosophila melanogaster. *Genetics* **118**, 247–259 (1988).

108. M. Furia, P. P. D'Avino, S. Crispi, D. Artiaco, L. C. Polito, Dense cluster of genes is located at the ecdysone-regulated 3C puff of Drosophila melanogaster. *J Mol Biol* **231**, 531–538 (1993).

109. S. K. Beckendorf, F. C. Kafatos, Differentiation in the salivary glands of Drosophila melanogaster: characterization of the glue proteins and their developmental appearance. *Cell* **9**, 365–373 (1976).

110. R. Farkas, B. M. Mechler, The timing of Drosophila salivary gland apoptosis displays an l(2)gl -dose response. *Cell Death & Differentiation* **7**, 89–101 (2000).

111. E. W. Abrams, D. J. Andrew, CrebA regulates secretory activity in the Drosophila salivary gland and epidermis. *Development* **132**, 2743–2758 (2005).

112. M. Lehmann, F. Wattler, G. Korge, Two new regulatory elements controlling the Drosophila Sgs-3 gene are potential ecdysone receptor and fork head binding sites. *Mech. Dev.* **62**, 15–27 (1997).

113. M. Lehmann, G. Korge, The fork head product directly specifies the tissue-specific hormone responsiveness of the Drosophila Sgs-4 gene. *EMBO J* **15**, 4825–4834 (1996).

114. A. J. Andres, P. Cherbas, Tissue-specific ecdysone responses: regulation of the Drosophila genes Eip28/29 and Eip40 during larval development. *Development* **116**, 865–876 (1992).

115. R. S. Mann, S. B. Carroll, Molecular mechanisms of selector gene function and evolution. *Curr Opin Genet Dev* **12**, 592–600 (2002).

116. A. C. Mullen, *et al.*, Master transcription factors determine cell-type-specific responses to TGF-β signaling. *Cell* **147**, 565–576 (2011).

117. T. H. I. Fakhouri, J. Stevenson, A. D. Chisholm, S. E. Mango, Dynamic chromatin organization during foregut development mediated by the organ selector gene PHA-4/FoxA. *PLoS Genet* **6** (2010).

118. T.-H. Pham, *et al.*, Mechanisms of in vivo binding site selection of the hematopoietic master transcription factor PU.1. *Nucleic Acids Res* **41**, 6391–6402 (2013).

119. X. Li, *et al.*, Transcription factors bind thousands of active and inactive regions in the Drosophila blastoderm. *PLoS Biol* **6**, e27 (2008).

120. E. Z. Kvon, G. Stampfel, J. O. Yáñez-Cuna, B. J. Dickson, A. Stark, HOT regions function as patterned developmental enhancers and have a distinct cis-regulatory signature. *Genes Dev* **26**, 908–913 (2012).

121. C. S. Lee, J. R. Friedman, J. T. Fulmer, K. H. Kaestner, The initiation of liver development is dependent on Foxa transcription factors. *Nature* **435**, 944–947 (2005).

122. I. C. Taylor, J. L. Workman, T. J. Schuetz, R. E. Kingston, Facilitated binding of GAL4 and heat shock factor to nucleosomal templates: differential function of DNA-binding domains. *Genes Dev* **5**, 1285–1298 (1991).

123. M. Kohwi, C. Q. Doe, Temporal fate specification and neural progenitor competence during development. *Nat Rev Neurosci* **14**, 823–838 (2013).

124. T. Isshiki, B. Pearson, S. Holbrook, C. Q. Doe, Drosophila neuroblasts sequentially express transcription factors which specify the temporal identity of their neuronal progeny. *Cell* **106**, 511–521 (2001).

125. T. Erclik, *et al.*, Integration of temporal and spatial patterning generates neural diversity. *Nature* **541**, 365–370 (2017).

126. Y.-B. Shi, Unliganded thyroid hormone receptor regulates metamorphic timing via the recruitment of histone deacetylase complexes. *Curr Top Dev Biol* **105**, 275–297 (2013).

127. R. D. Romeo, Puberty: a period of both organizational and activational effects of steroid hormones on neurobehavioural development. *J Neuroendocrinol* **15**, 1185–1192 (2003).

128. C. S. Thummel, Ecdysone-regulated puff genes 2000. *Insect Biochem Mol Biol* **32**, 113–120 (2002).

129. K. King-Jones, C. S. Thummel, Nuclear receptors--a perspective from Drosophila. *Nat Rev Genet* **6**, 311–323 (2005).

130. D. Shlyueva, *et al.*, Hormone-responsive enhancer-activity maps reveal predictive motifs, indirect repression, and targeting of closed chromatin. *Mol Cell* **54**, 180–192 (2014).

131. D. J. McKay, J. D. Lieb, A common set of DNA regulatory elements shapes Drosophila appendages. *Dev Cell* **27**, 306–318 (2013).

132. C. Estella, R. S. Mann, Non-redundant selector and growth-promoting functions of two sister genes, buttonhead and Sp1, in Drosophila leg development. *PLoS Genet* **6**, e1001001 (2010).

133. G. Halder, *et al.*, The Vestigial and Scalloped proteins act together to directly regulate wing-specific gene expression in Drosophila. *Genes Dev* **12**, 3900–3909 (1998).

134. Y. Guo, K. Flegel, J. Kumar, D. J. McKay, L. A. Buttitta, Ecdysone signaling induces two phases of cell cycle exit in Drosophila cells. *Biology Open* **5**, 1648–1661 (2016).

135. D. W. Huang, B. T. Sherman, R. A. Lempicki, Systematic and integrative analysis of large gene lists using DAVID bioinformatics resources. *Nat Protoc* **4**, 44–57 (2009).

136. F. Supek, M. Bošnjak, N. Škunca, T. Šmuc, REVIGO summarizes and visualizes long lists of gene ontology terms. *PLoS One* **6**, e21800 (2011).

137. J. T. Robinson, *et al.*, Integrative genomics viewer. *Nat Biotechnol* **29**, 24–26 (2011).

138. M. D. Robinson, D. J. McCarthy, G. K. Smyth, edgeR: a Bioconductor package for differential expression analysis of digital gene expression data. *Bioinformatics* **26**, 139–140 (2010).

139. A. R. Quinlan, I. M. Hall, BEDTools: a flexible suite of utilities for comparing genomic features. *Bioinformatics* **26**, 841–842 (2010).

140. F. Ramírez, *et al.*, deepTools2: a next generation web server for deep-sequencing data analysis. *Nucleic Acids Res.* **44**, W160-165 (2016).

141. M. Lawrence, *et al.*, Software for computing and annotating genomic ranges. *PLoS Comput Biol* **9**, e1003118 (2013).

142. M. Lawrence, R. Gentleman, V. Carey, rtracklayer: an R package for interfacing with genome browsers. *Bioinformatics* **25**, 1841–1842 (2009).

143. A. Akalin, V. Franke, K. Vlahoviček, C. E. Mason, D. Schübeler, Genomation: a toolkit to summarize, annotate and visualize genomic intervals. *Bioinformatics* **31**, 1127–1129 (2015).

144. R. C. McLeay, T. L. Bailey, Motif Enrichment Analysis: a unified framework and an evaluation on ChIP data. *BMC Bioinformatics* **11**, 165 (2010).

145. T. L. Bailey, *et al.*, MEME SUITE: tools for motif discovery and searching. *Nucleic Acids Res.* **37**, W202-208 (2009).

146. L. Jiang, J. C. Pearson, S. T. Crews, Diverse modes of Drosophila tracheal fusion cell transcriptional regulation. *Mech Dev* **127**, 265–280 (2010).

147. C. Han, L. Y. Jan, Y.-N. Jan, Enhancer-driven membrane markers for analysis of nonautonomous mechanisms reveal neuron-glia interactions in Drosophila. *Proc. Natl. Acad. Sci. U.S.A.* **108**, 9673–9678 (2011).

148. Michael. Bate, A. Martinez Arias, *The Development of Drosophila melanogaster* (Cold Spring Harbor Laboratory Press, 1993).

149. P. N. Adler, J. Liu, J. Charlton, Cell size and the morphogenesis of wing hairs in Drosophila. *Genesis* **28**, 82–91 (2000).

150. P. G. Giresi, J. Kim, R. M. McDaniell, V. R. Iyer, J. D. Lieb, FAIRE (Formaldehyde-Assisted Isolation of Regulatory Elements) isolates active regulatory elements from human chromatin. *Genome Res* **17**, 877–885 (2007).

151. S. Fraichard, *et al.*, Tenectin is a novel alphaPS2betaPS integrin ligand required for wing morphogenesis and male genital looping in Drosophila. *Dev Biol* **340**, 504–517 (2010).

152. L. F. Sobala, P. N. Adler, The Gene Expression Program for the Formation of Wing Cuticle in Drosophila. *PLOS Genetics* **12**, e1006100 (2016).

153. F. J. Cifuentes, A. García-Bellido, Proximo-distal specification in the wing disc of Drosophila by the nubbin gene. *Proc Natl Acad Sci U S A* **94**, 11405–11410 (1997).

154. T. L. Lovato, A. R. Benjamin, R. M. Cripps, Transcription of Myocyte enhancer factor-2 in adult Drosophila myoblasts is induced by the steroid hormone ecdysone. *Dev Biol* **288**, 612–621 (2005).

155. X. Mou, D. M. Duncan, E. H. Baehrecke, I. Duncan, Control of target gene specificity during metamorphosis by the steroid response gene E93. *Proc Natl Acad Sci U S A* **109**, 2949–2954 (2012).

156. N. J. Fuda, *et al.*, GAGA factor maintains nucleosome-free regions and has a role in RNA polymerase II recruitment to promoters. *PLoS Genet* **11**, e1005108 (2015).

157. K. J. T. Venken, *et al.*, MiMIC: a highly versatile transposon insertion resource for engineering Drosophila melanogaster genes. *Nat Methods* **8**, 737–743 (2011).

158. T. L. Bailey, DREME: motif discovery in transcription factor ChIP-seq data. *Bioinformatics* **27**, 1653–1659 (2011).

159. M. Slattery, *et al.*, Divergent transcriptional regulatory logic at the intersection of tissue growth and developmental patterning. *PLoS Genet* **9**, e1003753 (2013).

160. A. B. Stergachis, *et al.*, Developmental fate and cellular maturity encoded in human regulatory DNA landscapes. *Cell* **154**, 888–903 (2013).

161. L. Dobens, K. Rudolph, E. M. Berger, Ecdysterone regulatory elements function as both transcriptional activators and repressors. *Mol Cell Biol* **11**, 1846–1853 (1991).

162. A. Carbonell, A. Mazo, F. Serras, M. Corominas, Ash2 acts as an ecdysone receptor coactivator by stabilizing the histone methyltransferase Trr. *Mol. Biol. Cell* **24**, 361–372 (2013).

163. J. Kreher, *et al.*, EcR recruits dMi-2 and increases efficiency of dMi-2-mediated remodelling to constrain transcription of hormone-regulated genes. *Nat Commun* **8**, 14806 (2017).

164. M. H. Syed, B. Mark, C. Q. Doe, Steroid hormone induction of temporal gene expression in Drosophila brain neuroblasts generates neuronal and glial diversity. *Elife* **6** (2017).

165. A. Hitrik, *et al.*, Combgap Promotes Ovarian Niche Development and Chromatin Association of EcR-Binding Regions in BR-C. *PLoS Genet* **12**, e1006330 (2016).

166. G. J. Fisk, C. S. Thummel, The DHR78 nuclear receptor is required for ecdysteroid signaling during the onset of Drosophila metamorphosis. *Cell* **93**, 543–555 (1998).

167. C. M. Uyehara, *et al.*, Hormone-dependent control of developmental timing through regulation of chromatin accessibility. *Genes Dev.* (2017) https:/doi.org/10.1101/gad.298182.117 (May 30, 2017).

168. A. Dobin, *et al.*, STAR: ultrafast universal RNA-seq aligner. *Bioinformatics* **29**, 15–21 (2013).

169. Y. Liao, G. K. Smyth, W. Shi, The Subread aligner: fast, accurate and scalable read mapping by seed-and-vote. *Nucleic Acids Res.* **41**, e108 (2013).

170. M. I. Love, W. Huber, S. Anders, Moderated estimation of fold change and dispersion for RNA-seq data with DESeq2. *Genome Biology* **15**, 550 (2014).

171. A. A. J. Rahnenfuhrer, topGO. *topGO: Enrichment Analysis for Gene Ontology* (2018) (November 26, 2018).

172. B. Langmead, S. L. Salzberg, Fast gapped-read alignment with Bowtie 2. *Nat Methods* **9**, 357–359 (2012).

173. H. Li, *et al.*, The Sequence Alignment/Map format and SAMtools. *Bioinformatics* **25**, 2078–2079 (2009).

174. W. J. Kent, A. S. Zweig, G. Barber, A. S. Hinrichs, D. Karolchik, BigWig and BigBed: enabling browsing of large distributed datasets. *Bioinformatics* **26**, 2204–2207 (2010).

175. Y. Zhang, *et al.*, Model-based Analysis of ChIP-Seq (MACS). *Genome Biology* **9**, R137 (2008).

176. P. Stempor, J. Ahringer, SeqPlots - Interactive software for exploratory data analyses, pattern discovery and visualization in genomics. *Wellcome Open Res* **1**, 14 (2016).

177. L. J. Zhu, *et al.*, ChIPpeakAnno: a Bioconductor package to annotate ChIP-seq and ChIP-chip data. *BMC Bioinformatics* **11**, 237 (2010).

178. C. E. Grant, T. L. Bailey, W. S. Noble, FIMO: scanning for occurrences of a given motif. *Bioinformatics* **27**, 1017–1018 (2011).

179. M. A. Crickmore, R. S. Mann, Hox control of organ size by regulation of morphogen production and mobility. *Science* **313**, 63–68 (2006).

180. D. Fristrom, M. Wilcox, J. Fristrom, The distribution of PS integrins, laminin A and F-actin during key stages in Drosophila wing development. *Development* **117**, 509–523 (1993).

181. J. Colombani, *et al.*, Antagonistic Actions of Ecdysone and Insulins Determine Final Size in Drosophila. *Science* **310**, 667–670 (2005).

182. L. Herboso, *et al.*, Ecdysone promotes growth of imaginal discs through the regulation of Thor in D. melanogaster. *Sci Rep* **5**, 12383 (2015).

183. C. K. Mirth, J. W. Truman, L. M. Riddiford, The Ecdysone receptor controls the post-critical weight switch to nutrition-independent differentiation in Drosophila wing imaginal discs. *Development* **136**, 2345–2353 (2009).

184. S. Nagarkar-Jaiswal, *et al.*, A genetic toolkit for tagging intronic MiMIC containing genes. *eLife* **4**, e08469 (2015).

185. P. J. Skene, J. G. Henikoff, S. Henikoff, Targeted in situ genome-wide profiling with high efficiency for low cell numbers. *Nat Protoc* **13**, 1006–1019 (2018).

186. S. Nagarkar-Jaiswal, *et al.*, A library of MiMICs allows tagging of genes and reversible, spatial and temporal knockdown of proteins in Drosophila. *eLife* **4**, e05338 (2015).

187. L. von Kalm, K. Crossgrove, D. Von Seggern, G. M. Guild, S. K. Beckendorf, The Broad-Complex directly controls a tissue-specific response to the steroid hormone ecdysone at the onset of Drosophila metamorphosis. *EMBO J* **13**, 3505–3516 (1994).

188. H. L. D. Brown, L. Cherbas, P. Cherbas, J. W. Truman, Use of time-lapse imaging and dominant negative receptors to dissect the steroid receptor control of neuronal remodeling in Drosophila. *Development* **133**, 275–285 (2006).

189. J. F. de Celis, A. Garcia-Bellido, S. J. Bray, Activation and function of Notch at the dorsal-ventral boundary of the wing imaginal disc. *Development* **122**, 359–369 (1996).

190. P. J. Kooh, R. G. Fehon, M. A. Muskavitch, Implications of dynamic patterns of Delta and Notch expression for cellular interactions during Drosophila development. *Development* **117**, 493–507 (1993).

191. F. Huang, C. Dambly-Chaudiere, A. Ghysen, The emergence of sense organs in the wing disc of Drosophila. *Development* **111**, 1087–1095 (1991).

192. S. S. Huppert, T. L. Jacobsen, M. A. Muskavitch, Feedback regulation is central to Delta-Notch signalling required for Drosophila wing vein morphogenesis. *Development* **124**, 3283–3291 (1997).

193. M. Schubiger, C. Carre, C. Antoniewski, J. W. Truman, Ligand-dependent de-repression via EcR/USP acts as a gate to coordinate the differentiation of sensory neurons in the Drosophila wing. *Development* **132**, 5239–5248 (2005).

194. S. Wang, J. Wang, Y. Sun, Q. Song, S. Li, PKC-mediated USP phosphorylation at Ser35 modulates 20-hydroxyecdysone signaling in Drosophila. *J Proteome Res* **11**, 6187–6196 (2012).

195. S. C. Biddie, *et al.*, Transcription Factor AP1 Potentiates Chromatin Accessibility and Glucocorticoid Receptor Binding. *Molecular Cell* **43**, 145–155 (2011).

196. S. John, *et al.*, Interaction of the Glucocorticoid Receptor with the Chromatin Landscape. *Molecular Cell* **29**, 611–624 (2008).

197. Y. Ma, L. Buttitta, Chromatin organization changes during the establishment and maintenance of the postmitotic state. *Epigenetics Chromatin* **10**, 53 (2017).

198. A. Niedziela-Majka, M. Kochman, A. Ozyhar, Polarity of the ecdysone receptor complex interaction with the palindromic response element from the hsp27 gene promoter. *Eur. J. Biochem.* **267**, 507–519 (2000).

199. U. Dressel, *et al.*, Alien, a highly conserved protein with characteristics of a corepressor for members of the nuclear hormone receptor superfamily. *Mol. Cell. Biol.* **19**, 3383–3394 (1999).

200. S. Kimura, *et al.*, Drosophila arginine methyltransferase 1 (DART1) is an ecdysone receptor co-repressor. *Biochem Biophys Res Commun* **371**, 889–893 (2008).

201. S. Sawatsubashi, *et al.*, Ecdysone receptor-dependent gene regulation mediates histone poly(ADP-ribosyl)ation. *Biochem Biophys Res Commun* **320**, 268–272 (2004).

202. A. Tulin, A. Spradling, Chromatin loosening by poly(ADP)-ribose polymerase (PARP) at Drosophila puff loci. *Science* **299**, 560–562 (2003).

203. J. Zhu, L. Chen, G. Sun, A. S. Raikhel, The Competence Factor βFtz-F1 Potentiates Ecdysone Receptor Activity via Recruiting a p160/SRC Coactivator. *Mol. Cell. Biol.* **26**, 9402–9412 (2006).

204. Y. Sedkov, *et al.*, Methylation at lysine 4 of histone H3 in ecdysone-dependent development of Drosophila. *Nature* **426**, 78–83 (2003).

205. M. Y. Mazina, E. V. Kovalenko, N. E. Vorobyeva, The negative elongation factor NELF promotes induced transcriptional response of Drosophila ecdysone-dependent genes. *Sci Rep* **11**, 172 (2021).

206. X.-J. Xie, *et al.*, CDK8-Cyclin C Mediates Nutritional Regulation of Developmental Transitions through the Ecdysone Receptor in Drosophila. *PLoS Biol* **13**, e1002207 (2015).

207. L. Wang, *et al.*, A genetic screen identifies new regulators of steroid-triggered programmed cell death in Drosophila. *Genetics* **180**, 269–281 (2008).

208. F. D. Karim, C. S. Thummel, Temporal coordination of regulatory gene expression by the steroid hormone ecdysone. *EMBO J* **11**, 4083–4093 (1992).

209. C. M. Uyehara, D. J. McKay, Direct and widespread role for the nuclear receptor EcR in mediating the response to ecdysone in Drosophila. *Proc Natl Acad Sci U S A* **116**, 9893–9902 (2019).

210. T. Rousso, E. D. Schejter, B.-Z. Shilo, Orchestrated content release from Drosophila glue-protein vesicles by a contractile actomyosin network. **18** (2016).

211. C. Cao, Y. Liu, M. Lehmann, Fork head controls the timing and tissue selectivity of steroid-induced developmental cell death. *J Cell Biol* **176**, 843–852 (2007).

212. M. M. Oliveira, A. W. Shingleton, C. K. Mirth, Coordination of Wing and Whole-Body Development at Developmental Milestones Ensures Robustness against Environmental and Physiological Perturbations. *PLOS Genetics* **10**, e1004408 (2014).

213. K. Ahmad, CUT&RUN with Drosophila tissues (2018) https:/doi.org/10.17504/protocols.io.umfeu3n (April 1, 2021).

214. Z. Cebeci, Comparison of Internal Validity Indices for Fuzzy Clustering. *Journal of Agricultural Informatics*, 1–14 (2019).

215. W. N. Venables, B. D. Ripley, *Modern Applied Statistics with S*, Fourth (Springer, 2002).

216. H. Wickham, *ggplot2: Elegant Graphics for Data Analysis* (Springer-Verlag New York, 2016).

217. T. L. Pedersen, *patchwork: The Composer of Plots* (2020).

218. H. Wickham, A Layered Grammar of Graphics. *null* **19**, 3–28 (2010).

219. S. Sayols, *rrvgo: a Bioconductor package to reduce and visualize Gene Ontology terms* (2020).

220. P. J. Skene, S. Henikoff, An efficient targeted nuclease strategy for high-resolution mapping of DNA binding sites. *Elife* **6** (2017).

221. Y. Liao, G. K. Smyth, W. Shi, featureCounts: an efficient general purpose program for assigning sequence reads to genomic features. *Bioinformatics* **30**, 923–930 (2014).

222. A. J. Simmonds, W. J. Brook, S. M. Cohen, J. B. Bell, Distinguishable functions for engrailed and invected in anterior-posterior patterning in the Drosophila wing. *Nature* **376**, 424–427 (1995).

223. J. O. MacKay, *et al.*, An in vivo analysis of the vestigial gene in Drosophila melanogaster defines the domains required for Vg function. *Genetics* **163**, 1365–1373 (2003).

224. A. H. Brand, N. Perrimon, Targeted gene expression as a means of altering cell fates and generating dominant phenotypes. *Development* **118**, 401–415 (1993).

225. C. Jiang, A. F. Lamblin, H. Steller, C. S. Thummel, A steroid-triggered transcriptional hierarchy controls salivary gland cell death during Drosophila metamorphosis. *Mol Cell* **5**, 445–455 (2000).

226. M. A. Horner, T. Chen, C. S. Thummel, Ecdysteroid regulation and DNA binding properties of Drosophila nuclear hormone receptor superfamily members. *Dev Biol* **168**, 490–502 (1995).

227. A. Hurtado, K. A. Holmes, C. S. Ross-Innes, D. Schmidt, J. S. Carroll, FOXA1 is a key determinant of estrogen receptor function and endocrine response. *Nat Genet* **43**, 27–33 (2011).

228. S. S. Blair, Wing Vein Patterning in Drosophila and the Analysis of Intercellular Signaling. *Annual Review of Cell and Developmental Biology* **23**, 293–319 (2007).

229. G. Richards, Sequential gene activation by ecdysteroids in polytene chromosomes ofDrosophila melanogaster : VII. Tissue specific puffing. *Wilehm Roux Arch Dev Biol* **191**, 103–111 (1982).

230. S. John, *et al.*, Chromatin accessibility pre-determines glucocorticoid receptor binding patterns. *Nat Genet* **43**, 264–268 (2011).

231. S. L. Nystrom, M. J. Niederhuber, D. J. McKay, Expression of E93 provides an instructive cue to control dynamic enhancer activity and chromatin accessibility during development. *Development* **147** (2020).

232. M. J. Niederhuber, D. J. McKay, Mechanisms underlying the control of dynamic regulatory element activity and chromatin accessibility during metamorphosis. *Curr Opin Insect Sci* **43**, 21–28 (2020).

233. Z. Pillidge, S. J. Bray, SWI/SNF chromatin remodeling controls Notch-responsive enhancer accessibility. *EMBO Rep* **20** (2019).

234. P. Varga-Weisz, ATP-dependent chromatin remodeling factors: nucleosome shufflers with many missions. *Oncogene* **20**, 3076–3085 (2001).

235. J. D. Buenrostro, B. Wu, H. Y. Chang, W. J. Greenleaf, ATAC-seq: A Method for Assaying Chromatin Accessibility Genome-Wide. *Curr Protoc Mol Biol* **109**, 21.29.1-21.29.9 (2015).

236. M. R. Corces, *et al.*, An improved ATAC-seq protocol reduces background and enables interrogation of frozen tissues. *Nat Methods* **14**, 959–962 (2017).

237. M. Lehmann, G. Korge, Ecdysone regulation of the Drosophila Sgs-4 gene is mediated by the synergistic action of ecdysone receptor and SEBP 3. *EMBO J* **14**, 716–726 (1995).

238. X. Liu, *et al.*, 20-Hydroxyecdysone (20E) Primary Response Gene E93 Modulates 20E Signaling to Promote Bombyx Larval-Pupal Metamorphosis. *J. Biol. Chem.* **290**, 27370–27383 (2015).

239. M. B. Davis, I. SanGil, G. Berry, R. Olayokun, L. H. Neves, Identification of common and cell type specific LXXLL motif EcR cofactors using a bioinformatics refined candidate RNAi screen in Drosophila melanogaster cell lines. *BMC Developmental Biology* **11**, 66 (2011).

240. H. S. Kaya-Okur, *et al.*, CUT&Tag for efficient epigenomic profiling of small samples and single cells. *Nat Commun* **10**, 1930 (2019).

241. N. C. Mitchell, *et al.*, The Ecdysone receptor constrains wingless expression to pattern cell cycle across the Drosophila wing margin in a Cyclin B-dependent manner. *BMC Dev Biol* **13**, 28 (2013).

242. M. Y. Mazina, R. H. Ziganshin, M. D. Magnitov, A. K. Golovnin, N. E. Vorobyeva, Proximity-dependent biotin labelling reveals CP190 as an EcR/Usp molecular partner. *Sci Rep* **10**, 4793 (2020).

243. M. E. Fortini, Notch signaling: the core pathway and its posttranslational regulation. *Dev Cell* **16**, 633–647 (2009).

244. C. B. González-Blas, *et al.*, Identification of genomic enhancers through spatial integration of single-cell transcriptomics and epigenomics. *bioRxiv*, 2019.12.19.882381 (2019).

245. J. Jacobs, *et al.*, The transcription factor Grainy head primes epithelial enhancers for spatiotemporal activation by displacing nucleosomes. *Nat. Genet.* (2018) https:/doi.org/10.1038/s41588-018-0140-x.

246. R. Loker, J. E. Sanner, R. S. Mann, Ubx orchestrates tissue identity through regional and bidirectional changes to chromatin accessibility. *bioRxiv*, 2021.01.15.426863 (2021).

247. L. I. Mortin, J. W. Sedat, Structure of Drosophila polytene chromosomes. Evidence for a toroidal organization of the bands. *J Cell Sci* **57**, 73–113 (1982).

248. J. C. J. Eeken, "Polytene Chromosomes" in *Brenner's Encyclopedia of Genetics (Second Edition)*, S. Maloy, K. Hughes, Eds. (Academic Press, 2001), pp. 405–406.

249. E. H. Mok, *et al.*, Maintenance of the DNA puff expanded state is independent of active replication and transcription. *Chromosoma* **110**, 186–196 (2001).

250. C. Pelling, T. D. Allen, Scanning electron microscopy of polytene chromosomes (I). *Chromosome Res* **1**, 221–237 (1993).

251. A. Pauli, *et al.*, A direct role for cohesin in gene regulation and ecdysone response in Drosophila salivary glands. *Curr Biol* **20**, 1787–1798 (2010).

252. Y. Ji, A. V. Tulin, The roles of PARP1 in gene control and cell differentiation. *Curr Opin Genet Dev* **20**, 512–518 (2010).

253. N. S. Benabdallah, *et al.*, Decreased Enhancer-Promoter Proximity Accompanying Enhancer Activation. *Mol Cell* **76**, 473-484.e7 (2019).